The Preserve: Lehigh Library Digital Collections

Asymptotic Structure Of Supersonic Turbulent Boundary Layers.

Citation

He, Jun. *Asymptotic Structure Of Supersonic Turbulent Boundary Layers.* 1994, https://preserve.lehigh.edu/lehigh-scholarship/graduate-publications-theses-dissertations/theses-dissertations/asymptotic-3.

Find more at https://preserve.lehigh.edu/

This document is brought to you for free and open access by Lehigh Preserve. It has been accepted for inclusion by an authorized administrator of Lehigh Preserve. For more information, please contact preserve@lehigh.edu.

INFORMATION TO USERS

This manuscript has been reproduced from the microfilm master. UMI films the text directly from the original or copy submitted. Thus, some thesis and dissertation copies are in typewriter face, while others may be from any type of computer printer.

The quality of this reproduction is dependent upon the quality of the copy submitted. Broken or indistinct print, colored or poor quality illustrations and photographs, print bleedthrough, substandard margins, and improper alignment can adversely affect reproduction.

In the unlikely event that the author did not send UMI a complete manuscript and there are missing pages, these will be noted. Also, if unauthorized copyright material had to be removed, a note will indicate the deletion.

Oversize materials (e.g., maps, drawings, charts) are reproduced by sectioning the original, beginning at the upper left-hand corner and continuing from left to right in equal sections with small overlaps. Each original is also photographed in one exposure and is included in reduced form at the back of the book.

Photographs included in the original manuscript have been reproduced xerographically in this copy. Higher quality 6" x 9" black and white photographic prints are available for any photographs or illustrations appearing in this copy for an additional charge. Contact UMI directly to order.

U·M·I

University Microfilms International
A Bell & Howell Information Company
300 North Zeeb Road, Ann Arbor, MI 48106-1346 USA
313/761-4700 800/521-0600

Order Number 9414994

Asymptotic structure of supersonic turbulent boundary layers

He, Jun, Ph.D.

Lehigh University, 1994

U·M·I
300 N. Zeeb Rd.
Ann Arbor, MI 48106

ASYMPTOTIC STRUCTURE OF SUPERSONIC TURBULENT BOUNDARY LAYERS

by

Jun He

Presented to the Graduate and Research Committee

of Lehigh University

in Candidacy for the Degree of

Doctor of Philosophy

in

Applied Mathematics

Lehigh University

December 1993

Approved and recommended for acceptance as a dissertation in partial fulfillment of the requirements for the degree of Doctor of Philosophy.

Dec. 9, 1993
Date

Dr. J. D. Walker, Professor,
Department of Mech. Enrg. & Mechanics.
(Dissertation Advisor and Chairman of the Special Committee)

Dec. 13, 1993
Accepted Date

Dr. P. A. Blythe, Professor,
Department of Mech. Enrg. & Mechanics.

Dr. H. S. Caram, Professor,
Department of Chemical Engineering.

Dr. J. Y. Kazakia, Professor,
Department of Mech. Enrg. & Mechanics.

Dr. C. R. Smith, Professor,
Department of Mech. Enrg. & Mechanics.

ACKNOWLEDGMENTS

I would like to thank Professor J. D. A. Walker, Professor J. Y. Kazakia for introducing me to this problem and for their guidance throughout the course of this research. A special debt of gratitude is owed to Professor Walker for serving as my advisor and for the many hours of individualized instruction he has given to me.

I would also like to thank Professors P. A. Blythe, C. R. Smith and H. S. Caram for serving as members of my special committee.

My sincerest thanks is extended to Mrs. Joann Casciano for her assistance in typing this manuscript.

In addition, the author gratefully acknowledges support of this work by NASA-Langley Research Center under grant number NAG-1-832 and AFOSR under grant number AFOSR 89-0487.

TABLE OF CONTENTS

LIST OF TABLES

LIST OF FIGURES

NOMENCLATURE

English Symbols

A	constant in equation (2.52)
A_l^+	integral defined in equation (5.52)
a	similarity parameter, see equation (5.41)
a_w	speed of sound at the wall. see equation (3.3)
B	constant in equation (2.52)
B_i	inner logarithmic law "constant" for thermal boundary layer
B_o	outer logarithmic law "constant" for thermal boundary layer
B_l^+	integral defined in equation (5.52)
c_f	skin friction coefficient
C_i	inner logarithmic law "constant" for momentum boundary layer
C_o	outer logarithmic law "constant" for momentum boundary layer
C_p	constant in Baldwin-Lomax turbulence model
c_p^*	specific heat (constant pressure)
c_v^*	specific heat (constant volume)
e_1	inner and outer gauge function in the asymptotic expansion for σ

F	normalized streamwise velocity
F_1	outer region defect streamfunction
$F_{1\infty}$	limiting value of F_1 at infinity
F_{com}	composite velocity defined in equation (5.72)
f_1	inner region expansion function for the streamfunction
f_n	wall layer expansion functions, see equations (4.11) and (4.12)
g_1	inner region gauge function in the asymptotic expansion for ϕ
H	dimensionless mean total enthalpy
H_c	leading order composite total enthalpy
$I = H/H_e$	normalized mean total enthalpy
I_{com}	composite total enthalpy defined in equation (5,73)
K	eddy viscosity "constant", see equation (5.14)
K_h	eddy conductivity "constant", see equation (5.17)
k	dimensionless thermal conductivity
k_t	dimensionless turbulent thermal conductivity
L_x	characteristic length of wall-layer streaks
l	mixing length, see equation (2.9)
M	local Mach number, see equation (1.24)

M_e	Mach number at the edge of boundary layer
M_o	representative parameter, see equation (3.4.1)
M_{ref}	reference Mach number, see equation (1.12)
n	dimensionless normal coordinate
P	constant in equation (6.38)
Pr	Prandtl number, see equation (1.22)
Pr_t	turbulent Prandtl number, see equation (2.26)
Pr_M	mixed Prandtl number, see equation (2.32)
p	dimensionless instantaneous pressure
p_o	fluctuating pressure due to the vortex motion above the wall layer
p_1	pressure variation due to organized motion within the wall layer
p_e	steady mainstream pressure (dimensionless)
p^+	scaled mainstream pressure gradient defined in equation (4.10)
$\hat{p}^+$	transformed pressure gradient defined in equation (4.19)
q	heat flux
q_w	heat flux at the wall
q_τ	heat flux temperature defined in equation (2.13)
$q_{\tau o}$	heat flux temperature defined in equation (4.34)

q_*	normalized heat flux, see equation (3.104)
R	gas constant
Re	Reynolds number based upon the reference quantities, see equation (1.22)
Re_o	Reynolds number based upon the fluid properties evaluated at T_o, see equation (3.86)
Re_{δ^*}	Reynolds number based on displacement thickness
Re_θ	Reynolds number based on momentum thickness
r	recovery factor
r	dimensionless radius of revolution for an axisymmetric body
S^*	constant in Sutherland relation (1.7)
St	Stanton number, see equation (5.65)
s	dimensionless tangential coordinate
T	dimensionless mean temperature
T_B	time period of the "burst"
T_c	average time period between bursts (mean burst period)
T_o	inner-region representative temperature
T_q	quiescent time period
T_w	temperature at the wall

T_r	recovery temperature defined in equation (2.43)
t	time (dimensionless)
t^+	scaled time in the wall layer formulation, see equation (4.4)
U_1	defect velocity
U_e	mainstream velocity
U^+	inner region velocity function
u	dimensionless mean streamwise velocity
u_c	leading order composite velocity
u_{eff}	Von Driest effective velocity, see equation (2.55)
$\tilde{u}_n$	expansion functions for the streamwise velocity in the wall-layer model, see equation (4.30)
u_τ	dimensionless friction velocity
$u_{\tau o}$	friction velocity defined in equation (3.24)
u_*	normalized friction velocity with respect to U_e
$\tilde{u}^+$	dimensionless instantaneous streamwise velocity (scaled on wall variables)
v	dimensionless mean normal velocity
$\tilde{v}$	transformed mean normal velocity, see equation (3.4)

$\tilde{v}^+$	dimensionless instantaneous normal velocity (scaled on wall variables)
$\hat{v}^+$	transformed instantaneous normal velocity, see equation (4.20)
W	wake function
w	dimensionless spanwise mean velocity
$\tilde{w}^+$	dimensionless instantaneous spanwise velocity (scaled on wall variables)
x	dimensionless streamwise coordinate
x^+	scaled inner region streamwise coordinate
Y	transformed normal coordinate (dimensionless)
Y^+	scaled inner region normal coordinate
Y_l^+	wall-layer characteristic range of Y^+, see equation (5.51)
Y_θ^+	scaled inner region normal coordinate for thermal boundary layer
y	dimensionless normal coordinate
y^+	scaled inner region normal coordinate
y_{max}	local of maximum $\tilde{F} = y \mid \partial u/\partial n \mid$
z	dimensionless spanwise coordinate
z^+	scaled inner region spanwise coordinate

Greek Symbols

α	parameter defined in equation (3.9)
β	equilibrium pressure gradient parameter, see equation (2.5)
Γ_1	outer region velocity scale
γ	ratio of specific heats c_p^*/c_v^*
γ_1	velocity scale in the inner region
γ_o	Eulers constant, $\gamma_o = 0.5772156649\ldots$
Δ_i	dimensionless inner region length scale, see equation (3.43)
Δ_o	dimensionless outer length scale, see equations (3.25), (5.40)
δ	boundary-layer thickness (dimensionless)
δ^*	kinetic displacement thickness defined in equation (5.8)
δ_c^*	displacement thickness
δ_t	thickness of thermal boundary layer
ϵ	dimensionless eddy-viscosity function
ϵ_a	dimensionless eddy-conductivity function, see equation (6.38)
ϵ_H	dimensionless eddy-conductivity function
ζ	intermediate matching variable defined in equation (3.80)
ζ_x^+	scaled streamwise vorticity

η	scaled normal coordinate in the outer region
η_1	parameter defined in equations (5.27) and (5.31)
η_m	parameter defined in equations (5.27) and (5.31)
η_θ	scaled outer coordinate for thermal boundary layer
Θ	momentum thickness
Θ_1	leading order outer-region expansion function for the total enthalpy
Θ_2	leading order outer-region expansion function for the total enthalpy in adiabatic flows
θ^+	leading order inner expansion function for the total enthalpy
θ_2^+	leading order inner expansion function for the total enthalpy in adiabatic flows
$\widetilde{\theta}^+$	scaled instantaneous total enthalpy function, see equation (4.33)
κ	von Kármán constant; inverse of the slope in the logarithmic region of the velocity profile
κ_a	logarithmic function constant for adiabatic flows
κ_θ	inverse of the slope in the logarithmic region of the temperature profile
Λ_1	outer region total enthalpy scale
λ	dimensionless mean streak spacing

λ_1	inner region total enthalpy scale
λ^+	normalized wall-layer streak spacing
μ	coefficient of viscosity
μ_o	characteristic viscosity
μ_t	turbulent viscosity, see equation (2.3.9)
μ_w	viscosity at the wall
ν	kinematic viscosity
Π	velocity wake strength parameter, see equation (5.1)
Π_i	dimensionless inner length scale of thermal boundary layer
Π_o	dimensionless outer length scale of thermal boundary layer
ρ	dimensionless density
ρ_o	characteristic density
Σ_1	outer region expansion function for the Reynolds stress term
σ	Reynolds stress term, see equation (3.30)
σ_1	inner region expansion function for the Reynolds stress term
τ	shear stress
τ_l	laminar shear stress
τ_w	wall shear stress

Φ_1	outer region expansion function for ϕ
ϕ	turbulence product term, see equation (3.3.19)
ϕ_1	inner region expansion function for ϕ
ϕ_2	inner region expansion function for ϕ in adiabatic flows
ψ	streamfunction

Subscripts

aw	adiabatic wall
e	boundary-layer edge
r	recovery
ref	reference quantity
w	wall

Superscripts

$-$	time mean
$\sim$	instantaneous variable
$'$	differentiation; turbulent fluctuation
$+$	scaled inner region variable
$*$	dimensional variable

ABSTRACT

The problem of high speed two-dimensional turbulent boundary layers is considered. An asymptotic analysis of the compressible boundary-layer equations is carried out for large Reynolds numbers and mainstream Mach numbers O(1). A self-consistent two-layer asymptotic structure is described wherein the time-mean velocity and total enthalpy are logarithmic within the overlap zone but in terms of the Howarth-Dorodnitsyn variable; the proposed structure leads to a compressible law of the wall for high speed turbulent flows and expressions are obtained relating the friction coefficient and surface heat flux to the slope of the velocity and total enthalpy profiles in the fully turbulent (logarithmic) zone. Representative velocity and total enthalpy profiles are obtained for the inner region of the boundary layer through consideration of typical time-dependent motions within the wall layer. The outer layer profiles are determined from the leading order outer layer equations; simple outer region Boussinesq eddy-viscosity and eddy-conductivity turbulence models are formulated to reflect the effects of compressibility of the flow. The conditions for self-similarity in a high-speed boundary layer are examined and a set of self-similar velocity and temperature profiles are obtained for constant pressure flows to test the proposed asymptotic structure and turbulence models; these are combined with wall-layer profiles to form a set of composite profiles valid across the entire boundary layer. A direct comparison with experimental data shows good agreement over a wide range of conditions for flows with and without surface heat transfer. To complete the analysis the case of an adiabatic wall is considered and an expression for the adiabatic wall temperature is derived. It is shown that the asymptotic analysis constrains the types of turbulence closures that can be used to represent the effects of viscous dissipation. A simple algebraic model is proposed and comparisons with measured total enthalpy profile data show good agreement.

1. INTRODUCTION

1.1 Overview

The need to predict the behavior of compressible turbulent boundary layers is encountered in a wide variety of applications, such as the design of compressor blades and airfoils for supersonic vehicles. In many situations technological or cost constraints rule out a detailed experimental investigation and the need for the accurate prediction of friction and heat transfer behaviors becomes important. Over the past two decades, the development of modern computational techniques, dramatic increases in computer capability and high quality experimental measurements have been directly responsible for an increase in the reliability of incompressible turbulent boundary-layer flow predictions. This increasing success with low-speed flow problems has naturally led many investigators to consider similar approaches for the prediction of high-speed compressible flows. Unfortunately, supersonic boundary layers are considerably more complex than their subsonic counterparts, since it is necessary to account for temperature and density variations. The thermal boundary-layer solution is generally coupled to that of the velocity boundary layer and plays an important role in the determination of the skin friction and heat transfer distribution at the wall. In practice, the wall may be adiabatic or it may conduct heat energy either to (the hot wall) or from (the cold wall) the gas above. The influence of heat transfer at the wall can dramatically alter mean profile behavior in the boundary layer. A potential additional complication is that, at sufficiently high Mach numbers, density fluctuations may affect the structure of the boundary-layer turbulence.

A major obstacle in the development of compressible turbulence models is the inherent difficulty in obtaining good experimental velocity and temperature profile data. It is much more difficult to take reliable data in the high-speed environment and measurements of the temperature distribution appear to be especially challenging. Compared to the substantial data base that has been developed for subsonic flows, a relatively small base exists for velocity and temperature profiles in supersonic flow with heat transfer. Because a supersonic boundary layer is often extremely thin, accurate measurements near the wall are very difficult and hence rather rare. Established theoretical results for high-speed compressible turbulent boundary layers are also relatively scarce and many competing and controversial theories exist.

It is well known that simple algebraic turbulence models yield good predictions for attached turbulent boundary layers (see, for example, White, 1992) at low to moderate subsonic speeds. In this study consideration will be limited to simple algebraic models for transport of momentum and energy in a high-speed compressible boundary layer, as opposed to more complicated higher-order turbulence closure schemes. Examples of modern algebraic models include the Cebeci-Smith (1974), the Baldwin-Lomax (1978), and the Johnson-King (1985) models. Algebraic models normally consist of an eddy viscosity formulation in the outer portion of the boundary layer that is then typically modified to a mixing length form in the near-wall region. The term "overlap zone" denotes a region between the viscous wall layer and the effectively inviscid outer part of the boundary layer; here the velocity profile in incompressible flow is observed to be logarithmic and thereby conform to the so-called "law of the wall". The mixing

length is typically taken to be linear in the coordinate normal to the wall within the overlap zone, but is then reduced toward the wall through multiplication by a van Driest damping factor (see, for example, Cebeci and Smith, 1974); for prediction methods this produces the intense variation in the velocity profile through the wall layer that is required to complete the adjustment to the no-slip condition at the surface. This type of model has been validated reasonably well in incompressible flow and is often used, almost without modification, in prediction methods for supersonic turbulent boundary layers (see, for example, Talcott and Kumar, 1985). The implicit assumption in such approaches is that a compressible "law of the wall" exists which is similar to the incompressible form (see, for example, Viegas et al., 1985). However, the generalization of the "law of the the wall" to compressible flow has been somewhat controversial and a number of different functional forms have been proposed (for example, van Driest, 1951; Rotta, 1960; White and Christopher, 1972; Barnwell and Wahls, 1989).

Perhaps the most popular formulation for compressible boundary layers is based on the effective velocity approach of van Driest (1951), which is critically discussed by Fernholz and Finley (1980). This scheme consists of an extrapolation of a popular incompressible formulation wherein the mixing length for compressible turbulence is also assumed to be linear in physical distance from the wall within an anticipated overlap zone between the wall layer and outer region. Upon accounting for a variation in density, an incompressible form of the "law of the wall" is ultimately obtained (see, for example, Cebeci and Smith, 1974) but in terms of an "effective velocity"; the latter quantity is calculated from the actual mean streamwise velocity through a transformation involving an inverse sine function.

This has come to be known as the van Driest transformation and strictly should be expected to yield only a localized description of the velocity profile (since it is based on a specific type of mixing length model within the overlap zone). However, Maise and McDonald (1968) found that a substantial amount of compressible profile data for an adiabatic wall could be collapsed when an "effective velocity" was defined across the entire boundary layer. The van Driest transformation is used extensively in analysis of profile data and sometimes to infer values of skin friction at the surface from measured velocity profile data.

There are aspects of the van Driest transformation which could be regarded as disadvantageous. First the transformation is based on a particular turbulence model (mixing length) in the overlap zone, and although it produces a logarithmic behavior in the "effective velocity", other types of models, such as eddy viscosity, are found to produce a somewhat different functional form for the actual velocity in the overlap zone (Degani et al., 1991). This situation may be contrasted with the case of incompressible flow where all turbulence models are implicitly constructed to produce a universal logarithmic "law of the wall". A second point is that the van Driest mixing-length model is based on a local analysis within the overlap zone; therefore no information about the boundary layer as a whole can be deduced to elucidate the changes of various features with Mach number. Lastly, the inverse sine behavior in the actual velocity distribution is somewhat awkward to deal with. For these reasons a principal objective of the present study was to look for an alternative, and perhaps simpler, theoretical description of the compressible turbulent boundary layer.

It is well known (Stewartson, 1964) that the Howarth-Dorodnitsyn variable

Y is an appropriate normal coordinate in the description of compressible laminar boundary layers. This variable Y is defined in terms of an integral of the density in a direction normal to the surface and may be interpreted as a density-averaged distance from the wall. A main thrust of this study is to introduce the same variable in the description of the turbulent boundary layer and further to determine whether the mean velocity profile in the overlap zone may be conveniently represented in a form which is logarithmic in Y. It is then subsequently shown that a self-consistent asymptotic two-layer structure valid in the limit of large Reynolds number, Re, exists. To obtain velocity and temperature profiles, a simple algebraic turbulence model, which is a generalization of existing incompressible turbulence models, is formulated. The eventual test of the proposed structure carried out here is a direct comparison with experimental profile data. These comparisons strongly support the premise of universal compressible law of the wall for velocity in terms of the Howarth-Dorodnitsyn variable.

Established theoretical results are relatively scarce for the total enthalpy and temperature distributions in compressible boundary layers. In low speed subsonic flows with heat transfer, data for the static temperature distribution (Weigand, 1978) clearly displays a logarithmic behavior in the overlap zone. However, the value of the slope of the temperature profile in the overlap zone appears to vary with pressure gradient and local flow conditions, unlike that of the velocity profile. In supersonic boundary layers the total enthalpy plays a similar role to the static temperature at low speeds, but direct measurements of this quantity, particularly in the overlap zone, are relatively rare. Consequently, it is

difficult to determine the slope of the total enthalpy profile in the overlap zone from existing experimental data, or in some cases even if the total enthalpy is logarithmic there. At subsonic speeds, the turbulent heat flux terms in the energy equation are usually represented by an algebraic model, in which an "eddy conductivity" is related to the eddy viscosity through a turbulent Prandtl number. Unfortunately, turbulent Prandtl numbers are generally found not to be constant in thermal boundary-layer flows (Crawford and Kays, 1980), and often semi-empirical relations are introduced so that the turbulent Prandtl number varies with distance across the boundary layer. For high-speed compressible flow, similar modeling concepts are often employed, as well as various semi-empirical versions of the Crocco relations (Fernholz and Finley, 1980). In the present study one goal was to treat the thermal problem independent from the velocity problem and without introducing a turbulence model based explicitly on either a turbulent Prandtl number, a Reynolds analogy argument, or an empirical version of the Crocco integral. In this study a self-consistent, two-layer structure is developed for the total enthalpy distribution in the boundary layer, in which the enthalpy is logarithmic in the overlap zone in the Howarth-Dorodnitsyn variable. A formula for the slope of the total enthalpy is derived, as well as a relationship from which the surface heat transfer at the wall can be evaluated. Again, the proposed structure is tested by comparing total enthalpy directly with the existing experimental data.

One motivation of this investigation was to establish a theoretical foundation for more efficient algorithms for the prediction of high-speed compressible turbulent boundary layers. For subsonic two-dimensional boundary

layers, it is well-known that the inner wall layer exhibits a self-similar behavior (Fendell, 1972). In the embedded function methodology described by Walker, Werle and Ece (1991), this self-similar wall-layer structure is incorporated in a prediction method by representing the mean velocity and total enthalpy distributions by analytical profiles across the entire wall layer; the profile models are derived through consideration of the coherent structure and dynamics of the near-wall flow (Walker et al., 1989; Smith et al., 1991). In the algorithm a conventional numerical solution is matched systematically to embedded wall-layer functions, and Walker et al. (1991) demonstrate that up to a 50% reduction in total mesh points (as well as computational effort) can be achieved with no degradation in accuracy, as compared to a conventional scheme that computes the flow all the way to the wall.

Because the embedded-function approach involves the smooth joining of an exterior numerical solution to a set of embedded functionals which are logarithmic near the surface, the numerical algorithms involved are not straightforward. A crucial step in the methodology is the determination of the appropriate asymptotic scaling laws for the velocity and total enthalpy in the overlap zone. This is carried out in the present study through the development of asymptotic expansions, which describe the structure of the solution of the compressible boundary-layer equations for large Reynolds number. The analysis is based on the Howarth-Dorodnitsyn variable Y which implicitly incorporates the influence of mean density variations across the boundary layer. As a test of the asymptotic results, as well as the new turbulence models, a limiting case is considered corresponding to self-similar profiles that evolve in a constant pressure flow; in this situation, the governing

equations in the outer region of the boundary layer reduce to ordinary differential equations, for which both exact analytic solutions and accurate numerical solutions may be found.

1.2 Governing Equations

The governing equations of interest in this study describe the transport of momentum and thermal energy in either a two-dimensional or axisymmetric compressible turbulent boundary layer. The general assumptions that are applied throughout are:

1) the velocity components and total enthalpy may be written as a sum of a conventional time-mean term and a fluctuating component;
2) the influence of density fluctuations is negligible;
3) the fluid properties such as viscosity μ and conductivity k are functions of temperature alone;
4) the effects of normal pressure gradients due to curvature are negligible.

The basic coordinate system used in the present study is depicted in Figure 1.1. An orthogonal coordinated system (s^*,n^*) is selected, measuring distance along the contour and normal to the wall respectively; the corresponding time-mean velocity components are u^* and v^*, with instantaneous components being $u^{*\prime}$ and $v^{*\prime}$. Here and throughout this study, an asterisk superscript denotes a dimensional quantity. The mean total enthalpy H^* is defined in terms of u^* and the mean static temperature T^* by

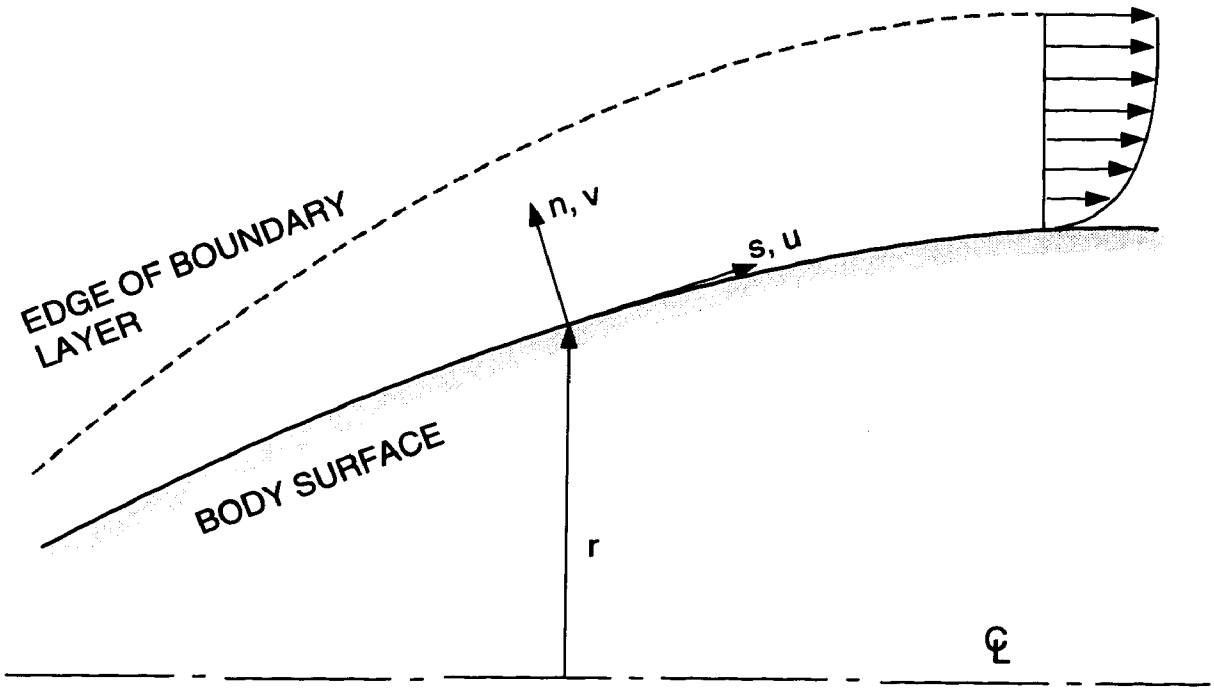

Figure 1.1. Boundary-layer coordinate system for an axisymmetric body

$$H^* = c_p^* T^* + \frac{1}{2} u^{*2} \ , \tag{1.1}$$

where c_p^* is the specific heat at constant pressure and is assumed to be constant.

The turbulent boundary-layer equations describing compressible nominally steady flow in dimensional form are (Cebeci and Smith, 1974):

continuity

$$\frac{\partial}{\partial s^*}(r^* \rho^* u^*) + \frac{\partial}{\partial n^*}(r^* \overline{\rho^* v^*}) = 0 \ ; \tag{1.2}$$

streamwise momentum

$$\rho^* u^* \frac{\partial u^*}{\partial s^*} + \overline{\rho^* v^*} \frac{\partial u^*}{\partial n^*} = -\frac{\mathrm{d}p_e^*}{\mathrm{d}s^*} + \frac{\partial}{\partial n^*}\left[\mu^* \frac{\partial u^*}{\partial n^*} - \rho^* \overline{u^{*\prime} v^{*\prime}}\right] ; \tag{1.3}$$

energy equation (written in terms of static temperature)

$$\rho^* u^* c_p^* \frac{\partial T^*}{\partial s^*} + \overline{\rho^* v^*} c_p^* \frac{\partial T^*}{\partial n^*} = u^* \frac{\mathrm{d}p_e^*}{\mathrm{d}s^*} + \frac{\partial}{\partial n^*}\left[k^* \frac{\partial T^*}{\partial n^*} - \rho^* \overline{v^{*\prime} T^{*\prime}}\right]$$

$$+ \left(\mu^* \frac{\partial u^*}{\partial n^*} - \rho^* \overline{u^{*\prime} v^{*\prime}}\right) \frac{\partial u^*}{\partial n^*} \ ; \tag{1.4}$$

or in terms of total enthalpy,

$$\rho^* u^* \frac{\partial H^*}{\partial s^*} + \overline{\rho^* v^*} \frac{\partial H^*}{\partial n^*} = \frac{\partial}{\partial n^*}\left[\frac{k^*}{c_p^*} \frac{\partial H^*}{\partial n^*} + u^*\left(1 - \frac{1}{P_r}\right) \mu^* \frac{\partial u^*}{\partial n^*} - \rho^* \overline{v^{*\prime} H^{*\prime}}\right] . \tag{1.5}$$

Here ρ^*, μ^* and p_e^* denote the dimensional time-mean density, absolute viscosity and mainstream pressure respectively and $\overline{\rho^* v^*}$ denotes a time-average of the

density/normal velocity product. $r^* = r^*(s^*)$ is the dimensionless radius of revolution for an axisymmetric body. The primes denote instantaneous fluctuations about the mean values and the overbar indicates a long time average.

In the derivation of equations. (1.2) through (1.5) it has been assumed that density fluctuations are not significant to the leading order; this assumption is sometimes known as the Morkovin's hypothesis and is discussed in §1.3. In the above equations, the principal unknowns are u^*, v^*, ρ^* and H^*; the viscosity μ^* and conductivity k^* are properties of the fluid which taken to vary only with temperature T^*. To complete the system, an equation of state is required and in this study a calorically perfect gas is assumed so that,

$$p_e^* = R\rho^* T^* \ , \tag{1.6}$$

thereby relating the density and static temperature across the boundary layer to the mainstream pressure $p_e^*(s^*)$; here R is the gas constant. Another quantity of interest is the ratio of the specific heats defined as $\gamma = c_p^*/c_v^*$; for practical purposes γ can be considered as virtually invariant for the diatomic gases of interest here (air, nitrogen) and for helium (which is found not diatomic recently). For a pure, nonreacting gas, the viscosity coefficient is dependent only on temperature and at moderate temperatures may be calculated from the Sutherland relation

$$\frac{\mu^*}{\mu_w^*} = \left(\frac{T^*}{T_w^*}\right)^{3/2} \left(\frac{T_w^* + \mathrm{S}^*}{T^* + \mathrm{S}^*}\right), \tag{1.7}$$

where S^* has the value 110K for air.

The effects of normal pressure gradients due to curvature effects are

assumed negligible. The n^* – momentum equation implies that at a given s^* station, the pressure is invariant across the boundary layer and $p^* = p_e^*(s^*)$. The boundary conditions for the system (1.2) through equation (1.5) are

$$u^* = v^* = 0, \quad T^* = T_w^*(s^*), \text{ and } H^* = H_w^*(s^*) \text{ at } n^* = 0$$

and (1.8)

$$u^* \to U_e^*(s^*), \quad T^* \to T_e^*(s^*), \quad \text{and} \quad H^* \to H_e^* \quad \text{as} \quad n^* \to \infty.$$

Here and throughout this study, the subscripts w and e are used to denote quantities evaluated at the wall and boundary-layer edge respectively. The limiting behavior of the turbulence correlations is also known. At the outer edge of the boundary layer, the turbulence terms must vanish and

$$\rho^*\overline{u^{*\prime}v^{*\prime}}, \quad \rho^*\overline{v^{*\prime}T^{*\prime}}, \quad \rho^*\overline{v^{*\prime}H^{*\prime}} \to 0 \text{ as } n^* \to \infty. \tag{1.9}$$

Near the wall Reichardt (1951) has shown that $\overline{u^{*\prime}v^{*\prime}}$ behaves as a cubic function of n^* and using similar arguments, it is easily demonstrated that

$$\rho^*\overline{u^{*\prime}v^{*\prime}}, \quad \rho^*\overline{v^{*\prime}T^{*\prime}}, \quad \rho^*\overline{v^{*\prime}H^{*\prime}} = O(n^{*3}) \text{ as } n^* \to 0. \tag{1.10}$$

The governing equations may be cast in dimensionless form using a reference length L_{ref}^* , velocity U_{ref}^*, viscosity μ_{ref}^* and density ρ_{ref}^*; in addition T^* and H^* are made dimensionless with respect to a reference temperature T_{ref}^* and $c_p^*\, T_{ref}^*$ respectively. The dimensionless total enthalpy is therefore given by

$$H = T + \frac{\gamma - 1}{2} M_{ref}^2 \, u^2, \tag{1.11}$$

where the reference Mach number is defined by

$$M_{ref}^2 = \frac{{U_{ref}^*}^2}{\gamma R T_{ref}^*} \, . \tag{1.12}$$

Lastly, the pressure is made dimensionless with respect to $\rho_{ref}^* {U_{ref}^*}^2$. The boundary- layer equations (1.2) through (1.6) become:

$$\frac{\partial}{\partial s}(r\rho u) + \frac{\partial}{\partial n}(r\overline{\rho v}) = 0 \; ; \tag{1.13}$$

$$\rho u \frac{\partial u}{\partial s} + \overline{\rho v} \frac{\partial u}{\partial n} = -\frac{\mathrm{d}p_e}{\mathrm{d}s} + \frac{\partial}{\partial n}\left(\frac{\mu}{Re}\frac{\partial u}{\partial n} - \rho\overline{u'v'}\right); \tag{1.14}$$

$$\rho u \frac{\partial T}{\partial s} + \overline{\rho v}\frac{\partial T}{\partial n} = (\gamma - 1) M_{ref}^2 u \, \frac{\mathrm{d}p_e}{\mathrm{d}s} + \frac{\partial}{\partial n}\left(\frac{\mu}{PrRe}\frac{\partial T}{\partial n} - \rho\overline{v'T'}\right)$$

$$+ (\gamma - 1) M_{ref}^2 \left(\frac{\mu}{Re}\frac{\partial u}{\partial n} - \rho\overline{u'v'}\right)\frac{\partial u}{\partial n} \; ; \tag{1.15}$$

$$\rho u \, \frac{\partial H}{\partial s} + \overline{\rho v} \, \frac{\partial H}{\partial n} = \frac{\partial}{\partial n}\left(\frac{\mu}{PrRe}\frac{\partial H}{\partial n} + (\gamma - 1)\mathrm{M}_{ref}^2 \frac{\mu}{Re}\left(1 - \frac{1}{P_r}\right)u\frac{\partial u}{\partial n} - \rho\overline{v'H'}\right), \tag{1.16}$$

where the fact that r = r(s) in the boundary layer (to leading order) has been used. For two-dimensional plane flow r is set to be unity for convenience. The dimensionless form of the equation of state is

$$p_e = \frac{\rho T}{\gamma M_{ref}^2} \,. \tag{1.17}$$

and the boundary conditions are

$$u = v = 0, \qquad T = T_w(s), \qquad H = H_w(s) \,, \qquad \text{at} \;\; n = 0 \,, \tag{1.18}$$

$$u \to u_e(s) \,, \qquad T \to T_e(s) \,, \qquad H \to H_e \qquad \text{as} \;\; n \to \infty \tag{1.19}$$

and

$$\rho\overline{u'v'}, \quad \rho\overline{v'T'}, \quad \rho\overline{v'H'} = O(n^3), \qquad \text{as } n \to 0 \,, \tag{1.20}$$

$$\rho\overline{u'v'}, \quad \rho\overline{v'T'}, \quad \rho\overline{v'H'} \to 0, \qquad \text{as } n \to \infty. \tag{1.21}$$

Two important dimensionless parameters appear in these equations

$$Re = \frac{\rho^*_{ref} u^*_{ref} L^*_{ref}}{\mu^*_{ref}} \,, \qquad Pr = \frac{\mu^* c^*_p}{k^*} \,, \tag{1.22}$$

namely the reference Reynolds number and Prandtl number, respectively. Although both μ^* and k^* vary with temperature, the Prandtl number can generally be assumed constant in the temperature ranges of practical interest.

The boundary-layer equations given here apply to compressible flow and are equally applicable to subsonic and supersonic flows. In principle, they also apply to hypersonic flows. Although it is difficult to draw a distinction between the "supersonic" and the "hypersonic" regime on the basis of Mach number alone. It is expected that at sufficiently high Mach number, density fluctuations and fluctuations in the transport properties such as μ and κ (which depend upon T) may have to be taken into consideration. In addition, viscous dissipation within

the boundary layer gives rise to high temperatures which in turn promotes chemical reactions such as ionization and dissociation. Such cases might be classified as truly hypersonic and here the system of equations given by equations (1.13) to (1.17) is not complete; diffusion of chemical species, energy changes due to chemical reactions and a more realistic equation of state must then be considered.

1.3 Morkovin's Hypothesis

In writing down equations (1.2) to (1.5), it has implicitly been assumed that density fluctuations are not significant to leading order, and this assumption will be discussed briefly here, following Fernholz and Finley (1980). Denoting dimensionless instantaneous quantities by a tilde, the instantaneous total enthalpy is given by

$$\tilde{H} = \tilde{T} + \frac{(\gamma-1)}{2} M_{ref}^2 (\tilde{u}^2 + \tilde{v}^2 + \tilde{w}^2). \tag{1.23}$$

Upon writing each quantity as a sum of mean and fluctuating quantities (i.e. $\tilde{H} = H + H'$), it can be shown that

$$\frac{H'}{H} = \left(\frac{T'}{T} + (\gamma-1) M^2 \frac{u'}{u} \right) \left(1 + \frac{\gamma-1}{2} M^2\right)^{-1} \tag{1.24}$$

where $M^2 = u^2 M_{ref}^2 / T$ denotes a local Mach number; in obtaining equation (1.24), it has been assumed that second order quantities such as $u'^2 - \overline{u'^2}$ are negligible. Since H represents the total energy of the flow, it is reasonable to expect for adiabatic walls that the left side of equation (1.24) is at least an order of magnitude

smaller than the fluctuating terms on the right side. This assumption is the so-called "strong Reynolds analogy" (Morkovin, 1960) and is supported by experiments, at least for boundary layers with adiabatic walls (Kistler, 1959); for situations with strong heat transfer at the wall, the assumption may be questionable. In any event, for either an adiabatic wall or for moderate heat transfer at the wall, it follows from equation (1.24) that

$$\frac{T'}{\overline{T}} \approx -(\gamma-1)M^2\,\frac{u'}{u} \tag{1.25}$$

A relationship between the fluctuating temperature, pressure, and density may be obtained from the equation of state $P = \rho T/(\gamma M_{ref}^2)$ (cf. equation (1.17)). Assuming that $\rho T \ll \overline{\rho' T'}$, it is easily shown that

$$\frac{T'}{\overline{T}} \approx -\frac{\rho'}{\overline{\rho}} + \frac{p'}{\overline{p}} \tag{1.26}$$

Measurements by Kistler (1959) indicated that p'/p is small and combining equations (1.25) and (1.26) leads to

$$\frac{T'}{\overline{T}} \approx -\frac{\rho'}{\overline{\rho}} \approx -(\gamma-1)M^2\,\frac{u'}{u} \tag{1.27}$$

This relation was obtained by Morkovin (1960) who argued that if $(\gamma-1)M^2$ is not large, density fluctuations are small compared to the mean density ρ and that turbulence structure should not be influenced by compressibility effects. Here the term "turbulence structure" is used to denote relationships between the statistical properties of turbulence (Bradshaw and Ferris, 1971). The premise that

compressibility effects do not affect turbulence structure is evidently partially based in empirical measurements and is known as Morkovin's hypothesis. Experiments suggest that, for example, $< T' > /T$ is less than 0.1 and $< H' > /H$ is less than 0.05 throughout the boundary layer for Mach numbers up to 5; here the symbol $<\ >$ stands for the rms fluctuation.

As discussed by Cebeci and Smith (1974), the compressible equations of motion are most appropriately written in terms of mass-weighted or Favre variables; for the streamwise velocity, the Favre variable is

$$\overline{u} = \frac{\overline{\rho u}}{\overline{\rho}} \tag{1.28}$$

Using relations (1.27), it can be shown for $\rho'/\overline{\rho} \ll 1$ and in a boundary layer (Bradshaw and Ferriss, 1971; Cebeci and Smith, 1974) that the governing equations can be written in terms of conventional time-averaged quantities utilized in equations (1.2) through (1.5).

It is worthwhile to bear in mind that the Morkovin hypothesis is rooted strongly in empiricism and may be expected to become invalid at some stage with increasing Mach number. Measurements in a hypersonic boundary layer at $M_e = 9.4$ over a cooled wall by Laderman and Demetriades (1974) have shown values of p'/p approaching 0.15 and, furthermore, a large departure from Morkovin's "strong Reynolds analogy" was found, i.e.

$$\frac{T'}{\overline{T}} \neq -(\gamma - 1)M^2 \frac{u'}{\overline{u}}\,, \tag{1.29}$$

even though $< \rho'/\rho >$ was always smaller than 0.1. In this case, the strong heat transfer in this flow may possibly be responsible for the departure from the Morkovin hypothesis.

1.4 Discussion of the Problem

The problem to be addressed here is the development of prediction techniques for the behavior of velocity and temperature profiles in two-dimensional compressible turbulent boundary-layer flows. Interest will be confined to flows with Prandtl number O(1) in the supersonic to hypersonic regime which are free from shock-boundary layer interactions and flow separation. Throughout the analysis, a rational theoretical approach is emphasized using singular perturbation methods to derive leading order expressions for the governing equations in each region of the flow.

A principal motivation of the present study was to develop the foundation for embedded-function methods for high-speed compressible turbulent flows. In conventional schemes, a large number of mesh points are required in order to resolve the intense variations in the velocity and temperature distributions that occur in the near-wall region. Such grids put a severe strain on computer resources and for approaches based on the full Navier-Stokes equations, the relatively small grid sizes near the surface can give rise to stability problems in the numerical algorithm. In an attached two-dimensional incompressible turbulent flow, the wall layer exhibits an essentially universal and similar behavior; thus, to a large extent, expending a major portion of the computation on a known (and unexceptional) wall-layer solution seems wasteful. For a three-dimensional flow, the problems

associated with using a refined mesh in the wall layer are even more acute; however, recent asymptotic analyses (Degani, Smith and Walker, 1992, 1993) are strongly suggestive that a generic wall-layer structure also exists in this case. Consequently, there has been an increasing interest in wall-function methods (Viegas et al., 1985) wherein the composite structure of the turbulent boundary layer is exploited. In such schemes, velocity and temperature profiles are computed in the outer part of the boundary layer and then systematically joined to some form of the "law of the wall" near the surface. This procedure obviates the need for a densely packed mesh near the surface, and, in principle, is much more efficient.

A necessary step in the development of the embedded function method for compressible flows is to determine the asymptotic structure of the boundary layer in the limit of large Reynolds number. Such analyses for incompressible flow have been considered by Yajnik (1970), Fendell (1972) and Mellor (1972), who were able to establish the nature and leading-order Reynolds number dependence of the scales in each region of the boundary layer, as well as the leading order equations for the velocity components and the Reynolds stress. The results of the asymptotic analyses are consistent with most of classical behavior observed in experimental measurements, but it must be recognized that these analyses do not resolve the closure problem. In order to make progress with closure, it is necessary to either guess the functional form of the unknown turbulence terms or to model them through consideration of representative time-dependent motions within the boundary layer. The latter approach has been adopted for incompressible flow in the wall layer by Walker et al. (1989) (see also, Walker, 1990a, 1990b) and for

weakly compressible flow by Weigand (1978). A similar approach will be taken here to model the wall-layer profile for total enthalpy and velocity in a compressible boundary layer.

1.5 General Objectives

The basic objectives of this study are summarized in the following points:

1) A first objective is to isolate the simplest possible self-consistent two-dimensional asymptotic structure for compressible turbulent boundary layers, which is valid for large Reynolds number. The relevant scaling laws have been controversial and here a number of approaches will be considered, with the most appropriate being verified through direct comparison with experimental data. One controversial issue concerns the nature of the functional form of the tangential mean velocity in the overlap zone near the surface and whether it is logarithmic in the physical variable y. Here, the possibility of a "compressible law of the wall" in which the mean velocity u is logarithmic, but in terms of the Howarth-Dorodnitsyn variable Y, will be considered in depth.

2) A second objective is to develop a theory for the total enthalpy equation, which is independent from any type of Reynolds analogy argument or semi-empirical version of the Crocco integral. A self-consistent structure will be proposed for the total enthalpy distribution in the boundary layer which is logarithmic in Y within the overlap zone; a formula for the slope of the total enthalpy there will be derived through asymptotic analysis, as well as a

relationship to evaluate the total heat transfer at the wall;

3) A third objective is to formulate relatively simple algebraic models for the outer layer, which account for the significant density variations that can occur in supersonic boundary layers.

4) A fourth objective is to determine the conditions necessary for the existence of self-similar velocity and temperature profiles and to develop a uniformly valid set of such profiles. Direct comparison will then be made with measured experimental data in order to validate the results of the asymptotic analysis, as well as the turbulence models. Since a substantial portion of available data has been taken in constant pressure conditions, this study will focus on these types of flows. However, the problem of pressure gradient flows will also be addressed.

The plan of the thesis is as follows. A literature review for high-speed compressible flow is presented in §2. In §3 the general asymptotic structure of the high-speed compressible turbulent boundary layer is addressed. In §4 a turbulence model is developed for the wall layer. In §5 simple outer region algebraic turbulence models are formulated to reflect the effects of compressibility. To test the proposed asymptotic structure and turbulence models, a set of self-similar outer region profiles for velocity and total enthalpy is obtained for constant pressure flow; these are combined with wall-layer profiles to form a set composite profiles valid across the entire boundary layer. Direct comparisons with experimental data are carried out in a wide range of Mach number and heat transfer rates. Lastly, the

influence of viscous dissipation and an appropriate turbulence model is taken up in §6 Conclusions and a Summary are given in §7.

2 LITERATURE REVIEW

2.1 Introduction

Accurate prediction of turbulent flows near surfaces is currently inhibited by two basic problems, one of which is primarily computational, while the other is associated with the uncertainty of how well a given turbulence model actually represents a particular flow environment. The first problem is related to the necessity of resolving the large velocity and enthalpy gradients typically encountered in the vicinity of a solid surface in the near-wall region; these gradients are always substantially larger in the near-wall region than in a laminar flow and, hence, the computational grid must be relatively small there in order to accurately determine skin friction and surface heat transfer. The second problem is more complex and is associated with questions of validity of the turbulence model. For incompressible two-dimensional boundary layers, the existence of a large experimental data base has led to the development of reasonably reliable semi-empirical turbulence models. However, more complex effects, such as property variations and three-dimensionality, are considerably more difficult to predict, partially because the data base is not as extensive and, in addition, two-dimensional incompressible models often do not extrapolate in an obvious way. Previous efforts in the modeling of compressible turbulent boundary layers will be reviewed in this section. Since most approaches have been carried out by attempting to extend established incompressible results to the compressible case, the behavior of incompressible turbulent boundary layers will be considered briefly first.

2.2 Incompressible Turbulent Boundary Layers

All present turbulent flow analyses are semi-empirical in nature, and considerable success has been achieved over the years in developing theoretical results and prediction methods for incompressible boundary layers. The reason is that empirically-motivated concepts as "eddy viscosity", "law of the wall", and "law of the wake" were found to have a wide range validity for two-dimensional boundary layers, and this has permitted the development of a class of reasonably good models. A common feature of turbulent boundary-layer and internal flows is that, in normal circumstances, the mean flow field is found to be double-structured, consisting of an outer inviscid defect region and a relatively thin inner wall layer adjacent to the surface. In the wall layer, the effects of viscosity are important to leading order, and here the flow is relatively insensitive to the conditions remote from the wall as well as upstream. Consider a boundary layer of thickness δ with a free-stream velocity U_e, with n measuring normal distance from the surface. Empirical observations suggest that for small enough n/δ, the flow should not depend directly on δ or U_e; rather a direct dependence on the distance n from the surface, the shear stress τ_w, and the fluid properties ρ and μ should be anticipated, viz.

$$u = g(\tau_w, \rho, \mu, n). \tag{2.1}$$

For a constant property flow, a velocity scale (called the friction velocity) may be defined by $u_\tau = \sqrt{\tau_w/\rho}$. Consequently, ν/u_τ has the dimension of length, and dimensional analysis suggests a functional relationship of the form

$$\frac{u}{u_\tau} = f\left(\frac{u_\tau n}{\nu}\right), \tag{2.2}$$

for the velocity within the wall layer. Empirical observations reveal that at the outer edge of the wall layer, f is logarithmic and this relationship is usually described as the "law of the wall".

The outer layer is usually referred to as the wake region; here the instantaneous flow is observed to be dominated by vortex motion and is effectively inviscid. Thus, the mean outer velocity is expected to be independent of viscosity and to depend only upon the wall shear stress τ_w and the distances n and δ. The effect of upstream history is not usually accounted for explicitly but is implicit since in a boundary layer having a streamwise pressure gradient, the profile shape at any station s depends in a complicated way on the upstream boundary-layer development. For the outer layer, the velocity is measured as a difference from the free-stream value U_e since the wall layer (where a substantial velocity difference does occur) is not accounted for as yet; consequently a functional relation of the form

$$U_e - u = f(\tau_w, \rho, n, \delta, \mathrm{d}p_e/\mathrm{d}s) \tag{2.3}$$

is proposed and dimensional analysis yields the relation

$$\frac{U_e - u}{u_\tau} = F\left(\frac{n}{\delta}, \frac{\delta}{\tau_w}\frac{\mathrm{d}p_e}{\mathrm{d}s}\right), \tag{2.4}$$

where F is an arbitrary function. This relationship is called the velocity-defect law, with $(U_e - u)$ being the "defect" or retardation of the flow due to effects near

the wall. The parameter involving the pressure gradient is characteristic of the mean flow in the outer layer, and in a set of classic papers, Clauser (1954, 1956) developed the concept of specific situations which he termed equilibrium turbulent flows. Clauser replaced the ill-defined boundary-layer thickness δ by the rigorously defined displacement thickness and introduced an equilibrium pressure gradient parameter by

$$\beta = \frac{\delta^*}{\tau_w} \frac{\mathrm{d}p_e}{\mathrm{d}s} . \tag{2.5}$$

After considerable experimental effort, Clauser (1954, 1956) showed clearly that a boundary layer with variable $p_e(s)$, but constant β, is in turbulent equilibrium in the sense that all the gross properties of the boundary layer can be scaled with a single parameter called the defect thickness $\Delta_0 = U_e \delta^* / u_\tau$. A zero-pressure-gradient flow is a special case of an equilibrium boundary layer. It has been found empirically that for such a flow, the function F is independent of Reynolds number (except in boundary layers at rather low Reynolds numbers) and, significantly, independent of surface roughness. These special situations may also be referred to as self-similar turbulent boundary layers.

Between the inner and outer layers there is a "region of common validity", usually referred to as the overlap region. A variety of arguments (see, for example, White, 1992 and Bradshaw, 1984) suggest a logarithmic behavior for the mean streamwise velocity profile in the overlap region, according to

$$\frac{u}{u_\tau} = \frac{1}{\kappa} \log \frac{u_\tau n}{\nu} + C_i , \tag{2.6}$$

in inner variables and

$$\frac{u-U_e}{u_\tau} = \frac{1}{\kappa} \log \frac{n}{\delta} + C_o \ , \tag{2.7}$$

in terms of outer variables. Here, the von Karman constant κ and C_i are found to be near-universal constants for turbulent flow past smooth impermeable walls, having values of about 0.41 and 5.1 respectively; on the other hand, the outer logarithmic function constant C_o varies with the pressure gradient parameter β, as well as with streamwise distances. The validity of the law of the wall (given in equation (2.6)) is strongly supported by experimental data, but should be primarily regarded as an empirical law.

In order to close the equations governing the mean flow and temperature field, it has traditionally been assumed that there exists some unknown functional relation between the $\rho\overline{u'v'}$ ($\rho\overline{v'T'}$) product and the mean velocity (temperature) field. This view is adopted throughout this study; however, it must always be recognized that no general such functional relationship has ever been shown to exist and for the present any such hypothesis must be regarded as no more than a useful approximation. The main reasons for adopting such models for boundary layer flows are (1) their simplicity and (2) the relatively high degree of success that this type of model has enjoyed in prediction methods.

Boussinesq (1877) suggested a model for the Reynolds stress $\overline{u'v'}$ based on an analogy with the coefficient of viscosity μ in Stokes' law for laminar flow and the eddy viscosity function ϵ was defined according to

$$-\rho\overline{v'u'} = \rho\epsilon\frac{\partial u}{\partial n} . \tag{2.8}$$

It should be noted that ϵ has no physical relation to the fluid properties. A criticism often leveled at the Boussinesq-type approximations is that they lack generality and depend only on the local flow parameters. A wide variety of much more complicated closure schemes have been proposed over the years (see, for example, White, 1992). However, it is not clear whether the increasing variety of these much more involved higher-order closure schemes offers any significant advantage in connection with predicting turbulent boundary-layer flows.

Prandtl (1925) formulated the mixing-length hypothesis in an attempt to improve Boussinesq's eddy-viscosity hypothesis. Using an intuitive argument, Prandtl hypothesized that turbulent transport is analogous (but on a much larger scale) to molecular transport which has traditionally been modeled by kinetic theory. In the mixing-length model, the Reynolds stress is represented by,

$$-\rho\overline{u'v'} = \rho l^2 \mid \frac{\partial u}{\partial n} \mid \frac{\partial u}{\partial n} , \tag{2.9}$$

where l is the mixing-length function which is to be modeled. In the kinetic theory of gases, l is the mean free path; however l is not as clearly defined for the mixing-length hypothesis and only represents some local characteristic length within the turbulence.

When there is a temperature difference between the wall and the mainstream, heat transfer occurs in incompressible flow. The list of independent variables for the temperature profile will again exhibit a dependence on n, τ_w, ρ and μ because

the temperature field for a forced convective flow is mainly governed by the character of the velocity field; in addition, the assumptions used to model the turbulence in the velocity field are usually carried over to the heat transfer problem for situations when the Prandtl number Pr is O(1). Since the velocity field depends on the rate of transfer of momentum toward the surface, τ_w, the temperature field may be expected to depend, analogously, on the rate of heat transfer from the surface to the flow, q_w. A total flux of heat q may be defined by

$$q = -\frac{\mu}{PrRe}\frac{\partial T}{\partial n} + \rho\overline{v'T'}, \tag{2.10}$$

where $q = q^*/\rho^*_{ref}u^*_{ref}c^*_p T^*_{ref}$ because the thermal wall layer is thin, a generally accepted approximation is that the heat flux at any height is constant and equal to the wall value; thus, from equation (2.10)

$$q_w = -\frac{\mu}{PrRe}\frac{\partial T}{\partial n} + \rho\overline{v'T'}, \qquad q_w = q|_{n=0}. \tag{2.11}$$

Denoting the thickness of the thermal boundary layer by δ_t, it may be expected that the temperature profile does not depend on δ_t in the inner region where $n^* \ll \delta_t$. Thus, the form of equation (2.11) suggests that mean temperature in the inner region is a function of n, q_w, τ_w, ρ, μ, Pr and $T_w - T$; using dimensional analysis. Squire (1951) showed that in the inner region

$$\frac{T_w - T}{q_\tau} = f_t\left(\frac{u_\tau n}{\nu}, Pr\right), \tag{2.12}$$

where q_τ is the so-called heat flux temperature defined by

$$q_\tau = \frac{q_w}{\rho u_\tau} \tag{2.13}$$

and f_t is an arbitrary function, whose behavior has usually been guessed or developed from semi-theoretical considerations.

For flow at large Reynolds number, the outer region of the boundary layer is essentially a rotational inviscid flow, and here the turbulent transport of thermal energy is expected to be considerably larger than conduction; thus, far away from the wall it is generally assumed that the mean temperature is independent of molecular properties. This assumption is often referred to as the Reynolds and Peclet number similarity principle (the Peclet number is defined as $Pe = RePr$). This principle indicates that the mean temperature in the outer layer (analogous to the mean velocity) should be in the form of a defect law

$$\frac{T - T_e}{q_\tau} = F_t\left(\frac{n}{\delta_t}\right). \tag{2.14}$$

Experimental data suggests a region of common validity with a logarithmic variation for the normalized temperature difference in the overlap region

$$\frac{T_w - T}{q_\tau} \sim \frac{1}{\kappa_\theta} \log \frac{u_\tau n}{\nu} + B_i \tag{2.15}$$

in inner variables and

$$\frac{T - T_e}{q_\tau} \sim \frac{1}{\kappa_\theta} \log \frac{n}{\delta_t} + B_o \tag{2.16}$$

in outer variables. Here κ_θ plays the role of the von Karman constant in the velocity distribution, but κ_θ is not constant in general and depends on local flow conditions (Weigand, 1978). A detailed description of the general behavior of the temperature profile in each of these flow regions can be found in the thesis of Weigand (1978).

For compressible turbulent boundary layer flows, the composite double layer structure found in incompressible boundary-layer flows should also apply for variable-property flows at least over a range of Mach numbers, provided that the local mean density and other temperature dependent quantities are used in differential equations or algebraic formulae relating turbulence terms to the mean velocity and temperature fields. There have been many attempts, both analytical and empirical to describe the mean velocity, temperature, as well as turbulence field distributions in compressible turbulent boundary layers. The most popular and commonly used approaches are reviewed next.

2.3 The Crocco-Walz Relation

In a compressible flow, the velocity and temperature problems are coupled, and it is not possible to determine the mean velocity profile without knowing how the temperature and density vary across the boundary layer (and vice versa). Over the years many authors have sought to develop exact or semi-empirical solutions yielding relationships between the mean static enthalpy h (or the mean static temperature T) and the mean velocity u; in these relationships, the Mach number, specific heat ratio, and some type of heat transfer quantity appear as parameters. In this section, the approach developed first by van Driest (1954, 1956) and

subsequently by Walz (1959) will be outlined. The end result is a semi-empirical temperature/velocity relationship. It is convenient to introduce Crocco variables in which $\xi = s$ and $u = u(s,n)$ are utilized as independent variables while the laminar shear term

$$\tau_l = \frac{\mu}{Re}\frac{\partial u}{\partial n} \tag{2.17}$$

is used as the dependent variable; note that τ_l has been made dimensionless with respect to $\rho_{ref}U_{ref}^2$. The derivatives transform according to

$$\frac{\partial}{\partial s} = \frac{\partial}{\partial \xi} + \frac{\partial u}{\partial s}\frac{\partial}{\partial u}, \quad \frac{\partial}{\partial n} = \frac{\partial u}{\partial n}\frac{\partial}{\partial u}. \tag{2.18}$$

By using the first of equations (2.18) to differentiate n, it can be shown that

$$\frac{\partial u}{\partial s} = -\frac{\partial u}{\partial n}\frac{\partial n}{\partial \xi}\bigg|_u, \tag{2.19}$$

and in equations (2.18) and (2.19) $\partial u/\partial n$ may be related to τ_l through equation (2.17). However, it is convenient to leave the transformed derivatives in the form (2.18) on the understanding that $\partial u/\partial n$ and $\partial u/\partial s$ are given by equations (2.17) and (2.19). Substitution in the momentum equation (1.14) and energy equation gives

$$\rho u\frac{\partial u}{\partial s} + \overline{\rho v}\frac{\partial u}{\partial n} = -\frac{\mathrm{d}p_e}{\mathrm{d}\xi} + \frac{\partial u}{\partial n}\frac{\partial}{\partial u}\left(\tau_l - \rho\overline{u'v'}\right) \tag{2.20}$$

and

$$\rho u\frac{\partial T}{\partial \xi} + \left(\rho u\frac{\partial u}{\partial s} + \overline{\rho v}\frac{\partial u}{\partial n}\right)\frac{\partial T}{\partial u} = (\gamma - 1)\,M_{ref}^2\,u\frac{\mathrm{d}p_e}{\mathrm{d}\xi} + \frac{\partial u}{\partial n}\frac{\partial}{\partial u}$$

$$\left(-\rho\overline{u'v'} + \frac{\mu}{Re}\frac{\partial u}{\partial n}\right) + (\gamma - 1)M_{ref}^2\left(-\rho\overline{v'T'} + \frac{\mu}{PrRe}\frac{\partial u}{\partial n}\frac{\partial T}{\partial u}\right)\frac{\partial u}{\partial n}. \tag{2.21}$$

Elimination of $\overline{\rho v}$ using equation (2.20) leads to the following form of the energy equation:

$$\rho u\frac{\partial T}{\partial \xi}+\left\{-\frac{\mathrm{d}p_e}{\mathrm{d}\xi}+\frac{\partial u}{\partial n}\frac{\partial}{\partial u}\left(-\rho\overline{u'v'}+\tau_l\right)\right\}\frac{\partial T}{\partial u}=(\gamma-1)\,M_{ref}^2\,u\frac{\mathrm{d}p_e}{\mathrm{d}\xi}$$

$$+\frac{\partial u}{\partial n}\frac{\partial}{\partial u}\left(-\rho\overline{u'v'}\frac{1}{Pr_t}+\frac{\tau_l}{Pr}\right)\frac{\partial T}{\partial u}+(\gamma-1)M_{ref}^2\left(-\rho\overline{u'v'}+\tau_l\right)\frac{\partial u}{\partial n}\,, \tag{2.22}$$

where the turbulent Prandtl number is defined by the relation

$$Pr_t=\frac{\overline{u'v'}}{\overline{v'T'}}\,\frac{\partial T/\partial n}{\partial u/\partial n}\,. \tag{2.23}$$

It is worthwhile to digress briefly to discuss the turbulent Prandtl number. In dimensional variables, the relevant turbulence quantities are often related to the mean profile gradients by Bousinesq-type relations of the form

$$-\rho\overline{u'v'}\Big|^*=\mu_t^*\,\frac{\partial u^*}{\partial n^*}\,,\qquad -\rho c_p\overline{v'T'}\Big|^*=k_t^*\,\frac{\partial T^*}{\partial n^*}\,, \tag{2.24}$$

where μ_t^* and k_t^* are the so-called turbulent viscosity and conductivity which are to be modeled in general. In the present dimensionless variables, the equivalent relations to equations (2.24) are

$$-\rho\overline{u'v'} = \frac{\mu_t}{Re}\frac{\partial u}{\partial n}, \qquad -\rho\overline{v'T'} = \frac{k_t}{Re}\frac{\partial T}{\partial n}, \tag{2.25}$$

where $\mu_t = \mu^*/\mu^*_{ref}$ and $k_t = k^*_t/(\mu^*_{ref}c^*_p)$ are the dimensionless eddy viscosity and conductivity functions respectively. The turbulent Prandtl number defined by equation (2.23) is therefore also described by

$$Pr_t = \frac{\mu_t}{k_t} = \frac{\mu^*_t c^*_p}{k^*_t}, \tag{2.26}$$

which evidently derives its designation by analogy with the definition of the Prandtl number in equations (1.22). In introducing the turbulent Prandtl number concept, the best that can be hoped for is that Pr_t is a constant, at least for some classes of turbulent flows; then, if a model for $\overline{u'v'}$ is known, an expression for $\overline{v'T'}$ follows directly from equation (2.23), and it is not necessary to model the turbulent thermal problem independently. Unfortunately, experimental measurements in modern times indicate that Pr_t varies across a thermal boundary layer, and this brings into question the usefulness of introducing the turbulent Prandtl number concept at all. Nevertheless the quantity appears in most classical analyses of turbulent thermal boundary layers and will be utilized in this section.

Consider now the simplest case of a compressible boundary layer, being at constant pressure and with constant wall temperature; the last condition suggests that $\partial T/\partial\xi = 0$ and equation (2.22) reduces to

$$\tau_l\left\{(\gamma-1)M^2_{ref} + \frac{\partial}{\partial u}\left(\frac{1}{Pr}\frac{\partial T}{\partial u}\right)\right\} + \left\{\frac{1-Pr}{Pr}\frac{\partial \tau_l}{\partial u} - \frac{1-Pr_t}{Pr_t}\frac{\partial}{\partial u}(\rho\overline{u'v'})\right\}\frac{\partial T}{\partial u}$$

$$-\rho\overline{u'v'}\left\{(\gamma-1)M^2_{ref} + \frac{\partial}{\partial u}\left(\frac{1}{Pr_t}\frac{\partial T}{\partial u}\right)\right\} = 0 \tag{2.27}$$

The simplest form of equation (2.27) occurs for the so-called model fluid with $Pr = 1$ (Stewartson, 1964) and for laminar flow wherein equation (2.27) reduces to

$$\frac{\mathrm{d}}{\mathrm{d}u}\left(\frac{\mathrm{d}T}{\mathrm{d}u}\right) = -(\gamma-1)M_{ref}^2. \tag{2.28}$$

The solution of equation (2.28) subject to the boundary conditions

$$T = T_w \quad \text{at} \quad n = u = 0; \quad T = T_e \quad \text{as} \quad u \rightarrow U_e. \tag{2.29}$$

is the famous Crocco-Buseman relation given by

$$\frac{T}{T_e} = \frac{T_w}{T_e} + \left(1 - \frac{T_w}{T_e}\right)\frac{u}{U_e} + \frac{\gamma-1}{2}M_e^2\,\frac{u}{U_e}\left(1 - \frac{u}{U_e}\right) \tag{2.30}$$

where the fact that $M_e^2 = M_{ref}^2 U_e^2/T_e$ has been used. This relation applies for laminar boundary layers with $Pr = 1$ and U_e, T_e and T_w constant.

The eventual form of the Crocco-Walz equation is similar to equation (2.30) and is based on the objective of extending the Crocco-Buseman relation to arbitrary but constant Prandtl number for both laminar and turbulent compressible boundary layers. To this end van Driest (1955) considered a somewhat different form of the energy equation. The total dimensionless shear stress is given by

$$\tau = \tau_l - \rho\overline{u'v'} = \frac{\mu}{Re}\frac{\partial u}{\partial n} - \rho\overline{u'v'}, \tag{2.31}$$

and Van Driest (1955) defined a mixed Prandtl number by

$$Pr_M = \frac{\mu + \mu_t}{k + k_t} = c_p^* \frac{(\mu^* + \mu_t^*)}{k^* + k_t^*} \,. \tag{2.32}$$

Upon using equations (2.25), (2.31) and (2.32), it may be shown that equation (2.27) can be written according to

$$\tau \left\{ (\gamma - 1) M_{ref}^2 + \frac{\partial}{\partial u}\left(\frac{1}{Pr_M} \frac{\partial T}{\partial u} \right) \right\} + \frac{1 - Pr_M}{Pr_M} \frac{\partial T}{\partial u} \frac{\partial \tau}{\partial u} = 0 \tag{2.33}$$

This equation is equivalent to equation (2.27), and although it appears to be a simpler form, it must be understood that the "mixed" Prandtl number Pr_M is a hybrid quantity involving actual and turbulent viscosity; in general Pr_M is not known, and its actual variation across a boundary layer may be quite complicated.

Defining a normalized velocity and temperature by

$$\overline{u} = u/U_e, \quad \overline{T} = T/T_e \,, \tag{2.34}$$

equation (2.33) may be written in the form

$$\left(\frac{\overline{T}'}{Pr_M}\right)' + (1 - Pr_M) \frac{\tau'}{\tau} \left(\frac{\overline{T}'}{Pr_M}\right) = -(\gamma - 1)\, M_e^2 \,, \tag{2.35}$$

which is a linear, first-order differential equation in $(\overline{T}'/Pr_M)$ as a function of $\overline{u}$; it is valid for constant pressure flows which have U_e, T_e and T_w constant and for which the solution is independent of ξ and a function of $\overline{u}$ along. Integration of equation subject to conditions (2.29) yields

$$\frac{T}{T_e} = \frac{T_w}{T_e} + \left(1 - \frac{T_w}{T_e}\right) \frac{\mathrm{S}(\overline{u})}{\mathrm{S}(1)} + (\gamma - 1) M_e^2 \left\{ \frac{\mathrm{S}(\overline{u})}{\mathrm{S}(1)} \mathrm{R}(1) - \mathrm{R}(\overline{u}) \right\} , \tag{2.36}$$

as given first by Van Driest (1955); here $S(\bar{u})$ and $R(\bar{u})$ are the following integrals:

$$S(\bar{u}) = \int_0^{\bar{u}} Pr_M \exp\Big(-\int_{\tau_w}^{\tau} \frac{1-Pr_M}{\tau}\, d\tau\Big)\, dt\ , \tag{2.37}$$

$$R(\bar{u}) = \int_0^{\bar{u}} Pr_M \exp\Big(-\int_{\tau_w}^{\tau} \frac{1-Pr_M}{\tau}\, d\tau\Big)\Big\{\int_o^t \exp\Big(\int_{\tau_w}^{\tau} \frac{1-Pr_M}{\tau}\, d\tau\Big)\, d\zeta\Big\}\, dt, \tag{2.38}$$

Equation (2.36) relates the temperature to the velocity distribution but is useful only if Pr_M and τ are known as functions of $\bar{u}$. Walz (1959) made what may be regarded as questionable assumption by assuming that Pr_M is constant; this leads to

$$S(\bar{u}) = Pr_M \int_0^{\bar{u}} \Big(\frac{\tau}{\tau_w}\Big)^{Pr_M - 1} dt, \quad R(\bar{u}) = \int_0^{\bar{u}} S(t) \int_0^t \Big(\frac{\tau}{\tau_w}\Big)^{1-Pr_M} d\zeta dt. \tag{2.39}$$

Walz (1959) further assumed that Pr_M was close to 1 and then, to leading order; it follows from equation (2.39) that

$$\frac{S(\bar{u})}{S(1)} = \bar{u} + \ldots, \quad \frac{R(\bar{u})}{R(1)} = \bar{u}^2 + \ldots. \tag{2.40}$$

Introducing these relationships into equation (2.36) gives

$$\frac{T}{T_e} = \frac{T_w}{T_e} + \Big(1 - \frac{T_w}{T_e}\Big)\frac{u}{U_e} + r\frac{(\gamma-1)}{2} M_e^2 \Big\{\frac{u}{U_e} - \Big(\frac{u}{U_e}\Big)^2\Big\}\ , \tag{2.41}$$

where r is a constant defined by

$$r = 2R(1) = 2\int_0^1 \Big\{\Big(\frac{\tau}{\tau_w}\Big)^{Pr_M - 1} \int_0^t \Big(\frac{\tau}{\tau_w}\Big)^{1-Pr_M} d\zeta\Big\}\, dt\ . \tag{2.42}$$

It is easily seen that r is the recovery factor. By differentiating equation (2.41) with respect to n and taking zero heat transfer at the wall, the recovery temperature T_r is then obtained

$$T_r = T_e\left(1 + \mathrm{r}\,\frac{\gamma-1}{2}\,M_e^2\right). \tag{2.43}$$

Consequently, r is the recovery factor; note from equation (2.42) that $\mathrm{r} = 1$ when $Pr_M = 1$. Using equation (2.43), equation (2.36) may be written in terms of the recovery temperature to give the following temperature/velocity relation.

$$\frac{T}{T_e} = \frac{T_w}{T_e} + \left(\frac{T_r - T_w}{T_e}\right)\frac{u}{U_e} - \mathrm{r}\,\frac{(\gamma-1)}{2}M_e^2\left(\frac{u}{U_e}\right)^2, \tag{2.44}$$

which is equivalent (using equation (2.43)) to the Crocco-Buseman relation (2.30) when $\mathrm{r} = 1$. The temperature/velocity relation (2.44) is called Walz's equation or Crocco-Walz relationship.

It may be noted that Walz's relation (2.44)) is exact only when either $Pr_M \equiv 1$ or $\tau \equiv$ constant. The latter condition is never true in a boundary-layer flow. Most technically important gases have the molecular Prandtl number in the range of $0.7 \leq Pr \leq 1$ and thus there is a reasonable expectation that equation (2.44) may apply as an approximation in a boundary-layer flow. A complete survey of measured and predicted temperature profiles has been carried out by Fernholz and Finley (1977), based on a variety of measurements in compressible turbulent boundary layers with zero pressure gradient along adiabatic and isothermal walls. They concluded that in the approximate parameter range of $Pr \approx 0.71$, $M_e < 10$, and $0.2 < T_w/T_e < 1$, the mean temperature distribution is adequately represented

by the Walz relationship within an error range of 10%.

However, the Walz (1955) formula must be regarded as a semi-empirical approximate formula. There are so few measurements in the wall layer that it is impossible to judge whether the relation can predict the slope of the temperature profile ($\partial T/\partial n$) at the wall, in order to determine the surface heat transfer rate. The relationship is potentially useful in the outer layer of the boundary layer to obtain an expression for the mean temperature distribution when the mean velocity is known. However, there are certain conditions which the profile cannot describe, such as adiabatic boundary layers; here a total temperature overshoot (i.e. values of $T > T_e$ near the boundary layer edge is typically found in data. In summary, the Walz relation is a simple formula but is restricted to constant temperature and pressure flows; even here the assumptions concerning the behavior of the mixed Prandtl number seem rather restrictive, and the formula should be regarded as a useful approximation at best.

2.4 The Van Driest Effective Velocity Concept

In analogy with incompressible flow, it is commonly assumed that in the thin inner region of the boundary layer, the convection terms and the pressure gradient are negligibly small with respect to the viscous and Reynolds stresses in the streamwise momentum equation; this result will be shown to hold formally in the limit Re$\rightarrow\infty$ in Chapter 3. It follows from equation (1.14) that, to leading order, the total stress

$$\tau = -\rho\overline{u'v'} + \frac{\mu}{Re}\frac{\partial u}{\partial n} \tag{2.45}$$

is constant in the inner region and equal to the value at the wall (1951) τ_w. Van Driest (1951) argued that the viscous term is negligible with respect to the Reynolds stress near the outer edge of the wall layer and here the turbulence term was represented using the same mixing length formulation (2.9) as for incompressible flow according to

$$\tau_w = \rho\, l^2\, |\frac{\partial u}{\partial n}|\, \frac{\partial u}{\partial n}\,. \tag{2.46}$$

The same mixing length $\ell = \kappa n$ was assumed to hold for compressible boundary layers, where $\kappa = 0.41$ is von Karman's constant. Note that this is the fundamental basis of the van Driest theory and constitutes what may be regarded as a questionable extrapolation of an incompressible theory. It follows that near the outer edge of the wall layer

$$\frac{\partial u}{\partial n} = \sqrt{\frac{\rho_w}{\rho}}\, u_\tau\, \frac{1}{\kappa n}\,, \tag{2.47}$$

where

$$u_\tau = \sqrt{\frac{\tau_w}{\rho_w}}\,. \tag{2.48}$$

Formula (2.47) is the same as the incompressible result, except that it contains a density variation. Because the pressure is constant across the boundary layer, the ideal gas law yields

$$\frac{\rho_w}{\rho} = \frac{T}{T_w}\,, \tag{2.49}$$

and introducing the Crocco-Walz relation (2.44), it follows that

$$\frac{\rho_w}{\rho} = \frac{T}{T_w} = 1 + \left(\frac{T_r}{T_w} - 1\right)\frac{u}{U_e} - \mathrm{r}\,\frac{\gamma-1}{2}\,M_e^2\,\frac{T_e}{T_w}\left(\frac{u}{U_e}\right)^2 \tag{2.50}$$

Substitution into equation (2.47) gives

$$\frac{1}{\left\{1 + B(u/U_e) - A^2(u/U_e)^2\right\}^{1/2}}\,\mathrm{d}\left(\frac{u}{U_e}\right) = \frac{u_\tau}{\kappa U_e}\,\frac{\mathrm{d}n}{n}\ , \tag{2.51}$$

where the constants A and B are defined by

$$A^2 = \mathrm{r}\,\frac{\gamma-1}{2}\,M_e^2\,\frac{T_e}{T_w}\,, \qquad\qquad B = \frac{T_\mathrm{r}}{T_w} - 1\ . \tag{2.52}$$

Integration of equation (2.51) yields

$$\frac{1}{A}\sin^{-1}\left\{\frac{2A^2(u/U_e) - B}{(B^2+4A^2)^{1/2}}\right\} = \frac{u_\tau}{U_e}\,\frac{1}{\kappa}\log(n) + D\ , \tag{2.53}$$

where D is a constant. Since equations (2.47) (and hence (2.53)) hold only near the outer edge of the wall layer, the constant D cannot be found by applying conditions at either the wall or the mainstream. Instead, a value of D is obtained by letting $M_e \to 0$ and forcing equation (2.53) to be equivalent to the incompressible law of the wall for no heat transfer (i.e. $T_w = T_e$); in this limit $A, B \to 0$. This procedure can be accomplished in a variety of ways and the result is therefore not unique; the particular form adopted by van Driest (1951) is

$$\frac{1}{A}\sin^{-1}\left\{\frac{2A^2(u/U_e) - B}{(B^2+4A^2)^{1/2}}\right\} + \frac{1}{A}\sin^{-1}\left\{\frac{B}{(B^2+4A^2)^{1/2}}\right\}$$

$$= \frac{u_\tau}{U_e}\left\{\frac{1}{\kappa}\log\left(\frac{\rho_w u_\tau n}{\mu_w}\right) + C\right\}. \tag{2.54}$$

Here C is the log-law constant for incompressible flow ($C \simeq 5.0$). Note that this step is somewhat ad hoc since a number of other functional forms for D could also be used. If an "effective" velocity is defined by

$$u_{eff} = \frac{U_e}{A} \sin^{-1}\left\{ \frac{2A^2(u/U_e) - B}{(B^2+4A^2)^{1/2}} \right\} + \sin^{-1}\left\{ \frac{B}{(B^2+4A^2)^{1/2}} \right\}, \tag{2.55}$$

then with $B \equiv 0$ and $A \to 0$, the inverse sine function may be expanded for small argument, and it is easily shown that $u_{eff} \to u$. Consequently, equation (2.54) reduces to the incompressible law of the wall in the limit $M_e \to 0$.

Equation (2.55) is called the van Driest effective velocity or van Driest transformation; it can be regarded as transforming the velocity profile in the overlap zone of a compressible boundary layer, $u(n)$, to an equivalent incompressible flow $u_{eff}(n)$ that obeys the standard logarithmic formula given by the right side of equation (2.54). Fernholz and Finley (1977) have concluded from their survey of two-dimensional compressible turbulent boundary-layer that the transformed logarithmic law agreed satisfactorily with measurements in boundary layers with zero pressure gradient along isothermal walls, and the same value of $C \simeq 5.0$ as for incompressible flow appeared to apply in equation (2.54) for the compressible case. The Mach number range investigated by Fernholz and Finley (1977) is $3 < M_e < 7.2$ and a range of heat transfer parameters corresponding to $0.31 < T_w/T_r < 1.0$ were considered, where T_w is the wall temperature and T_r is the recovery temperature. Deviations between the logarithmic law and measurements were sometimes attributed to upstream history effects or to a systematic error in the skin friction measurement in high Mach number flows with strong heat transfer. Although equation (2.55) is derived on the basis of a local analysis of the

compressible overlap zone, it is sometimes used to define a transformation for the entire boundary layer. Maise and McDonald (1968) found that compressible boundary-layer data for an adiabatic wall could be collapsed to an almost universal form using the van Driest effective velocity transformation; however, the approach was found to be much less impressive in flows with heat transfer. Consequently, the van Driest effective velocity method should be viewed as an interesting representation of velocity in the overlap zone of a compressible turbulent boundary layer but for which the range of validity is not clearly established.

2.5 A General Velocity Transformation

The van Driest transformation is based partially on the Crocco-Walz relation which is an approximate equation for the temperature distribution in the entire boundary layer and applies to a constant pressure flow along an isothermal wall. An alternative theory can be developed for the compressible turbulent wall layer which does not have some of these restrictions. In the wall layer, the total stress τ is constant and equation (2.33) reduces to

$$(\gamma-1)M_{ref}^2+\frac{\partial}{\partial u}\left(Pr_M\,\frac{\partial T}{\partial u}\right)=0, \tag{2.56}$$

where the mixed Prandtl number Pr_M is defined by equation (2.32). It may be noted that equation (2.56) also applies to flows with pressure gradient since the terms due to $\partial P_e/\partial\xi$ that are omitted in equation (2.33) are generally negligible in the wall layer to leading order (cf. Chapter 3). For constant Pr_M, equation (2.56) may be integrated from the wall, and the solution having $u=u_s=u(n_s)$, $T=T_s=T(n_s)$ at some point in the wall layer where $n=n_s$ is

$$\frac{T}{T_w} = 1 + \left(\frac{T_s - T_w}{T_w}\right)\frac{u}{u_s} + Pr_M \frac{\gamma - 1}{2} M_s^2 \frac{T_s}{T_w}\left\{\frac{u}{u_s} - \left(\frac{u}{u_s}\right)^2\right\}, \tag{2.57}$$

where $M_s^2 = u_s^{*2}/(\gamma R T_s^*)$. For constant Pr_M, it can be verified by differentiation of equation (2.57) that the recovery temperature may be related to the temperature T_s and Mach number M_s at $n = n_s$ by

$$T_r = T_s \left(1 + Pr_M \frac{\gamma - 1}{2} M_s^2\right), \tag{2.58}$$

or equivalently

$$T_r = T_s + Pr_M \frac{\gamma - 1}{2} M_{ref}^2 u_s^2 . \tag{2.59}$$

Substituting into equation (2.57) yields a temperature-velocity relation for the inner layer according to

$$\frac{T}{T_w} = 1 + \left(\frac{T_r - T_w}{T_w}\right)\frac{u}{u_s} - Pr_M \frac{\gamma - 1}{2} M_s^2 \frac{T_s}{T_w}\left(\frac{u}{u_s}\right)^2. \tag{2.60}$$

This relationship is somewhat more general than the Crocco-Walz relationship and can be applied to flows with varying wall temperature which have a pressure gradient. Here u_s and T_s should be interpreted as a velocity and temperature characteristic of the wall layer and evaluated at a representative location $n = n_s$.

The relation (2.60) can now be introduced in equation (2.7) to obtain an alternate effective velocity definition given by

$$u_{eff} = \frac{U_e}{\tilde{A}} \sin^{-1}\left\{\frac{2\tilde{A}^2(u/U_e) - \tilde{B}}{(\tilde{B}^2 + 4\tilde{A}^2)^{1/2}}\right\} + \sin^{-1}\left\{\frac{\tilde{B}}{(\tilde{B}^2 + 4\tilde{A}^2)^{1/2}}\right\} \tag{2.61}$$

where

$$\tilde{A}^2 = Pr_M \frac{\gamma-1}{2} M_e^2 \frac{T_e}{T_w}, \qquad \tilde{B} = \left(\frac{T_r}{T_w} - 1\right) \frac{U_e}{u_s}, \tag{2.62}$$

such that

$$u_{eff} = u_\tau \left\{ \frac{1}{\bar{\kappa}} \log\left(\frac{\rho_w u_\tau n}{\mu_w}\right) + c \right\}. \tag{2.63}$$

To utilize this relation, a representative value of n_s must be selected for the wall layer. This general approach will be revised subsequently in this thesis.

2.6 The Van Driest Skin Friction Formula

Van Driest (1951) developed a skin friction formula for compressible turbulent flat plate flows which was based on his effective velocity concept. These formulae are still in wide use today, and it is therefore of interest to understand the basis of these expressions. Consider flow over a flat plate at arbitrary Mach number and wall temperature. Van Driest (1951) assumed that the major contributions to the integral thickness could be evaluated by using u_{eff} in the overlap zone of the boundary layer. The compressible momentum thickness is defined by

$$\Theta = \int_0^\delta \frac{\rho u}{\rho_e U_e}\left(1 - \frac{u}{U_e}\right) dn. \tag{2.64}$$

The velocity distribution in this integral is then represented using equation (2.54), and rewriting (2.54) to obtain n as a function of u/U_e gives

$$n = \frac{\mu_w}{\rho_w u_\tau} \exp(-\kappa C) \exp\left\{\kappa \frac{U_e}{A u_\tau}\left\{\sin^{-1}\left(\frac{2A^2(u/U_e) - B}{(B^2+4A^2)^{1/2}}\right)\right.\right. \\ \left.\left. + \sin^{-1}\left(\frac{B}{(B^2+4A^2)^{1/2}}\right)\right\}\right\}. \tag{2.65}$$

Upon differentiation of equation (2.65) with respect to n and using the Crocco-Walz relation (2.44) for the density ratio in equation (2.64), along with the ideal gas law, it is readily shown

$$\Theta = e^{-\kappa C} \frac{\mu_w}{\kappa \rho_e u_e} a^2 \exp\left\{\frac{a}{A} \sin^{-1} \frac{B}{(B^2+4A^2)^{1/2}}\right\} \times \mathbb{J}, \tag{2.66}$$

where $\mathbb{J}$ is the integral

$$\mathbb{J} = \int_o^1 \frac{z(1-z)}{(1+Bz-A^2z^2)^{3/2}} \exp\left\{\frac{a}{A} \sin^{-1} \frac{2A^2z - B}{(B^2+4A^2)^{1/2}}\right\} dz, \tag{2.67}$$

and a and z are defined by

$$a = \kappa U_e / u_\tau, \qquad z = u/U_e. \tag{2.68}$$

If y denotes

$$y = \exp\left\{\frac{a}{A} \sin^{-1}\left(\frac{2A^2z - B}{(B^2+4A^2)^{1/2}}\right)\right\}, \tag{2.69}$$

it is easily verified that

$$y = \sqrt{\frac{1+Bz-A^2z^2}{a}} \frac{dy}{dz}, \tag{2.70}$$

and this relation may be used to facilitate an evaluation of $\mathbb{J}$ by successive integration by parts to produce a descending series in a^{-1}. Since $a \gg 1$ as Re becomes large, the leading order term for $\mathbb{J}$ follows from two integrations by parts and is given by

$$\mathbb{J} \approx \frac{1}{a^2(1+B-A^2)^{1/2}} \exp\left\{\frac{a}{A} \sin^{-1}\frac{2A^2-B}{(B^2+4A^2)^{1/2}}\right\}$$

$$+\frac{1}{a^2} \exp\left\{-\frac{a}{A} \sin^{-1}\frac{B}{(B^2+4A^2)^{1/2}}\right\}, \tag{2.71}$$

with an error $O(a^{-3})$. Since the exponent of the second term in equation (2.71) is negative, and A is usually larger than unity, the second term in equation (2.71) can normally be neglected to yield

$$\mathbb{J} \approx \frac{1}{a^2(1+B-A^2)^{1/2}} \exp\left\{\frac{a}{A} \sin^{-1}\frac{2A^2-B}{(B^2+4A^2)^{1/2}}\right\}. \tag{2.72}$$

The result is now substituted into equation (2.66), and using the fact

$$A^2 = \left(\frac{T_r}{T_w} - 1\right)\frac{T_e}{T_w}, \tag{2.73}$$

an expression for the skin friction coefficient c_f defined as

$$c_f = \frac{\rho_w U_\tau^2}{\frac{1}{2}\rho_e U_e^2} \tag{2.74}$$

may be obtained in the form

$$\frac{1}{\sqrt{c_f}} = \left\{ \frac{1}{\bar{\kappa}} \log \left(Re_\theta \frac{\mu_e}{\mu_w} \left(\frac{T_e}{T_w} \right)^{1/2} \right) + \text{constant} \right\} \sqrt{F_c} \,, \tag{2.75}$$

where the momentum thickness Reynolds number is defined as

$$Re_\theta = \frac{\rho_e U_e \Theta}{\mu_e} \,. \tag{2.76}$$

Here F_c is regarded as a compressibility correction and is defined by

$$F_c = \frac{T_r/T_e - 1}{2(\sin^{-1}\alpha_c + \sin^{-1}\beta_c)^2} \,, \tag{2.77}$$

with α_c and β_c given by

$$\alpha_c = \frac{2A^2 - B}{(B^2 + 4A^2)^{1/2}} \,, \qquad \beta_c = \frac{B}{(B^2 + 4A^2)^{1/2}} \,. \tag{2.78}$$

Equation (2.75) is usually referred to as van Driest formula I. As the Mach number becomes large, the representation of the skin friction is found to be progressively worse; in addition, the predicted values are poor when the heat transfer rates at the surface are high. Sometime later van Driest (1956) developed a second skin-friction formula which has been widely used and is referred to by White (1992) as "the best of its type ever developed."

The van Driest I formula is based on the Prandtl mixing-length formula $l = \kappa n$ in the overlap zone, which, combined with Walz relationship, leads to the effective velocity concept. If the procedure leading to formula I is repeated with the mixing-length expression given instead by von Karman's similarity law

$$l = \kappa \left| \frac{\partial u/\partial n}{\partial^2 u/\partial n^2} \right|, \tag{2.79}$$

a formula similar to equation (2.75) is obtained except that the temperature ratio $\sqrt{T_e/T_w}$ inside the logarithmic term is not present. This formula is known as van Driest II and is of the form

$$\frac{1}{\sqrt{c_f}} = \left\{ \frac{1}{\kappa} \log \left(Re_\theta \frac{\mu_e}{\mu_w} \right) + \text{constant} \right\} \sqrt{F_c} \, . \tag{2.80}$$

The constants in equations (2.75) and (2.80) can be determined from a requirement that, when $M_e \rightarrow 0$ and $T_w/T_e = 1$ both equations must reduce to the incompressible flow case, namely, approximately 5.0. Several surveys (see, for example, Bradshaw, 1977) have been carried out concerning the accuracy of these skin-friction formulae and formula II generally shows better agreement with experimental data than formula I. This is somewhat surprising because the von Karman mixing-length formula (2.79) has never gained wide acceptance, partially because it is not possible to obtain a useful velocity expression from it. Both formulae should be regarded as interesting semi-empirical relations which are based on a number of questionable assumptions. Although Van Driest II is believed to give a better representation of data, the range of validity is uncertain and the problem is compounded by uncertainties in the data to which the formulae are compared. For example, there are discrepancies between similar experiments because of differences in the method of finding Re_θ. It can be seen from the definition of momentum thickness in equation (2.64) that the quality of temperature measurements has a strong effect on the integral as Mach number increases. Generally, a lack of reliable inner region velocity and temperature data makes the situation worse, especially in the hypersonic range since the wall layer grows as a percentage of the total boundary

layer thickness as Mach number increases. At $M_e = 5$ (the approximate start of the hypersonic range), the wall layer is ten time as thick as in low-speed flow at the same Reynolds number. Of course, whether or not the Van Driest theory applies in the hypersonic regime is questionable at all.

2.7 Compressibility Transformations

The use of a mathematical transformation to account for the effect of compressibility has been extensively applied to laminar boundary layers and wakes. Howarth (1948), Stewartson (1949), and many others have used this approach. The motivation behind such transformations is to attempt to convert the system of equations describing compressible boundary layers into a simpler form which is similar to the incompressible problem. For laminar flow, the Stewartson-Illingworth transformation (Stewartson, 1964) provides such a relationship. It might be expected that similar transformation can be used in compressible turbulent flow. This question has been considered by Burgraff (1962), Crocco (1963), Coles (1964) among others. A potential problem in the turbulent case has been identified by Crocco (1963) as follows:

> "Since the mechanism determining the distribution of the turbulent shearing stress is unknown, one cannot be assured of the physical validity of the transformation, even if this correctly transforms the inertia and pressure terms of the equations".

However, Coles (1964) argued to the contrary accordingly:

> "The accelerations and the pressure force are well-defined quantities that can be evaluated experimentally. The unbalance between these quantities may simply be taken to define an apparent shearing stress, and numerical values for the latter may thus be inferred from measurements of velocity and pressure. It is clearly irrelevant, for example, that this apparent stress

may have a turbulent part that can be independently defined in terms of certain velocity fluctuations capable of being measured directly. If a transformation can be found to treat the acceleration and pressure terms in the equations, and if this transformation is required to be physically realistic, then it must follow without reference to any special definition of the shearing stresses that these stresses can also be treated by the transformation".

The use of compressibility transformations in turbulent compressible flow has been controversial and was debated in the literature (see, for example, Economs, 1970 and Lewis, 1970) without apparent resolution.

A variety of approaches to compressibility transformations have been discussed by Burggraf (1962) and Coles (1964). Implicit in many of these approaches is the notion of a reference condition at which the variable thermodynamic properties are to be evaluated in the hope that the gross properties of the boundary layer may be represented by incompressible formulae. One example discussed by Burggraf (1962) which will be used in the present study is the Howarth-Dorodnitsyn variable defined by

$$Y = \int_o^n \frac{\rho}{\rho_o}\, dn \tag{2.81}$$

where ρ_o is a "reference density" and ρ is the dimensionless time-mean density. The use of this transformation is common in laminar boundary-layer analysis where the wall density is often used for ρ_o. However, the problem of compressible turbulent boundary layers poses a dilemma because a suitable reference density is not immediately apparent. In the outer region of the boundary layer, the mean density can be expressed as a perturbation about the mainstream value. On the

other hand, the density at the wall is often substantially different from the mainstream value, and an intense variation occurs in density and temperature across the compressible turbulent wall layer. Consequently, there is a difficulty in the turbulent case in defining a reference density which is characteristic of both regions. In Burggraf's (1962) approach, the reference conditions were defined at $Y^+ = Y u_\tau / \nu_w = 11$ which is a location part way through the wall layer; the value of 11 is where the extension of a logarithmic law (for large Y^+) intersects the linear relation (which is valued for small Y^+). The velocity distribution in this new scaled coordinate was then assumed to conform to known incompressible results, such as the "law of the wall". A variety of similar approaches are discussed by Coles (1964). In this study, the concept of a reference state will also be utilized and the approach first considered by Burggraf (1962) will be pursued.

2.8 Status of Experimental Knowledge

It is extremely difficult to measure skin friction directly with good accuracy. Unfortunately detailed knowledge of the surface shear stress is vital to prediction of performance and design of structural requirements in both supersonic and hypersonic aircraft. In general, the design of aircraft and material selection depends heavily on a predicted skin friction distribution over the entire aircraft configuration and of the convective heat flux along the various surfaces. In supersonic flight, the surface temperature of the aircraft is normally close to adiabatic wall temperature. However, at hypersonic speeds temperatures near the surface are generally much larger, and as a result of the relative importance of radiative cooling to the atmosphere (as well as possible heat transfer to the interior of the aircraft), the cooled-wall situation is of most importance, since the surface

temperature is often 30 to 50 percent of the adiabatic wall temperature. Considerable effort has been devoted to developing accurate means to measure skin friction. Evidently the direct measurement of skin friction (such as by floating element balances on the surface) would be most desirable, but various difficulties associated with applying such methods in a variety of common situations, such as flows with pressure gradients, has led to the development of a number of indirect means of inferring skin friction distributions from other more easily measured quantities. In a survey article, Hopkins (1971) has given a critical review of these indirect methods which include: (1) surface heat transfer measurements in which skin friction is then inferred by assuming the skin friction is proportional to the wall heat flux (the Reynolds analogy); (2) skin friction is estimated from the momentum integral equation by estimating the rate of change of momentum thickness with longitudinal distance from measured velocity profiles; (3) attempts to estimate the velocity gradient at the surface from data taken close to the wall (where experimental errors are of the large and (4) schemes such as the Clauser plot in which the velocity profile is assumed to conform to some functional form, such as the incompressible law of the wall, containing the skin friction as a parameter; this parameter is then adjusted until a "best fit" to measured velocity profile data is obtained. All of these indicated methods suffer from various uncertainties, and those which rely on the availability of velocity profile data close to the wall are especially problematic, in view of the difficulty of obtaining accurate data in the very thin boundary layers characteristic of high speed compressible flows.

As discussed by Hopkins (1971), there is a long history of attempts at direct measurement of wall shear stress using floating element balances, however, the

technique is beset by many pitfalls which can be overcome in particular situations, and unfortunately a priori specifications of the requirements that must be met in any situation to achieve accurate results remains difficult. Questions associated with the effects of: (1) the necessary gaps around the floating element, (2) local wall temperature changes, and (3) surface heat transfer and a variety of other influences are far from being well understood. Unless the floating element is very large, it is difficult to be certain that various forms of systematic gap-induced-errors are not present; unfortunately the measurement is not local when the element is large. Furthermore, gap-induced errors are likely to be more significant when complicated by inflow and outflow associated with pressure gradients. If the floating element has a temperature different from that of the wall, significant errors may arise in flows in heat transfer and/or varying wall temperature. For example, an uncooled floating element in a cooled wall may give unrealistically low shear stress values; a difference on the order of 20% was found by Voisinet and Lee (1972) for a case with $T_w/T_r = 0.22$ (Fernholz and Finley 1977). A survey of errors in obtaining skin friction arising from various causes has also been given by Winter (1977).

Another means of inferring skin friction is through use of the Preston (1954) tube, which consists of a circular pitot tube lying on the surface. Preston demonstrated using a range of sizes of tube in fully developed pipe flow that a unique relationship could be obtained between the measured pressure and velocity if it was assumed that the velocity profile had a specific form. This is known as the calibration. Although some investigators consider this approach to be reliable in compressible flow, there remain many uncertainties concerning the effects of pressure gradient, flow unsteadiness, heat transfer and three dimensional effects.

Both this method and the Clauser cross-plot method are questionable in compressible flow because they rely on knowing the form of the velocity profile near the wall and the form of the "law of the wall" for compressible flow is not well established (particularly with increasing Mach number). As yet there is no universal agreement on Preston tube calibration; experimentalists often present several different values of skin friction obtained by various methods and leave it to the reader to choose (Carvin 1988) the most reliable. In fact, it may not be possible at present to extend the Preston tube calibration to supersonic flow because there is no general agreement of the "law of wall" for compressible boundary layer flow. This therefore appears to leave floating element balances as the preferred way to measure the skin friction in a supersonic boundary layer.

The measurement of mean flow velocity profile data should be relatively straightforward if it were easy and inexpensive to carry out supersonic experiments in steady flow facilities at large scale. However, most supersonic flow data are usually obtained from relatively small size facilities and are often "blow down" facilities with relatively short run times to keep the costs low; in the hypersonic range such facilities are often derivatives of shock tubes. The relatively small size of most of these facilities, as well as probe size limitations, do not significantly affect the quantity of experimental data taken throughout most of the boundary layer. Unfortunately there are serious restrictions as the wall is approached. As a consequence, there are virtually no high-speed compressible flow experiments for which a significant number of data points are in the wall-layer region, and thus it is not possible to place a high level of confidence in estimates of wall shear stress and heat flux obtained from extrapolating the slope of the velocity and total temperature data near the surface. It is therefore not possible to check wall

measurements against profile data unless it can be assumed that the profile as a whole obeys a general similarity relationship. Much of the existing mean boundary-layer data has been measured through use of Pitot tubes which measure the difference between the static pressure and the local stagnation pressure. The static pressure at any s-station is constant to leading order across the boundary layer, and the static pressure can therefore be obtained from a surface measurement. In order to obtain velocity from the Pitot data, it is necessary to know the local density. In many cases, temperature and hence density (from the ideal gas law with p constant at any s location) were obtained approximately from the Crocco-Walz relation. In some experiments, total temperature is measured directly with a stagnation temperature probe (STP) consisting of a tube in which the flow is brought to rest and the temperature is measured using a thermocouple. Another common means of velocity measurement is with a hot wire, although the Pitot measurements are believed to be more reliable. Recently a non-intrusive technique, namely the laser-Doppler-velocimeter (LDV) has been used to measure velocity directly in compressible turbulent boundary layers. LDV measurements yield mean and fluctuating velocity data by evaluating the motion of individual particles in the flow, and at least for velocity, total temperature information is not needed; in principle, LDV measurements provide a direct check on the calibration and data reduction procedures used in the classical compressible boundary-layer experiments. Unfortunately, for reasons related to the optics, it is very difficult to make measurements close to the wall, and often results for the thin wall layer may not be very precise. Therefore once again important information in the near wall region is often lacking.

Measurements of turbulence quantities (i.e. time-averaged velocity and

temperature fluctuation products) are principally used as an aid to the modeling of turbulence terms in the mean equations. Direct experimental measurements of the Reynolds shear stress are relatively scarce. Such measurements have been common in incompressible flow for some time (see, for example, Kleblanoff, 1955, and Townsend, 1956). Some measurements of the fluctuating velocities and temperature in supersonic boundary layers have been made, but thus far the results cannot be considered conclusive in the sense that it is not clear how the Reynolds stress is influenced by Mach number and heat transfer rate. Fluctuating velocities are normally measured with either hot wires or an LDV. Fluctuating temperature measurements are relatively rare and difficult to obtain; they are normally carried out with a stagnation temperature probe using a thermocouple to measure temperature. There have been many attempts to find a means to collapse compressible data for either $\overline{u'v'}$ or $\rho\overline{u'v'}$ at various longitudinal stations to a single curve in the search for some type of similarity law. Such attempts have been inconclusive as surveyed by Fernholz and Finley (1981), who carried out an exhaustive but futile attempt to find similarity in distributions of Reynolds normal stresses; no common trends could be found and the search was hampered by large discrepancies between similar experiments. It appears that systematic investigations of fluctuating velocities, even in constant pressure compressible boundary layers are needed which cover a wide range of Reynolds numbers, Mach numbers and surface heat transfer. The question whether self-similarity can exist in compressible turbulent boundary layers will be discussed in §5.

2.9 Summary

The current state of knowledge for high-speed compressible turbulent

boundary layers may be summarized as follows. Data for velocity and temperature profiles, as well as turbulence quantities within the wall layer are scattered and often of uncertain reliability. Although a number of approaches have been developed to represent the velocity and temperature distributions in the near-wall region, many are based on questionable assumptions that are difficult to verify. It has been common practice to extrapolate results of incompressible theories, almost without modification to the compressible regime. This approach seems to give plausible predictions for moderate Mach number boundary layers, but the entire approach for the hypersonic range needs to be critically assessed.

At least for a range of Mach numbers, the direct effects of density fluctuations on turbulence are believed to be small (Morkovin's hypothesis) if the root-mean-square fluctuation is small compared with the absolute density. Thus it is expected that within some Mach number range (usually take up to $\mathrm{Me} = 5$), the "turbulence structure" of boundary layers is closely related to that in a constant-property flow; the term "structure" means that the composite nature of turbulent boundary layers holds for compressible flows and further that the effect of mean density variations in s or n directions on the turbulence is essentially parametric. Consequently, assumptions concerning turbulence structure that apply to constant-density flow will, if properly scaled, carry over to compressible boundary layers as long as Morkovin's hypothesis holds. Unfortunately the range of validity in Me is not known, and it is often not clear which incompressible results can be carried over and which cannot; in the end all turbulence models are empirically based to one degree or another, and a major difficulty here lies in the fact that even many incompressible theories cannot be considered to be firmly established.

The Crocco-Walz (1959) temperature relationship and van Driest (1954,

1956) effective velocity concept form the basis of most current prediction methods for compressible turbulent boundary layers. However, both theories involve questionable assumptions and restrictions which would seem to be limiting in their application. For example, the Walz formula cannot describe the total temperature overshoot near the boundary-layer edge observed in high speed flows with adiabatic walls. Generally the theory for energy transport can be considered incomplete and lacking relations for the mean temperature profile when: (1) the wall temperature varies in s or (2) a longitudinal pressure gradient dp/ds exists Without a general treatment of the wall layer, it is impossible to predict either the skin friction or the surface heat transfer rates.

It is evident from the brief synopsis in this chapter that there are many controversial and unresolved issues. An asymptotic analysis has the potential of systematically addressing and resolving some of these aspects. In the end, however, some appeal or comparison to experimental data is always necessary in theoretical turbulence research. Unfortunately, there is a relatively small database of velocity and temperature profile for the near-wall region in high-speed compressible flows.

3. ASYMPTOTIC STRUCTURE FOR Re→∞

3.1 Introduction

Concepts which have proven successful for incompressible flows provide a useful starting point for the analysis of compressible boundary layers. At low speeds (when the mainstream Mach number approaches zero), the fluid has constant transport quantities μ and k, and the velocities and lengths depend on the Reynolds number in a specific way; for example, the incompressible laminar boundary layer thickness is easily shown to be $O(Re^{-1/2})$. A systematic rational analysis is more difficult for turbulent boundary layers because the equations contain Reynolds stress terms such as $\rho\overline{u'v'}$, whose functional form and precise order of magnitude (in terms of Reynolds number) is not known. In principle, this difficulty can be resolved by introducing a specific closure model which relates the turbulent stress to the mean profiles. However, a multitude of different closure schemes exist, and since the objective in this study is to obtain general results, a minimum number of assumptions will be made concerning the turbulence models.

In addition to the Reynolds number, compressible turbulent boundary layers depend on at least two more parameters, namely the Mach number and the surface heat transfer, and it is important to determine how the length and velocity scales depend on these parameters. An immediate problem is associated with the representative Reynolds number, since all transport coefficients are temperature dependent and large variations in temperature (and density) are typical across supersonic boundary layers. It is also important to attempt to determine the asymptotic structure with a minimum appeal to experiment, especially since the experimental data for velocity and temperature in supersonic flows is not as

complete as for incompressible flows. In the analysis described in this chapter, an explicit closure model is not adopted, and the goal is to extract as much information as possible using the method of matched asymptotic expansions from a minimal number of reasonable physical assumptions.

The problem under consideration is a fully developed compressible turbulent boundary layer with finite Mach number and large Reynolds number, satisfying either the two-dimensional or axisymmetric nominally steady turbulent boundary layer equations. In addition, it is assumed that the boundary layer can be subdivided into a relatively thin wall layer and an outer defect layer, as in the incompressible case. In this chapter, the leading order expansions and equations for velocity and total enthalpy will be established without recourse to a specific closure assumption. The plan of this chapter is as follows. In §3.2 and §3.3 supersonic flow experimental data are analyzed and a velocity scale appropriate for compressible turbulent boundary layer flows is proposed. The governing equations in terms of Howarth-Dorodnitsyn variable is also given in §3.3. The leading order asymptotic expansions of the time-mean equations will be developed for the inner-region and outer-region profiles respectively in §3.4 and §3.5. The resulting leading order expressions are matching to form complete composite expansions in §3.6. Finally a summary is given in §3.7 to put the leading order results of the asymptotic expansion in an organized fashion.

3.2 The Nature of Compressible Turbulent Boundary Layers

An important feature that distinguishes high-speed compressible turbulent boundary layers from their incompressible counterparts is the large changes in density and temperature which typically occur across the boundary layer. Some

representative temperature profiles for constant pressure flows with adiabatic walls are shown in Figure 3.1 for increasing Mach number. The numbering scheme used is that given in Fernholz and Finley (1977) with the first two digits indicating the year in which the data was taken. Because the mainstream pressure is in general impressed across the boundary layer, the density at any station in a boundary layer is inversely proportional to the temperature. It may be noted that the density and temperature changes become more severe with increasing Mach number; these changes are a result of compressibility and viscous dissipation and can be strongly influenced by heat transfer at the wall. Such changes generally imply a variation in the transport properties such as viscosity μ and heat conductivity k across the boundary layer.

In Figure 3.2, a set of mean velocity profiles, corresponding to the temperature profiles in Figure 3.1, measured in fully turbulent boundary layer is shown; these profiles correspond to the temperature profiles shown in Figure 3.1. Although the Mach numbers differ considerably, the velocity distributions all look very similar; they are characterized by a rapid velocity change in a relatively thin region near the wall with a slowly varying profile in the outer part of the boundary layer. The profiles in the outer part of the boundary layer are similar to that observed in a wake and are sometimes referred to as "wake-like". An important trend should be noted and this is the growth of the viscous wall layer as a fraction of the total boundary-layer thickness; in the hypersonic range, the wall layer comprises a much larger portion of the boundary layer in low-speed flow, and the velocity reaches a significantly higher percentage of the local mainstream speed at the edge of wall layer. This effect is believed to be associated with increased dissipation in the wall layer with increasing Mach number and, consequently,

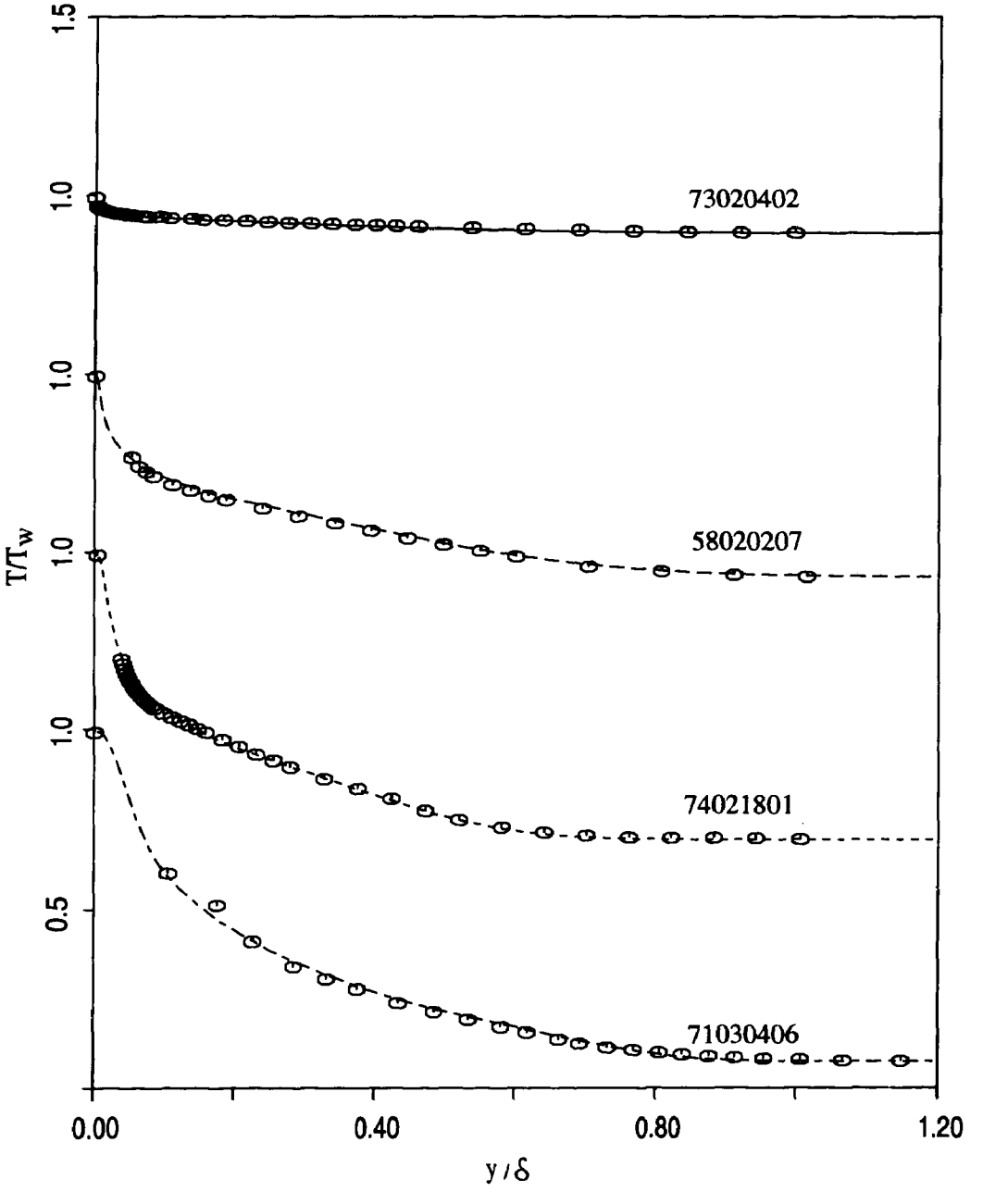

Figure 3.1. Temperature profiles in constant pressure gradient boundary layers with different Mach numbers; 73020402, Me=0.79; 58020207, Me=2.74; 74021801, Me=4.52; 71030406, Me=6.69(in helium). Note the staggered origins.

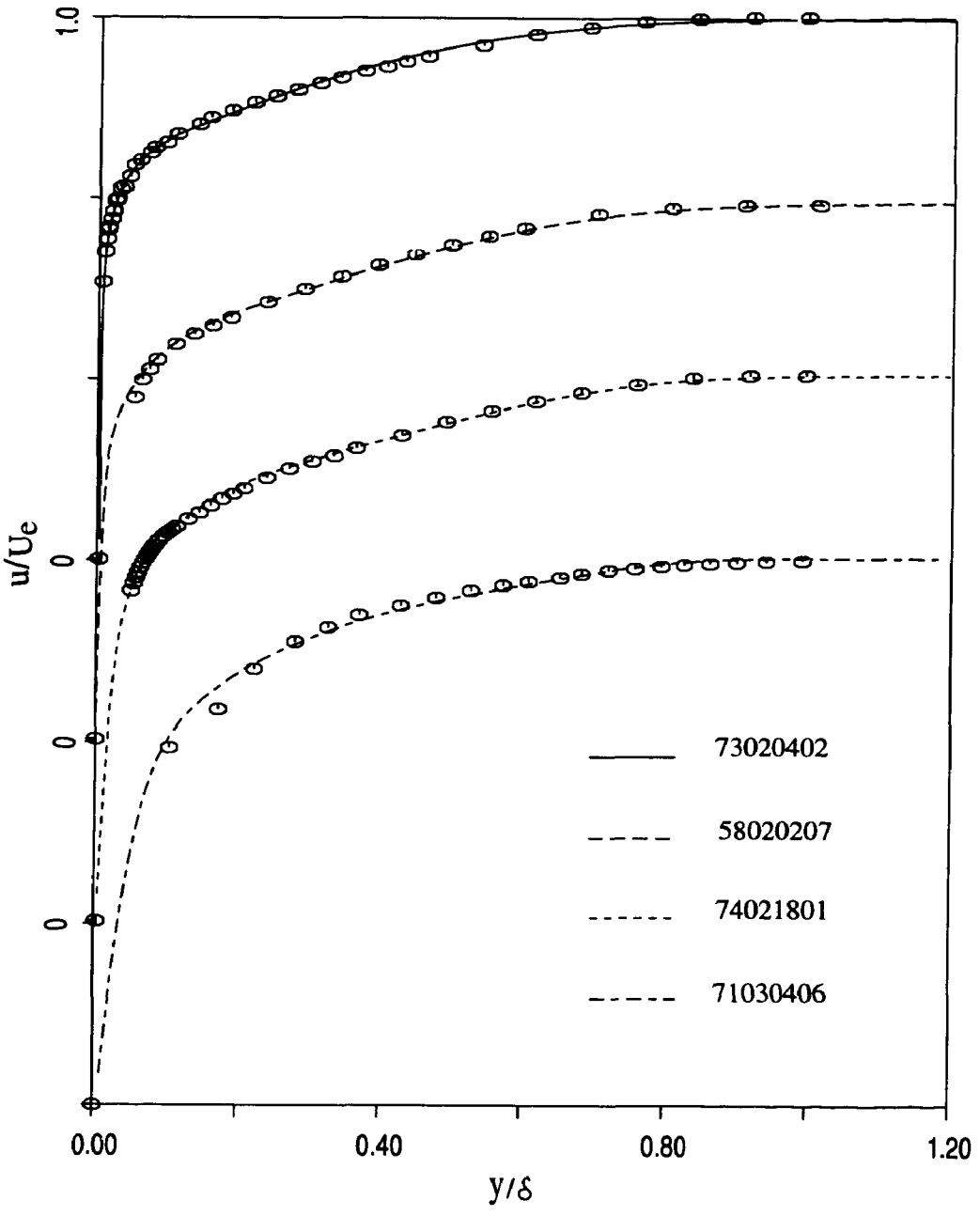

Figure 3.2. Velocity profiles in constant pressure gradient boundary layers with different Mach numbers; 73020402, Me=0.79; 58020207, Me=2.74; 74021801, Me=4.52; 71030406, Me=6.69(in helium). Note the staggered origins.

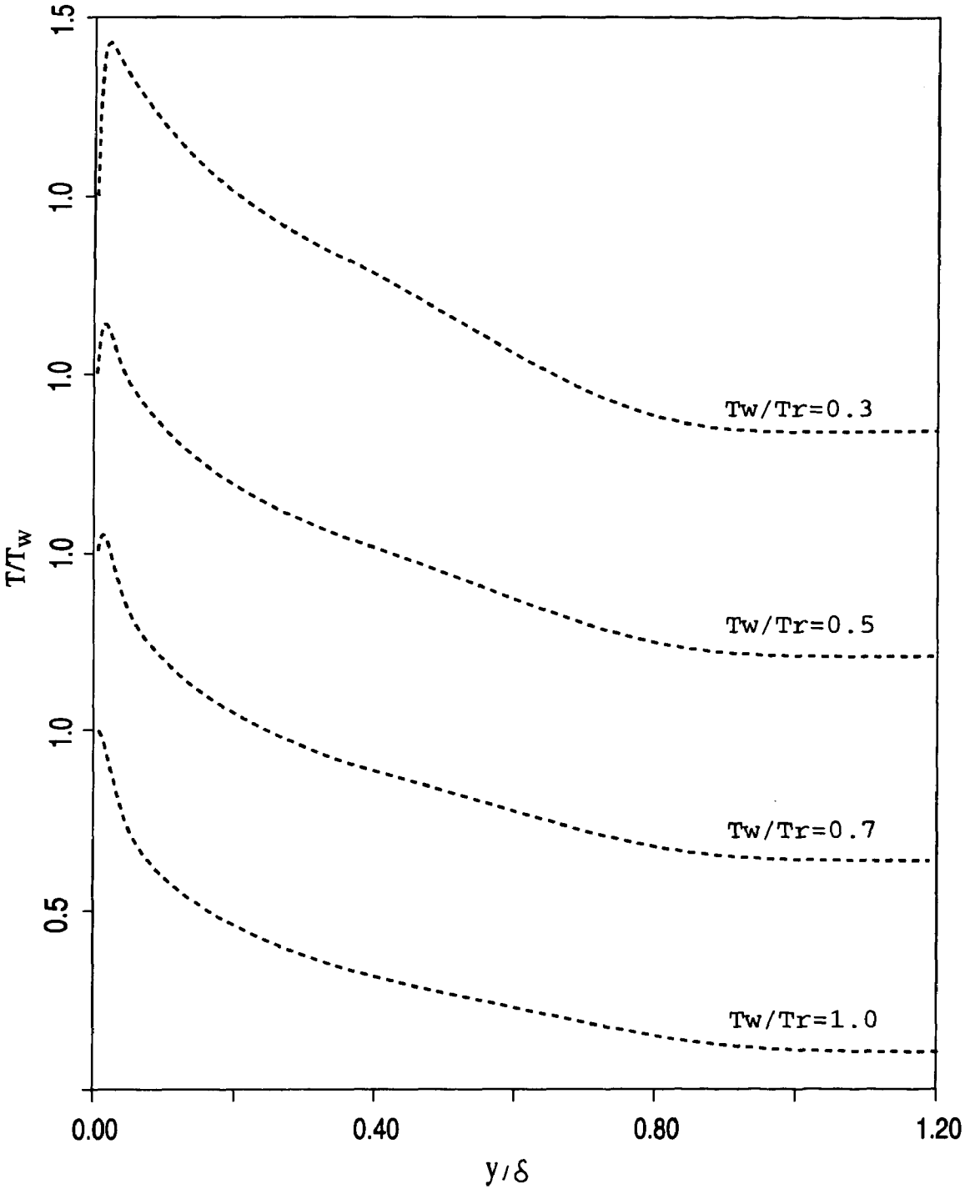

Figure 3.3. Temperature profiles in constant pressure gradient boundary layers with different surface heat transfer rate; 72040601, Me=6.5, Tw/Tr=0.51; 72021203, Me=4.9, Tw/Tr=0.23. Note the staggered origins.

higher temperatures; this is believed to influence the velocity profile near the wall and thereby reduce the shear stress. A similar effect is of course responsible for the observed increase in the thickness of a laminar boundary layer at high Mach numbers. Another distinguishing feature of hypersonic flow is the relatively slower variation of velocity in the outer part of the boundary layer. In an incompressible flow $\partial u/\partial n$ approaches zero rapidly away from the wall, but in hypersonic flows the decay is less rapid; this makes comparisons of hypersonic data sets on the basis of boundary-layer thickness δ problematic, especially since δ is not precisely defined. Density and temperature variations are also associated with this problem. Most of the total-pressure gradient across the boundary layer is attributable to $\partial \rho/\partial n$ instead of $\partial u/\partial n$. Bushnell and Morris (1971) have indicated that at $M_e = 20$, δ_{995} is only about half a thickness defined with pitot-pressure profile as a basis. Bradshaw (1977) has suggested that an alternative definition of δ should be the distance from the surface at which the total pressure P_{total} (or more accurately the pressure difference $P_{total} - p$) reaches 0.995 of its maximum value at the mainstream.

Issues associated with temperature and density variations across the boundary layer will receive the most attention in this chapter. The relative importance of such variations is illustrated for the Mach 6 flow in helium shown in Figure 3.1; here for an adiabatic wall, the temperature ratio of the wall to the mainstream value is more than 10! A large fraction of this total variation occurs across the wall layer. As a second example, Figure 3.3 shows two temperature profiles containing rare near-wall measurements at similar Mach numbers; here T_w/T_r denotes the ratio of wall temperature to the adiabatic wall temperature. One profile corresponds to a moderately cooled wall, while the second represents a

strongly cooled wall having the temperature ratio between that of the wall and the mainstream close to one. The strongly cooled case demonstrates well the potential influence of temperature and density variations in each portion of a compressible turbulent boundary layer. The temperature rapidly "recovers" or increases from the wall value, near the edge of the wall layer a value of T is achieved which is not radically different from the corresponding adiabatic flow temperature. In fact, as the temperature decreases toward the mainstream, the profile soon becomes almost indistinguishable from a corresponding profile with an adiabatic wall. The plotted results in Figure 3.3 suggest that the flow in the outer region is almost unaware of the precise value of the wall temperature and two conclusions can be drawn: 1) in defining an appropriate asymptotic structure for the boundary layer, it should be expected that neither the wall temperature nor the density should appear in the leading terms for the asymptotic expansions in the outer layer, and 2) it may be necessary to define characteristic temperature or density which is representative of conditions in the outer portion of the wall layer.

3.3 General Considerations

By analogy with incompressible flows, analyses of the inner compressible wall layer are normally based upon neglecting the convection and pressure gradient terms; then in an argument based on Morkovin's hypothesis, the velocity in the wall layer of a compressible boundary layer is hypothesized to have a form similar to that in incompressible flows, viz.

$$u = f(\tau_w,\ \rho,\ \mu,\ n), \tag{3.1}$$

with, however, the fluid properties ρ and μ varying with n, it is commonly argued that all the temperature dependent parameters in equation (3.1) can be represented by some empirical relationships. For example, μ can be expressed as a function of T, such as $\mu \propto T^{\omega}$ for some ω, which is often a good approximation for common gases over a range of temperature. Bradshaw (1984) assumed an inner velocity form according to

$$u = f(\tau_w,\ \rho_w,\ \mu_w,\ q_w,\ c_p,\ T_w,\ k_w,\ \gamma,\ n), \tag{3.2}$$

and dimensional analysis yields

$$\frac{u}{u_\tau} = f_1\left(\frac{\rho_w u_\tau n}{\mu_w}\ ,\ \frac{q_w}{\rho_w c_p u_\tau T_w}\ ,\ \frac{u_\tau}{a_w}\ ,\ \gamma,\ Pr\right) \tag{3.3}$$

where $u_\tau = \sqrt{\tau_w/\rho_w}$ is the wall friction velocity and $a_w = \sqrt{\gamma R T_w}$ is the speed of sound at the wall. The quantity u_τ/a_w is called the friction Mach number. Bradshaw (1984) has suggested that the local value of $\sqrt{\tau_w/\rho}$ should provide a better velocity scale than the wall value u_τ where the density now varies with n. However, the reasoning is not clear, and in any case it is difficult to accommodate this in an asymptotic expansion. Most authors attempt to expand the density about the value at the wall ρ_w. However, it is evident (cf. Figure 3.3) that the density variation across the wall layer can be substantial, and the density in the outer portion of the wall layer is comparable to that in the outer layer. In summary, it is evident that the direct extrapolation of constant-property flow concepts to compressible case may produce plausible models for low Mach numbers, but will become less satisfactory with increasing Mach number.

The possibility of using a compressibility transformation for high speed turbulent boundary layer flows was discussed in §2 and will be pursued here. The Howarth-Dorodnitsyn transformation is defined by

$$Y = \int_o^n \left(\frac{\rho}{\rho_o}\right) dn, \qquad \tilde{v} = \frac{\overline{\rho v}}{\rho_o} + u\,\frac{\partial Y}{\partial s}\,, \tag{3.3.4}$$

where ρ_o is a reference density and Y measures a density-weighted distance from the surface. Under this transformation, the governing equations (1.13), (1.14) and (1.16) become

$$\frac{\partial}{\partial s}(ru) + \frac{\partial}{\partial Y}(r\tilde{v}) = 0\ ; \tag{3.5}$$

$$u\frac{\partial u}{\partial s} + \tilde{v}\,\frac{\partial u}{\partial Y} = -\left(\frac{\rho_e}{\rho}\right)\frac{1}{\rho_e}\,\frac{dp_e}{ds} + \frac{1}{\rho_o}\,\frac{\partial}{\partial Y}\left(-\rho\overline{u'v'} + \frac{\mu\rho}{\rho_o}\,\frac{1}{Re}\,\frac{\partial u}{\partial Y}\right); \tag{3.6}$$

$$u\,\frac{\partial H}{\partial s} + \tilde{v}\,\frac{\partial H}{\partial Y} = \frac{1}{\rho_o}\,\frac{\partial}{\partial Y}\left(-\rho\overline{v'H'} + \frac{\mu\rho}{\rho_o}\,\frac{1}{PrRe}\,\frac{\partial H}{\partial n}\right)$$

$$+ (\gamma-1)M_{ref}^2\frac{1}{\rho_o}\,\frac{\partial}{\partial Y}\left[\left(1-\frac{1}{Pr}\right)\frac{\mu\rho}{\rho_o}\,\frac{1}{Re}\,\frac{\partial}{\partial Y}\left(\frac{u^2}{2}\right)\right]. \tag{3.7}$$

Here the energy equation in terms of total enthalpy H has been listed since it is the form that will be used throughout.

For a nominally steady flow, the time-mean total enthalpy in the mainstream, H_e, is a constant and the Mach number at the outer edge of the boundary layer is related to H_e and U_e by

$$U_e^2 = \frac{\alpha\, H_e}{(\gamma-1)M_{ref}^2} \tag{3.8}$$

where α is defined by

$$\alpha = \frac{(\gamma-1)\, M_e^2}{1+\left(\frac{\gamma-1}{2}\right) M_e^2} \,. \tag{3.9}$$

The density is related to the static temperature T through the equation of state, equation (1.17) and it is easily shown that the temperature is related to H and u by

$$\frac{T}{T_e} = \left\{1+\frac{\gamma-1}{2}M_e^2\right\}\left\{\frac{H}{H_e}-\frac{1}{2}\,\alpha\,\frac{u^2}{U_e^2}\right\}. \tag{3.10}$$

The pressure is independent of n to leading order across the boundary layer and equal to the value $p_e(s)$ at the boundary-layer edge and the Bernoulli equation for steady compressible flow gives

$$\frac{dp_e}{ds} = -\rho_e U_e \frac{dU_e}{ds} \,. \tag{3.11}$$

In addition, it follows from the ideal gas relation equation (1.17)

$$\rho T = \rho_o T_o = \rho_e T_e \,, \tag{3.12}$$

where ρ_o and T_o can be taken at any location within the boundary layer. Consequently, the density ratio in equation (3.6) may be replaced by the right side of equation (3.10) and the compressible problem is thereby expressed solely in terms of the unknowns u, $\tilde{v}$, H and the turbulence terms according to

$$\frac{\partial}{\partial s}(ru) + \frac{\partial}{\partial Y}(r\tilde{v}) = 0 \; ; \tag{3.13}$$

$$u\frac{\partial u}{\partial s} + \tilde{v}\frac{\partial u}{\partial Y} = \frac{1}{M_e}\frac{dM_e}{ds}\left(\frac{H}{H_e}U_e^2 - \frac{\alpha}{2}u^2\right) + \frac{1}{\rho_o}\frac{\partial \tau}{\partial Y} \; ; \tag{3.14}$$

$$u\frac{\partial H}{\partial s} + \tilde{v}\frac{\partial H}{\partial Y} = \frac{1}{\rho_o}\frac{\partial q}{\partial Y} \; . \tag{3.15}$$

Here the total shear stress and heat flux are defined as

$$\tau = \sigma + \frac{\mu\rho}{\rho_o}\frac{1}{Re}\frac{\partial u}{\partial Y} \; ; \tag{3.16}$$

$$q = \phi + \frac{\mu\rho}{\rho_o}\frac{1}{PrRe}\frac{\partial H}{\partial Y} + \frac{(\gamma-1)}{2}M_{ref}^2\frac{\partial}{\partial Y}\left[\left(1-\frac{1}{Pr}\right)\frac{\mu\rho}{\rho_o}\frac{1}{Re}\frac{\partial}{\partial Y}\left(u^2\right)\right] . \tag{3.17}$$

respectively, where σ and ϕ are the Reynolds stress and turbulent heat flux given by

$$\sigma = -\rho\overline{u'v'} \; , \qquad \phi = -\rho\overline{v'H'} . \tag{3.18}$$

The boundary conditions are

$$u = \tilde{v} = 0, \qquad T = T_w(s), \text{ and } H = H_w(s) \qquad \text{at } Y = 0 \; ; \tag{3.19}$$

for specified wall temperature and

$$\frac{\partial H}{\partial Y} = 0 \qquad \text{at} \qquad Y = 0 \tag{3.20}$$

for an adiabatic wall. At the mainstream

$$u \to U_e(s)\,, \qquad T \to T_e(s)\,, \qquad \text{and } H \to H_e \qquad \text{as } Y \to \infty\,. \tag{3.21}$$

At this stage, the reference density ρ_o that has been used to define the transformed variables should be regarded as a density characteristic of either the inner or outer part of the boundary layer; a specific selection will be made subsequently in this thesis. Consider first the wall layer where the viscous and turbulent stress dominate and where the total shear stress is therefore constant with $\tau = \tau_w$, to the leading order. For a compressible laminar boundary layer, ρ and μ can be formally removed from the viscous term in the transformed equation of motion if the Chapman relation $\rho\mu = \text{constant}$ (Stewartson, 1964) is used. In a boundary layer this is equivalent to $\mu \propto \mathrm{T}$, and for such a relation the compressible-to-incompressible transformation is complete for laminar boundary layers. For a turbulent flow, the situation is complicated because knowledge of the Reynolds stress terms is inexact. In general, the Reynolds stress vanishes at the surface and asymptotes to a maximum value of τ_w, in the overlap zone between the inner and outer layer; this behavior has been confirmed by a number of experiments in both compressible and incompressible flow. Based on this type of behavior, it does seem reasonable that the turbulence term can also be treated by the compressibility transformation and the transformed Reynolds stress σ can be independent of compressibility, if a characteristic density ρ_o is suitably defined using the new variable Y. The velocity profile for the inner layer should therefore be determined by the distance Y, the shear stress τ_w, and the characteristic fluid properties ρ_o and μ_o; because the convective terms are negligible to leading order, the dependence of the wall-layer relation on the streamwise variable s can at most be parametric and hence

$$u = f(\tau_w, \rho_o, \mu_o, Y) \ . \tag{3.22}$$

It is easily shown that a normalized relation can then be obtained by dimensional analysis which is analogous to the incompressible law of the wall according to

$$\frac{u}{u_{\tau_o}} = f\left(\frac{\rho_o u_{\tau_o} Y}{\mu_o}\right), \tag{3.23}$$

where here

$$u_{\tau_o} = \sqrt{\frac{\tau_w}{\rho_o}} = \sqrt{\frac{\rho_w}{\rho_o}}\, u_\tau \ , \tag{3.24}$$

is a generally defined velocity scale.

The flow in the outer portion of the boundary layer is inviscid to leading order, and here for a constant pressure flow the shear stress τ reaches a maximum τ_w near the surface in order to match with the inner layer profile; a τ asymptotes to zero towards the outer edge of the boundary layer. Because the shear-stress has this simple profile shape, the change of the τ distribution with Mach number is not seen to be large. Therefore the velocity profile for a constant pressure flow can plausibly be assumed to depend only on τ_w, ρ_o, Y, and some outer-layer length scale Δ_o proportional to the local boundary-layer thickness. The outer defect velocity is therefore

$$U_e - u = F(\tau_w, \rho_o, Y, \Delta_o) \ . \tag{3.25}$$

and dimensionless analysis yields

$$\frac{U_e - u}{u_{\tau_o}} = F\left(\frac{Y}{\Delta_o}\right) \tag{3.26}$$

for a constant pressure compressible turbulent boundary layer. Note that u_{τ_o} is again a generally defined velocity scale defined in terms of the characteristic density.

Two conclusions can be drawn from the above brief analysis. First, although in principle the velocity scales for inner and outer layer profiles could be selected separately, there must be a velocity scale of common validity between the inner and outer layers, and this requires a single selection for ρ_o so that u_{τ_o} is the same for both layers, in other words only a single velocity scale is feasible. Secondly, ρ_o cannot be selected at either the surface temperature or the mainstream temperature; in the former case, the velocity profile in the outer layer would then depend on a wall parameter, and this is a situation which is excluded from the current analysis. The latter case is also not acceptable since it would require a dependence of the wall layer solution on the external density. It therefore appears that the characteristic density should be representative of the density in both layers, and this would suggest that this quantity should be selected to be representative of the overlap zone. This possibility will be pursued subsequently.

3.4 Asymptotic Structure of the Inner Layer

The asymptotic structure of the velocity field in the limit of large Reynolds number has been considered for a constant-property two-dimensional turbulent boundary layer by a number of authors (e.g., Fendell, 1972, and Mellor, 1972). A procedure similar to that of Fendell (1972) was followed by Weigand (1978) in an

analysis of thermal boundary layers in low flow speeds where the asymptotic structure is deduced for first principles using a minimum of empirically motivated assumptions. Here a similar analysis will be carried out for high-speed compressible turbulent boundary-layer flow utilizing the transformed form of governing equations (3.13) through (3.18) in terms of the Horwarth-Dorodnitsyn variable Y.

Experimental evidence strongly suggests that the boundary layer consists of a thin inner wall layer and a relatively thick outer defect layer. In the wall layer, the asymptotic expansions for the stream function and velocity are written

$$\psi(s,Y) = \Delta_i(s;\ Re,M_o)\ \gamma_1(s;\ Re,M_o)\ r(s)\ f_1(s,Y^+) + \cdots \tag{3.27}$$

$$u(s,Y) = \gamma_1(s;\ Re,M_o)\ U^+(s,Y^+) + \cdots \tag{3.28}$$

where Δ_i and γ_1 are gauge functions to be found, and $r(s)$ is the dimensionless radius of revolution for an axisymmetric body. The velocity function $U^+(s,Y^+)$ is defined here according to $U^+ = \partial f_1/\partial Y^+$ and

$$Y^+ = \frac{Y}{\Delta_i(s;Re,M_o)}\,. \tag{3.29}$$

Here Y^+ is the scaled normal coordinate in the inner layer and Δ_i is the dimensionless inner-layer length scale, representing a typical normal length scale in the inner region; γ_1 is the inner velocity scale. A characteristic Mach number M_o is introduced to allow for possible Mach number effects associated with compressibility and heat transfer, described in §3.3. The final results will contain

the influence of M_o implicitly in such parameters as ρ_o and μ_o. The Reynolds stress σ is zero at the wall and asymptotes to a maximum value near the outer edge of the wall layer, but is otherwise unknown. To leading order σ is written

$$\sigma(s,Y) = e_1(s;\ Re,M_o)\ \sigma_1(s,Y^+) + \cdots , \tag{3.30}$$

where the gauge function e_1 is to be found.

In a compressible flow the equations governing the transport of energy and momentum are normally strongly coupled, and here the structure of the thermal problem is taken up. At low subsonic speeds, Weigand (1978) has reviewed an extensive amount of experimental data showing that the static temperature distribution clearly displays a logarithmic behavior in the overlap zone. With increasing Mach number, there are relatively fewer data points in the overlap zone, as well as less experiments that measure temperature directly; in addition the influence of dissipation is expected to become significant. In most of the data considered by Weigand (1978), the total and static temperatures are quantitatively equivalent. It is not obvious that the static temperature is the appropriate dependent variable, and here the total enthalpy will be used instead as the primary thermal independent variable, in view of the fact that equation (3.15) is more analogous to the energy equation in low speed flows. In the wall layer, the total enthalpy is written as a perturbation about the wall value, according to

$$H = H_w + \lambda_1(s;\ Re,Pr,M_o)\ \theta^+(s,Y_\theta^+) + \cdots , \tag{3.31}$$

where

$$Y_\theta^+ = \frac{Y}{\Pi_i(s;Re,Pr,M_o)} . \tag{3.32}$$

Here Y_θ^+ is the scaled normal coordinate for the thermal wall layer where the length scale and the total enthalpy scale λ_1 are to be found subject to the requirement that $\lambda_1 \to 0$ and $\Pi_i \to 0$ as $Re \to \infty$. It may be noted that a model for the dynamics of the wall layer will be discussed in §4. It will be argued that the thermal normal scale should differ from the corresponding hydrodynamic scale only through a function of Prandtl number. Thus, for the common gases of interest here where Pr = O(1), both Δ_i and Π_i should be of comparable magnitude.

Both the functional form and Reynolds number dependence associated with the turbulent heat flux term ϕ are unknown, and unfortunately there is little reliable data in high speed flows for ϕ. From low-speed experiments (see, for example, Orlando et al., 1974), $-\rho\overline{v'T'}$ or $-\rho\overline{v'H'}$ behave much the same as the Reynolds-stress term σ increasing from zero at the wall to a maximum in the overlap zone. Here the turbulent heat flux term ϕ is written

$$\phi(s,Y) = g_1(s;\ Re, Pr, M_o)\ \phi_1(s, Y_\theta^+) + \cdots . \tag{3.33}$$

where g_1 is a gauge function to be found.

Substituting equations (3.17) through (3.31) into the momentum equation (3.14) leads to

$$\gamma_1 \frac{\partial f_1}{\partial Y^+}\left(\gamma_1' \frac{\partial f_1}{\partial Y^+} + \gamma_1 \frac{\partial^2 f_1}{\partial s \partial Y^+}\right) - \left((\Delta_i \gamma_1)' f_1 + \Delta_i \gamma_1 \frac{\partial f_1}{\partial Y^+} + \Delta_i \gamma_1 \frac{r'}{r} f_1\right) \frac{\gamma_1}{\Delta_i} \frac{\partial^2 f_1}{\partial Y^{+2}}$$

$$= \frac{1}{M_e} \frac{dM_e}{ds} \left\{ \left(\frac{H_w}{H_e} + \frac{\lambda_1}{H_e} \theta^+ \right) U_e^2 - \left(\gamma_1 \frac{\partial f_1}{\partial Y^+} \right)^2 \right\}$$

$$+ \frac{1}{\rho_o \Delta_i} \frac{\partial}{\partial Y^+} \left(\frac{\mu \rho}{\rho_o} \frac{\gamma_1}{Re \Delta_i} \frac{\partial^2 f_1}{\partial Y^{+2}} \right) + \frac{e_1}{\rho_o \Delta_i} \frac{\partial \sigma_1}{\partial Y^+} , \tag{3.34}$$

where the primes denote total differentiation with respect to s. Balancing in equation (3.34) is carried out here by assuming (subject to verification) that to leading order the viscous and Reynolds stress are comparable while the convection terms are negligible. Specifically, it is assumed that

$$e_1 = \mathrm{O}\left(\frac{\mu_o \gamma_1}{Re\Delta_i}\right), \qquad \gamma_1 \Delta_i^2 Re \to 0 \quad \text{as } Re \to \infty \,. \tag{3.35}$$

Here the Chapman density-viscosity relation $\mu\rho \simeq \mu_o \rho_o$ has been used to delineate the various orders of magnitude; this relationship is not quantitatively accurate over significant temperature ranges but is valid for representing qualitative relationships. It will be verified subsequently that the pressure gradient term in equation (3.34) is also negligible to the leading order and, as a result, equation (3.34) reduces to

$$\frac{\partial}{\partial Y^+}\left(\frac{\mu\rho}{\rho_o}\frac{\gamma_1}{Re\Delta_i}\frac{\partial^2 f_1}{\partial Y^{+2}}\right) + e_1 \frac{\partial \sigma_1}{\partial Y^+} = 0 \,. \tag{3.36}$$

in the limit $Re \to \infty$.

The gauge functions γ_1 and e_1 may now be related to a conventionally defined friction velocity u_τ in terms of quantities at the wall according to

$$u_\tau^2 = \frac{\mu_w}{\rho_w Re}\left.\frac{\partial u}{\partial n}\right|_{n=0}, \tag{3.37}$$

which in terms of inner variables is

$$u_\tau^2 = \frac{\mu_w \gamma_1}{\rho_o Re\Delta_i}\frac{\partial^2 f_1(s,0)}{\partial Y^{+2}} \,. \tag{3.38}$$

It is convenient to define the following wall normalization

$$\frac{\partial U^+}{\partial Y^+}(s,0) = \frac{\partial^2 f_1(s,0)}{\partial Y^{+2}} = 1 \ , \tag{3.39}$$

and equation (3.38) becomes

$$u_\tau^2 = \frac{\mu_w \gamma_1}{\rho_o Re \Delta_i} \ . \tag{3.40}$$

It now follows from equation (3.35) that the Reynolds stress scale e_1 is $O(\rho_w u_\tau^2)$. Without loss of generality the gauge function may be selected according to

$$e_1(s;\ Re) = \rho_w(s) u_\tau^2(s;\ Re) \ . \tag{3.41}$$

It may be noted that the reference Mach number M_o is not involved in the definition of e_1 since the Chapman relation has been assumed.

The scale for Reynolds stress is now fixed in terms of the friction velocity and the density at the wall. However, γ_1 is still unknown and that some additional information related to the characteristics of compressible turbulent boundary layers is required. As discussed in §3.3, one proposed velocity scale is

$$\gamma_1(s;Re;M_o) = u_{\tau o}(s;Re,M_o) = \sqrt{\frac{\rho_w}{\rho_o}}\, u_\tau(s;Re) \ , \tag{3.42}$$

and it then follows from equation (3.40) that Δ_i is given by

$$\Delta_i(s;Re,M_o) = \frac{\mu_w \rho_w}{\rho_o^2 Re\ u_{\tau o}} \ . \tag{3.43}$$

For reasons discussed in §3.3, this definition of the wall layer velocity scale is believed to be superior to the choice $\gamma_1 = u_\tau$. The wall layer equation (3.36) may now be integrated from 0 to Y^+ using the boundary condition (3.39), as well as the fact that $\sigma = 0$ at $Y^+ = 0$, to obtain

$$\sigma + \rho_o u_{\tau o}\left(\frac{\mu\rho}{\mu_w\rho_w}\right)\frac{\partial u}{\partial Y^+} = \rho_o u_{\tau o}^2 \,, \tag{3.44}$$

where the total stress $\tau = \rho_w u_\tau^2 = \rho_o u_{\tau o}^2$ is constant across the inner layer, to leading order. Furthermore, since the viscous stress becomes small as $Y^+ \to \infty$, it must follow that

$$\sigma \to \rho_o u_{\tau o}^2 = \rho_w u_\tau^2 \quad \text{as} \quad Y^+ \to \infty, \tag{3.45}$$

to leading order. It may be noted that any model which is adopted for the Reynolds stress in the outer layer must conform to the behavior indicated by equation (3.45) in the overlap zone. By using equations (3.28), (3.30), (3.41), and (3.42), the final form of the wall layer momentum equation is

$$\sigma_1 + \left(\frac{\mu\rho}{\mu_w\rho_w}\right)\frac{\partial U^+}{\partial Y^+} = 1 \,. \tag{3.46}$$

Now consider the energy equation in the wall layer. Upon substituting the expansions for the total enthalpy (3.31), velocity (3.28) and the turbulent heat flux (3.33) into the energy equation (3.15), it follows

$$u_{\tau o}\frac{\partial f_1}{\partial Y^+}\left(H_w' + \lambda_1'\theta^+ + \lambda_1\frac{\partial\theta^+}{\partial s}\right) - \left((\Delta_i u_{\tau o})' f_1 + \Delta_i u_{\tau o}\frac{\partial f_1}{\partial Y^+}\right.$$

$$\left. + \Delta_i u_{\tau o}\frac{r'}{r} f_1\right)\frac{\lambda_1}{\Pi_i}\frac{\partial\theta^+}{\partial Y_\theta^+} = \frac{1}{\rho\Pi_i}\frac{\partial q}{\partial Y^+} \,, \tag{3.47}$$

to leading order, where the total energy flux q is

$$q = g_1\phi_1 + \frac{\mu\rho}{\rho_o}\frac{\lambda_1}{PrRe\Pi_i}\frac{\partial\theta^+}{\partial Y_\theta^+} + \frac{(\gamma-1)}{2}\frac{M_{ref}^2 u_{\tau o}^2}{Re\Delta_i}\left[\frac{Pr-1}{Pr}\frac{\mu\rho}{\rho_o}\frac{\partial(U^{+2})}{\partial Y^+}\right]. \tag{3.48}$$

If the convection terms are again assumed negligible to leading order (subject to verification), equation (3.47) reduces to

$$\frac{\partial q}{\partial Y^+} = 0\ . \tag{3.49}$$

Consequently, the total flux q is invariant, to leading order, across the wall layer and equal to the value at the wall $q_w(s)$. Since U^+ and ϕ_1 vanish at $Y^+ = 0$, it follows from equation (3.48) that

$$q_w(s) = \frac{\mu_w\rho_w}{\rho_o}\frac{\lambda_1}{PrRe\Pi_i}\frac{\partial\theta^+(s,0)}{\partial Y_\theta^+}\ , \tag{3.50}$$

where q_w denotes a dimensionless heat flux at the wall defined by

$$q_w(s) = \frac{q_w^*}{\rho_{ref}^* U_{ref}^* c_p^* T_{ref}^*}\ , \qquad q_w^* = k_w^*\left.\frac{\partial T^*}{\partial n^*}\right|_{n=0}\ . \tag{3.51}$$

Here k_w^* is the dimensional thermal conductivity of the fluid at the wall. Note that q_w denotes a heat flux from *fluid to the wall.*

It will subsequently be argued that $\lambda_1/H_e = O(u_{\tau o}/U_e)$ if the heat transfer between the flow and the wall is significant. It is then easily seen that the last term on the right side of equation (3.48) (which is related to viscous-dissipation) is negligible to leading order and, consequently, the only acceptable balance is

between the viscous diffusion term and the turbulent heat flux term; thus, it is assumed that

$$g_1 = \mathrm{O}\left(\frac{\mu_o \lambda_1}{Re\Pi_i}\right) \quad \text{as} \quad Re \to \infty \,, \tag{3.52}$$

where again the Chapman relation has been assumed. An additional assumption that has been made here is that the wall-temperature gradient dH_w/ds is sufficiently small (at most O(1)) so that the associated term on the left side of equation (3.47) does not enter the balance to leading order. Consequently, the energy equation in the wall layer reduces to

$$\frac{\mu\rho}{\rho_o}\frac{\lambda_1}{Pr Re\Pi_i}\frac{\partial\theta^+}{\partial Y_\theta^+} + g_1\,\phi_1 = q_w \,, \tag{3.53}$$

to leading order. The auxiliary equation (3.50) may now be used to relate the heat flux q_w to the gauge functions λ_1 and g_1.

The study of Walker, Abbott, Scharnhorst and Weigand (1986) on the dynamics of wall-layer turbulence suggests that the normal scale in the energy equation is related to that in the momentum equation by a factor of the square root of the Prandtl number. Since Pr is assumed to be O(1) in this study, this scaling may be adopted without loss of generality, viz.

$$\Pi_i(s; Re, Pr, M_o) = \Delta_i(s; Re, M_o)/\sqrt{Pr} \,, \qquad Y_\theta^+ = \sqrt{Pr}\, Y^+ \quad , \tag{3.54}$$

and it is therefore convenient to select the wall normalization

$$\frac{\partial \theta^+(s,0)}{\partial Y_\theta^+} = \sqrt{Pr} \ . \tag{3.55}$$

As a result equation (3.50) reduces to

$$q_w(s) = \frac{\mu_w \rho_w}{\rho_o} \frac{\lambda_1}{Re \Delta_i} \ . \tag{3.56}$$

It follows from equations (3.52) and (3.56) that g_1 is $O(q_w)$, and without loss in generality, the leading order term for the turbulent heat flux may be selected as

$$g_1(s) = q_w(s) \ . \tag{3.57}$$

With the inner-layer length scale Δ_i specified by equation (3.43), the gauge function for the total enthalpy in the wall layer is found from equation (3.56), viz.

$$\lambda_1(s; Re, Pr, M_o) = \frac{q_w}{\rho_o u_{\tau o}} \ . \tag{3.58}$$

Consequently, the energy equation in the wall layer may now be written as

$$\phi_1 + \left(\frac{\mu \rho}{\mu_w \rho_w}\right) \frac{1}{\sqrt{Pr}} \frac{\partial \theta^+}{\partial Y_\theta^+} = 1 \tag{3.59}$$

to leading order.

At this point the leading order inner-layer expansions for both velocity and total enthalpy have been established and the outer-layer expansions will be considered next.

3.5 The Outer Layer

In the outer layer the streamwise velocity will be written as a small perturbation about the mainstream value in accordance with the concept of velocity defect in the outer layer. This was originally hypothesized by von Kármán (1930), who argued that the velocity in the outer layer is retarded due to the presence of the wall in a manner which is independent of the viscosity, but depends on the wall shear stress and a length scale characteristic of the normal distance over which the presence of the wall is felt. The outer-layer expansion for the longitudinal velocity is written in the form

$$u(s,Y) = U_e(s) + \Gamma_1(s;\ Re,M_o)\ U_1(s,\eta)\ + \cdots \tag{3.60}$$

where $U_1(s,\eta)$ is the defect velocity and η is the scaled normal coordinate

$$\eta\ =\ \frac{Y}{\Delta_o(s;\ Re,M_o)}\,. \tag{3.61}$$

Here Δ_o is the dimensionless outer region length scale and Γ_1 is the scale of the perturbed velocity in the outer region. Both Δ_o and Γ_1 are to be found subject to the requirements that $\Delta_o/\Delta_i \to \infty$ and $\Gamma_1 \to 0$ as $Re \to \infty$.

A stream function may be defined by

$$\frac{\partial\psi(s,Y)}{\partial Y} = ru\ ,\qquad \frac{\partial\psi(s,Y)}{\partial s} = -r\widetilde{v}\ , \tag{3.62}$$

which satisfies the continuity equation (3.13) identically. It follows from equation (3.60) that ψ has the expansion

$$\psi(s,Y) = \Delta_o(s;Re,M_o)\ r(s)\left[U_e(s)\eta + \Gamma_1(s;Re,M_o)F_1(s,\eta) + \cdots\right] \tag{3.63}$$

where $F_1(s,\eta)$ is defined as $U_1 = \partial F_1/\partial\eta$. The normal velocity function $\tilde{v}$ is given by

$$\tilde{v} = -\frac{1}{r}\left(\Delta_o r U_e\right)'\eta - \frac{\partial}{\partial s}\left(\Delta_o r \Gamma_1 F_1\right) + \cdots , \tag{3.64}$$

where the prime denotes differentiation with respect to s. It is assumed here (subject to verification) that $\partial\Gamma_1/\partial s$ is at most $O(\Gamma_1)$.

Consider next the expansion for the Reynolds stress σ in the outer region. The Reynolds stress vanishes at the mainstream and reaches a maximum near the overlap zone, and it is therefore reasonable to expect the Reynolds stress to have the same gauge function in the inner and outer regions and to enter the equations to leading order in both regions; for this reason the outer layer expansion for σ has a form similar to equation (3.30) and

$$\sigma(s,Y) = e_1(s;\ Re,M_o)\ \Sigma_1(s,\eta) + \cdots . \tag{3.65}$$

where the gauge function e_1 is given by equations (3.41) and (3.42) according to

$$e_1(s;\ Re,M_o) = \rho_o(s)\ u_{\tau o}^2(s;\ Re,M_o) . \tag{3.66}$$

In the outer region the total enthalpy is written as a perturbation about the mainstream value in accordance with experimental evidence according to

$$H(s,Y) = H_e + \Lambda_1(s;Re,Pr,M_o)\ \Theta_1(s,\eta) + \cdots , \tag{3.67}$$

where $\eta = Y/\Delta_o$ and Λ_1 is the order of the perturbed total temperature. Here because the major heat transfer processes occur near the surface and Pr is O(1), the thickness of the thermal layer is assumed to be comparable to that of the velocity boundary layer. The gauge function Λ_1 is to be found subject to $\Lambda_1 \to 0$ as $Re \to \infty$. The scale for the turbulent heat flux ϕ in the outer layer is selected as for the inner layer for reasons previously discussed and from equation (3.57)

$$\phi(s,Y) = q_w(s)\Phi_1(s,\eta) + \cdots . \tag{3.68}$$

Substituting equations (3.60) through (3.67) into (3.14) and neglecting terms of $O(\Gamma_1^2)$ yields

$$U_e\Gamma_1 \frac{\partial^2 F_1}{\partial s \partial \eta} + (U_e\Gamma_1)' \frac{\partial F_1}{\partial \eta} - \Gamma_1 \frac{(\Delta_o r U_e)'}{\Delta_o r}\, \eta \frac{\partial^2 F_1}{\partial \eta^2} = \frac{1}{M_e}\frac{dM_e}{\partial s} U_e^2 \left(\frac{\Lambda_1}{H_e}\Theta_1 - \alpha \frac{\Gamma_1}{U_e}\frac{\partial F_1}{\partial \eta} \right)$$

$$+ \frac{e_1}{\rho_o \Delta_o}\frac{\partial \Sigma_1}{\partial \eta} + \frac{\Gamma_1}{\rho_o \Delta_o^2}\frac{\partial}{\partial \eta}\left(\frac{\mu\rho}{\rho_o Re}\frac{\partial^2 F_1}{\partial \eta^2} \right), \tag{3.69}$$

where the primes denote total differentiation with respect to s. A balance between the Reynolds stress and the convective terms implies that

$$\Gamma_1 = O\left(\frac{e_1}{\rho_o U_e \Delta_o} \right). \tag{3.70}$$

In addition, it will be assumed (subject to verification) that the viscous stress is negligible to leading order, viz.

$$Re\Delta_o^2 \to \infty \quad \text{as} \quad Re \to \infty \,. \tag{3.71}$$

Effectively this is a statement that the thickness of the outer layer is greater than that of the laminar boundary layer, and this is a result which is well-substantiated by experiment (Cebeci and Smith, 1974; Fernholz, 1976). The momentum equation in the outer layer is therefore

$$U_e\Gamma_1 \frac{\partial^2 F_1}{\partial s \partial \eta} + (U_e\Gamma_1)' \frac{\partial F_1}{\partial \eta} - \Gamma_1 \frac{(\Delta_o r U_e)'}{\Delta_o r} \eta \frac{\partial^2 F_1}{\partial \eta^2}$$

$$= \frac{1}{M_e} \frac{dM_e}{\partial s} U_e^2 \left(\frac{\Lambda_1}{H_e}\Theta_1 - \alpha \frac{\Gamma_1}{U_e} \frac{\partial F_1}{\partial \eta} \right) + \frac{e_1}{\rho_o \Delta_o} \frac{\partial \Sigma_1}{\partial \eta} \tag{3.72}$$

to leading order. The outer asymptotic analysis is not complete until the outer velocity scale Γ_1 is formally specified, and the solution is matched to that in the wall layer. The question of matching will be taken up in the next section where it will be argued that a self-consistent structure can be obtained if the scale for the deflect velocity is the same as that for the velocity in the wall layer, viz.

$$\Gamma_1(s; Re, M_o) = u_{\tau o}(s;\ Re, M_o) = \sqrt{\frac{\rho_w}{\rho_o}}\, u_\tau(s;\ Re) \,. \tag{3.73}$$

Note that ρ_o and the outer length scale Δ_o are as yet unspecified.

The leading order energy equation is obtained next upon substituting the expansions for the total enthalpy (3.67), the turbulent heat flux (3.68), the velocities (3.60) and (3.64) into the governing equation (3.15) and retaining terms linear in Λ_1 and $u_{\tau o}$ to obtain

$$U_e\Lambda_1 \frac{\partial \Theta_1}{\partial s} + U_e\Lambda_1' \Theta_1 - \Lambda_1 \frac{(\Delta_o r U_e)'}{\Delta_o r} \eta \frac{\partial \Theta_1}{\partial \eta}$$

$$= \frac{g_1}{\rho_o \Delta_o} \frac{\partial \Phi_1}{\partial \eta} + \frac{\Lambda_1}{\rho_o \Delta_o^2} \frac{\partial}{\partial \eta} \left(\frac{\mu \rho}{\rho_o Pr Re} \frac{\partial \Theta_1}{\partial \eta} \right). \tag{3.74}$$

Here the primes represent differentiation with respect to s. Note that the term associated with viscous dissipation is second order in magnitude and is therefore negligible to leading order. It is assumed (subject to verification) that the convective terms balance the turbulent heat flux to leading order so that

$$\Lambda_1 = O\left(\frac{g_1}{\rho_o U_e \Delta_o} \right). \tag{3.75}$$

In view of equation (3.71), the conduction term on the right side of equation (3.74) is negligible and, consequently, the energy equation in the outer region is

$$U_e\Lambda_1 \frac{\partial \Theta_1}{\partial s} + U_e\Lambda_1'\Theta_1 - \Lambda_1 \frac{(\Delta_o r U_e)'}{\Delta_o r} \eta \frac{\partial \Theta_1}{\partial \eta} = \frac{g_1}{\rho_o \Delta_o} \frac{\partial \Phi_1}{\partial \eta} \tag{3.76}$$

to leading order. In a manner similar to the momentum equation, the scale of the defect for total enthalpy is selected equal to that in the inner layer according to

$$\Lambda_1(s; Re, Pr, M_o) = \frac{q_w}{\rho_o u_{\tau o}}. \tag{3.77}$$

The matching of the outer expansions to the wall layer will be considered next.

3.6 The Overlap Zone

In the asymptotic structure described thus far, there are two terms in the

outer expansion which must be matched to a single term in the wall layer; moreover, at this stage the Reynolds number (as well as the Mach number) dependence of the outer layer length scale is unknown. Further information or assumptions are required concerning the turbulent problem before it is possible to proceed further. Both Millikan (1939) and Gill (1968) have discussed a matching procedure where the quantity $n\partial u/\partial n$ is matched initially and a logarithmic dependence in the velocity profile is obtained. However, this type of argument in effect assumes the experimental result for the following reason. In any type of double layer, this type of matching condition is independent of the normal coordinate scale simply because the length scale on n for the inner or the outer layer cancels out. For an arbitrary velocity profile u, there are three possibilities for the behavior of $n(\partial u/\partial n)$ in the overlap region:

(1) $n(\partial u/\partial n) \to \infty$ in the matching region (e.g., $u \sim n^a$ for $a > 0$);

(2) $n(\partial u/\partial n) \to 0$ (e.g., $u \sim n^a$ or $u \sim n \log n$, $a < 0$);

(3) $n(\partial u/\partial n) \to$ c (if $u \sim \log n$).

There exists a wide variety of functional forms which will satisfy possibilities (1) and (2) but only the logarithm which satisfies possibility (3). Consequently, in selecting (3) Millikan (1939) essentially assumed the logarithmic dependence he was attempting to prove. It should be kept in mind that the difficulty is due to lack of complete information about turbulence terms, and if the functional form of both the Reynolds stress and turbulent heat flux terms were known, the matching can be carried out in the conventional way. Rather than assume a specific turbulence model, the approach that will be adopted here is to assume that the analog of the law of the wall for high speed compressible flow is given by

$$U^+(Y^+) \sim \frac{1}{\kappa(s)} \log Y^+ + C_i\,, \qquad \text{as} \qquad Y^+ \to \infty. \tag{3.78}$$

Here κ is the von Kármán constant and C_i is the inner log-law constant, usually assumed to have universal values of $\kappa = 0.41$ and $C_i = 5.0$; in general both κ and C_i could be functions of s, depending on the particular constitutive model adopted for the Reynolds stress. For the total enthalpy problem, the wall-layer function θ^+ is similar in form to U^+ and the following form is assumed

$$\theta^+(Y_\theta^+) \sim \frac{1}{\kappa_\theta} \log Y_\theta^+ + B_i \,, \qquad \text{as} \qquad Y_\theta^+ \to \infty. \tag{3.79}$$

Here κ_θ plays the role of the von Kármán constant in the velocity distribution, but both κ_θ and B_i are not constant in general and can depend on local flow condition (Weigand, 1978). Equations (3.78) and (3.79) constitute the two main assumptions of this study, i.e. that the wall layer profiles for velocity and total enthalpy are logarithmic in Y, the Howarth-Dorodnitsyn variable. It will now be demonstrated that a set of self-consistent asymptotic expansions can be developed. The test of the original hypotheses will be carried out subsequently through direct comparisons with experimental data.

To carry out the matching, an intermediate variable is first introduced by

$$\zeta = \frac{Y}{\Delta_{io}} \,, \qquad \Delta_o \gg \Delta_{io} \gg \Delta_i \quad \text{as} \quad Re \to \infty \,. \tag{3.80}$$

Thus, $\eta = Y/\Delta_o = (\Delta_{io}/\Delta_o)\zeta \to 0$ and $Y^+ = Y/\Delta_i = (\Delta_{io}/\Delta_i)\zeta \to \infty$ as $Re \to \infty$ with s and ζ fixed. It is easily seen that the same ζ can be used for the thermal problem for $Pr = O(1)$. In general, it is required that the slope of the profile and the profile itself merge smoothly in the overlap region according to the relations

$$\left[U_e + u_{\tau o}\frac{\partial F_1}{\partial \eta} + \cdots\right]_{\eta = \frac{\Delta_{io}}{\Delta_o}\zeta \to 0} = \left[u_{\tau o}\, U^+ + \cdots\right]_{Y^+ = \frac{\Delta_{io}}{\Delta_i}\zeta \to \infty} \tag{3.81}$$

and

$$\left[\frac{u_{\tau o}}{\Delta_o}\frac{\partial^2 F_1}{\partial \eta^2} + \cdots\right]_{\eta = \frac{\Delta_{io}}{\Delta_o}\zeta \to 0} = \left[\frac{u_{\tau o}}{\Delta_i}\frac{\partial U^+}{\partial Y^+} + \cdots\right]_{Y^+ = \frac{\Delta_{io}}{\Delta_i}\zeta \to \infty} \tag{3.82}$$

The limits in both relations are taken for the fixed s and ζ, and for $Re \to \infty$. Using equation (3.78), it is easily determined that the outer defect profile must behave logarithmically with

$$\frac{\partial F_1(s,\eta)}{\partial \eta} \sim \frac{1}{\kappa(s)} \log \eta + C_o \qquad \text{for} \qquad \eta \to 0\ , \tag{3.83}$$

where the outer log-law constant C_o is, in general, a function of s.

Matching the velocity using equations (3.78), (3.81) and (3.83) leads to match condition

$$\frac{U_e}{u_{\tau o}} = \frac{1}{\kappa(s)} \log\left(\frac{\Delta_o}{\Delta_i}\right) + C_i - C_o\ . \tag{3.84}$$

Introducing the inner region length scale Δ_i defined by equation (3.43), it follows that

$$\frac{U_e}{u_{\tau o}} = \frac{1}{\kappa(s)} \log\left(\frac{\rho_o^2}{\mu_w \rho_w} Re\ u_{\tau o}\Delta_o\right) + C_i - C_o\ , \tag{3.85}$$

which relates the velocity scale $u_{\tau o}$ to the unknown outer layer length scale Δ_o. It follows from equations (3.70) and (3.73) that Δ_o is $O(u_{\tau o}/U_e)$, and consequently from equation (3.85)

$$\frac{u_{\tau o}}{U_e} = O\left(\frac{1}{\log Re_o}\right) \quad \text{as} \quad Re \to \infty , \tag{3.86}$$

or, in terms of the friction velocity u_τ

$$\frac{u_\tau}{U_e} = O\left(\frac{\sqrt{\rho_w/\rho_o}}{\log Re_o}\right) \quad \text{as} \quad Re \to \infty . \tag{3.87}$$

This relation should be compared with the incompressible result $u_\tau/U_e = 0(1/\log Re)$. The Mach number and the heat transfer influence are contained in equation (3.87) where $Re_o = \rho_o^* U_{ref}^* L_{ref}^*/\mu_o^*$ is a Reynolds number with the fluid properties evaluated at the characteristic conditions. From equation (3.43), the inner length scale can also be shown to have the following order of magnitude:

$$\Delta_i = O\left(\frac{\log Re_o}{Re_o}\right) \quad \text{as} \quad Re \to \infty . \tag{3.88}$$

It is worthwhile to note that many of the assumptions leading to the inner and outer leading order equations of motion may now be verified. In the outer layer analysis the viscous stress was assumed negligible with $Re\Delta_o^2 \to \infty$ as $Re \to \infty$. With the order of outer length scale known, it is evident that

$$Re\Delta_o^2 = O\left(\frac{Re}{\log^2 Re_o}\right) \to \infty \quad \text{for} \quad Re \to \infty , \tag{3.89}$$

and so the assumed behavior is consistent. The other assumptions made during the course of the analysis may be easily justified similarly.

The matching for velocity is complete to leading order, and composite expansions can now be formed across the entire boundary layer according to the procedures discussed by Van Dyke (1975). The composite expansion is formed as the sum of the inner and outer layer expansions and then subtracting the common part. The common part is defined to be either the limiting form of the inner layer asymptotic expansion $Y^+ \to \infty$, or equivalently, the limiting form of the outer layer asymptotic expansion as $\eta \to 0$. The composite leading order expansion for the velocity profile is formed using equations (3.18), (3.60), (3.78), (3.83) and (3.84), and it follows

$$u_{com} = u_{\tau o}\left[\frac{\partial F_1}{\partial \eta}(s,\eta) + U^+(s,Y^+) - \frac{1}{\kappa(s)}\log\eta - C_o(s)\right]. \tag{3.90}$$

The inner layer and outer layer Reynolds-stress expansions are matched according to the relation

$$\left[\rho_o u_{\tau o}^2 \Sigma_1 + \cdots\right]_{\eta = \frac{\Delta_{io}}{\Delta_o}\zeta \to 0} = \left[\rho_w u_{\tau o}^2 \sigma_1 + \cdots\right]_{Y^+ = \frac{\Delta_{io}}{\Delta_i}\zeta \to \infty}. \tag{3.91}$$

Note that $\rho_o u_{\tau o}^2 = \rho_w u_\tau^2$ and using equations (3.46) and (3.78), it follows that the wall layer Reynolds-stress function σ_1 behaves according to

$$\sigma_1(s,Y^+) \sim 1 + \cdots \quad \text{for} \quad Y^+ \to \infty \tag{3.92}$$

and furthermore from equation (3.91), it follows that

$$\Sigma_1(s,\eta) \sim 1 + \cdots \quad \text{for} \quad \eta \to 0 \ . \tag{3.93}$$

Matching for the energy equations is carried out in a similar manner by requiring the total enthalpy and its slope to merge smoothly in the overlap region. A logarithmic dependence also occurs for the outer total enthalpy according to

$$\Theta_1(s,\eta) \sim \frac{1}{\kappa_\theta(s)} \log \eta + B_o \quad \text{for} \quad \eta \to 0 \ , \tag{3.94}$$

where B_o is, in general, a function of s. The actual streamwise distribution of κ_θ and B_o is strongly influenced by the outer-region flow conditions; there is no universally agreed upon constant value of κ_θ, and careful comparisons (Weigand, 1978) with measured temperature profile data in low-speed subsonic boundary layers show that κ_θ depends on local flow conditions. A means to evaluate κ_θ will be developed subsequently in §5.

Matching of the total enthalpy leads to the matching condition

$$\frac{(H_e - H_w)\rho_o u_{\tau o}}{q_w} = \frac{1}{\kappa_\theta(s)} \log\left(\frac{\Pi_o}{\Pi_i}\right) + B_i - B_o \ , \tag{3.95}$$

which relates the dimensionless heat flux q_w to u_τ and the outer-layer length scale. Recall that the outer length scale Π_o has been taken to be Δ_o while the inner scale Π_i is selected with $\Pi_i = \Delta_i\sqrt{Pr}$; thus equation (3.95) may be written

$$\frac{(H_e - H_w)\rho_o u_{\tau o}}{q_w} = \frac{1}{\kappa_\theta(s)} \log\left(\frac{\rho_o^2}{\mu_w \rho_w} Re u_{\tau o} \Delta_o \sqrt{Pr}\right) + B_i - B_o \ . \tag{3.96}$$

It follows from this relation and the velocity matching condition (3.85) that if H_w

is significantly different to H_e due to the heat transfer between the flow and the surface

$$\frac{q_w}{\rho_o U_e H_e} = \mathrm{O}\left(\frac{u_{\tau o}^2}{U_e^2}\right) \quad \text{as} \quad Re \to \infty \,. \tag{3.97}$$

The matching is now complete for the energy equation and a composite profile H_{com} can be formed from the inner and outer total enthalpy expansions according to

$$H_{com} = H_w + \frac{q_w}{\rho_o u_{\tau o}}\left[\Theta_1(s,\eta) + \theta^+(s,Y^+) - \frac{1}{\kappa_\theta(s)}\log\eta - B_o(s)\right]. \tag{3.98}$$

It may be noted that the assumptions made in arriving at this set of asymptotic expansions may easily be verified using equation (3.97). For example, in the inner-layer analysis the total enthalpy scale λ_1/H_e was assumed to be $\mathrm{O}(u_{\tau o}/U_e)$; now it is easily verified using equation (3.58) to obtain

$$\lambda_1/H_e = \frac{q_w}{\rho_o u_{\tau o} H_e} = \mathrm{O}\left(\frac{u_{\tau o}}{U_e}\right). \tag{3.99}$$

The matching of the turbulent product terms is straightforward. By using equations (3.53) and (3.79), the limiting form of inner turbulence heat flux function ϕ_1 is shown to be

$$\phi_1(s,Y^+) \sim 1 + \cdots \quad \text{for} \quad Y^+ \to \infty \,, \tag{3.100}$$

and the outer turbulence function Φ_1 must then have

$$\Phi_1(s,\eta) \sim 1 + \cdots \quad \text{for} \quad \eta \to 0 \,. \tag{3.101}$$

3.7 Summary of the Asymptotic Expansions

In the previous three sections asymptotic expansions have been developed for velocity and total enthalpy profiles in the compressible turbulent boundary layer. The leading order results can be summarized as follows.

In the inner region, the velocity u and total enthalpy H, Reynolds stress σ and turbulent product ϕ may be expanded to leading order as

$$\frac{u}{U_e}(s,Y) = u_* U^+(s,Y^+) + \cdots \,,$$

$$\frac{H}{H_e}(s,Y) = \frac{H_w}{H_e}(s) + q_* \theta^+(s,Y_\theta^+) + \cdots \,. \tag{3.102}$$

$$\sigma(s,Y) = \rho_o u_{\tau o}^2 \sigma_1(s,Y^+) + \cdots \,, \quad \phi(s,Y) = q_w \phi_1(s,Y_\theta^+) + \cdots \,. \tag{3.103}$$

Here u_* and q_* are normalized velocity and total enthalpy scales defined as

$$u_* = \frac{u_{\tau o}}{U_e} \,, \qquad q_* = \frac{q_w}{\rho_o u_{\tau o} H_e} \,, \tag{3.104}$$

with $u_{\tau o} = \sqrt{\rho_w/\rho_o}\; u_\tau$, and u_τ is the dimensionless friction velocity at the wall. These scales are defined in terms of a characteristic reference density ρ_o. The scaled wall layer variables Y^+ and Y_θ^+ are

$$Y^+ = \frac{Y}{\Delta_i} \,, \qquad Y_\theta^+ = \frac{\sqrt{Pr}\, Y}{\Delta_i} \,, \tag{3.105}$$

with the wall layer length scale defined by

$$\Delta_i = \frac{\mu_w \rho_w}{\rho_o^2 Re u_{\tau o}} \,. \tag{3.106}$$

The velocity and total enthalpy functions U^+ and θ^+ satisfy the following leading order equations in the wall layer:

$$\sigma_1 + \left(\frac{\mu\rho}{\mu_w\rho_w}\right)\frac{\partial U^+}{\partial Y^+} = 1 \,, \quad \phi_1 + \left(\frac{\mu\rho}{\mu_w\rho_w}\right)\frac{1}{\sqrt{Pr}}\frac{\partial \theta^+}{\partial Y_\theta^+} = 1 \,, \tag{3.107}$$

and have the following asymptotic behavior:

$$U^+(Y^+) \sim \frac{1}{\kappa(s)} \log Y^+ + C_i \,,$$

$$\theta^+(Y_\theta^+) \sim \frac{1}{\kappa_\theta} \log Y_\theta^+ + B_i \qquad \text{as} \qquad Y^+, Y_\theta^+ \to \infty \tag{3.108}$$

and

$$\sigma_1(s, Y^+) \sim 1 + \cdots \,, \qquad \phi_1(s, Y^+) \sim 1 \qquad \text{as} \qquad Y^+ \to \infty \,. \tag{3.109}$$

The asymptotic expansions for velocity and total enthalpy in the outer layer have the following defect forms

$$\frac{u}{U_e}(s, Y) = 1 + u_* \frac{\partial F_1}{\partial \eta}(s, \eta) + \cdots \,, \quad \frac{H}{H_e}(s, Y) = 1 + q_* \Theta_1(s, \eta) + \cdots \,, \tag{3.110}$$

$$\sigma(s, Y) = \rho_o u_{\tau o}^2 \Sigma_1(s, \eta) + \cdots \,, \quad \phi(s, Y) = q_w \Phi_1(s, \eta) + \cdots \,, \tag{3.111}$$

where the scaled outer region variable $\eta = Y/\Delta_o$. The velocity and total temperature functions $\partial F_1/\partial \eta$ and Θ_1 satisfy the equations

$$\frac{\partial^2 F_1}{\partial s \partial \eta} + \frac{u_*'}{u_*}\frac{\partial F_1}{\partial \eta} - \frac{(\Delta_o r U_e)'}{\Delta_o r U_e}\eta\frac{\partial^2 F_1}{\partial \eta^2} = \frac{1}{M_e}\frac{dM_e}{\partial s}\left(\frac{q_*}{u_*}\Theta_1 - 2\frac{\partial F_1}{\partial \eta}\right) + \frac{u_*}{\Delta_o}\frac{\partial \Sigma_1}{\partial \eta} \ . \quad (3.112)$$

and

$$\frac{\partial \Theta_1}{\partial s} + \frac{q_*'}{q_*}\Theta_1 - \frac{(\Delta_o r U_e)'}{\Delta_o r U_e}\eta\frac{\partial \Theta_1}{\partial \eta} = \frac{\mu_w \rho_w u_*}{\mu_o \rho_o \Delta_o}\frac{\partial \Phi_1}{\partial \eta} \ , \quad (3.113)$$

to leading order and have the asymptotic behavior

$$\frac{\partial F_1(s,\eta)}{\partial \eta} \sim \frac{1}{\kappa(s)}\log \eta + C_o, \ \ \Theta_1(s,\eta) \sim \frac{1}{\kappa_\theta(s)}\log \eta + B_o \ \text{ for } \ \eta \to 0 \ . \quad (3.114)$$

$$\Sigma_1(s,\eta) \sim 1 + \cdots, \qquad \Phi_1(s,\eta) \sim 1 + \cdots \qquad \text{for} \qquad \eta \to 0 \ . \quad (3.115)$$

In the above equations, primes denote total differentiation with respect to s.

Finally the velocity and the total enthalpy matching conditions are given by:

$$\frac{U_e}{u_{\tau o}} = \frac{1}{\kappa(s)}\log\left(\frac{\rho_o^2}{\mu_w \rho_w} Re u_{\tau o}\Delta_o\right) + C_i - C_o \ . \quad (3.116)$$

$$\frac{(H_e - H_w)\rho_o u_{\tau o}}{q_w} = \frac{1}{\kappa_\theta(s)}\log\left(\frac{\rho_o^2}{\mu_w \rho_w} Re u_{\tau o}\Delta_o\sqrt{Pr}\right) + B_i - B_o \ . \quad (3.117)$$

The asymptotic expansions summarized above have been obtained using perturbation methods applied to the time-mean, two-dimensional or axisymmetric compressible turbulent boundary layer problem. An important aspect is that the

leading order boundary-layer structure was determined without recourse to specific turbulence closure models. The leading order Reynolds number dependence in the velocity, total enthalpy, and length scales has been established in the limit of large Reynolds number. Actual solutions in each layer are not possible until a functional form is developed for the unknown turbulence terms, and this aspect is taken up next.

4. THE WALL LAYER MODELS FOR COMPRESSIBLE TURBULENT BOUNDARY LAYERS

4.1 Introduction

As a result of over two decades of experimental work, it has been possible to identify a repeatable and cyclic process that occurs in low-speed turbulent flows near walls; in this process, the turbulent wall layer is observed to grow slowly over a period of time and then interact strongly with the outer flow in an event usually referred to as bursting. These events are known to dominate the dynamics of the wall-layer flow. If observations are carried out over a fixed area of the wall, the wall layer will be seen to be in a quiescent state for a large majority of the total observation time. During this quiescent period, the wall-layer streaks can be observed when a visualization medium such as dye or hydrogen bubbles is introduced into the near-wall flow in a water tunnel. These streaks are a result of the tendency of the hydrogen bubbles to collect in the wall layer near vertical surfaces across which there is no relative spanwise motion and where the motion in the cross flow plane is away from the wall. The streaks are relatively stable and separated by an average spanwise distance of 100 ν/u_τ (Willmarth, 1975 and Smith, 1983), where ν is the kinematic viscosity and u_τ is the local mean friction velocity; the streaks are elongated in the streamwise direction and typically may have a length on the order of 1000 ν/u_τ. The streamwise velocity in the vicinity of the streaks is generally less than that of the mean profile and thus the terminology "low-speed streaks" is common. The cause of the wall-layer streaks is not generally agreed upon but it is reasonable to suppose that the streaks are the signature of

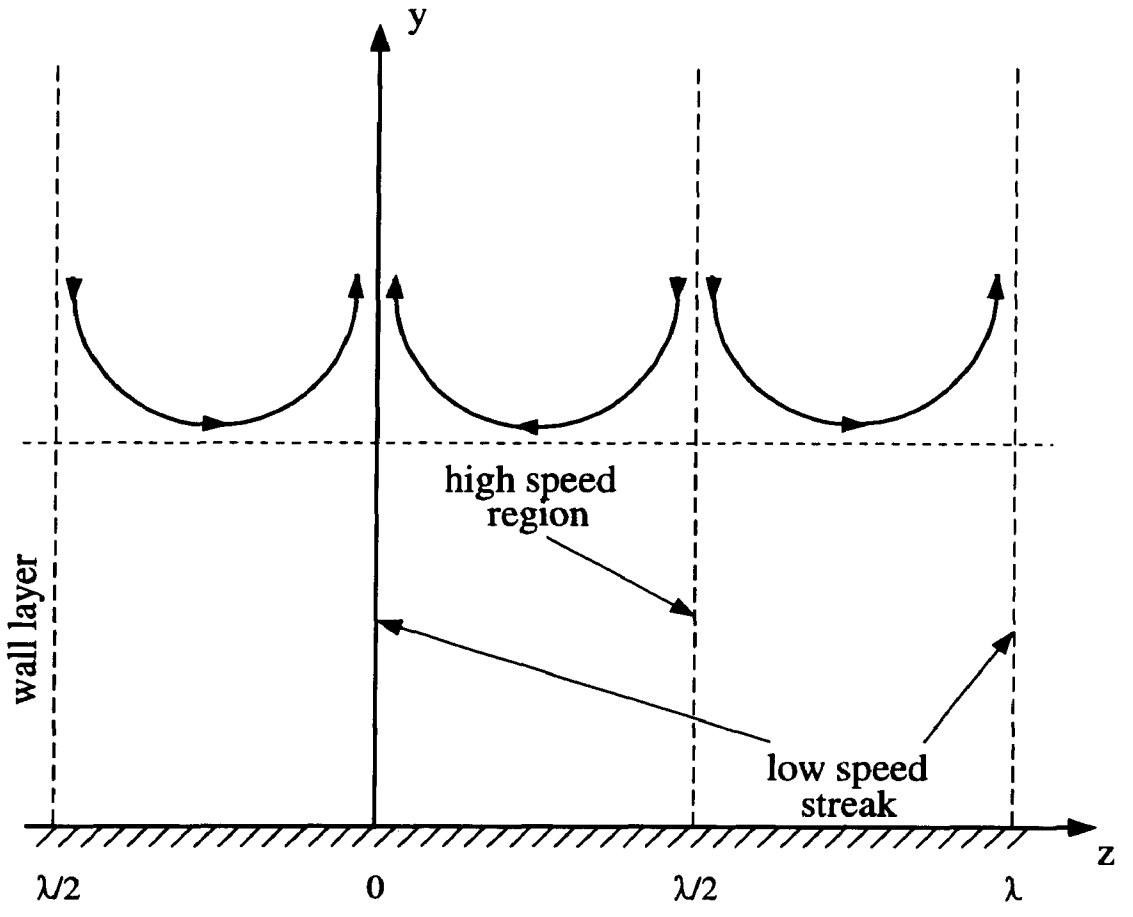

Figure 4.1 Schematic diagram of average wall-layer structure during the quiescent state.

vortices which are being convected over the wall within the boundary layer but above the streaks (Smith et al., 1991).

While the observed portion of the wall layer is in the quiescent state, the time-dependent flow in the turbulent boundary layer may be considered to have a distinct double structure; that is, there is a well defined inner wall layer and an outer layer. The wall layer is very thin with respect to the whole boundary layer; furthermore, at this stage, the wall layer only responds passively to events which are taking place in the outer layer. In other words, there are no strong interactions between the inner and outer regions during the quiescent period. The quiescent period is generally observed to initiate with the "sweep" which is characterized by a penetration of high speed fluid from the outer region of the boundary layer toward the wall; in the latter stages of the sweep event, the wall-layer streaks appear. At this stage the wall layer is very thin. There then ensues a relatively long quiescent in which there are no major interactions with the outer flow and the wall layer continuously thickens due to viscous diffusion.

The quiescent period is observed to terminate at isolated spanwise and streamwise locations in the bursting process. Eventually the organized motion of the quiescent period is interrupted by a rapid and violent ejection of fluid into the outer layer. The ejection process is observed to originate deep within the wall layer and culminate in an inviscid-viscous interaction with the outer layer. As the bursting fluid leaves the wall layer, it is followed almost simultaneously by an inrush of fluid from the outer layer into the inner layer; this event has been called the sweep by Corino and Brodkey (1969). In the latter stages of the sweep event the streak pattern near the wall reappears but now at different spanwise locations

and the quiescent flow behavior begins a new cycle. Over a long period of time the distribution of the streaks near the wall appears to be essentially random; of course, for a two-dimensional time-mean flow this is the expected mathematical behavior.

At present the cause of the streaks and the bursts is still regarded as controversial. It was demonstrated by Wallace, Eckelmann and Brodkey (1972) that the vast majority of the contribution to the Reynolds stress occurs during bursting for both the inner and the outer layer. Clearly, to arrive at a theoretical model over the entire boundary layer for the Reynolds stress, the dynamics of this bursting process must be understood. An early explanation for the wall layer breakdown is that the breakup of the quiescent growth and subsequent burst are induced by the passage of a vorticular disturbance (Walker, 1977). There are various studies of the large-scale motions in the outer part of the boundary layer. The observations by Head and Bandyopadhyay (1981) are of particular note. These authors used flow visualization to study a zero-pressure-gradient boundary layer over a wide range of Reynolds numbers based on the momentum thickness ($500 < Re_\theta < 17500$). They found clear evidence of hairpin-type vortices that had been assumed to have a connection with the near-wall bursting process (see, for example, Kline et al., 1967, and Offen and Kline, 1974) may extend throughout the entire boundary layer. In the visualization studies, the layer appeared to contain hairpin eddies attached to the wall region and inclined to the wall at a characteristic angle of $40^\circ - 50^\circ$. Recently a comprehensive model of the turbulent boundary layer has been given by Smith et al. (1991), in which the main observed features of the time-dependent flow have been explained in terms of the motion of hairpin vortices and their influence on each other and the near-wall flow. In this

model the wall layer streaks are attributed to the motion of hairpin vortices which are convected above the wall layer and induce an upwelling; the streaks are described as the passive trails of a moving vortex in the near-wall flow. The bursting process is described as an inviscid-viscous interaction between the wall layer and the outer inviscid region which is also induced by the motion of hairpin vortices. It is argued that the hairpin vortex induces an adverse pressure gradient on the wall layer flow and, after a period of time, separation of the wall layer is provoked locally. The separation culminates in a strong localized interaction in which wall-layer vorticity is sharply compressed in the streamwise direction and abruptly thrown into the outer portion of the boundary layer. As indicated by the model of Smith et al. (1991), as well as other considerations and measurements, the principal lasting contributions to the Reynolds stress are made during the brief periods when localized breakdowns of the wall layer occur. The nature of the interaction when this occurs is very complex and well beyond the scope of modern computational methods. On the other hand, the wall layer is in a passive order state for a majority of any total observation time, and this suggests an alternative strategy for turbulence modeling for the wall layer. In this approach (Walker and Abbott, 1977; Walker et al., 1989), the idea is to focus on the development of the mean velocity profile in the wall layer. In view of the relatively long duration of the quiescent state, the vast majority of contributions to the mean profile are made during this period when the wall-layer flow is reasonably well-ordered and when no strong interactions occur between the wall layer and the outer layer. Another important piece of experimental information used in the modeling is related to the spanwise spacing of the streaks. Experimental evidence (at least in a limited Reynolds number range) indicates that the streaks possess an average dimensionless

spanwise spacing of $\lambda^+ = \lambda u_\tau Re/\nu = 100$ where λ is the mean streak spacing (Smith and Metzler, 1983). Walker and Abbott (1977) have cataloged values of the average streak spacing over the existing experimental range of Reynolds numbers; unfortunately there is still insufficient data for large Reynolds numbers to definitively determine a trend. However, it is clear that either $\lambda^+ \rightarrow \infty$ or a large positive constant as $Re \rightarrow \infty$. It is also evident that $\overline{\lambda}$ constitutes the appropriate length scale in the spanwise direction for the time-dependent wall-layer flow. This modeling approach has been successful for incompressible flow and extensive comparisons with data (Walker and Scharnhorst, 1977; Walker et al., 1989) indicate that the "unsteady wall layer model" represents measured data very well. A formula for the Reynolds stress can then be recovered from the mean momentum equation. A similar modeling approach for thermal transport in low-speed flows was subsequently carried out by Weigand (1978), and excellent agreement was obtained with measured temperature profile data. In this chapter, the extension of this modeling approach to high-speed compressible flow will be considered.

4.2 Coherent Structures in High-Speed Flows

For incompressible flow, the unsteady wall layer model is based strongly on the observed coherent structure of the near wall flow. The first question that must be addressed is whether such structure is present in compressible flows and whether the model discussed by Smith et al. (1991) is appropriate in the compressible wall layer. Most of the common flow visualization methods, such as dye or hydrogen bubbles used in water tunnels, are not applicable to a supersonic boundary layer.

However, coherent structures can also be detected indirectly by using, for example, arrays of hot wires and wall pressure transducers to record the disturbances provoked by motions such as hairpin vortices. Most recent work has been confined to incompressible boundary-layer flows for a variety of technical reasons (see, for example, Robinson, 1985) and has indicated the presence of a complex hierarchy of organized motions. Combining this information with flow visualization results, it has been possible to put together a general descriptive account of the turbulent boundary layers (see, for example, Smith et al., 1991), even though a variety of questions concerning the causes and effects of the observed phenomena are still controversial.

There is evidence for the presence of coherent motions in supersonic flows, and this should be expected since the dynamical model described by Smith et al. (1991) should carry over in some form to compressible flows. The Schlieren photographs of Deckker and Weekes (1976) and Deckker (1980) show large-scale motions with boundaries inclined at about 45° to the wall in turbulent boundary layers at Mach numbers of 1.84 and 2.58 (see van Dyke 1982). By and large, however, quantitative study of turbulent boundary layer structure in compressible flows is relatively rare. Owen and Horstman (1972) have carried out extensive space-time correlation measurements in a hypersonic boundary layer and focused their main attention on mean convection velocities. More recently, Robinson (1986) has reported average measurements for the angle structures made with the surface for a supersonic flow, and these were found to bear a resemblance to those found in incompressible flows. Spina and Smits (1986) attempted to provide some of the first measurements of instantaneous structure in compressible flow, and their

work also suggests the existence of organized structures in a boundary layer. They evaluated instantaneous angle structures made with the wall, as well as the average structure-angle; these measurements produced results which are consistent with those associated with distributions of hairpin vortex loops found in incompressible flows. It was observed that near the wall, the majority of the structures make an angle below 45° with the wall, with the most populated state being $15° - 30°$. Away from the wall ($y/\delta = 0.3$), the angular distribution shifts towards 45°. At the edge of the boundary layer ($y/\delta = 0.9$), the population with angles between 75°-90° has increased dramatically and becomes dominant. These trends are consistent with what is known concerning the dynamics of hairpin vortices in a shear flow (see, for example, Head and Bandyopadhyay, 1981, Hon and Walker, 1991, Smith et al., 1991). Hairpins of all sizes populate the boundary layer. A typical hairpin vortex (see, for example, Smith, 1991, Smith et al., 1991) consists of elongated legs near the surface inclined at shallow angles to the wall, a central portion inclined at angles in the vicinity of 45°, and a head which bends back in the shear flow reaching angles close to 90°. Therefore, measurements of Spina and Smits (1986) are fairly consistent with similar structural observations in incompressible flow, and it appears that the effect of compressibility on the basic character of the structure is small.

In addition to the experimental evidence, Morkovin's (1962) hypothesis would also support these ideas. The strong correlation between temperature and velocity fluctuations shown in equation (1.25) is often used to imply that the density field has no more effect than a passive scalar and plays no role in the dynamics of turbulent mixing. Morkovin (1962) concluded on this basis that the

dynamics of compressible turbulent shear layers should correspond to the incompressible pattern closely, as long as the fluctuating Mach numbers remain small (i.e. the Mach number is moderate). It is worthwhile to point out that this does not imply that the turbulence quantities in incompressible and compressible flows have closely comparable distributions since the density will have at least a parametric influence on the turbulence shear stress, even if density fluctuations are negligible. Laderman and Demetriades (1979), for example, interpreted Morkovin's (1962) hypothesis to mean that the turbulent shear distribution across the boundary layer, when expressed in the form τ/τ_w, should be invariant with Mach number and correspond to the incompressible shear stress profile. In fact, Smits and Spina (1989) found from their data in the low supersonic range ($1.7 < M_e < 4.6$) that the Mach number dependence for the turbulence intensity $\sqrt{\overline{u'^2}}$ was no longer evident when the data were normalized by a velocity scale derived using the wall shear stress and the local density (i.e., $\sqrt{\tau_w/\rho}$). However, the situation in regards to proper scaling of the turbulence quantities is far from clear for compressible boundary layers. Most attempts to determine similarity with Mach number for turbulence terms are controversial. It may be evident that even though the pattern of turbulence motions appears to be similar to the incompressible case, density gradients in a compressible shear layer could possibly affect hairpin vortex motion. From a mathematical standpoint, it would not be surprising to find differences between compressible and incompressible boundary layers, since the vorticity transport equation describes the transport of vorticity per unit mass, rather than the absolute vorticity. Density gradients will therefore affect the vorticity dynamics to some extent, and the extent of this influence will clearly vary with Mach number and heat transfer rate.

Studies of unsteady compressible wall-layer structure would seem to be desirable although it must be admitted that the experimental difficulties are formidable. In this thesis it has been assumed that the wall-layer mean equations can be converted into a corresponding constant property problem through the Howarth-Dorodnitsyn transformation. Here this same transformation will be used to examine the unsteady compressible wall-layer flow, and it will be shown that to the leading order the wall layer problem is a corresponding incompressible form. The analysis closely follows that in low-speed flows described by Weigand (1978) and Walker et al. (1989). It is worthwhile to note that the physical basis of the use of the compressibility transformation is the belief that a similar coherent behavior occurs in the compressible wall layer as has been thoroughly documented for incompressible flows. Thus the compressible wall layer is expected to be in the quiescent state for a majority of any total observation time with localized breakdowns occurring only intermittently at isolated locations. Thus, the time-dependent flow in the wall layer is regarded as essentially ordered and stratified most of the time.

4.3 Unsteady Wall Layer Model for Compressible Flows

In this section the full Navier-Stokes equations will be investigated during the quiescent period and in limit of large Reynolds number with the overall objective of considering the nature of the flow evolution during a typical quiescent period. A complete solution for the wall-layer flow is not expected; instead, representative solutions will be considered with the main objective being to obtain

realistic expression for the time-mean velocity and total enthalpy distributions within the wall layer.

The main ideas inherent in the analysis are strongly motivated by experiment of incompressible flows and are as follows. For a fixed and small area of the surface, define T_q as the average period during which the wall layer is in quiescent state; during this period the wall layer is intact, the wall layer length scale associated with the normal coordinate is therefore $O(\mu_o/\rho_o u_{\tau o} Re)$ as discussed in §3.4. Note that as $M_e \to 0$ this scaling reduces to its incompressible expression of $O(\nu/u_\tau Re)$. Further, suppose that the average time associated with a localized breakdown corresponding to burst-sweep sequence is T_b. The experiments of Kline et al. (1967) and Offen and Kline (1974) suggest that the period over which a burst takes place is considerably smaller than the time scale associated with the quiescent period (i.e. $T_b \ll T_q$). Therefore, the actual average time period of a cycle T_c should be close to the quiescent time period T_q, and Walker and Scharnhorst (1977) and Walker et al. (1989) argue that the ratio T_q/T_b should become large as $Re \to \infty$. Consequently, consideration of representative time-dependent motions in the wall layer during the quiescent period and subsequent time averaging should produce a reasonable model (the unsteady wall layer model) for the mean profiles. The same argument should hold for compressible flows if the influence of density gradient to the turbulence motion is only parametric.

Another important assumption associated with the unsteady wall layer model is that the average spanwise spacing λ is such that the dimensionless spacing $\lambda^+ = \lambda u_\tau Re/\nu$ is large as $Re \to \infty$. There are two potential problems in extending the analysis to the compressible regime. First it is not well established from

experiment that wall layer streaks exist in compressible flow. However, the model of Smith et al. (1991), as well as Morkovin's (1962) hypothesis, would suggest that it is reasonable to assume wall-layer streaks are present. A second question then concerns the appropriate length scale that could characterize the spanwise spacing. In particular, what local parameters should be used in defining λ^+ in an environment where the fluid properties such as density ρ and viscosity μ vary across the boundary layer? The answers to these questions will remain partially unresolved until additional experimental work is carried out in the supersonic regime. For the present analysis, the reference temperature concept will be utilized again and a dimensionless mean streak spacing defined by $\lambda^+ = \lambda\,(\rho_o^2 u_{\tau o} Re/\mu_w \rho_w)$. Note that this expression reduces to the incompressible form as $M_e \to 0$. Furthermore, it is assumed that λ^+ is large in the limit $Re \to \infty$ as in the incompressible case.

Consider now a nominally steady two-dimensional boundary layer and let $(x,\ y,\ z)$ measure distances in the streamwise, normal and spanwise directions respectively with corresponding instantaneous velocities $(\tilde{u}\,,\ \tilde{v}\,,\ \tilde{w})$. Note that here x and y (instead of s and n in the previous chapters) are used to denote the streamwise and normal directions. Since the ratio of wall-layer to boundary layer thickness $\delta_i/\delta \to 0$ in the limit of large Reynolds number (cf. §3.4), and since in addition it has been assumed that $\delta \ll r(s)$, where r is the radius of revolution for an axisymmetric body, it is easily inferred that $r/\delta_i \to \infty$, and it follows that the wall layer can be simply treated as a three-dimensional problem along an essentially flat surface. Therefore it is convenient to simply use conventional notations in the study of wall-layer modeling that apply to either the two-

dimensional or axisymmetric cases.

During a typical quiescent period, the wall layer is well-defined and the low-speed streaks are present. It is well established from experiment that the turbulent intensities $\overline{u'^2}$, $\overline{v'^2}$, $\overline{w'^2}$ as well as the Reynolds stress $-\overline{v'u'}$ are $O(\tau_w/\rho)$ in the wall layer, and this suggests that the velocity scale obtained in §3.4 is also appropriate for the instantaneous velocities during the quiescent period. First define the scaled velocity components in the streamwise and spanwise directions by

$$\tilde{u}^{+} = \tilde{u}/u_{\tau o}\,, \qquad \tilde{w}^{+} = \tilde{w}/u_{\tau o}\,. \tag{4.1}$$

Note that the tilde is used to denote instantaneous quantities here and throughout this study. It is also assumed that the length scale associated with typical time-dependent motions in the normal direction is comparable to the mean wall-layer thickness. At the same time, variations in the streamwise direction are considered to be less important, in view of the long length of the streaks relative to their spacing. The characteristic length in the spanwise direction is known to be λ and therefore the following scaled coordinates are introduced:

$$x^{+} = \frac{x}{L_x}\,, \quad y^{+} = \frac{y}{(\mu_w\rho_w/\rho_o^2 u_{\tau o} Re)}\,, \quad z^{+} = \frac{z}{\lambda} = \frac{z}{\lambda^{+}(\mu_w\rho_w/\rho_o^2 u_{\tau o} Re)}\,. \tag{4.2}$$

Here L_x is a characteristic length in the x direction which is not known but is expected to be associated with the streamwise extent of the outer-region structures responsible for the creation and evolution of the wall-layer streaks; recent evidence

(Smith et al., 1991) indicates that these are convected hairpin vortices. In any event it is assumed, in accordance with experiment, that $L_x \gg \mu_w \rho_w / \rho_o^2 u_{\tau o} Re$, the normal direction length scale. It then follows from the continuity equation (1.13) and equations (4.1) and (4.2) that the scaled normal velocity should be defined by

$$\tilde{v}^{+} = \tilde{v}\,(\lambda^{+}/u_{\tau o})\,; \tag{4.3}$$

here the balance is between the terms $\partial(\rho\tilde{v})/\partial y$ and $\partial(\rho\tilde{w})/\partial z$ in the continuity equation. The proper scaling in time follows from a balance between the viscous diffusion and unsteady terms in the streamwise momentum equation and

$$t^{+} = \frac{t}{(\mu_w \rho_w / \rho_o^2 u_{\tau o}^2 Re)}\,. \tag{4.4}$$

Finally the pressure may be written in a general form as

$$p = p_e(x) + \rho_o u_{\tau o}^2 \left\{ \frac{Re \rho_o^2 u_{\tau o}}{\mu_w \rho_w} p_o(x^{+}, t^{+}) + \frac{1}{\lambda^{+}} p_1(x^{+}, y^{+}, z^{+}, t^{+}) + \cdots \right\}, \tag{4.5}$$

where $p_e(x)$ is the steady mainstream pressure distribution outside the boundary layer. The term p_1 is associated with the relatively organized motion between the streaks during the quiescent period. The pressure p_o is an unsteady pressure variation which is impressed across the wall layer during the quiescent period and which may be thought of as due to the motion of convected disturbances in the outer region (such as hairpin vortices); it is easily verified, upon substitution in the

Navier-Stokes equations, that p_o is independent of y^+ and z^+ as indicated in equation (4.5). In general, the p_o term in the x-momentum equation is not known and potentially poses a problem. The data of Emmerling (1973) provides evidence of intense localized centers of pressure within the turbulent boundary layer and large fluctuating pressure gradients may not be ruled out entirely. However, it is believed that the observed large pressure fluctuations are probably associated with the bursting process and localized wall-layer breakdowns and, therefore, probably do not have significant influence during quiescent periods. Walker and Abbott (1977) have suggested that if such a large pressure fluctuation is convected into the region under consideration and above the wall layer, then a rapid breakdown of quiescent period might be expected. On the other hand, small scale pressure gradient fluctuations are possible if they are truly random with a zero time-mean average. It may be concluded from the observed well-ordered motion in the wall layer during the quiescent period that it is not reasonable to expect that small scale unorganized pressure fluctuations dominate the wall layer flow. Thus, it is not necessary to consider motions arising from small scale pressure fluctuations at the edge of the wall layer since in the end such motions will not produce lasting contributions to the mean profile.

Throughout this analysis the density ρ is viewed as a function whose distribution is the same as the mean. Thus, the density is akin to a more passive scalar whose fluctuations play no important role in the dynamics of leading-order turbulence motion. This is in line with the view that the compressible wall layer is essentially stably stratified during the quiescent state. Two simplifications result from this assumption. First, the momentum and thermal boundary-layer problems

decouple, and second, the time derivative of density does not appear in the governing equations. Upon substitution of equations (4.1) to (4.5) into the unsteady Navier-Stokes equations, the following equations governing the wall layer are obtained

$$\rho \frac{\partial \tilde{u}^+}{\partial t^+} + \frac{\rho \tilde{v}^+}{\lambda^+} \frac{\partial \tilde{u}^+}{\partial y^+} + \frac{\rho \tilde{w}^+}{\lambda^+} \frac{\partial \tilde{u}^+}{\partial z^+} = -p^+ + \frac{\partial}{\partial y^+}\left(\frac{\rho_o^2 \mu}{\mu_w \rho_w} \frac{\partial \tilde{u}^+}{\partial y^+}\right)$$

$$+ \frac{1}{\lambda^{+2}} \frac{\partial}{\partial z^+}\left(\frac{\rho_o^2 \mu}{\mu_w \rho_w} \frac{\partial \tilde{u}^+}{\partial z^+}\right), \tag{4.6}$$

$$\rho \frac{\partial \tilde{v}^+}{\partial t^+} + \frac{\rho \tilde{v}^+}{\lambda^+} \frac{\partial \tilde{v}^+}{\partial y^+} + \frac{\rho \tilde{w}^+}{\lambda^+} \frac{\partial \tilde{v}^+}{\partial z^+} = -\rho_o \frac{\partial p_1}{\partial y^+} + \frac{\partial}{\partial y^+}\left(\frac{\rho_o^2 \mu}{\mu_w \rho_w} \frac{\partial \tilde{v}^+}{\partial y^+}\right)$$

$$+ \frac{1}{\lambda^{+2}} \frac{\partial}{\partial z^+}\left(\frac{\rho_o^2 \mu}{\mu_w \rho_w} \frac{\partial \tilde{v}^+}{\partial z^+}\right), \tag{4.7}$$

$$\rho \frac{\partial \tilde{w}^+}{\partial t^+} + \frac{\rho \tilde{v}^+}{\lambda^+} \frac{\partial \tilde{w}^+}{\partial y^+} + \frac{\rho \tilde{w}^+}{\lambda^+} \frac{\partial \tilde{w}^+}{\partial z^+} = -\frac{\rho_o}{\lambda^{+2}} \frac{\partial p_1}{\partial z^+}$$

$$+ \frac{\partial}{\partial y^+}\left(\frac{\rho_o^2 \mu}{\mu_w \rho_w} \frac{\partial \tilde{w}^+}{\partial y^+}\right) + \frac{1}{\lambda^{+2}} \frac{\partial}{\partial z^+}\left(\frac{\rho_o^2 \mu}{\mu_w \rho_w} \frac{\partial \tilde{w}^+}{\partial z^+}\right), \tag{4.8}$$

$$\frac{\partial(\rho\, \tilde{v}^+)}{\partial y^+} + \frac{\partial(\rho\, \tilde{w}^+)}{\partial z^+} = 0\,. \tag{4.9}$$

where $\rho = \rho(x^+, y^+)$. Here p^+ is the scaled mainstream pressure gradient defined

by

$$p^+ = -\frac{\mu_w \rho_w}{\rho_o^2 u_{ro}^3 Re} \frac{dp_e}{dx} . \tag{4.10}$$

During a typical quiescent state the presence of the wall-layer streaks indicates that there are planes at certain spanwise locations which on average are aligned in the streamwise direction and across which there is no spanwise flow. Consider therefore the flow development between a typical pair of wall-layer streaks located at $z^+ = 0$ and $z^+ = 1$; since w^+ must vanish at $z^+ = \mathrm{n}/2$, here $\mathrm{n} = 0,\ 1,\ \cdots$, it follows from the continuity equation that it is possible to write $\tilde{v}^+$ and $\tilde{w}^+$ during a typical quiescent period according to (4.91)

$$\tilde{w}^+ = -\frac{\rho_o}{\rho} \sum_{n=1}^{\infty} \frac{\partial \mathrm{f}_n}{\partial y^+} \sin(2\mathrm{n}\pi z^+) , \tag{4.11}$$

$$\tilde{v}^+ = -2\pi \frac{\rho_o}{\rho} \sum_{n=1}^{\infty} \mathrm{n}\, \mathrm{f}_n \cos(2\mathrm{n}\pi z^+) . \tag{4.12}$$

Here $\mathrm{f}_n(y^+,\ t^+)$ are the functional coefficients of the Fourier series which are to be determined subject to the following boundary conditions at the wall

$$\mathrm{f}_n = \frac{\partial \mathrm{f}_n}{\partial y^+} = 0 \quad \text{at} \quad y^+ = 0 . \tag{4.13}$$

A variety of different conditions could be considered for the asymptotic behavior of the instantaneous flow in the outer edge of the wall layer subject to the restriction

that $\tilde{w}^+$ is at most O(1) as $y^+ \to \infty$; this restriction is necessary since the motions represented by equations (4.11), (4.12) should make significant contributions to the turbulence intensities and measurements show that $\overline{w'^2}$ is at most $O(u_{\tau o}^2)$ for large y^+. The simplest outer condition that will produce the observed type of wall-layer structure, corresponding to the situation depicted schematically in Figure 4.1, is obtained for

$$\frac{\partial f_1}{\partial y^+} \to \frac{\rho}{\rho_o} W_1 , \quad \frac{\partial f_n}{\partial y^+} \to 0 , \; n > 1 , \quad \text{as} \quad y^+ \to \infty . \tag{4.14}$$

Here W_1 represents an average spanwise velocity at the wall-layer edge. This external motion is similar to the type of flow that might be induced on the wall layer from above by a convecting hairpin vortex. It is evident that the solution of equations (4.7) to (4.9) develops independently from that of the streamwise momentum (4.6). Equations (4.6) through (4.14) form the basis of the unsteady wall-layer model.

To consider the compressible problem, the Howarth-Dorodnitsyn transformation

$$Y^+ = \int_o^{y^+} \left(\frac{\rho}{\rho_o} \right) dy^+ \tag{4.15}$$

is introduced and equations (4.6) – (4.14) become

$$\frac{\partial \tilde{u}^{+}}{\partial t^{+}} + \frac{\hat{v}^{+}}{\lambda^{+}} \frac{\partial \tilde{u}^{+}}{\partial Y^{+}} + \frac{\tilde{w}^{+}}{\lambda^{+}} \frac{\partial \tilde{u}^{+}}{\partial z^{+}} = -\hat{p}^{+}$$

$$+ \frac{\partial}{\partial Y^{+}} \left(\frac{\mu\rho}{\mu_w \rho_w} \frac{\partial \tilde{u}^{+}}{\partial Y^{+}} \right) + \frac{1}{\lambda^{+2}} \frac{\partial}{\partial z^{+}} \left(\frac{\mu\rho_o}{\mu_o \rho} \frac{\partial \tilde{u}^{+}}{\partial z^{+}} \right), \tag{4.16}$$

$$\frac{\partial \tilde{v}^{+}}{\partial t^{+}} + \frac{\hat{v}^{+}}{\lambda^{+}} \frac{\partial \tilde{v}^{+}}{\partial Y^{+}} + \frac{\tilde{w}^{+}}{\lambda^{+}} \frac{\partial \tilde{v}^{+}}{\partial z^{+}} = -\frac{\partial p_1}{\partial Y^{+}}$$

$$+ \frac{\partial}{\partial Y^{+}} \left(\frac{\mu\rho}{\mu_w \rho_w} \frac{\partial \tilde{v}^{+}}{\partial Y^{+}} \right) + \frac{1}{\lambda^{+2}} \frac{\partial}{\partial z^{+}} \left(\frac{\mu\rho_o}{\mu_o \rho} \frac{\partial \tilde{v}^{+}}{\partial z^{+}} \right), \tag{4.17}$$

$$\frac{\partial \tilde{w}^{+}}{\partial t^{+}} + \frac{\hat{v}^{+}}{\lambda^{+}} \frac{\partial \tilde{w}^{+}}{\partial Y^{+}} + \frac{\tilde{w}^{+}}{\lambda^{+}} \frac{\partial \tilde{w}^{+}}{\partial z^{+}} = -\frac{1}{\lambda^{+2}} \frac{\rho_o}{\rho} \frac{\partial p_1}{\partial z^{+}}$$

$$+ \frac{\partial}{\partial Y^{+}} \left(\frac{\mu\rho}{\mu_w \rho_w} \frac{\partial \tilde{w}^{+}}{\partial Y^{+}} \right) + \frac{1}{\lambda^{+2}} \frac{\partial}{\partial z^{+}} \left(\frac{\mu\rho_o}{\mu_o \rho} \frac{\partial \tilde{w}^{+}}{\partial z^{+}} \right), \tag{4.18}$$

$$\frac{\partial \hat{v}^{+}}{\partial Y^{+}} + \frac{\partial \tilde{w}^{+}}{\partial z^{+}} = 0\,, \tag{4.19}$$

where $\hat{v}^{+} = (\rho/\rho_o)\tilde{v}^{+}$ and a newly defined mainstream pressure gradient parameter $\hat{p}^{+}$ has the form

$$\hat{p}^{+} = -\frac{\mu_w \rho_w}{\rho_o^2 u_{\tau o}^3 Re} \frac{1}{\rho} \frac{dp_e}{dx} = \frac{\mu_w \rho_w}{\rho_o^2 u_{\tau o}^3 Re} \frac{1}{M_e} \frac{dM_e}{dx} \left(\frac{H}{H_e} U_e^2 - \frac{\alpha}{2} u^2 \right), \tag{4.20}$$

which follows from §3.3. Note that in most cases $\hat{p}^{+}$ is negligibly small and can

only become and O(1) term when the pressure gradient in the mainstream dp_e/dx becomes $O(u_{\tau o}^3 Re)$; with the Reynolds number large, this can occur only as $u_{\tau o} \to 0$ or more specifically when $u_{\tau o} = O(Re^{-1/3})$. This latter case is only possible in a very large pressure gradient flow or near a point of time-mean separation. This type of flow is not considered in this analysis. Thus, the $\hat{p}^+$ term is negligible to leading order as $Re \to \infty$ and may be omitted from the leading order momentum equations.

The density still appears in the transformed equations, (4.16) through (4.19), in two different forms, one of which is the density-viscosity product ratio $\mu\rho/\mu_w\rho_w$. Again the Chapman law will be assumed so that this ratio is taken to be unity. The density also appears either in the form ρ_o/ρ or with the viscosity μ/ρ; however, each of these terms contains inverse powers of λ^+, and since it is argued that λ^+ is large for $Re \to \infty$, terms containing $1/\lambda^+$ and $(1/\lambda^+)^2$ may be treated as higher order and the unsteady Navier-Stokes equations are therefore in a constant property form

$$\frac{\partial \tilde{u}^+}{\partial t^+} = -\hat{p}^+ + \frac{\partial}{\partial Y^+}\left(\frac{\partial \tilde{u}^+}{\partial Y^+}\right), \tag{4.21}$$

$$\frac{\partial \tilde{v}^+}{\partial t^+} = -\frac{\partial p_1}{\partial Y^+} + \frac{\partial}{\partial Y^+}\left(\frac{\partial \tilde{v}^+}{\partial Y^+}\right), \tag{4.22}$$

$$\frac{\partial \tilde{w}^+}{\partial t^+} = \frac{\partial}{\partial Y^+}\left(\frac{\partial \tilde{w}^+}{\partial Y^+}\right), \tag{4.23}$$

$$\frac{\partial \hat{v}^{+}}{\partial Y^{+}} + \frac{\partial \tilde{w}^{+}}{\partial z^{+}} = 0 . \tag{4.24}$$

Equations (4.11) and (4.12) may now be written in a constant property form according to

$$\tilde{w}^{+} = -\sum_{n=1}^{\infty} \frac{\partial f_n}{\partial Y^{+}} \sin(2n\pi z^{+}) , \tag{4.25}$$

$$\hat{v}^{+} = -2\pi \sum_{n=1}^{\infty} n f_n \cos(2n\pi z^{+}) . \tag{4.26}$$

Finally, the boundary conditions are

$$f_n = \frac{\partial f_n}{\partial Y^{+}} = 0 \quad \text{at} \quad Y^{+} = 0 , \tag{4.27}$$

$$\frac{\partial f_1}{\partial Y^{+}} \to W_1 , \quad \frac{\partial f_n}{\partial Y^{+}} \to 0 , \; n > 1 , \quad \text{as} \quad Y^{+} \to \infty . \tag{4.28}$$

At this point, the density has been formally removed from the unsteady wall-layer equations using the Howarth-Dorodnitsyn transformation, the Chapman density viscosity law, and the perfect gas law relation. In addition, it has been assumed that characteristic spanwise spacing λ^{+} is large as $Re \to \infty$. The range of validity of this last assumption is not known and can only be verified through future experimental work. However, with increasing Mach number, it is known that the wall layer thickens and occupies a much larger portion of the whole

boundary layer than in low-speed flows. Thus it is entirely possible that the present analysis may eventually become invalid in the hypersonic regime.

It is evident that the solution of equations (4.22) – (4.24) develops independently from that of equation (4.21); in fact these equations describe the evolution of the scaled streamwise vorticity ζ_x^+ defined by

$$\zeta_x^+ = \frac{\partial \tilde{w}^+}{\partial Y^+} - \frac{\partial \hat{v}^+}{\partial z^+} . \tag{4.29}$$

The motions represented by the streamwise vorticity transport equation produce contributions to the turbulence intensities $\overline{v'^2}$ and $\overline{w'^2}$. However, there will be no neat contribution to an average value of either w or v from the time-dependent motions represented by equations (4.25) and (4.26). This is because after each wall-layer breakdown and subsequent sweep, the low-speed streaks appear at different spanwise locations; over a large number of cycles the spanwise distribution of the streaks must be random. Walker and Abbott (1977) have discussed typical values of $\hat{v}^+$ and $\tilde{w}^+$ across the span from $z^+ = 0$ to λ^+. At least for incompressible flow, the present theoretical picture is consistent with the known mean results that $w = 0$ and v is small and $O(Re^{-1})$. It may be verified upon substitution of equations (4.25) and (4.26) into equation (4.21) that $\tilde{u}^+$ may be written according to

$$\tilde{u}^+ = \tilde{u}_o(Y^+, t^+) + \sum_{n=1}^{\infty} \tilde{u}_n(Y^+, t^+) \cos(2n\pi z^+) . \tag{4.30}$$

A variation in x^+ has not been written explicitly in this equation, since the dependence on x^+ is at most parametric (entering from the outer conditions for $\tilde{u}^+$ as $Y^+ \to \infty$). The procedure of Walker and Scharnhorst (1977) and Walker et al. (1989) may now be followed to obtain the representative solutions and a subsequent expression for the time-mean streamwise velocity distribution U^+. For completeness the final form of the time-mean inner region velocity profile approximation U^+ will be given in Appendix A.

4.4 Wall Layer for the Thermal Boundary Layer

In this section an expression for the wall-layer total enthalpy profile will be developed through consideration of the leading order form of the time-dependent energy equation in the wall layer for large Reynolds number. The total enthalpy equation for a three-dimensional flow is

$$\rho\frac{\partial\tilde{H}}{\partial t}+\rho\tilde{u}\frac{\partial\tilde{H}}{\partial x}+\rho\tilde{v}\frac{\partial\tilde{H}}{\partial y}+\rho\tilde{w}\frac{\partial\tilde{H}}{\partial z}=(\gamma-1)M_{ref}^2\frac{\partial\tilde{p}}{\partial t}$$

$$+\frac{\partial}{\partial x}\Big(\frac{\mu}{PrRe}\frac{\partial\tilde{H}}{\partial x}\Big)+\frac{\partial}{\partial y}\Big(\frac{\mu}{PrRe}\frac{\partial\tilde{H}}{\partial y}\Big)+\frac{\partial}{\partial z}\Big(\frac{\mu}{PrRe}\frac{\partial\tilde{H}}{\partial z}\Big)+\Phi\ , \tag{4.31}$$

where the dissipation function is

$$\Phi = \frac{\gamma-1}{2}M_{ref}^2\Bigg\{\Big(1-\frac{1}{Pr}\Big)\Big\{\frac{\partial}{\partial x}\Big(\frac{\mu}{Re}\frac{\partial \tilde{u}^2}{\partial x}\Big)+\frac{\partial}{\partial y}\Big(\frac{\mu}{Re}\frac{\partial \tilde{u}^2}{\partial y}\Big)+\frac{\partial}{\partial z}\Big(\frac{\mu}{Re}\frac{\partial \tilde{u}^2}{\partial z}\Big)$$

$$+\frac{\partial}{\partial x}\Big(\frac{\mu}{Re}\frac{\partial \tilde{v}^2}{\partial x}\Big)+\frac{\partial}{\partial y}\Big(\frac{\mu}{Re}\frac{\partial \tilde{v}^2}{\partial y}\Big)+\frac{\partial}{\partial z}\Big(\frac{\mu}{Re}\frac{\partial \tilde{v}^2}{\partial z}\Big)+\frac{\partial}{\partial x}\Big(\frac{\mu}{Re}\frac{\partial \tilde{w}^2}{\partial x}\Big)$$

$$+\frac{\partial}{\partial y}\Big(\frac{\mu}{Re}\frac{\partial \tilde{w}^2}{\partial y}\Big)+\frac{\partial}{\partial z}\Big(\frac{\mu}{Re}\frac{\partial \tilde{w}^2}{\partial z}\Big)\Big\}+\frac{2\mu}{Re}\Big\{\Big(\frac{\partial \tilde{u}}{\partial x}\Big)^2+\Big(\frac{\partial \tilde{v}}{\partial y}\Big)^2+\Big(\frac{\partial \tilde{w}}{\partial z}\Big)^2$$

$$+2\Big(\frac{\partial \tilde{u}}{\partial y}\frac{\partial \tilde{v}}{\partial x}\Big)+2\Big(\frac{\partial \tilde{v}}{\partial z}\frac{\partial \tilde{w}}{\partial y}\Big)+2\Big(\frac{\partial \tilde{w}}{\partial x}\frac{\partial \tilde{u}}{\partial z}\Big)-\frac{2}{3}\Big(\frac{\partial \tilde{u}}{\partial x}+\frac{\partial \tilde{v}}{\partial y}+\frac{\partial \tilde{w}}{\partial z}\Big)^2\Big\}\Bigg\}. \qquad (4.32)$$

The function Φ contains a long list of terms involving the derivatives of velocity components whose terms are associated with the viscous dissipation of kinetic energy into thermal internal energy. It might be anticipated that with increasing mainstream Mach number, the influence of viscous dissipation will become significant at some stage.

Unfortunately, measurements of the fluctuating total enthalpy are very scarce; however, it is expected that the turbulent fluctuations in temperature or total enthalpy should have scales comparable to those associated with velocity fluctuations. It is known from experiment that the time-mean and instantaneous velocities have the same order of magnitude, and therefore it is not unreasonable to assume the scale of $\tilde{H}$ to be the same of the mean total enthalpy. Consequently, the following scale total enthalpy function for the wall layer is defined

$$\tilde{\theta}^{+} = \frac{\tilde{H} - H_w}{q_{\tau o}} , \tag{4.33}$$

where the scale for total enthalpy is

$$q_{\tau o} = \frac{q_w}{\rho_o u_{\tau o}} . \tag{4.34}$$

When the surface heat transfer rate is moderate or large, it was shown in §3.6 that $q_{\tau o}$ is $O(u_{\tau o})$. The wall temperature H_w is permitted to vary in the x-direction but dH_w/dx is taken to be small so that streamwise variation of H_w is always slow in x according to the inner-layer asymptotic analysis described in §3.4. Since the scales of velocity components are all $u_{\tau o}$, it is easily verified that Φ will only enter the leading-order form equation (4.32) for total enthalpy when $(\gamma - 1)M_{ref}^2 u_{\tau o} = O(1)$. This estimate is consistent with current physical views of the structure of the supersonic turbulent boundary layer and in the present wall layer analysis the influence of dissipation will be neglected. Upon substitution of equations (4.1) through (4.5) and (4.33) into the unsteady energy equation (4.31), it may be verified that total-enthalpy equation reduces to

$$\rho \frac{\partial \tilde{\theta}^{+}}{\partial t^{+}} + \frac{\rho \tilde{v}^{+}}{\lambda^{+}} \frac{\partial \tilde{\theta}^{+}}{\partial y^{+}} + \frac{\rho \tilde{w}^{+}}{\lambda^{+}} \frac{\partial \tilde{\theta}^{+}}{\partial z^{+}} =$$

$$\frac{\partial}{\partial y^{+}}\left(\frac{\rho_o^2 \mu}{Pr \mu_w \rho_w} \frac{\partial \tilde{\theta}^{+}}{\partial y^{+}}\right) + \frac{1}{\lambda^{+2}} \frac{\partial}{\partial z^{+}}\left(\frac{\rho_o^2 \mu}{Pr \mu_w \rho_w} \frac{\partial \tilde{\theta}^{+}}{\partial z^{+}}\right) , \tag{4.35}$$

to leading order in the limit of large Reynolds number. Note that equation (4.35) and the x-momentum equation (4.6) are the same in mathematical form for $Pr = 1$.

For most practical situations Pr is O(1), and it is convenient to introduce new scalings to eliminate the Prandtl number from leading order terms in the final equations. This procedure results in

$$\frac{\partial \tilde{\theta}^{+}}{\partial t^{+}} = \frac{\partial}{\partial Y_{\theta}^{+}}\left(\frac{\partial \tilde{\theta}^{+}}{\partial Y_{\theta}^{+}}\right), \tag{4.36}$$

where

$$Y_{\theta}^{+} = \sqrt{Pr}\int_{o}^{y^{+}} \left(\frac{\rho}{\rho_o}\right) dy^{+} \ . \tag{4.37}$$

The form of equation (4.36) is now identical to the streamwise velocity equation (4.16) to the leading order and the analysis leading to the final profile result for θ^{+} is exactly the same as the velocity problem. For completeness the final form of the time-mean inner region profiles U^{+} and θ^{+} are given in Appendix A.

The development of the thermal inner-layer model for the case when these is significant heat transfer at the surface is now complete. However as indicated in equation (4.36), the terms associated with viscous dissipation do not appear in the leading-order equation and it is of interest to ascertain when such terms will become important. To this stage it has been implicitly assumed that the total-enthalpy scaling for the wall layer $q_{\tau o}$, defined in equation (4.34) is O($u_{\tau o}$), and because of this the viscous dissipation terms in equation (4.31) were neglected. There appear to be at least two situations where the viscous dissipation, Φ, will be import. The first occurs for a nearly adiabatic surface and the second is in the hypersonic regime. If the leading order terms in the dissipation term are retained in

equation (4.31), it follows that

$$\frac{\partial \tilde{\theta}^{+}}{\partial t^{+}} = \frac{\partial}{\partial Y_{\theta}^{+}}\left(\frac{\partial \tilde{\theta}^{+}}{\partial Y_{\theta}^{+}}\right) + D_{\tau o}\frac{\partial}{\partial Y_{\theta}^{+}}\left[\frac{\partial}{\partial Y_{\theta}^{+}}\left(\frac{\tilde{u}^{+2} + \tilde{w}^{+2}}{2}\right)\right], \tag{4.38}$$

where

$$D_{\tau o} = (Pr-1)(\gamma-1)M_{ref}^{2}\,\frac{u_{\tau o}^{2}}{q_{\tau o}}\,. \tag{4.39}$$

If $q_{\tau o}$ is $O(u_{\tau o})$ and M_{ref} is O(1), then $D_{\tau o} \ll 1$. Here situations where $D_{\tau o}$ is O(1) are considered; such cases occur when total-enthalpy scale

$$q_{\tau o} = O\Big((Pr-1)(\gamma-1)M_{ref}^{2}\,u_{\tau o}^{2}\Big)\,. \tag{4.40}$$

This can happen either when $q_{\tau o}$ is $O(u_{\tau o}^{2})$ and M_{ref} is O(1) corresponding to a nearly adiabatic supersonic flow case, or when $(\gamma-1)M_{ref}^{2}u_{\tau o}$ is O(1) corresponding to hypersonic flows. Note that the instantaneous kinetic energy $k \approx (\tilde{u}^{+2} + \tilde{w}^{+2})/2$ appears in the leading order energy equation (4.38), and the normal $\tilde{v}$-velocity related component is not present since it is $O(1/\lambda^{+})$.

It follows from equations (4.33) and (4.40) that for a nearly adiabatic wall the unsteady total enthalpy in the wall layer may be expanded according to

$$\tilde{H} = H_{w} + \alpha(1-Pr)H_{e}\,u_{*}^{2}\,\tilde{\theta}_{2}^{+} + \cdots\,. \tag{4.41}$$

Note that αH_{e} is related to the reference Mach number through equation (3.8). When this limiting form is introduced into the instantaneous energy equation, it

yields a relation similar to equation (4.38),

$$\frac{\partial \tilde{\theta}_2^+}{\partial t^+} = \frac{\partial}{\partial Y_\theta^+}\left(\frac{\partial \tilde{\theta}_2^+}{\partial Y_\theta^+}\right) + \frac{\partial}{\partial Y_\theta^+}\left[\frac{\partial}{\partial Y_\theta^+}\left(\frac{\tilde{u}^{+2} + \tilde{w}^{+2}}{2}\right)\right]. \tag{4.42}$$

Unfortunately this equation is very different to analyze and the extension of the wall-layer analysis of Walker et al (1989) to consider representative time-dependent motions in the wall layer is not easily extended. The difficulty is associated with the quadratic terms in velocity on the right side of equation (4.42); during a typical quiescent state these velocities are representable as Fourier series and thus they give rise to a very complicated forcing function in equation (4.42). For this reason a time dependent analysis of equation (4.42) was not attempted. Fortunately the deviation of the total enthalpy from H_w is not large (cf. equation (4.41)) for an insulated wall and an expression for the time-average of $\tilde{\theta}_2^+$ is not needed to give an adequate representation of H in a composite profile for the entire boundary layer.

4.5 Summary

In this chapter a theory has been presented in which representative motions have been considered during a typical assumed quiescent period in the compressible turbulent wall layer. A time average of these motions has produced expressions for the mean streamwise velocity u^+ and the total enthalpy θ^+ in the wall layer. These wall layer profiles constitute the turbulence model for the wall layer and no

further modeling, say of the Reynolds stress, is required. The quality of the models will ultimately be tested through direct comparison with experimental data.

Having successfully described the wall-layer distributions, it might be thought that a similar line of reasoning could be pursued to develop a profile in the outer region. However, the outer layer problem is much more complicated since the outer region receives vorticity in sharp short bursts from the near wall. Thus the bursting problem cannot be avoided as it was for the wall layer analysis. Unfortunately, the mathematical problems associated with the strong unsteady viscous-inviscid interaction that occurs during the burst are formidable, and there is little hope for a resolution to this problem in the foreseeable future. Consequently, it is necessary at present to use some sort of conventional model for the outer region flow, and this is considered in Chapter 5.

5. TURBULENT BOUNDARY LAYERS WITH HEAT TRANSFER

5.1 Introduction

The asymptotic analysis given in §3 has identified the leading-order equations in the inner and outer region of the compressible turbulent boundary layer without recourse to a specific turbulence closure model. Actual solutions of these equations cannot be produced until the turbulence terms are modeled. In §4 an unsteady wall-layer model has been developed for the wall layer, and this yields mean profiles for the wall-layer velocity and total enthalpy that are based on the observed coherent behavior of the flow in the near-wall region. The question of a model for the outer layer is more complex however. Recent studies (e.g., Smith et al., 1991) suggest that the outer layer dynamics are dominated by the complicated motion of hairpin vortices that provoke intermittent eruptions of the wall layer thereby giving rise to the production of new turbulence. Although many of the mechanisms of vortex interactions in the outer layer are understood, there are still formidable difficulties in formulating a model for the time-mean flow in the outer layer based on these dynamics. At present there are two possible alternatives for dealing with the outer layer, namely: (1) use an empirically-motivated outer region profile approximations, or (2) introduce some type of turbulence closure model for the Reynolds stress and turbulent heat flux terms and then seek solutions of the outer-layer equations for velocity and total enthalpy.

The first approach is often used in momentum integral prediction methods, and the most popular velocity profile approximation for the outer layer is "law of

the wake" described by Coles (1956) for incompressible turbulent boundary layers. Coles (1956) assumed that the velocity profile could be expressed as a combination of the logarithmic "law of the wall" and a wake component according to

$$\frac{u}{u_\tau} = \frac{1}{\kappa}\log\left(\frac{\rho u_\tau n}{\mu}\right) + C_i + \frac{\Pi(s)}{\kappa} W\left(\frac{n}{\delta}\right). \tag{5.1}$$

Here $W(n/\delta)$ is the wake function and $\Pi(s)$ is the so-called wake-strength parameter. The wake function W is essentially an empirical correlation based upon velocity data taken in wide variety of conditions with and without pressure gradients. The wake function W is often assumed to be effectively universal, and when different data sets were reduced to this form, they appeared to exhibit a common behavior. Hinze (1959) has suggested that the wake function could be adequately described by

$$W(\eta) = 1 + \sin\left[\frac{\Pi}{2}(2\eta - 1)\right]. \tag{5.2}$$

The so-called "wake-strength" parameter Π is selected to reflect a dependence on the pressure gradient and, to a lesser extent, Reynolds number (White, 1992). A detailed description of the "law of the wake" can be found in Coles and Hirst (1969) where the results of data fitting carried out for the 1968 Stanford Conference is given.

The question now arises as to how a formula based on low speed data can be extended to supersonic boundary layers if at all. As previously discussed, data for

the velocity profile in compressible boundary layers, especially in the hypersonic range, are sparse and sometimes of uncertain reliability near the surface. However, there have been various attempts to extrapolate the incompressible "law of the wake" to the compressible regime. Both Stalmach (1958) and Maise and McDonald (1968) utilized the van Driest effective-velocity transformation to try to express the compressible profile in an equivalent incompressible form and then use modeling concepts based on the "Law of the Wake". The approach enjoyed some success, although it lacks a sound theoretical basis and moreover seems to perform poorly in flows with significant heat transfer. Consequently, this approach will not be considered further here.

In connection with the second approach, it should be noted that there are an enormous number of turbulence models for the Reynolds stress currently in use for incompressible flows. For simplicity, the discussion here will relate primarily to algebraic turbulence models which are the simplest possible class of models. Examples of algebraic models that are in common use include the Cebeci-Smith (1974) model and the Baldwin-Lomax (1978) model. The essence of this type of model is a simple ramp function for eddy viscosity which behaves linearly in distance from the wall near the surface and then abruptly changes to a uniform value further from the surface that depends on the local flow conditions. In conventional boundary-layer prediction methods, the eddy viscosity model is typically modified to a mixing length formulation in the wall-layer region; the mixing length is linear in distance from the wall in the overlap zone, but is reduced toward the wall through multiplication by a van Driest damping factor (Cebeci and Smith, 1974).

It should be noted that because of the rapid variation of the damping factor, relatively large numbers of mesh points are required in the wall layer to ensure reasonable accuracy in any computational algorithm which seeks to compute the velocity profile all the way to the wall. In the embedded-function method developed by Walker, Werle and Ece (1987) and Weigand and Walker (1978), the mean velocity and temperature profiles are represented by smooth analytical functions throughout the wall layer. In an attached two-dimensional turbulent flow, the wall layer exhibits an essentially universal and self-similar behavior, and thus expending a major portion of the computational resources on a known wall-layer solution seems wasteful. In the embedded-function algorithm, the analytical wall-layer functionals are smoothly matched to an outer-region numerical solution of the turbulent boundary-layer equations. Therefore only simple outer region closure models are needed and the analytical functionals provide the turbulent model for the wall layer; thus, inner models involving the van Driest damping factor are no longer necessary. The embedded-function approach has been effectively applied to the calculation of low-speed compressible flows (Walker et al., 1989).

The work described in this chapter represents a first step toward extending the embedded-function methodology to the computation of high-speed compressible turbulent flows. It has been previously argued that both regions of a compressible turbulent boundary layer can potentially be treated using a compressibility transformation and that certain features of constant property turbulent flow may then carry over. The major premise of this chapter is that the profiles for velocity and total enthalpy conform to the law of the wall in which both exhibit a

logarithmic dependence, but in terms of a density weighted variable Y instead of the physical distance y. In this chapter turbulence models will be constructed in order to ensure that this behavior is realized in a self-consistent manner. One constraint in deriving these models is that they must reduce to conventional incompressible models in the limit $M_{ref} \to 0$. The quality of the theory thus constructed will ultimately be decided on the basis of direct comparisons of the results with experimental data.

It is worthwhile to note that the embedded-function approach of interest here can only be sensibly applied to an attached turbulent flow. As a turbulent flow separates, it is well known that the logarithmic behavior in the velocity profile disappears. Although there is some evidence that there may be a logarithmic portion of the profile in the back-flow region beyond the separation point, it is evidently a far different functional form than in the upstream boundary layer. This is simply an indication that the physics in the back-flow zone are different from the well-documented behavior of the attached wall layer upstream of separation. At the same time, it is also important to appreciate that in most practical flow problems, the turbulent boundary layer layer is attached over a large portion of the total surface.

5.2 Turbulence Closure Models

As discussed in §2.2, the Reynolds shear stress σ and turbulent heat flux ϕ in a boundary layer may be represented by gradient diffusion models of the form

$$\sigma = -\rho\overline{u'v'} = \rho\epsilon\,\frac{\partial u}{\partial n}\,, \tag{5.3}$$

$$\phi = -\rho\overline{v'H'} = \rho\epsilon_H\,\frac{\partial H}{\partial n}\,, \tag{5.4}$$

where ϵ and ϵ_H are the eddy viscosity and eddy conductivity, respectively. The Cebeci-Smith (1974) and Baldwin-Lomax (1978) models are representative of a number of eddy viscosity models currently in common use and will therefore be described here. Both models behave linearly in distance from the wall near the surface having the form

$$\epsilon = \kappa u_\tau n \qquad n \le n_m\,, \tag{5.5}$$

for incompressible flow; here n_m represents a patch point where the formula switches to a simple expression (which is constant for fixed s) such as

$$\epsilon = \mathrm{K}U_e\delta^* \qquad n > n_m\,, \tag{5.6}$$

for the Cebeci-Smith (1974) model and

$$\epsilon = \mathrm{C}_p\ \mathrm{K}n_{max}\tilde{\mathrm{F}}_{max}\,, \tag{5.7}$$

for the Baldwin-Lomax (1978) model. In these formulae, κ is the von Kármán constant, K is a constant normally having a value $\mathrm{K} = 0.0168$, and δ^* is the displacement thickness defined by

$$\delta^* = \int_o^\infty \left(1 - \frac{u}{U_e}\right) dn \ . \tag{5.8}$$

For the Baldwin-Lomax (1978) model, n_{max} is the physical location in the boundary layer where the function $\tilde{F} = n\,|\,\partial u/\partial n\,|$ achieves a maximum, and $\tilde{F}_{max}$ is the corresponding value of $\tilde{F}$; in addition, C_p is a constant which was originally adjusted by Baldwin and Lomax (1978) so that the model produced essentially similar results to the Cebeci-Smith (1974) model in constant-pressure boundary layers; usually a value of $C_p = 1.65$ is employed. In this study, an exact value of C_p has been determined in Appendix B through a similarity analysis of incompressible two-dimensional flows. In particular, It is shown that the Baldwin-Lomax (1978) model with $C_p = 1.7332$ produces identical results to the Cebeci-Smith (1974) model in the limit of $M_{ref} \to 0$ for two-dimensional constant pressure boundary layers.

It is evident from equations (5.5) through (5.7) that this type of model is a simple ramp function, with the junction point being n_m determined by the location where equation (5.5) intersects either equation (5.6) or (5.7). In addition, a so-called "intermittency" factor is often introduced as an option, in order to reduce the eddy viscosity to zero far from the wall. At the outer edge of the boundary layer, the turbulence is observed to become intermittent for a fraction γ of any total observation. An intermittency factor distribution was obtained by Klebanoff (1954) and can be fitted approximately by the expression

$$\gamma = \frac{1}{2}\left\{1 - \mathrm{erf}\left[5(n/\delta - 0.78)\right]\right\} . \tag{5.9}$$

Through multiplication of either equation (5.6) or (5.7) by γ, a model is obtained in which the eddy viscosity ϵ is reduced to zero at the boundary-layer edge. In this study the intermittancy factor will not be used, since it was found to have only a minor effect on computed profiles in the outer part of the boundary; thus γ may be regarded as an embellishment to the central model, which only serves to complicate the analysis and is not central to the main issues to be decided. Eddy-conductivity models are typically used for the turbulence terms in the energy equation, but these are often formulated as being proportional to the eddy viscosity by introducing a factor of proportionality (usually taken to be constant) and which is referred to as the turbulent Prandtl number. It is important to appreciate that such models were primarily developed and fine tuned for low-speed flows and, consequently, the arbitrary extension of this type of model to the prediction of high-speed compressible flows is questionable. At the same time, it is well known in high speed compressible flows that the Reynolds stress in the outer region does have a similar shape to that observed in incompressible flows, reaching a maximum, τ_w, near the surface, and asymptoting to zero at the outer edge of the boundary layer. Thus it is likely that a reasonable corresponding simple eddy-viscosity formulation is possible for compressible flows. An attractive feature of algebraic models is their relative simplicity, and it is therefore of interest to develop such an approach which adequately accounts for the effects of compressibility.

The leading order expansions for both turbulent stress σ and heat flux ϕ in the outer layer have been formally established in §3 and given in equations (3.111), which are repeated here for convenience,

$$\sigma(s,Y) = \rho_o u_{\tau o}^2 \Sigma_1(s,\eta) + \cdots , \qquad \phi(s,Y) = q_w \Phi_1(s,\eta) + \cdots . \tag{3.111}$$

Both functions must exhibit the asymptotic behavior of $\Sigma_1 \sim 1$ and $\Phi_1 \sim 1$ as $\eta \to 0$, where the scaled outer variable η is defined as $\eta = Y/\Delta_o$ and Δ_o denoted a thickness characteristic of the outer layer. Consider first the eddy viscosity function. In terms of the Howarth-Dorodnitsyn variable Y defined in equation (3.4) and the scaled outer variable η

$$\sigma = \frac{\rho^2}{\rho_o}\,\epsilon\,\frac{\partial u}{\partial Y} = \frac{\rho^2 \epsilon}{\rho_o \Delta_o}\,\frac{\partial u}{\partial \eta} . \tag{5.10}$$

In the outer layer, u is expressed in the form of a defect law as given in equations (3.110), and as indicated in equations (3.114), the defect function is logarithmic for small η. It follows that

$$\sigma \sim \frac{\rho^2 \epsilon u_{\tau o}}{\rho_o \Delta_o \kappa \eta} = \frac{\rho^2 \epsilon u_{\tau o}}{\rho_o \kappa Y} , \qquad \text{as } \eta \to 0 . \tag{5.11}$$

However, it follows from equations (3.111) and (3.115) that $\sigma \sim \rho_o u_{\tau o}^2$ as $\eta \to 0$. Comparing this with equation (5.11), it follows that the eddy viscosity function must have the following asymptotic form

$$\epsilon \sim \frac{\rho_o^2}{\rho^2}\, u_{\tau o} \kappa Y = \frac{\rho_o^2}{\rho^2}\, u_{\tau o} \Delta_o \kappa \eta , \qquad \text{as} \quad \eta \to 0 . \tag{5.12}$$

The linear form in Y shown in equation (5.12) is a necessary feature of all proper outer-region models in order to produce the logarithmic behavior in the mean profile. The important aspect of equation (5.12) is the functional dependence on the density. As $M_{ref} \to 0$ it is easily seen that the eddy-viscosity formula takes the incompressible form, $\epsilon \sim \kappa u_\tau n$.

For large distances from the wall, the linear dependence in ϵ on Y must be modified so that the turbulent shear stress σ will be reduced to zero at the outer edge of the boundary layer; in addition, the model should reduce to either equation (5.6) or (5.7) for low Mach numbers for large Y. Unfortunately, there is a wide variety of functional forms that would fulfill both of these requirements. A question arises first as to what characteristic boundary-layer thickness should be used in the compressible formulation. At first glance, it might seem reasonable to replace the displacement thickness δ^* with its corresponding compressible two-dimensional definition δ_c^*, given by

$$\delta_c^* = \int_o^\infty \left(1 - \frac{\rho u}{\rho_e U_e}\right) dn \ . \tag{5.13}$$

However, δ_c^* is not generally satisfactory for scaling turbulent profiles because it contains the influence of both the velocity distribution and density variations; δ_c^* is really characteristic of ρu, the mass flow rate distribution, while δ^* is related essentially to the velocity distribution in the boundary layer. It may be noted that compressible velocity profiles in the outer layer often have similar shapes over a

wide range of surface heat transfer conditions. Since the ratio of the inner-layer to outer-layer thickness approaches to zero as $Re \to \infty$ (see §3), δ^* is uniquely defined once the outer velocity distribution u/U_e is known and here δ^* will be taken to be the characteristic length scale for the outer layer.

An additional consideration relative to model selection was that the adopted form should represent the situation well over a range of Mach numbers without introducing additional empiricism. Here the modification of the Cebeci-Smith-type model will be described first. In view of the compressible nature of the turbulent field, it seems reasonable to carry the variation in density indicated by equation (5.12) across the outer layer and to define the outer portion of the model by

$$\epsilon = \frac{\rho_o \rho_e}{\rho^2} \, \mathrm{K} U_e \delta^* \, , \qquad \text{for} \quad \eta \geq \eta_m \, . \tag{5.14}$$

Here η_m is the value of η where equations (5.12) and (5.14) intersect. The form of equation (5.14) was adopted partially for convenience; the factor of density ρ^{-2}, mandated by the matching to the wall layer, is carried through the outer layer in order that patch point η_m between the two pieces of the ramp function is a function of streamwise distance alone and does not depend upon $\rho(s,\eta)$. The equivalent form for the Baldwin-Lomax model can be readily shown to be

$$\epsilon = \frac{\rho_o \rho_e}{\rho^2} \, \mathrm{K} \, \mathrm{C}_p \, n_{max} \, \tilde{\mathrm{F}}_{max} \, , \qquad \text{as} \quad \eta \geq \eta_m \, . \tag{5.15}$$

A number of formulations were tested in this study by producing profiles which could be compared directly with experimental data. The combination of parameters

$\rho_o\rho_e/\rho^2$ appearing in equations (5.14) and (5.15) has been found to produce the best results. A compact representation of these eddy viscosity functions will be given in §5.3.

Following similar arguments to those used for the eddy-viscosity function, it is easily shown using equations (3.111), (3.114) and (5.4) that the compressible eddy-conductivity function ϵ_H must have the following form for small η:

$$\epsilon_H \sim \frac{\rho_o^2}{\rho^2}\, u_{\tau o}\, \kappa_\theta Y = \frac{\rho_o^2}{\rho^2}\, u_{\tau o}\, \Delta_o\, \kappa_\theta \eta\ , \qquad \text{as} \quad \eta \to 0\ . \tag{5.16}$$

For large values of η, the linear dependence on η must be modified and a simple far-field eddy-conductivity formula for low-speed flow has been given by Weigand (1978) and Walker et al. (1986) according to

$$\epsilon_H = \mathrm{K}_h U_e \delta^*\ , \tag{5.17}$$

and extensive comparisons with temperature profile data in constant pressure low-speed boundary layers have shown that $\mathrm{K}_h = 0.0245$. Again, a generalization to high-speed compressible flow is sought which conforms to the equation (5.16) and reduces to equation (5.17) in the outer part of the boundary layer for low Mach numbers. The eddy-conductivity formula adopted is consistent with the form of equation (5.14) and is

$$\epsilon_H = \frac{\rho_o\rho_e}{\rho^2}\, \mathrm{K}_h\, U_e\, \delta^*\ , \qquad \text{as} \quad \eta \geq \tilde{\eta}_m\ , \tag{5.18}$$

where $\tilde{\eta}_m$ is the value of η_o where equations (5.16) and (5.18) intersect. It is worthwhile to note that κ_θ has been found (Weigand, 1978) to depend on the local flow variables such as the surface heat transfer rate and pressure gradient; a means for evaluating κ_θ will subsequently be discussed

At this point compressible formulae for both eddy viscosity and eddy conductivity have been proposed. The asymptotic results suggest a deficiency in the conventional form of outer-region algebraic models now in common use, and a modification to account for density variations has been suggested. The turbulence models used in the present study for the outer region are modifications of Cebeci-Smith (1974) and Baldwin-Lomax (1978) models and have been selected here as the simplest possible outer algebraic models in order to demonstrate the concepts involved. In order to test the results of the asymptotic theory, as well as the new turbulence models, a limiting case will be considered in the next subsection corresponding to self-similar profiles that evolve in a constant pressure flow with heat transfer; in this situation the governing equations in the outer region of the boundary layer reduce to ordinary differential equations and exact analytical solutions for the profiles can be found.

5.3 Self-Similar Profiles in the Outer Layer

The governing equation for the velocity and total-enthalpy profiles in the outer region and their associated boundary conditions were developed in §3 and are given in equations (3.112) – (3.114) in the form of defect velocity $U_1 = \partial F_1/\partial\eta$ and

defect total enthalpy Θ_1; the outer region equations are rewritten here according to

$$\frac{\partial^2 F_1}{\partial s \partial \eta} + \frac{u_*'}{u_*}\frac{\partial F_1}{\partial \eta} - \frac{(\Delta_o r U_e)'}{\Delta_o r U_e}\eta\frac{\partial^2 F_1}{\partial \eta^2}$$

$$= \frac{1}{M_e}\frac{dM_e}{\partial s}\left(\frac{q_*}{u_*}\Theta_1 - 2\frac{\partial F_1}{\partial \eta}\right) + \frac{1}{\rho_o u_* \Delta_o U_e^2}\frac{\partial \sigma}{\partial \eta} \quad , \tag{5.19}$$

and

$$\frac{\partial \Theta_1}{\partial s} + \frac{q_*'}{q_*}\Theta_1 - \frac{(\Delta_o r U_e)'}{\Delta_o r U_e}\eta\frac{\partial \Theta_1}{\partial \eta} = \frac{1}{\rho_o q_* \Delta_o U_e H_e}\frac{\partial \phi}{\partial \eta} \, , \tag{5.20}$$

where the primes denote differentiation with respect to streamwise distance s. The boundary conditions associated with these equations are

$$\frac{\partial F_1(s,\eta)}{\partial \eta} \sim \frac{1}{\kappa(s)}\log \eta + C_o \qquad \text{for} \quad \eta \to 0 \, , \tag{5.21}$$

$$\Theta_1(s,\eta) \sim \frac{1}{\kappa_\theta(s)}\log \eta + B_o \qquad \text{for} \quad \eta \to 0 \, , \tag{5.22}$$

and

$$\frac{\partial F_1}{\partial \eta} \, , \ \Theta_1 \to 0 \, , \qquad \text{as } \eta \to \infty \, . \tag{5.23}$$

The turbulence quantities σ and ϕ are defined in terms of eddy viscosity and

conductivity functions according to

$$\sigma = \rho\epsilon \frac{\partial u}{\partial n} = \frac{\rho^2}{\rho_o} \epsilon \frac{u_* U_e}{\Delta_o} \frac{\partial^2 F_1}{\partial \eta^2} , \tag{5.24}$$

$$\phi = \rho\epsilon_H \frac{\partial H}{\partial n} = \frac{\rho^2}{\rho_o} \epsilon_H \frac{q_* H_e}{\Delta_o} \frac{\partial^2 F_1}{\partial \eta^2} . \tag{5.25}$$

The first eddy viscosity function used here is a modification of the Cebeci-Smith (1974) model and has the simple ramp formula

$$\epsilon = \frac{\rho_o \rho_e}{\rho^2} U_e \delta^* \hat{\epsilon}(\eta) , \qquad \hat{\epsilon}(s,\eta) = \begin{cases} \mathrm{K} , & \eta > \eta_m , \\ \kappa\eta/\eta_1 , & \eta \le \eta_m , \end{cases} \tag{5.26}$$

where

$$\eta_1(s) = \frac{\rho_e U_e \delta^*}{\rho_o \Delta_o u_{\tau o}} , \qquad \eta_m = \frac{\mathrm{K}}{\kappa} \eta_1 , \qquad \mathrm{K} = 0.0168, \tag{5.27}$$

while the eddy conductivity is defined by

$$\epsilon_H = \frac{\rho_o \rho_e}{\rho^2} U_e \delta^* \hat{\epsilon}_H(\eta) , \quad \hat{\epsilon}_H(s,\eta) = \begin{cases} \mathrm{K}_h , & \eta > \tilde{\eta}_m , \\ \kappa_\theta \eta/\eta_1 , & \eta \le \tilde{\eta}_m , \end{cases} \tag{5.28}$$

where η_1 is defined in equation (5.27) and

$$\tilde{\eta}_m = \frac{\mathrm{K}_h}{\kappa_\theta} \eta_1 , \qquad \mathrm{K}_h = 0.0245. \tag{5.29}$$

For the modification of Baldwin-Lomax (1978) model, $U_e\delta^*$ is replaced by $C_p y_{max}\tilde{F}_{max}$ in the first of equations (5.26) and (5.28) while $U_e\delta^*$ is replaced by $y_{max}\tilde{F}_{max}$ in the definition of η_1 in equation (5.27). The explicit representation of eddy viscosity is

$$\epsilon = \frac{\rho_o \rho_e}{\rho^2} C_p y_{max} \tilde{F}_{max} \hat{\epsilon}(\eta) , \qquad \hat{\epsilon}(s,\eta) = \begin{cases} K , & \eta < \eta_m , \\ \kappa\eta/\eta_1 , & \eta < \eta_m , \end{cases} \tag{5.30}$$

with

$$\eta_1(s) = \frac{\rho_e y_{max} \tilde{F}_{max}}{\rho_o \Delta_o u_{\tau o}} , \qquad \eta_m = \frac{C_p K \eta_1}{\kappa} , \qquad K = 0.0168. \tag{5.31}$$

The Baldwin-Lomax (1978) model was originally introduced because of the difficulty of defining U_e and δ^* unambiguously in certain types of flows, especially internal flows. In the model y_{max} denotes the physical location where the function $\tilde{F} = y|\partial u|\partial y|$ achieves a maximum, normally at a location in the outer region. Note here that y denotes actual physical distance from the surface and, in general, y_{max} must be found iteratively. The determination of the constant C_p is discussed in Appendix B.

Here it is required that the governing equations must reduce to the corresponding incompressible form as $M_{ref} \to 0$. For constant-property flows, Clauser (1954) has examined a large number of outer region velocity profiles and demonstrated empirically that the outer velocity profile can exhibit self-similar behavior when scaled using the single length scale $\Delta_o = U_e\delta^*/u_\tau$, provided the parameter $\beta = (\delta^*/\tau_w)(dp_e/ds)$ is constant. The thickness Δ_o was introduced to

avoid the problems that are invariably encountered when dealing with the ill-defined boundary-layer thickness δ; note however that for each set of equilibrium profiles, Δ_o is generally proportional to δ. Clauser (1954) found that velocity profiles with constant β could be collapsed to a single curve and concluded that a turbulent flow is equilibrium (or is self-similar) when and only when β is constant in the incompressible boundary layer. Mellor and Gibson (1966) and Fendell (1972) later described theoretical arguments that support Clauser's (1954) empirical results, and there is a general acceptance that self-similar velocity profiles can occur in incompressible turbulent boundary layers. Later Weigand (1978) demonstrated that self-similar temperature distributions can occur in low-speed compressible turbulent boundary layers.

Consider now the momentum equation (5.19) and specifically the order of magnitude of the ratio u'_*/u_*. Matching of the inner and the outer layer velocity expansions has resulted in the match condition (3.116), which is rewritten here in terms of u_* according to

$$\frac{1}{u_*} = \frac{1}{\kappa(s)} \log\left(\frac{\rho_o^2}{\mu_w \rho_w} Re u_* \Delta_o U_e\right) + C_i - C_o \ . \tag{5.32}$$

Differentiation of equation (5.32) with respect to s leads to

$$\frac{u'_*}{u_*} = \frac{\kappa'}{\kappa} - \frac{u_*}{\kappa}\left\{\frac{\Delta'_o}{\Delta_o} + \frac{U'_e}{U_e} + \frac{u'_*}{u_*} + 2\frac{\rho'_o}{\rho_o} - \frac{\mu'_w}{\mu_w} - \frac{\rho'_w}{\rho_w} + \kappa'(C_i - C_o) + \kappa\left(C'_i - C'_o\right)\right\} . \tag{5.33}$$

It is now assumed that κ'/κ is negligibly small, and terms such as Δ'_o are at most

$O(\Delta_o)$ in the braces in equation (5.33); it is widely assumed in any event that κ is a universal constant and streamwise variations in a turbulent boundary layer are expected to be slow in s. Consequently, it follows that

$$u'_* = O(u_*^2) \,, \tag{5.34}$$

and the term containing u'_*/u_* may be neglected in equation (5.19). A similar argument may be applied to the matching condition (3.117) for the energy equation, which using equations (3.104) may be written

$$\frac{(1-I_w)}{q_*} = \frac{1}{\kappa_\theta(s)} \log\left(\frac{\rho_o^2}{\mu_w \rho_w} Re u_* \Delta_o U_e\right) + B_i - B_o \,, \tag{5.35}$$

where $I_w = H_w/H_e$. Comparison of equations (5.32) and (5.35) establishes that $q_* = O(u_*)$ for $\kappa_\theta = O(\kappa)$. From either the result or by differentiation of equation (5.35), it follows that

$$q'_* = O(u_*^2) \,, \tag{5.36}$$

and thus the term q'_*/q_* is negligible to leading order in the energy equation (5.20).

Therefore, to leading order equations (5.19) and (5.20) become

$$\frac{\partial}{\partial \eta}\left\{\hat{\epsilon}\frac{\partial^2 F_1}{\partial \eta^2}\right\} + a(s)\eta\frac{\partial^2 F_1}{\partial \eta^2} + b(s)\left\{\left(1-\frac{H_w}{H_e}\right)\frac{\kappa_\theta}{\kappa}\Theta_1 - 2\frac{\partial F_1}{\partial \eta}\right\} = c(s)\frac{\partial^2 F_1}{\partial s \partial \eta} \,, \tag{5.37}$$

$$\frac{\partial}{\partial \eta}\left\{\hat{\epsilon}_H \frac{\partial \Theta_1}{\partial \eta}\right\} + \mathrm{a}(s)\eta \frac{\partial \Theta_1}{\partial \eta} = \mathrm{c}(s) \frac{\partial \Theta_1}{\partial s}\,, \tag{5.38}$$

where the coefficients in these equations are given by

$$\mathrm{a}(s) = \frac{(\Delta_o r U_e)'}{r u_{\tau o} \eta_1}\,, \qquad \mathrm{b}(s) = \frac{\mathrm{c}(s)}{M_e}\frac{dM_e}{ds}\,, \qquad \mathrm{c}(s) = \frac{\Delta_o U_e}{u_{\tau o}\eta_1}\,. \tag{5.39}$$

On the basis the these equations a set of self-similar outer-layer velocity and total-enthalpy profiles will now be developed. These results will subsequently be combined with inner wall-layer profiles to form composite profiles across the entire boundary layer. A large portion of measured profile data in supersonic and hypersonic boundary layers has been taken in constant pressure conditions, and therefore this situation will be addressed here first; the problem of flows with pressure gradient will be considered subsequently.

Self-similar solutions of equations (5.37) and (5.38), for which $F_1 = F_1(\eta)$ and $\Theta_1 = \Theta_1(\eta)$ and M_e is constant ($\mathrm{b} = 0$), are now sought. For self-similar profiles to exist, the coefficients in the governing equations must be constant values; it follows from equations (5.22) and (5.24) that η_1 and $\hat{\epsilon}$ and $\hat{\epsilon}_H$ must be functions of η alone, which requires that η_1 be independent of s; a second requirement is that $\mathrm{a}(s)$ is constant. The first requirement may be satisfied by selecting the outer scale Δ_o according to

$$\Delta_o = \frac{\rho_e U_e \delta^*}{\rho_o u_{\tau o}}\,; \tag{5.40}$$

consequently, the two conditions are

$$\eta_1 = 1 \ , \quad \mathrm{a}(s) = \mathrm{a} \ , \tag{5.41}$$

where a is constant. Under these circumstances, equations (5.37) and (5.38) reduce to

$$\frac{d}{d\eta}\left\{\hat{\epsilon}\frac{d^2F_1}{d\eta^2}\right\} + \mathrm{a}\eta\,\frac{d^2F_1}{d\eta^2} = 0 \ , \tag{5.42}$$

$$\frac{d}{d\eta}\left\{\hat{\epsilon}_H\frac{d\Theta_1}{d\eta}\right\} + \mathrm{a}\eta\,\frac{d\Theta_1}{d\eta} = 0 \ , \tag{5.43}$$

where $\hat{\epsilon}$ and $\hat{\epsilon}_H$ are given by equations (5.26) and (5.28) but with $\eta_1 = 1$. The solution of equation (5.42) which satisfies conditions (5.21) and (5.23) is given by

$$\frac{dF_1}{d\eta} = \begin{cases} -\sqrt{\frac{\pi}{2\mathrm{Ka}}}\,\mathrm{e}^{-\mathrm{Ka}/2\kappa^2}\,\mathrm{erfc}\left\{\sqrt{\frac{\mathrm{a}}{2\mathrm{K}}}\,\eta\right\} & \eta > \eta_m \ , \\ -\frac{1}{\kappa}\mathrm{E}_1\left(\frac{\mathrm{a}\eta}{\kappa}\right) + C_o - \frac{1}{\kappa}\left[\gamma_o - \log\left(\frac{\kappa}{\mathrm{a}}\right)\right] & \eta \le \eta_m \ , \end{cases} \tag{5.44}$$

where C_o is the outer region log-law constant (cf. equation (5.21)) which is given by

$$C_o = \frac{1}{\kappa}\left\{\gamma_o - \log\left(\frac{\kappa}{\mathrm{a}}\right) + \mathrm{E}_1\left(\frac{\mathrm{aK}}{\kappa^2}\right)\right\} - \sqrt{\frac{\pi}{2\mathrm{Ka}}}\,\mathrm{e}^{-\mathrm{aK}/2\kappa^2}\,\mathrm{erfc}\left\{\sqrt{\frac{\mathrm{aK}}{2\kappa^2}}\right\} . \tag{5.45}$$

In the above equations erfc and E_1 denote the complementary error function and exponential integral, respectively and $\gamma_o = 0.577215...$ is Euler's constant. The solution for the total enthalpy function Θ_1 is also given by equation (5.44) but with K and κ replaced by K_h and κ_θ respectively; in addition B_o, the outer region log-law constant for total enthalpy (cf. equation (5.22)), replaces C_o. The constant B_o is also given by equation (5.45) but with $K = K_h$ and $\kappa = \kappa_\theta$. The exact solutions (5.44) and (5.45) provide a convenient representation of the defect profiles for the simple eddy-viscosity and eddy-conductivity functions. Note that more complicated models such as the Johnson-King (1985) model or other effects such as intermittency are included in the basic turbulence model, it is necessary to obtain solutions of the similarity equations numerically. This is easily accomplished using the two-tier scheme described in Yuhas and Walker (1982). In this approach, for example, numerical solution of equation (5.42) is obtained using finite difference methods in an outer tier defined by $\eta_m < \eta < \infty$, where η_m is given in equation (5.27) with $\eta_1 = 1$; this solution satisfies $dF_1/d\eta \to 0$ as $\eta \to \infty$. In the inner tier for $\eta \leq \eta_m$ power series solutions are constructed for small η containing the logarithmic behavior in equation (5.17). The set of solutions are jointed at $\eta = \eta_m$ so as to ensure that the defect functions and their derivatives are continuous there.

It should be noted that the solution described above depends on the, as yet, undetermined constant a. Integrating equation (5.42) across the boundary layer and making use of the boundary conditions (5.21) and (5.23), as well as the fact that $F_1(0) = 0$, it is easily shown that

$$a = -1/F_{1\infty}\,, \tag{5.46}$$

where $F_{1\infty}$ is the limiting value of $F_1(\eta)$ as $\eta \to \infty$. For incompressible flow ($M_e \to 0$), it is readily demonstrated that $F_{1\infty} = -1$ (see Fendell, 1972); however, for compressible flow $F_{1\infty}$ may be significantly different from one. In fact in compressible flows, the solutions of equations (5.42) and (5.43) are closely coupled through the parameter a; for incompressible flows $a = 1$ and the momentum equation can be solved independently. To an extent the value of a indicates the degree of coupling between the momentum and thermal equations as the Mach number increases. This will be demonstrated subsequently once the procedure to determine the appropriate value of a is described.

For each value of the solution of equation (5.42) gives profile for $\partial F_1/\partial \eta$, which also satisfies the integral form (5.46) which may be rewritten according to

$$\int_o^\infty \left(\frac{dF_1}{d\eta}\right) d\eta = -\frac{1}{a} . \tag{5.47}$$

Using the defect velocity formula (3.111) and equation (5.40), it is easily shown from the definition of δ^* in equation (5.8) that

$$\int_o^\infty \frac{\rho_e}{\rho}\left(\frac{dF_1}{d\eta}\right) d\eta = -1 . \tag{5.48}$$

Therefore the constant a must be determined iteratively so that the integral condition (5.48) is satisfied. It should be noted that the integral (5.48) is taken across the outer layer, since contributions to δ^* due to the wall layer are negligible to leading order in the limit $Re \to \infty$. Because the pressure is invariant across the

boundary layer at any streamwise location, it follows from the ideal gas law and equation (3.10) that

$$\frac{\rho_e}{\rho} = \frac{T}{T_e} = \left\{1 + \frac{(\gamma-1)}{2} M_e^2\right\} \left\{\frac{H}{H_e} - \frac{\alpha}{2} F^2\right\}, \tag{5.49}$$

where α is defined by equation (3.9). It is evident from equation (5.49) that the solution of the momentum and energy equations is coupled through the parameter a.

5.4 The Reference Condition

The wall-layer profiles and the outer-region solutions described in §5.3 can now be combined to form profiles that are valid for the entire boundary layer once the reference density ρ_o is specified. It was argued in §3 that neither the wall value ρ_w nor the value at the edge of the boundary layer ρ_e is likely to be a suitable choice for ρ_o. Rather a suitable choice would appear to require a value which is representative of both layers. Here two possibilities will be considered to define ρ_o and the corresponding reference temperature T_o; this choice then formally defines the velocity scale u_{τ_o}. Recall that the major changes in density occur across the wall layer and, consequently, a choice based on either an average density (or temperature) or a mean density would seem logical. It has been suggested that a wall-layer characteristic density might be a suitable selection of ρ_o for the completion of asymptotic analysis of a turbulent boundary layer.

Consider first a definition of T_o based on an average wall-layer temperature

defined by

$$T_o = \frac{1}{Y_l^+} \int_o^{Y_l^+} T \, dY^+ \,, \tag{5.50}$$

where Y_l^+ is regarded as a universal value of Y^+ which is characteristic of the extent of the wall layer in equation (5.49) that

$$T_o = T_w - T_e \left\{ \frac{\gamma - 1}{2} M_e^2 \, u_*^2 \mathrm{A}_l^+ - \left(1 + \frac{\gamma - 1}{2} M_e^2\right) q_* \mathrm{B}_l^+ \right\}, \tag{5.51}$$

where the constants A_l^+ and B_l^+ are given by

$$\mathrm{A}_l^+ = \frac{1}{Y_l^+} \int_o^{Y_l^+} [U^+(Y^+)]^2 \, dY^+, \quad \mathrm{B}_l^+ = \frac{1}{Y_l^+} \int_o^{Y_l^+} \theta^+(Y^+) \, dY^+, \tag{5.52}$$

and the mean values of the wall-layer profile for $(U^+)^2$ and θ^+ in the wall layer. Since U^+ and θ^+ are known analytical functions of Y^+, A_l^+ and B_l^+ can be readily evaluated and the results depend only parametrically on the log-law constants κ, C_i and κ_θ, B_i .

Although Y_l^+ is assumed to be representative of the normal extent, it is not possible to define the quantity uniquely since there is not a distinct boundary between the inner and outer layer, but rather an overlap zone where the solutions merge smoothly together. To determine specific universal value for Y_l^+, a comparison with experiment is indicated. For experimental flow and heat transfer conditions, a set of wall-layer velocity and total-enthalpy profiles can be calculated for a specified Y_l^+, and a mean density ρ_o can be evaluated using equation (5.51).

In principle, the resulting profiles could then be compared with measured data to decide on which value of Y_l^+ produces optimal results. Unfortunately, data in the wall layer is sparse and often of uncertain reliability. and an alternative method to obtain the best value of Y_l^+ was carried out as follows.

Another basis for comparison with experiment is the quoted values of wall shear stress. Although it is difficult to measure skin friction directly, there has been much effort to improve reliability of these measurements using floating element balances (FEB), and currently there is data over a wide range of Mach number and surface heat transfer rates. This data is perhaps least reliable in the hypersonic regime and when large temperature differences exist across the boundary layer. Nevertheless skin friction data in the supersonic regime and with moderate heat transfer rates are generally considered reasonably credible and certainly more reliable than estimates based on an extrapolated slope of the velocity profile at the wall. Here a sufficient amount of skin friction data obtained in recent times using the direct FEB method was collected in the range of $0 \leq M_e \leq 11$ and $0.22 \leq T_w/T_r \leq 1$ to carry out a reasonably extensive comparison; here T_r is the recovery temperature defined in equation (2.43). For each given flow and heat transfer condition (taken from each experiment), a set of self-similar composite velocity and total-enthalpy profiles were calculated using the procedure to be described in §5.5. For each value of Y_l^+ used in defining T_o in equations (5.51) and (5.52), different skin-friction coefficient c_f will be obtained. The object here is to compare results for a large number of values of calculated c_f with the corresponding data, $c_{f,data}$, and through this process determine a "best" fixed value of Y_l^+. The principal difficulty with the fitting process is that there are

relatively large discrepancies between experiments, especially at hypersonic speeds or when the wall is strongly cooled. There are still many questions associated with the accuracy of the FEB measurement in high speed flows with heat transfer and, until a more reliable data base is established, it makes no sense to perform a highly refined optimization process. For this reason, the final value of Y_l^+ was obtained through trial and error and selected on a visual basis.

The results of this process are shown in Figures (5.1), (5.2) and (5.3) for $Y_l^+ = 40$, 60 and 70 respectively. The points denote the skin friction coefficient c_f obtained in the calculation procedure to be described in §5.5; this value constitutes a prediction for c_f, and a point will be on the straight line when c_f agrees exactly with its corresponding data $c_{f,data}$. The circles on these graphs represent cases where the wall is nearly adiabatic while the squares are for flows having significant heat transfer towards the wall (the strongly cooled wall). The data is presented in terms of the quantity $(\gamma-1)M_e^2 c_f$; consideration of several related quantities, this group of physical variables was found to be very convenient to represent the influence of Reynolds number, Mach number, and surface heat transfer. Suppose, for example, that the Mach number is held constant and the Reynolds number is increased; this will result in a decrease in c_f. However, an increase in Mach number will also result in a decrease in c_f. At the same time, cooling of the wall tends to result in an increase in c_f. Consequently, if c_f alone were used in Figures 5.1 to 5.3, most of the high speed data would appear shifted to the left while most of the cold wall data would appear far to the right of the graph. In a plot of $(\gamma-1)M_e^2 c_f$, the portion of the graph to the left represents high Reynolds number, low Mach number, and nearly adiabatic flows; on the other hand, the portion to

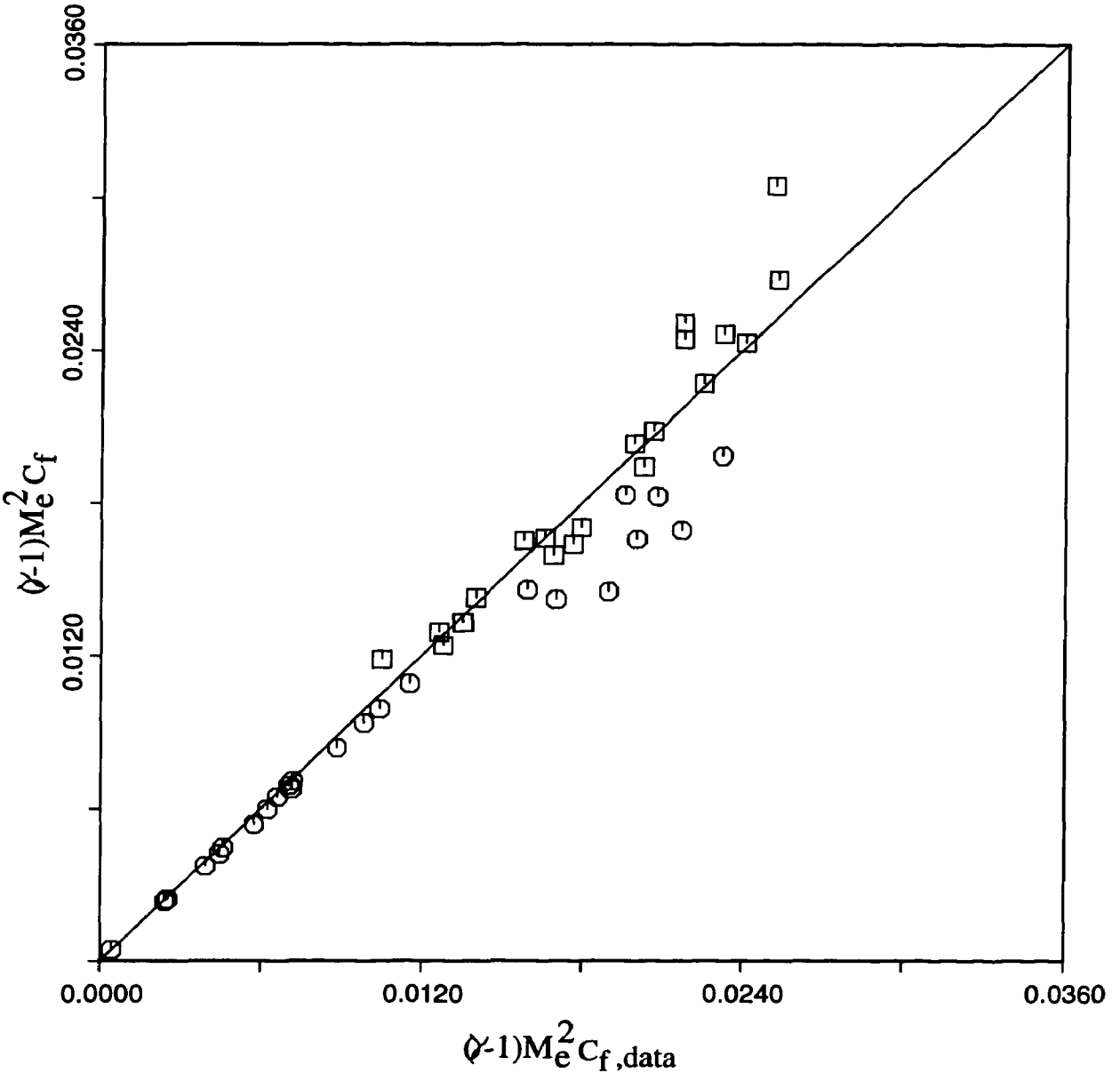

Figure 5.1. Comparison of theoretical skin friction with data, using the reference condition in equation (5.51) based on $Y_l^+ = 40$; the data is from Fernholz and Finley (1977, 1981) and tabulated results are given in Table 5.1.

Case No.	M_e	T_w/T_r	c_f (data) $\times 10^3$	c_f (theory) $\times 10^3$
53010401	2.540	≈ 1	2.420	2.312
53010601	2.578	≈ 1	1.660	1.578
53011302	4.544	≈ 1	1.260	1.196
58020103	1.739	≈ 1	1.900	1.940
58020207	2.739	≈ 1	1.515	1.481
58020304	3.667	≈ 1	1.306	1.280
58020306	3.681	≈ 1	1.220	1.189
65060101	2.445	0.9721	1.030	0.9774
67020701	6.430	0.9282	1.256	1.102
67020801	6.340	0.8607	0.9920	0.9041
73020402	0.793	≈ 1	1.650	1.706
73020914	2.208	≈ 1	1.290	1.242
74020303	2.500	1.0019	1.560	1.493
74021001	3.483	1.0098	1.470	1.453
74021204	3.496	1.0023	1.170	1.097
74021801	4.517	1.0242	1.080	1.024
74021805	4.493	0.9829	0.880	0.8345
77030101	5.994	0.8983	0.8017	0.7557
73050304(H)	9.830	≈ 1	0.3040	0.2836
73050504(H)	10.31	≈ 1	0.2400	0.1998
78040104(H)	11.04	1.0418	0.2826	0.2410
78040105(H)	11.23	1.0298	0.2578	0.2010
78040106(H)	11.40	1.0658	0.2311	0.1907
78040107(H)	11.51	1.0570	0.2148	0.1637

Table 5.1a. Parameters associated with near-adiabatic wall experiments; c_f (theory) is calculated for $Y_l^+ = 40$ in equation (5.51) and (H) denotes that the gas is helium.

Case No.	M_e	T_w/T_r	c_f (data) $\times 10^3$	c_f (theory) $\times 10^3$
65060103	4.915	0.7105	1.330	1.286
65060104	4.895	0.5951	1.410	1.383
65060105	4.961	0.5228	1.480	1.505
67020104	6.490	0.5253	1.336	1.344
72021203	4.857	0.2279	1.110	1.253
72021401	4.792	0.2107	1.720	1.794
72021501	4.929	0.2242	1.300	1.326
72040101	6.210	0.3330	1.560	1.572
72040201	6.390	0.3136	1.220	1.242
72040301	6.420	0.4377	1.230	1.176
72040401	6.420	0.4194	1.250	1.261
72040501	6.500	0.5082	1.060	1.006
72040601	6.500	0.5014	1.000	0.9409
72050102	7.200	0.4984	0.850	0.7881
72050103	7.200	0.4764	0.800	0.7991
N103838	8.013	0.2970	0.980	1.185
78040204(H)	11.17	0.4455	0.304	0.3201
78040205(H)	11.00	0.4319	0.288	0.3046
78040206(H)	11.47	0.4364	0.248	0.2855
78040207(H)	11.42	0.3808	0.250	0.2804

Table 5.1b. Parameters associated with cooled-wall experiments; c_f (theory) is calculated for $Y_l^+ = 40$ in equation (5.51) and (H) denotes that the gas is helium.

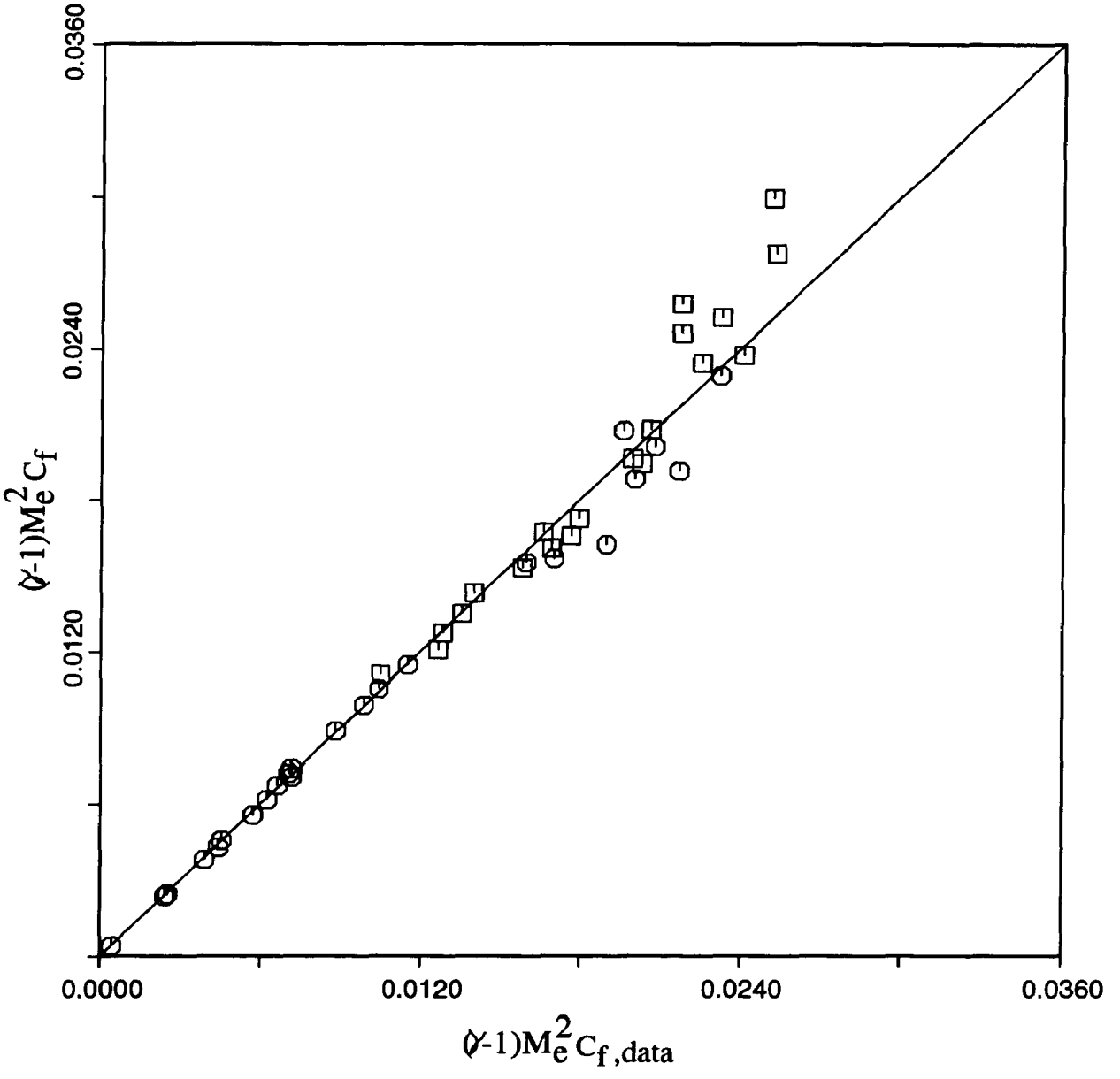

Figure 5.2. Comparison of theoretical skin friction with data using the reference condition in equation (5.51) based on $Y_t^+ = 60$; the data is from Fernholz and Finley (1977, 1981) and tabulated results are given in Table 5.2.

Case No.	M_e	T_w/T_r	c_f (data) $\times 10^3$	c_f (theory) $\times 10^3$
53010401	2.540	≈ 1	2.420	2.400
53010601	2.578	≈ 1	1.660	1.627
53011302	4.544	≈ 1	1.260	1.278
58020103	1.739	≈ 1	1.900	1.975
58020207	2.739	≈ 1	1.515	1.531
58020304	3.667	≈ 1	1.306	1.344
58020306	3.681	≈ 1	1.220	1.246
65060101	2.445	0.9721	1.030	1.038
67020701	6.430	0.9282	1.256	1.216
67020801	6.340	0.8607	0.9920	0.9658
73020402	0.793	≈ 1	1.650	1.713
73020914	2.208	≈ 1	1.290	1.267
74020303	2.500	1.0019	1.560	1.537
74021001	3.483	1.0098	1.470	1.527
74021204	3.496	1.0023	1.170	1.143
74021801	4.517	1.0242	1.080	1.091
74021805	4.493	0.9829	0.880	0.8755
77030101	5.994	0.8983	0.8017	0.7997
73050304(H)	9.830	≈ 1	0.3040	0.3220
73050504(H)	10.31	≈ 1	0.2400	0.2212
78040104(H)	11.04	1.0418	0.2826	0.2789
78040105(H)	11.23	1.0298	0.2578	0.2279
78040106(H)	11.40	1.0658	0.2311	0.2173
78040107(H)	11.51	1.0570	0.2148	0.1838

Table 5.2a. Parameters associated with near-adiabatic wall experiments; c_f (theory) is calculated for $Y_l^+ = 60$ in equation (5.51) and (H) denotes that the gas is helium. The $Y_l^+ = 60$ is believed to be the optimum choice.

Case No.	M_e	T_w/T_r	c_f (data) $\times 10^3$	c_f (theory) $\times 10^3$
65060103	4.915	0.7105	1.330	1.319
65060104	4.895	0.5951	1.410	1.405
65060105	4.961	0.5228	1.480	1.510
67020104	6.490	0.5253	1.336	1.388
72021203	4.857	0.2279	1.110	1.173
72021401	4.792	0.2107	1.720	1.663
72021501	4.929	0.2242	1.300	1.239
72040101	6.210	0.3330	1.560	1.536
72040201	6.390	0.3136	1.220	1.200
72040301	6.420	0.4377	1.230	1.176
72040401	6.420	0.4194	1.250	1.258
72040501	6.500	0.5082	1.060	1.019
72040601	6.500	0.5014	1.000	0.949
72050102	7.200	0.4984	0.850	0.797
72050103	7.200	0.4764	0.800	0.804
N103838	8.013	0.2970	0.980	1.164
78040204(H)	11.17	0.4455	0.304	0.333
78040205(H)	11.00	0.4319	0.288	0.312
78040206(H)	11.47	0.4364	0.248	0.293
78040207(H)	11.42	0.3808	0.250	0.282

Table 5.2b. Parameters associated with cooled-wall experiments; c_f (theory) is calculated for $Y_l^+ = 60$ in equation (5.51) and (H) denotes that the gas is helium. The value of $Y_l^+ = 60$ is believed to be the optimum choice.

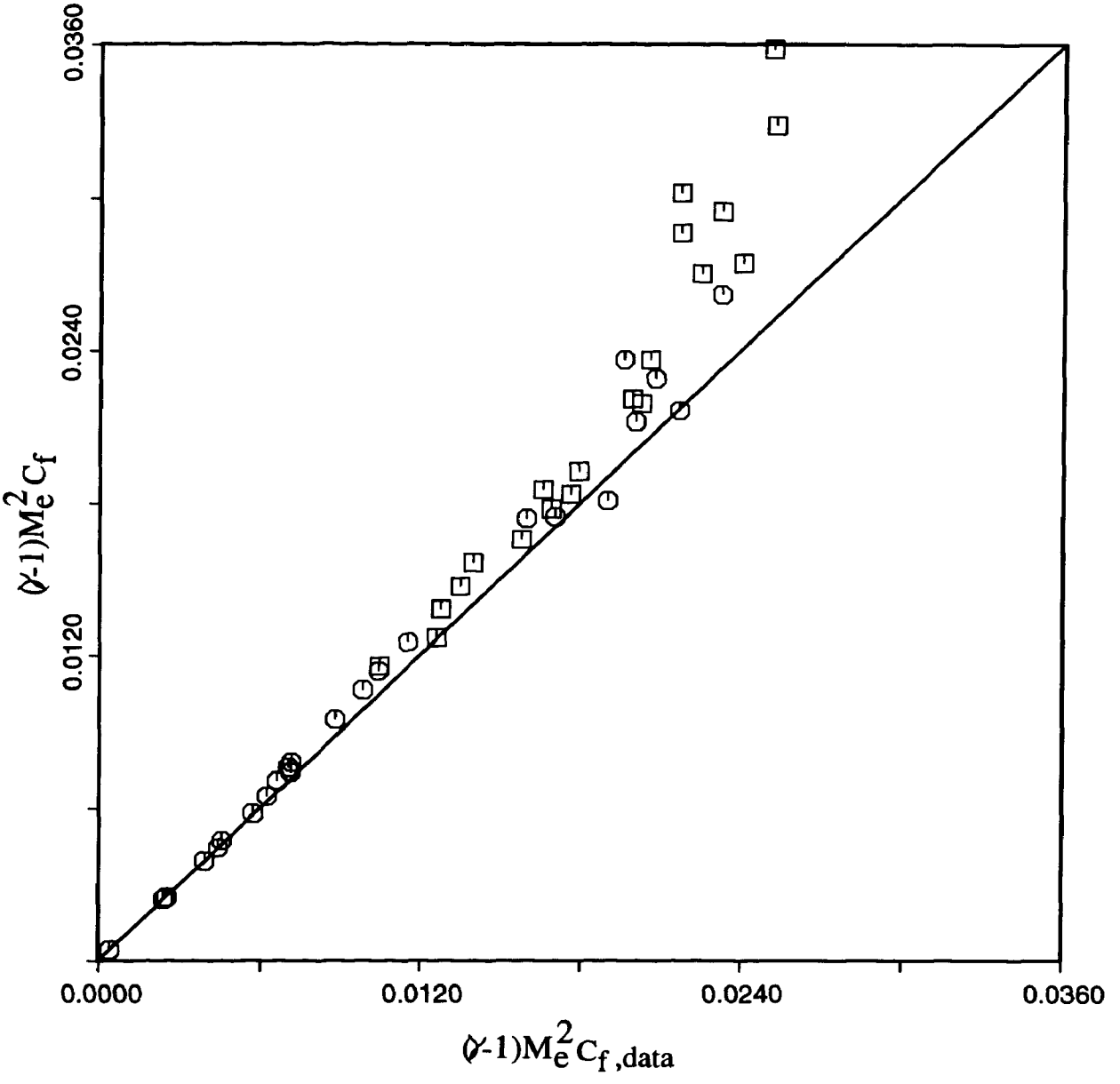

Figure 5.3. Comparison of theoretical skin friction with data using the reference condition in equation (5.51) based on $Y_l^+ = 70$; the data is from Fernholz and Finley (1977, 1981) and tabulated results are given in Table 5.3.

Case No.	M_e	T_w/T_r	c_f (data) $\times 10^3$	c_f (theory) $\times 10^3$
53010401	2.540	≈ 1	2.420	2.513
53010601	2.578	≈ 1	1.660	1.677
53011302	4.544	≈ 1	1.260	1.378
58020103	1.739	≈ 1	1.900	2.007
58020207	2.739	≈ 1	1.515	1.581
58020304	3.667	≈ 1	1.306	1.416
58020306	3.681	≈ 1	1.220	1.307
65060101	2.445	0.9721	1.030	1.115
67020701	6.430	0.9282	1.256	1.383
67020801	6.340	0.8607	0.9920	1.081
73020402	0.793	≈ 1	1.650	1.717
73020914	2.208	≈ 1	1.290	1.286
74020303	2.500	1.0019	1.560	1.577
74021001	3.483	1.0098	1.470	1.611
74021204	3.496	1.0023	1.170	1.188
74021801	4.517	1.0242	1.080	1.162
74021805	4.493	0.9829	0.880	0.9202
77030101	5.994	0.8983	0.8017	0.8709
73050304(H)	9.830	≈ 1	0.3040	0.3664
73050504(H)	10.31	≈ 1	0.2400	0.2461
78040104(H)	11.04	1.0418	0.2826	0.3184
78040105(H)	11.23	1.0298	0.2578	0.2573
78040106(H)	11.40	1.0658	0.2311	0.2445
78040107(H)	11.51	1.0570	0.2148	0.2046

Table 5.3a. Parameters associated with near-adiabatic wall experiments; c_f (theory) is calculated for $Y_l^+ = 70$ in equation (5.51) and (H) denotes that the gas is helium.

Case No.	M_e	T_w/T_r	c_f (data) $\times 10^3$	c_f (theory) $\times 10^3$
65060103	4.915	0.7105	1.330	1.432
65060104	4.895	0.5951	1.410	1.531
65060105	4.961	0.5228	1.480	1.651
67020104	6.490	0.5253	1.336	1.601
72021203	4.857	0.2279	1.110	1.223
72021401	4.792	0.2107	1.720	1.799
72021501	4.929	0.2242	1.300	1.302
72040101	6.210	0.3330	1.560	1.775
72040201	6.390	0.3136	1.220	1.350
72040301	6.420	0.4377	1.230	1.327
72040401	6.420	0.4194	1.250	1.431
72040501	6.500	0.5082	1.060	1.136
72040601	6.500	0.5014	1.000	1.049
72050102	7.200	0.4984	0.850	0.883
72050103	7.200	0.4764	0.800	0.8915
N103838	8.013	0.2970	0.980	1.393
78040204(H)	11.17	0.4455	0.304	0.3937
78040205(H)	11.00	0.4319	0.288	0.3644
78040206(H)	11.47	0.4364	0.248	0.3437
78040207(H)	11.42	0.3808	0.250	0.3284

Table 5.3b. Parameters associated with cooled-wall experiments; c_f (theory) is calculated for $Y_l^+ = 70$ in equation (5.51) and (H) denotes that the gas is helium.

the right tends to represent high Mach number flows (and relatively lower Reynolds numbers) and/or strongly cooled walls. The factor $(\gamma-1)M_e^2$ is introduced here because it appears naturally in compressible flow formulae (cf. equations (2.43) and (5.49) for example) and using the factor $(\gamma-1)$ facilitates comparisons for different gases.

It may be noted that the direct measurement of skin friction by the direct FEB method becomes increasingly more difficult in flows with high Mach number and/or strongly cooled walls; this is believed to be partially responsible for the increased scatter on each of Figures 5.1 to 5.3 for large values of $(\gamma-1)M_e^2 c_f$. It does appear that the calculated values of $(\gamma-1)M_e^2 c_f$ tend to be underpredicted in the hypersonic flows with adiabatic walls. However, in this Mach number ($M_e \approx 10$), the data are only for helium and are too scattered to make definite conclusions. At present there does not seem to be data taken in air flow at such high Mach numbers that could be used to confirm the trend shown in Figures 5.1 to 5.3. Data with strong heat transfer exhibit even more scatter, and there is a clear indication in Figures 5.1 to 5.3 that there is a tendency for the c_f values in the cold wall, hypersonic regime to be overpredicted for each of the Y_l^+ values used in obtaining Figures 5.1 to 5.3. In Tables 5.1 to 5.3, the test cases used in this comparison are listed along with the numerical values used in preparing the figures. In Tables 5.1(a) through 5.3(a), the cases for an almost adiabatic wall are listed, while situations with strongly cooled walls are given in Tables 5.1(b) through 5.3(b). The majority of the data was taken from the compilation due to Fernholz and Finley (1977), and their identification scheme for each profile is used in Tables 5.1 through 5.3. The calculated values of the skin friction coefficient are given in

these tables and may be compared directly with the quoted experimental values. Apart from some uncertainty in the hypersonic range, the calculated c_f are very close to the experimental values for the value $Y_l^+ = 60$, and this is believed to be fairly representative of an average across the wall layer. It is evident from comparing the graphs in Figures 5.1 through 5.3 that the value $Y_l^+ = 60$ gives the best representation of the data. For the cases where the wall is almost adiabatic, the discrepancies between calculated and measured skin-friction values are less than 4%. For hypersonic flows in helium, the c_f tend to be somewhat scattered; however, the mean average of the differences between $c_{f,data}$ and the predicted value is less than 6%. For the flows with heat transfer (in Table 5.2(b)), the calculated skin friction agrees with the data to within 5% of a Mach number of 7 and temperature ratio T_w/T_r of approximately 0.2; these results are also shown in Figure 5.2. It is worthwhile at this stage to reinforce the idea of using a realistic reference condition (for both parts of the boundary layer) by considering the case $Y_l^+ = 0$; this corresponds to taking the reference condition at the wall. It is evident from comparing Figure 5.2 with 5.4 that the representation of the data is much worse, and this confirms previous arguments that indicate wall values are not suitable as a reference condition for both portions of the boundary layer. It is evident that $T_o = T_w$ is not acceptable even in supersonic range. It is also interesting to note for a strongly cooled wall, T_o (evaluated at $Y_l^+ = 60$) can be substantially larger than either T_w or T_e, as may be evident from (3.4).

The results given in Figure 5.2 are based on defining the reference condition at an average temperature across the sublayer defined by equation (5.49). The evaluation of this value of T_o requires an integration of the wall-layer profiles

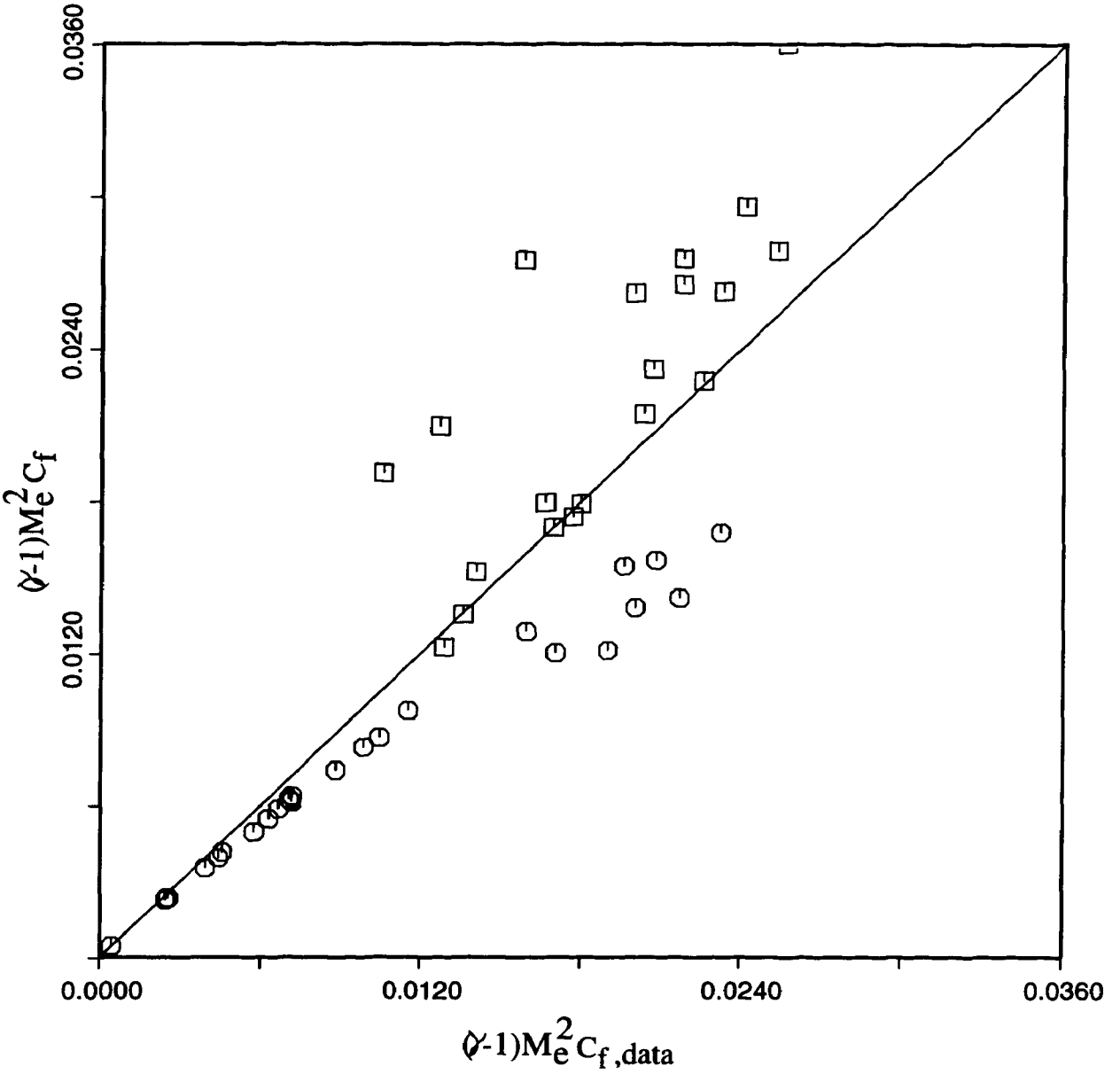

Figure 5.4. Comparison of theoretical skin friction with data using the value at the wall as the reference condition; the data is from Fernholz and Finley (1977, 1981) and tabulated results are given in Tbale 5.4.

Case No.	M_e	T_w/T_r	c_f (data) $\times 10^3$	c_f (theory) $\times 10^3$
53010401	2.540	≈ 1	2.420	2.114
53010601	2.578	≈ 1	1.660	1.475
53011302	4.544	≈ 1	1.260	1.046
58020103	1.739	≈ 1	1.900	1.866
58020207	2.739	≈ 1	1.515	1.380
58020304	3.667	≈ 1	1.306	1.155
58020306	3.681	≈ 1	1.220	1.078
65060101	2.445	0.9721	1.030	0.8656
67020701	6.430	0.9282	1.256	0.9459
67020801	6.340	0.8607	0.9920	0.7980
73020402	0.793	≈ 1	1.650	1.694
73020914	2.208	≈ 1	1.290	1.194
74020303	2.500	1.0019	1.560	1.404
74021001	3.483	1.0098	1.470	1.305
74021204	3.496	1.0023	1.170	1.009
74021801	4.517	1.0242	1.080	0.9020
74021805	4.493	0.9829	0.880	0.7577
77030101	5.994	0.8983	0.8017	0.6753
73050304(H)	9.830	≈ 1	0.3040	0.2391
73050504(H)	10.31	≈ 1	0.2400	0.1691
78040104(H)	11.04	1.0418	0.2826	0.2035
78040105(H)	11.23	1.0298	0.2578	0.1684
78040106(H)	11.40	1.0658	0.2311	0.1588
78040107(H)	11.51	1.0570	0.2148	0.1368

Table 5.4a. Parameters associated with near-adiabatic wall experiments; c_f (theory) is calculated using the value at the wall as the reference condition. (H) denotes that the gas is helium.

Case No.	M_e	T_w/T_r	c_f (data) $\times 10^3$	c_f (theory) $\times 10^3$
65060103	4.915	0.7105	1.330	1.265
65060104	4.895	0.5951	1.410	1.405
65060105	4.961	0.5228	1.480	1.602
67020104	6.490	0.5253	1.336	1.345
72021203	4.857	0.2279	1.110	2.019
72021401	4.792	0.2107	1.720	2.987
72021501	4.929	0.2242	1.300	2.150
72040101	6.210	0.3330	1.560	1.915
72040201	6.390	0.3136	1.220	1.599
72040301	6.420	0.4377	1.230	1.296
72040401	6.420	0.4194	1.250	1.403
72040501	6.500	0.5082	1.060	1.055
72040601	6.500	0.5014	1.000	0.9996
72050102	7.200	0.4984	0.850	0.8353
72050103	7.200	0.4764	0.800	0.8620
N103838	8.013	0.2970	0.980	1.468
78040204(H)	11.17	0.4455	0.304	0.3238
78040205(H)	11.00	0.4319	0.288	0.3241
78040206(H)	11.47	0.4364	0.248	0.3018
78040207(H)	11.42	0.3808	0.250	0.3159

Table 5.4b. Parameters associated with cooled-wall experiments; c_f(theory) is calculated using the value at the wall as the reference condition. (H) denotes that the gas is helium.

across the wall layer, and while this can be carried out once and for all for the velocity profile, the total enthalpy profile can vary from case to case depending on the value of κ_θ and the surface heat transfer. For $Y_l^+ = 60$ a value of $A_l^+ = 142.84$ is obtained while B_l^+ varied between 9.554 and 9.565; in principle an average value of $B_l^+ = 9.56$ could be used in applying this theory. Here following Burggraf (1962), an alternative and perhaps more convenient way of defining the reference condition is considered. Burggraf (1962) selected the reference condition at $Y^+ = 11$ and here various choices were considered. The value which seemed to produce the best overall correspondence with the experimental data was for $Y_o^+ = 23$. The comparisons using this simple criterion are shown in Figure 5.5 and Tables 5.5. It is evident that the data comparisons are in reasonable agreement with those shown in Figure 5.2. Consequently this simple definition of a reference temperature, i.e. $T_o = T_o\ (Y_o^+)$ where $Y_o^+ = 23$ is also a viable model; this definition of the reference temperature may be thought of as mean temperature for the compressible wall layer.

It is generally accepted that the wall layer ends somewhere in the range $y^+ \approx 40$ in an incompressible turbulent boundary layer, and beyond that range the wall layer blends into the outer layer. It has been shown that similar wall-layer functions are valid in compressible flow but in terms of Y^+; thus the wall layer should end in the similar range, but in terms of Y^+. The present results appear to confirm the wall-layer mean temperature concept, and it may be concluded that in nearly adiabatic flows with Mach numbers up to 10, or in strongly cooled wall cases with $T_w/T_r > 0.2$ and $M_e < 7$, the suggested compressible wall layer model produces good results. Beyond these ranges it is not clear yet whether the discrepancies

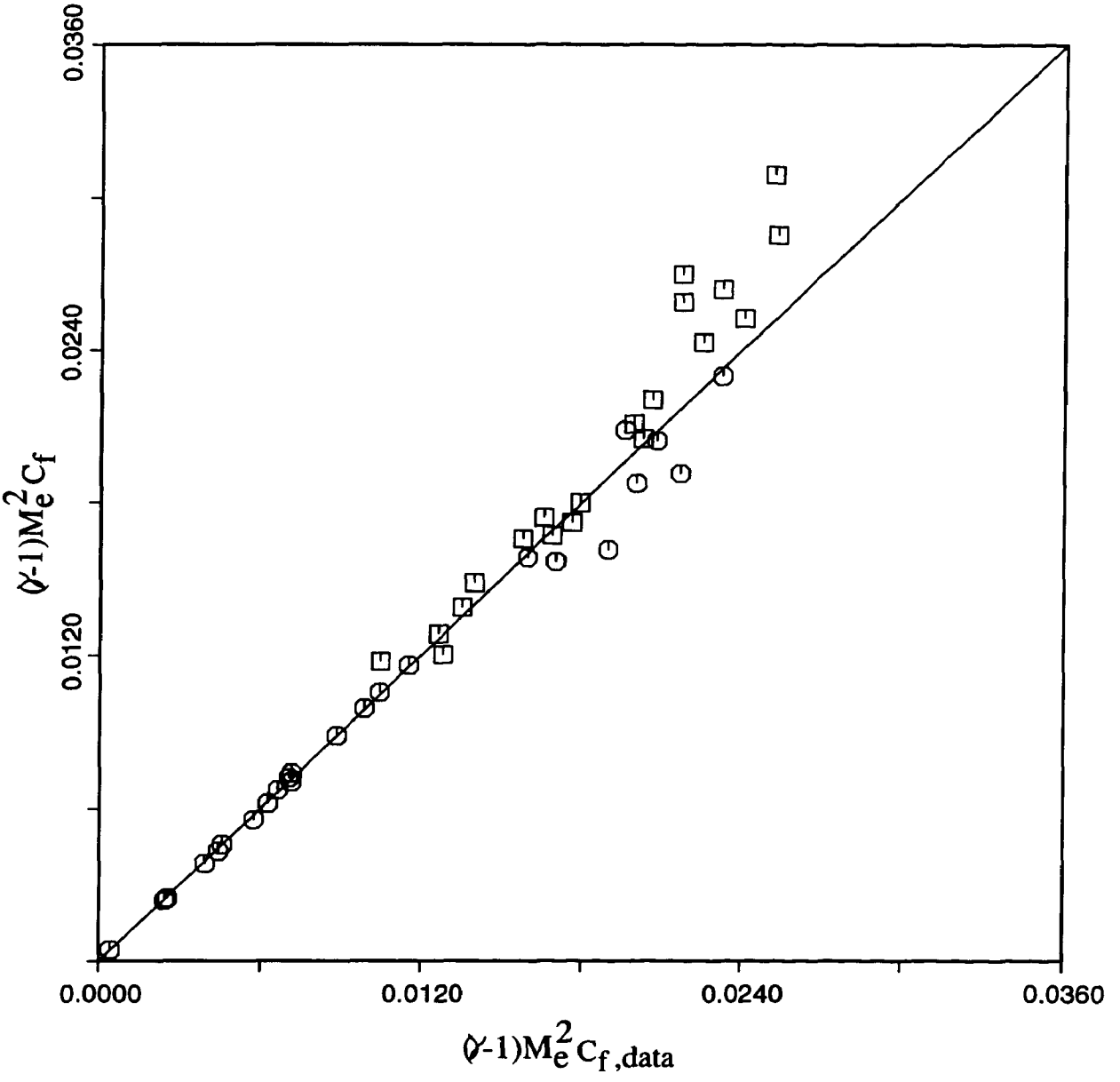

Figure 5.5. Comparison of theoretical skin friction with data, using the reference condition evaluated at $Y^+ = 23$; the data is from Fernholz and Finley (1977, 1981) and tabulated results are given in Table 5.5.

Case No.	M_e	T_w/T_r	c_f (data) $\times 10^3$	c_f (theory) $\times 10^3$
53010401	2.540	≈ 1	2.420	2.394
53010601	2.578	≈ 1	1.660	1.618
53011302	4.544	≈ 1	1.260	1.274
58020103	1.739	≈ 1	1.900	1.970
58020207	2.739	≈ 1	1.515	1.521
58020304	3.667	≈ 1	1.306	1.346
58020306	3.681	≈ 1	1.220	1.238
65060101	2.445	0.9721	1.030	1.038
67020701	6.430	0.9282	1.256	1.234
67020801	6.340	0.8607	0.9920	0.983
73020402	0.793	≈ 1	1.650	1.710
73020914	2.208	≈ 1	1.290	1.259
74020303	2.500	1.0019	1.560	1.527
74021001	3.483	1.0098	1.470	1.519
74021204	3.496	1.0023	1.170	1.134
74021801	4.517	1.0242	1.080	1.090
74021805	4.493	0.9829	0.880	0.870
77030101	5.994	0.8983	0.8017	0.805
73050304(H)	9.830	≈ 1	0.3040	0.3232
73050504(H)	10.31	≈ 1	0.2400	0.2208
78040104(H)	11.04	1.0418	0.2826	0.2791
78040105(H)	11.23	1.0298	0.2578	0.2276
78040106(H)	11.40	1.0658	0.2311	0.2161
78040107(H)	11.51	1.0570	0.2148	0.1824

Table 5.5a. Parameters associated with near-adiabatic wall experiments; c_f (theory) for the reference temperature taken at $Y^+ = 23$; (H) denotes that the flow is helium.

Case No.	M_e	T_w/T_r	c_f (data) $\times 10^3$	c_f (theory) $\times 10^3$
65060103	4.915	0.7105	1.330	1.249
65060104	4.895	0.5951	1.410	1.447
65060105	4.961	0.5228	1.480	1.569
67020104	6.490	0.5253	1.336	1.463
72021203	4.857	0.2279	1.110	1.245
72021401	4.792	0.2107	1.720	1.803
72021501	4.929	0.2242	1.300	1.321
72040101	6.210	0.3330	1.560	1.615
72040201	6.390	0.3136	1.220	1.251
72040301	6.420	0.4377	1.230	1.244
72040401	6.420	0.4194	1.250	1.307
72040501	6.500	0.5082	1.060	1.064
72040601	6.500	0.5014	1.000	0.9882
72050102	7.200	0.4984	0.850	0.8299
72050103	7.200	0.4764	0.800	0.8398
N103838	8.013	0.2970	0.980	1.283
78040204(H)	11.17	0.4455	0.304	0.3544
78040205(H)	11.00	0.4319	0.288	0.3324
78040206(H)	11.47	0.4364	0.248	0.2927
78040207(H)	11.42	0.3808	0.250	0.2906

Table 5.5b. Parameters associated with cooled-wall experiments; c_f (theory) for the reference temperature taken at $Y^+ = 23$. (H) denotes that the flow is helium.

between the calculations and data are due to a failure of the theory or error in measurements.

5.5 Comparison with Mean Profile Measurements

In this subsection the method of constructing composite profiles for total enthalpy and velocity will be described. Assume that at a given streamwise location along the surface, following dimensional data are known: (a) the mainstream velocity U_e^*, temperature T_e^* and density ρ_e^*, (b) the wall temperature T_w^*, and (c) the kinetic displacement thickness δ^{**}, which is related to the dimensionless thickness δ^* by $\delta^{**} = L_{ref}^* \delta^*$. In general the incompressible displacement thickness may be evaluated from measurements of u/U_e across the boundary layer through numerical integration and consequently only involves one source of experimental error; therefore δ^{**} should be considered to be one of the most reliable quantities quoted in experimental studies. The compressible displacement thickness and the momentum thickness, for example, implicitly contain experimental errors associated with mean temperature measurements and therefore may be considered to be somewhat less reliable.

Note that the formal definition of kinetic displacement thickness for an axisymmetric boundary layer is slightly different to that for a two-dimensional flow. In general, the kinetic displacement thickness is related to the difference in volumetric flux between that for the actual viscous profile and that which would occur if the flow were inviscid (i.e., $u \equiv U_e$). This difference is evaluated by integrating $(U_e - u)$ across the boundary layer, and δ^* is defined by imaging an equivalent inviscid flow in which the solid surface is displaced upward a distance to

make up for the "lost" volumetric flux associated with viscous effects. This thought process leads to the equation

$$U_e A^* = \int_o^\infty (U_e - u) dA \tag{5.53}$$

where A^* is the displaced area between $n = 0$ and $n = \delta^*$ given by

$$A^* = \pi\left\{(r+\delta^*)^2 - r^2\right\} = \pi\left(2r\delta^* + \delta^{*2}\right\} \tag{5.54}$$

for an axisymmetric flow, where r is the dimensionless radius of revolution for an axisymmetric body. It follows that

$$dA = \pi\left\{(r+n+dn)^2 - (r+n)^2\right\} \approx \pi\left\{2(r+n)dn\right\}, \tag{5.55}$$

and substitution of equations (5.54) and (5.55) into (5.53) yields

$$\delta^* + \frac{\delta^{*2}}{2\,r} = \int_o^\infty \left(U_e - u\right)\left(+\frac{n}{r}\right) dn \ . \tag{5.56}$$

For an axisymmetric body shaped like a needle, δ^* may be comparable to r. However, in many situations $\delta^* \ll r$, and to leading order equation (5.56) reduces to the two dimensional definition of δ^*, viz.

$$\delta^* = \int_o^\infty \left(1 - \frac{u}{U_e}\right) dn \tag{5.57}$$

However, since equation (5.56) has been used throughout the data compilation of

Fernholz and Finley (1977) for all axisymmetric flows, it will also be used in this study.

There are three gases commonly used in the compressible experiments (see Fernholz and Finley, 1977); these are air, nitrogen and helium and all are normally treated as perfect gas having constant specific heats. The gas properties assumed in the present calculations are listed in Table 5.6.

Gas	air	nitrogen	helium
Gas constant R (m^2/s^2K)	287.14	296.50	2078.74
Ratio of specific heats α	1.40	1.40	1.667

Table 5.6. Gas properties used in the calculations.

The transport properties are using formulae given by Keyes (1952) for diatomic gases and Neubert (1974) for helium. For the diatomic gases, the absolute viscosity is given by Keyes (1952).

$$\mu = \frac{10^{-6} a_o \sqrt{T}}{1 + a_1 T^{-1} 10^{-a_2/T}} \quad (\mathrm{Ns/m^2}) \tag{5.58}$$

where the constants and the associated range of validity are given in Table 5.7.

Gas	a_o	a_1	a_2	range of validity
air	1.488	122.1	5	$79°K < T < 1845°K$
nitrogen	1.418	116.4	5	$81°K < T < 1695°K$

Table 5.7. Constants used in equation (5.58) for viscosity.

For helium, Neubert (1974) gives the formula

$$\mu = \frac{50.23T^{0.647}}{1+\sqrt{T}(T-0.3)e^{-T/(T-0.3)}} + e^{-T}(61.273T^3$$

$$-199.1754T^1 + 179.1353T - 59.05466), \quad (10^{-8}\text{Ns/m}^2), \tag{5.59}$$

with the range of validity being $0.4\ \text{K} < T < 400\ \text{K}$.

A Reynolds number based on the kinetic displacement thickness may be defined by

$$Re_{\delta^*} = \frac{\rho_e^* U_e^* \delta^{**}}{\mu_w^*} = Re\,\frac{\rho_e U_e \delta^*}{\mu_w}\,, \tag{5.60}$$

and the velocity matching condition (5.32), with the definition of the outer scale given in equation (5.40) becomes

$$\frac{1}{u_*} = \frac{1}{\kappa} \log\left\{\frac{T_w}{T_o} Re_{\delta^*}\right\} + C_i - C_o \ . \tag{5.61}$$

Equation (5.61), combined with the definition of the reference temperature T_o (5.50), provides a relation to evaluate the skin friction coefficient c_f, which is given in terms of u_* by

$$c_f = 2 \frac{T_e}{T_o} u_*^2 \ . \tag{5.62}$$

The matching condition (5.35) for the total enthalpy profile and the definition of the outer scale in equation (5.40) yields

$$\frac{(1 - I_w)}{q_*} = \frac{1}{\kappa_\theta} \log\left\{\frac{T_w}{T_o} Re_{\delta^*} \sqrt{Pr}\right\} + B_i - B_o \ . \tag{5.63}$$

At this stage, equation (5.63) contains two unknowns κ_θ and q_*. It has been found (Weigand, 1978) that the value of the slope of the temperature profile in the overlap zone (which is related to κ_θ) appears to vary with local flow and heat transfer conditions. In a conventional approach (see, for example, Cebeci and Smith, 1974), some type of turbulent Prandtl formulation is used to define a turbulent heat flux model for the outer region which thereby implicitly defines a constant value for κ_θ. Here it is demonstrated that this approach may not yield a self-consistent formulation. In the limit of large Reynolds number, the logarithmic terms on the right side of equations (5.61) and (5.63) dominate, and it follows that

$$\frac{\kappa_\theta}{\kappa} \sim \frac{q_*}{(1 - I_w) u_*} \qquad \text{as} \qquad Re \to \infty \ . \tag{5.64}$$

Consequently κ_θ exhibits a strong dependence on local conditions and in particular on the local surface heat transfer. In this thesis the value of κ_θ is therefore taken to be defined by the asymptotic result in equation (5.64); this effectively fixes the most significant aspect associated with the turbulence model for the total enthalpy equation, namely the slope of the profile in the overlap zone. The thermal match condition (5.63) serves to determine the heat transfer parameter q_* for given values of Prandtl number, wall temperature and u_*; the characteristics of the outer-layer and inner-layer profiles enter through the log-law parameters B_o and B_i respectively. In practice, κ_θ may be calculated from equation (5.64) in a general iterative process for a given estimate of q_* and u_*, and then q_* may be updated using the full thermal match condition (5.63); both quantities may then be refined through an obvious iteration (Weigand, 1978).

For high-speed compressible flow, it is possible to calculate a Stanton number defined by

$$\mathrm{St} = \frac{q_w}{\rho_w U_e (H_e - H_w)} \,. \tag{5.65}$$

Combining equation (5.65) with the definitions of u_* and q_* defined in equations (3.104) gives

$$\mathrm{St} = \frac{\mu_w}{\mu_o (1 - I_w)} \, q_* u_* \,, \tag{5.66}$$

and using equation (5.64) gives

$$\kappa_\theta \sim \kappa \frac{\mu_o \mathrm{St}}{\mu_w u_*^2} . \tag{5.67}$$

However, it should be noted that a significant disadvantage of using the Stanton number in the analysis of high speed compressible flow is that for a heated wall St will become very large when H_w is close to H_e as is evident from equation (5.65). This is not a significant issue in low speed flows since the case $H_e = H_w$ implies that the static temperature is effectively constant and there is no heat transfer. An alternative heat transfer parameter Q_w was suggested by Fernholz and Finley (1977) which avoids the difficulty; this parameter is defined by

$$Q_w = \frac{q_w}{\rho_w U_e H_e} = \frac{\mu_w}{\mu_o} q_* u_* , \tag{5.68}$$

which is clearly bounded in all relevant situations.

Now consider the iterative procedure that was used to calculate the similarity constant a in equations (5.42) and (5.43), as well as self-similar velocity and total-enthalpy profiles at a given station along the wall. Using equations (3.110) for the defect velocity and definition of the outer variable, the definition of kinematic displacement thickness (5.56) becomes

$$\int_0^\infty \frac{\rho_e}{\rho} \left(\frac{dF_1}{d\eta}\right) \left(1 + \frac{n}{r}\right) d\eta = -1 - \frac{\delta^*}{r} , \tag{5.69}$$

for an axisymmetric flow and

$$\int_0^\infty \frac{\rho_e}{\rho}\left(\frac{\partial F_1}{\partial \eta}\right) d\eta = -1 \ , \tag{5.70}$$

for a two-dimensional flow (cf. equation (5.57)). In equation (5.69) $r = r^*/L^*_{ref}$ is the dimensionless radius of revolution for an axisymmetric body. The constant a must be determined so that either of equations (5.69) or (5.70) is satisfied. The following iterative procedure was used to find a. Starting from an initial guess for a, solutions for $F_1(\eta)$ and $\Theta_1(\eta)$, as well as C_o and B_o, are evaluated from equations (5.44) and (5.45). The profile $\Theta_1(\eta)$ is based on some initial estimate of κ_θ. With the wall layer constants B_i and C_i computed from the formulae given in Appendix C, κ_θ is then re-evaluated using equation (5.64). Since B_o and B_i are implicit functions of κ_θ, an inner iteration is carried out to determine a converged value of κ_θ. An estimate of q_* is then evaluated from equation (5.63) with u_* being obtained from the match condition (5.61). At this stage in the iteration composite, profiles for velocity and total enthalpy across the entire boundary layer are evaluated as follows. The inner variable Y^+ is related to η by

$$Y^+ = Re_{\delta^*}\, \eta \ , \tag{5.71}$$

and with the calculated value of u_*, a composite profile for the velocity across the boundary layer is defined by

$$F_{com} = 1 + u_* \left\{ \frac{dF_1(\eta)}{d\eta} + U^+(Y^+) - \frac{1}{\kappa}\left(\log Y^+ + C_i\right) \right\} . \tag{5.72}$$

A composite profile for total enthalpy may be constructed according to

$$I_{com} = 1 + q_* \left\{ \Theta_1(\eta) + \theta^+(Y^+) - \frac{1}{\kappa_\theta}\left(\log\left(Y^+\sqrt{Pr}\right) + B_i \right) \right\} . \qquad (5.73)$$

The integral in either of equations (5.69) or (5.70) was then evaluated numerically using either a trapezoidal or Simpsons rule; typically 150 to 300 mesh points across the entire boundary layer were found to yield good accuracy. The mesh chosen was tightly compacted near the surface. For a given value of a, either of equations (5.69) or (5.70) will not be satisfied in general, and the value of a is then refined using an iteration based on the secant method. This iterative procedure was continued until either of equations (5.69) or (5.70) is satisfied to within a given tolerance; for the present comparisons, the iterations were continued until successive values for a agreed to five significant figures. The final composite profiles in equations (5.72) and (5.73) were then used to make direct comparisons with experimental data.

In the following comparisons with measured profile data, both the modified Cebeci-Smith turbulence model (equation (5.26)) and the modified Baldwin--Lomax model (equation (5.3)) will be used. Between these two models the are some slight differences between the calculated values of skin friction and surface heat transfer, but the profiles obtained are virtually indistinguishable; thus only the results for the modified Cebeci-Smith model will be shown. The reference temperature T_o was evaluated in three ways using the average value defined by equation (5.51) with $Y_\ell^+ = 60$, a mean wall layer temperature evaluated at $Y^+ = 23$ and the wall temperature. As previously discussed, the first two options produce values of skin friction which are very close to the measured experimental values, while there is much more scatter with the third choice; again there is little

to choose between the plotted profiles. Results will be quoted here for the first two choices of the reference temperature T_o for the modified Cebeci-Smith model.

The corresponding fluid properties such as ρ_o and μ_o are assumed to be the functions of temperature alone and are evaluated at T_o. Direct comparisons were carried out with a representative selection of experimental data, and the theoretical profiles compare directly with the data listed in Table 5.8. The fifteen cases listed in Table 5.8 were taken from the data compilations of Fernholz and Finley (AGARD-223, 1977 and AGARD-263, 1981); here the same identification scheme is used. The first four digits identify a particular set of experiments while the last four designate a specific profile within that set. Generally, profiles nearest the end of the test section were selected for the present purposes, since such profiles were expected to be closest to equilibrium conditions. In all experiments in Table 5.8, the velocity distribution was measured across the boundary layer, but tabulated temperature data were generally inferred from Crocco-Walz relationship. In Table 5.8 T_r is the recovery temperature and $T_w/T_r \simeq 1$ denotes wall which is nearly adiabatic. The theory in this chapter does not account for the influence of viscous dissipation; therefore for an adiabatic wall, $q_w = 0$ and $H = H_e$ to leading order across the entire boundary layer. However, H_w will usually be measured as smaller than H_e in most adiabatic-wall experiments, and generally the difference $(H_e - H_w)$ increases with increasing Mach number. In order to consider such cases here, the value of the wall temperature quoted in the experimental data was used; this results in a calculated profile for total enthalpy having very small value of q_*. The case with $T_w/T_r < 1$ represents a cooled wall, while $T_w/T_r > 1$ corresponds to a heated wall.

Direct comparisons for the cases listed in Table 5.8 are illustrated in Figures 5.6 through 5.10. The comparisons with data for velocity are shown in Figures 5.6a through 5.10a, where it may be noted that the agreement is quite reasonable. Figure 5.6 considers the cases used in the illustrative Figure 3.1, in which the Mach number varies from subsonic through hypersonic range. Velocity profile comparisons are shown in Figure 5.6a with static temperature comparisons in Figure 5.6b. It is evident that the logarithmic region narrows with increasing Mach number with the velocity asymptoting to the mainstream value at much slower rate. The present self-similar profiles closely represent this behavior and, in addition, represents the data very well. In Figure 5.7, a set of supersonic flows over a nearly adiabatic surface are considered; Figures 5.8 and 5.9 illustrate situations with heat transfer at the surface where the wall is cooled. Figure 5.10 shows a set of hypersonic flows in helium; the highest Mach number, $M_e = 10$, occurs in flow No. 73050504. Since the ratio of specific heats in helium $\gamma = 1.667$ (as compared to 1.4 for air), compressibility effects in helium flow are more significant than that in air. There is evidently some scatter in the data near the wall in profiles 71030406 and 73050504, but otherwise the self-similar solutions agree with the data reasonably well.

It is worthwhile to note that closer correspondence with the data for a given profile can be achieved by adjusting the parameters in the turbulence models in equations (5.26) and (5.28), such as K and K_h. However, the objective here is to demonstrate that there is a degree of universality over a range of Mach numbers using the present models, and so no attempt to "fit" the data was made; the profiles were produced solely from the known physical quantities at each data

station, as well as δ^{**}, and clearly do represent the data reasonably well. At the same time, since true self-similarity will rarely be achieved in an experiment, a very close correspondence between the data and the theoretical profiles should not be expected. The calculated values of the skin friction parameter u_* are given in Table 5.8 along with the heat transfer parameter q_* which, as anticipated, is very small and at least an order of magnitude smaller than u_* for the nearly adiabatic cases; for flows with significant heat transfer, q_* and u_* are of comparable magnitude. The values given in Table 5.8 are for the modified Cebeci-Smith model using a reference temperature based on an average temperature across the wall; the corresponding results using a mean reference temperature (at $Y^+ = 23$) for the wall layer and also an outer region modified Baldwin-Lomax model are given in Tables 5.9 and 5.10 respectively. Note that the computed values are all very close, and the profiles cannot be distinguished graphically for all three models.

The data listed in Table 5.11 is of special interest because total temperature was measured directly for all these data. Again calculations were carried out for the modified Cebeci-Smith model for both an average and mean wall-layer reference temperature and a modified Baldwin-Lomax model; calculation results are given in Tables 5.11 through 5.13 where it may be noted that all predicted values are very similar. The first set of profiles presented in Figure 5.11 is taken from the recent experiments of Carvin (1988), where the velocity profile was measured by laser-Doppler-velocimetry. The experiments were at relatively low Mach number ($M_e \approx 2.2$) with supersonic flow over an adiabatic or a heated surface. Therefore this data affords an opportunity to examine the self-similar solutions in the temperature range of $T_w/T_r > 1$. The first two digits used in the identification

number of these profiles denote the value of the temperature ratio T_w/T_r; for example, 10 indicates that $T_w/T_r = 1.0$. The last two digits denote the distance (in cm) from the leading edge of the test section, and in this experiment 48 denotes the end of the test section. It should be noted that the trends in the data are unrealistic near the wall, and this problem appears to be persistent throughout Carvin's (1988) measurements. Otherwise, the agreement between theory and the data is quite reasonable. The total temperature was also measured directly in this experiment, and the present results shown in Figure 5.11 support the modeling of the total enthalpy equation developed here. The data shown in Figure 5.11 was taken using a hot wire in supersonic boundary-layer flows. Unfortunately, the velocity data does not appear to be of comparable quality to that taken with conventional techniques; this is particularly true as Mach number increases. In addition, the near-wall data were not taken in these experiments (Kistler, 1958). It is believed that calibration of a hot wire anemometer for the measurement in a flow with a large temperature gradient flow is extremely difficult. Despite these potential problems, the agreement of the present theory with experimental results for velocity and static temperature is still quite reasonable.

In Figures 5.13, profiles for axisymmetric flows with strong heat transfer and at high Mach number are shown; this environment is the practical situation for re-entry vehicles and missiles. The theoretical profiles again represent the experimental results well and within the uncertainty in the data. In Figures 5.14, three profiles are shown in which the test section was a nozzle wall and in these situations the flow is recovering from substantial upstream disturbances. In the flow from which profile 72021203 was taken, there was substantial heat transfer

(cooling) in the nozzle throat; consequently, there are downstream history effects due to both heat transfer and the pressure gradient in the nozzle. In the flow from which profile 72020205 was taken, the heat transfer history effect is not present since the nozzle region was not cooled. For the flow with profile 73010501, there is both upstream heat transfer and pressure gradient effects because the nozzle throat was heated and contained a predominately reflected-wave expansion. It is clear that none of the flows presented in Figures 5.14 are close to being self-similar; however, it can be seen that representation of the velocity profiles and temperatures is reasonable and is especially good in the wall layer conforming closely to the wall function solutions. In §3 it was shown that in the inner region: (1) the convection terms are negligible with respect to the viscous and turbulence terms and, hence, the flow only depends on local conditions, and (2) the pressure gradient term is negligible. These results are supported by Figure 5.14. It may be noted that the inner-region flow and temperature distribution recovers quickly from disturbances and depends mainly on local flow conditions.

Finally, it may be noted that calculations were also carried out using the wall temperature as the reference condition. This produces profiles which agree with the data in a manner which is visually indistinguishable from those presented here (see He, Kazakia, and Walker); as an example some results are shown in Figures 5.15 which may be compared with Figure 5.6. The influence of the reference temperature T_o is reflected implicitly in the calculation of the constant a and appears to have less influence on the outer region profiles than the skin friction coefficient. The over-riding consideration in using the reference temperature is that the prediction of skin friction is significantly improved relative to direct

experimental measurements obtained with a floating element balance.

5.6 Discussion of Self-Similarity

In any experiment, a turbulent boundary layer can at best be only "locally self-similar"; this means that the main feature of a turbulent boundary layer at any point can be mainly described (but not completely) in terms of mean flow boundary conditions at that point. The reason is that self-similar solutions can only be achieved at most in practice as "terminating solutions" of more general flows, in which the pressure gradient is constant and has acted over a substantial streamwise distance. In the comparisons carried out with experimental data, profiles were selected close to the end of the test section where the flow was believed to have recovered from conditions upstream. The comparisons with data seem to support the idea that these constant pressure flows are relatively close to being self-similar. Here the question of the range of validity of the constant pressure solutions, as well as the possibility of self-similar solutions in flows with pressure gradients, will be considered.

The leading order outer-region boundary layer equations were given in equations (5.37) and (5.38), and in order for self-similarity

$$\frac{\partial^2 F_1}{\partial s \partial \eta} = o(1), \qquad \text{and} \qquad \frac{\partial \Theta_1}{\partial s} = o(1), \tag{5.74}$$

while the derivatives of all the coefficients in equations (5.39) with respect to s must be o(1) in some limit, say $s \to \infty$. In addition with the choice (5.40) of the outer scale, the integral condition (5.48) must be satisfied. Because the pressure is

constant across the boundary layer, the variation in density across the boundary layer is given by equation (5.49) and substitution into equation (5.48) leads to

$$-F_{1\infty} = 1 + \left(1 + \frac{\gamma-1}{2}M_e^2\right)u_* \left[(1 - I_w)\frac{\kappa_\theta}{\kappa}\right]\int_o^\infty \Theta_1 d\eta$$

$$-(\gamma-1)M_e^2 u_* \int_o^\infty \left(\frac{\partial F_1}{\partial \eta}\right)^2 d\eta - \left(\frac{\gamma-1}{2}\right)M_e^2 u_*^2 \int_o^\infty \left(\frac{\partial F_1}{\partial \eta}\right)^3 d\eta \ , \qquad (5.75)$$

where $F_{1\infty}$ is the limiting value of F_1 as $\eta \to \infty$. For self-similarity $\theta_1 = \theta_1(\eta)$ and $\partial F_1/\partial \eta = F_1'(\eta)$; assuming such behavior and a constant Mach number M_e and then differentiating equation (5.75) with respect to s leads to

$$-\frac{\partial F_{1\infty}}{\partial s} = \left(1 + \frac{\gamma-1}{2}M_e^2\right) u_*' \left[(1 - I_w)\frac{\kappa_\theta}{\kappa}\right]\int_o^\infty \Theta_1 d\eta$$

$$-(\gamma-1)M_e^2 u_*' \int_o^\infty 2\left(\frac{\partial F_1}{\partial \eta}\right) d\eta - (\gamma-1)M_e^2 u_* u_*' \int_o^\infty \left(\frac{\partial F_1}{\partial \eta}\right)^3 d\eta \ . \qquad (5.76)$$

Here u_*' denotes the differentiation with respect to s and, as shown in equation (5.34), $u_*' = O(u_*^2)$. It is obvious that for $\partial F_{1\infty}/\partial s$ to be small (which is equivalent to $\partial^2 F_1/\partial s \partial \eta = o(1)$), the condition that must be satisfied is

$$(\gamma-1)M_e^2 \, u_*^2 = o(1) \ . \qquad (5.77)$$

Equation (5.77) therefore defines the condition for the existence of "local similarity" in constant pressure boundary layers. It combines the influences of Reynolds number, Mach number and fluid properties; when $M_e \leq 1$, $F_{1\infty} \approx 1$ from equation (5.71) and the condition (5.73) will be satisfied anyway. Actually since the

momentum and energy equations are not closely coupled, incompressible flow model may be used at this time. The next situation is $M_e > 1$ and $(\gamma-1)M_e^2 u_* = 0(1)$, which is the area of interest of this study. Finally as $M_e \to \infty$ and $(\gamma-1)M_e^2 u_*^2 = 0(1)$ the similarity solutions developed in this section are not valid anymore. It is worthwhile to note that according to equation (3.6.9), $u_* = 0(1/\log Re_o)$, therefore for each fixed M_e equation (5.73) will be eventually satisfied as $Re \to \infty$, however, as Mach number increases the similar profiles can only be reached at a far more downstream location.

When the boundary-layer flow is experiencing a longitudinal pressure gradient, mainstream Mach number M_e becomes a function of s; however, when $M_e \ll 1$, $\partial F_{1\infty}/\partial s = o(1)$ in some limit $s \to \infty$ with or without pressure gradient and therefore Clauser's "equilibrium" concept is valid; Clauser (1954) argued that a turbulent boundary-layer flow is self-similar when the "equilibrium constant" β is constant in incompressible turbulent boundary layers, here the constant β is defined as

$$\beta = \left(\delta^*/\tau_w\right)\left(dp_e/ds\right), \qquad M_e \ll 1 \,. \tag{5.78}$$

Now consider the situation of $(\gamma-1)M_e^2 u_* = O(1)$ where the variation of pressure may have significant influence on the defect velocity $\partial F_1/\partial\eta$. For convenience consider only the second term on the right hand of equation (5.75) to demonstrate the concept involved here; differentiating with respect to s yields the expression

$$\frac{\partial}{\partial s}\left\{(\gamma-1)M_e^2 u_* \int_o^\infty \left(\frac{\partial F_1}{\partial\eta}\right)^2 d\eta\right\} = (\gamma-1)M_e^2 u_* \left(\frac{M_e'}{M_e}\right)\int_o^\infty \left(\frac{\partial F_1}{\partial\eta}\right)^2 d\eta$$

$$+(\gamma-1)M_e^2 u'_* \int_o^\infty \left(\frac{\partial F_1}{\partial \eta}\right)^2 d\eta. \tag{5.75}$$

for a profile with $F_1 = F_1(\eta)$. It can evident that a further condition for self-similarity in a flow with pressure gradient is that $M'_e/M_e \ll 1$ in which case the coefficient b in equation (5.37) is small and the governing equation again reduces to equation (5.42). If a strong longitudinal pressure gradient occurs it is not known whether self-similar profile exist. However it does appear that self-similar may not occur and this is supported by experimental observations; by closely examining the data profiles presented in Figure (3.1) and Figure (5.6) it can be seen that appreciable Mach number changes lead to significant changes in the inner layer characteristics. With increasing M_e inner layer grows as a fraction of boundary-layer thickness and the variation of velocity in the outer region becomes slower with the logarithmic region becoming less distinct.

Case No.	M_e	T_w/T_r	Re_{δ^*}	u_*	q_*
73020402*	0.793	≈ 1	139480	0.0308	0.0005
58020207	2.739	≈ 1	12255	0.0422	0.0031
74021801*	4.517	1.0242	6945.5	0.0507	0.0037
73021203	2.799	≈ 1	66393	0.0355	0.0028
53010401	2.540	≈ 1	2635.5	0.0508	0.0035
53011302	4.544	≈ 1	4240.5	0.0546	0.0054
65060101	4.886	0.9755	6699.7	0.0515	0.0068
65060105	4.801	0.5228	4987.8	0.0461	0.0287
72090402*	7.780	0.7998	5686.5	0.0564	0.0188
79030103*(N)	8.788	0.3375	7518.1	0.0461	0.0382
72040201	6.390	0.3136	7667.2	0.0407	0.0348
72040601	6.500	0.5014	8435.7	0.0458	0.0297
71030207(H)	6.686	0.9811	33813	0.0721	0.0101
71030406(H)	6.686	0.9817	6580.2	0.0617	0.0086
73050504(H)	10.31	≈ 1	17177	0.0600	0.0072

Table 5.8 Computed dimensionless friction velocity and heat flux values for $Y_l^+ = 60$ in equation (5.51); (H) denotes that the gas is helium and (N) denotes nitrogen. An asterisk signifies that direct measurements of total temperature.

Case No.	M_e	T_w/T_r	Re_{δ^*}	u_*	q_*
73020402*	0.793	≈ 1	139480	0.0308	0.0005
58020207	2.739	≈ 1	12255	0.0422	0.0031
74021801*	4.517	1.0242	6945.5	0.0508	0.0037
73021203	2.799	≈ 1	66393	0.0355	0.0029
53010401	2.540	≈ 1	2635.5	0.0508	0.0035
53011302	4.544	≈ 1	4240.5	0.0546	0.0054
65060101	4.886	0.9755	6699.7	0.0515	0.0068
65060105	4.801	0.5228	4987.8	0.0463	0.0288
72090402*	7.780	0.7998	5686.5	0.0578	0.0211
79030103*(N)	8.788	0.3375	7518.1	0.0464	0.0384
72040201	6.390	0.3136	7667.2	0.0410	0.0349
72040601	6.500	0.5014	8435.7	0.0460	0.0299
71030207(H)	6.686	0.9811	33813	0.0714	0.0100
71030406(H)	6.686	0.9817	6580.2	0.0617	0.0086
73050504(H)	10.31	≈ 1	17177	0.0600	0.0072

Table 5.9 Computed dimensionless friction velocity and heat flux for the reference temperature taken at $Y^+ = 23$; (H) denotes that the gas is helium and (N) nitrogen. An asterisk denotes that direct measurements of total temperature were made.

Case No.	M_e	T_w/T_r	Re_{δ^*}	u_*	q_*
73020402*	0.793	≈ 1	139480	0.0309	0.0005
58020207	2.739	≈ 1	12255	0.0425	0.0032
74021801*	4.517	1.0242	6945.5	0.0509	0.0037
73021203	2.799	≈ 1	66393	0.0357	0.0029
53010401	2.540	≈ 1	2635.5	0.0509	0.0036
53011302	4.544	≈ 1	4240.5	0.0549	0.0055
65060101	4.886	0.9755	6699.7	0.0517	0.0069
65060105	4.801	0.5228	4987.8	0.0467	0.0289
72090402*	7.780	0.7998	5686.5	0.0565	0.0188
79030103*(N)	8.788	0.3375	7518.1	0.0463	0.0383
72040201	6.390	0.3136	7667.2	0.0412	0.0351
72040601	6.500	0.5014	8435.7	0.0462	0.0299
71030207(H)	6.686	0.9811	33813	0.0721	0.0101
71030406(H)	6.686	0.9817	6580.2	0.0617	0.0086
73050504(H)	10.31	≈ 1	17177	0.0600	0.0072

Table 5.10 Computed dimensionless friction velocity and heat flux values using Baldwin-Lomax model and $Y_l^+ = 60$ in equation (5.51). (H) denotes that the gas is helium and (N) nitrogen. Asterisk denotes that direct measurements of total temperature were made.

Case No.	M_e	T_w/T_r	Re_{δ^*}	u_*	q_*
f-1048	2.160	1.012	6450.5	0.0439	0.0021
f-1548	2.170	1.475	5139.6	0.0492	-0.0233
f-2048	2.140	1.961	4831.9	0.0526	-0.0539
58030101	1.720	1.006	31521	0.0362	0.0014
58030201	3.560	1.031	29121	0.0403	0.0022
58030301	4.670	1.045	13621	0.0465	0.0035
67010105	5.970	0.4888	14120	0.0414	0.0274
67010204	6.040	0.4257	12083	0.0409	0.0300
72050103	7.200	0.4764	10433	0.0451	0.0305
72020205	4.823	0.9277	20730	0.0435	0.0079
72021203	4.857	0.2279	56517	0.0275	0.0260
73010501	4.742	1.0212	12352	0.0473	0.0037

Table 5.11. Computed dimensionless friction velocity and heat flux values for $Y_l^+ = 60$ in equation (5.51). Direct measurements of total temperature were made.

Case No.	M_e	T_w/T_r	Re_{δ^*}	u_*	q_*
f-1048	2.160	1.012	6450.5	0.0439	0.0021
f-1548	2.170	1.475	5139.6	0.0491	-0.0233
f-2048	2.140	1.961	4831.9	0.0525	-0.0583
58030101	1.720	1.006	31521	0.0362	0.0014
58030201	3.560	1.031	29121	0.0403	0.0022
58030301	4.670	1.045	13621	0.0465	0.0035
67010105	5.970	0.4888	14120	0.0417	0.0276
67010204	6.040	0.4257	12083	0.0413	0.0301
72050103	7.200	0.4764	10433	0.0433	0.0307
72020205	4.823	0.9277	20730	0.0435	0.0079
72021203	4.857	0.2279	56517	0.0277	0.0261
73010501	4.742	1.0212	12352	0.0473	0.0037

Table 5.12. Computed dimensionless friction velocity and heat flux values for the reference temperature taken at $Y^+ = 23$. Direct measurements of total temperature were made.

Case No.	M_e	T_w/T_r	Re_{δ^*}	u_*	q_*
f-1048	2.160	1.012	6450.5	0.0441	0.0021
f-1548	2.170	1.475	5139.6	0.0492	-0.0233
f-2048	2.140	1.961	4831.9	0.0526	-0.0539
58030101	1.720	1.006	31521	0.0363	0.0014
58030201	3.560	1.031	29121	0.0406	0.0022
58030301	4.670	1.045	13621	0.0467	0.0035
67010105	5.970	0.4888	14120	0.0418	0.0276
67010204	6.040	0.4257	12083	0.0414	0.0302
72050103	7.200	0.4764	10433	0.0453	0.0306
72020205	4.823	0.9277	20730	0.0438	0.0080
72021203	4.857	0.2279	56517	0.0281	0.0265
73010501	4.742	1.0212	12352	0.0475	0.0037

Table 5.13. Computed dimensionless friction velocity and heat flux values using Baldwin-Lomax model and $Y_l^+ = 60$ in equation (5.51). Direct measurements of total temperature were made.

5.7 Summary

In this section, a theory and turbulence models have been developed which give good comparison between self-similar profiles for velocity and static temperature and experimental profile data over a wide range of Mach numbers and surface heat transfer rates. Extensions of simple algebraic turbulence models to high speed compressible flow have been suggested and both have been found to give similar results; the results presented in all figures were obtained using the extended Cebeci-Smith type model but are indistinguishable from plots obtained using the extended Baldwin-Lomax model. The good comparisons with experimental data tend to validate the simple asymptotic structure proposed in this study in which both the velocity and total enthalpy confirm to a simple logarithmic behavior in the overlap zone but in terms of the Howarth-Dorodnitsyn variable. The limiting condition for the self-similarity has been demonstrated to be $(\gamma-1)M_e^2 u_*^2 = o(1)$, as stated in equation (5.77). The variation of the self-similar profiles with Mach number can be seen in Figures (5.16) and (5.17) for a fixed value of $Re_{\delta^*} = 10{,}000$; the trends shown in these figures are similar for other values of Re_{δ^*}. The velocity profiles shown in Figure (5.16) illustrate the tendency for relative growth of the wall layer with the increasing Mach number, and the velocity achieves a higher percentage of the mainstream speed. As shown in Figure 5.17, the variation of static temperature in the near-wall region is more severe with increasing Mach number for an adiabatic wall. In Figure 5.18, the influence of wall cooling on the temperature profile is shown for a fixed mainstream Mach number. It may be observed that there is a significant variation of the temperature (and density) inside the wall layer for all different temperature ratios. At a certain stage in the limit

$M_e \to \infty$, the thickening wall layer will lead to breakdown of the present analysis.

It is of interest to compare the present theoretical results for the temperature distribution with that predicted by the Crocco-Walz relation given in equation (2.50). A comparison of the two profiles for two different Mach numbers and over a range of surface heat transfer conditions is shown in Figures 5.19a and 5.19b; it may be seen that the agreement is very close for nearly adiabatic walls (as expected), but becomes progressively less so for strong surface heat transfer rates.

In the preceding comparisons, the velocity and static temperature profiles have been compared with experimental data over a wide range of experimental conditions, and the agreement with data is seen to be quite reasonable. Similarly good agreement is obtained for the total enthalpy profile in flows with heat transfer. However for an adiabatic wall, the variation in total enthalpy is not substantial across the boundary layer, and the present theory appears to miss a phenomenon which is in most measurements of total temperature. This is depicted for the data sets shown in Figure 5.20 where the total enthalpy overshoots or exceeds the mainstream value in the outer portion of the boundary layer. Although the deviations from H_e are relatively small, they are observed consistently, and as shown in Figure 5.20, the present theoretical profiles for total enthalpy are incapable of capturing this effect. Thus the adiabatic wall case must be re-examined and this is the focus of next chapter.

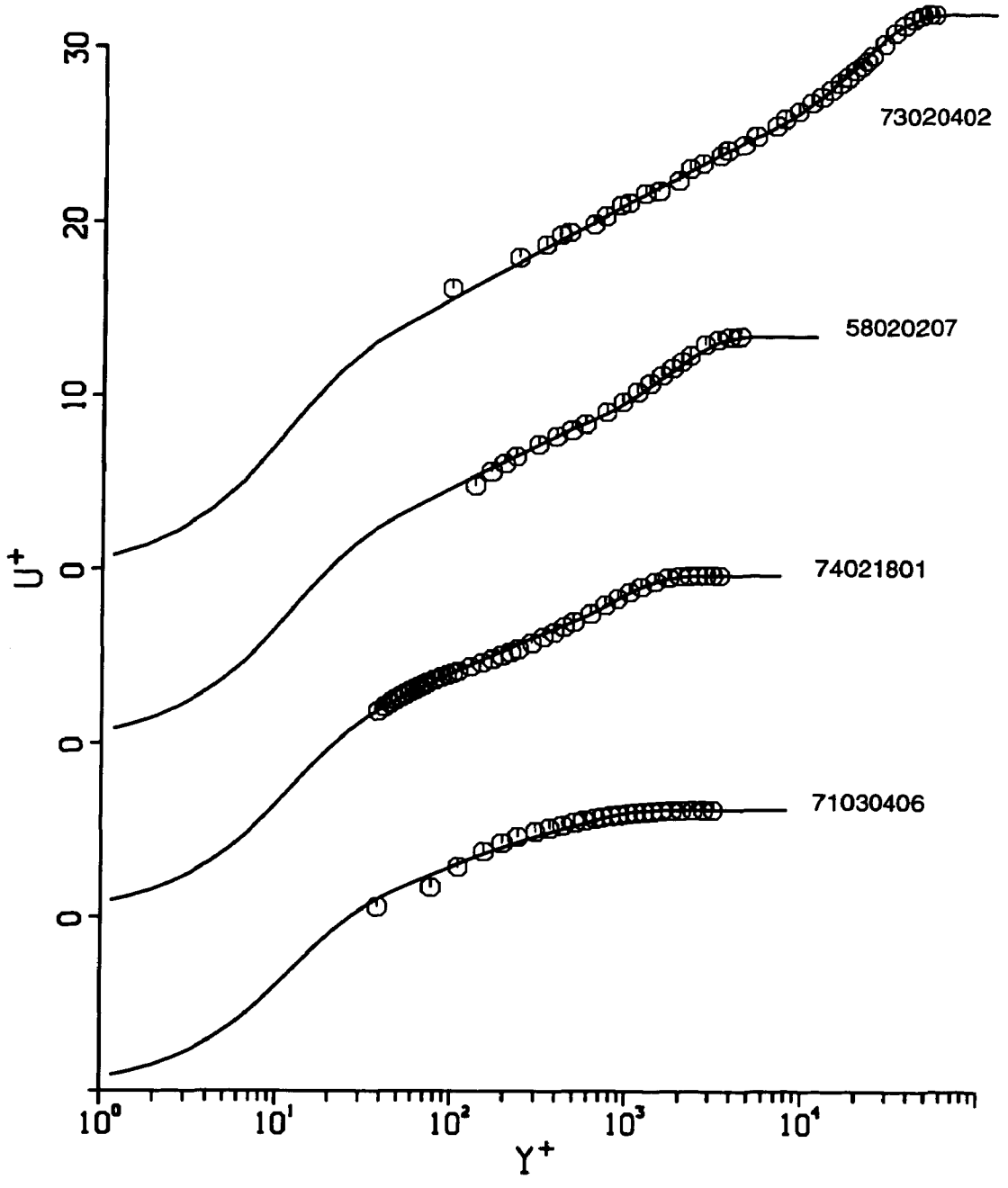

Figure 5.6a. Comparison of two-dimensional velocity data with the theoretical profile. Data from Fernholz and Finley, 1977 (5802-Stalmach; 7302-Winter and Gaude; 7402-Mabey et. al.; 7103-Fischer and Maddalon). Note the shifted origins.

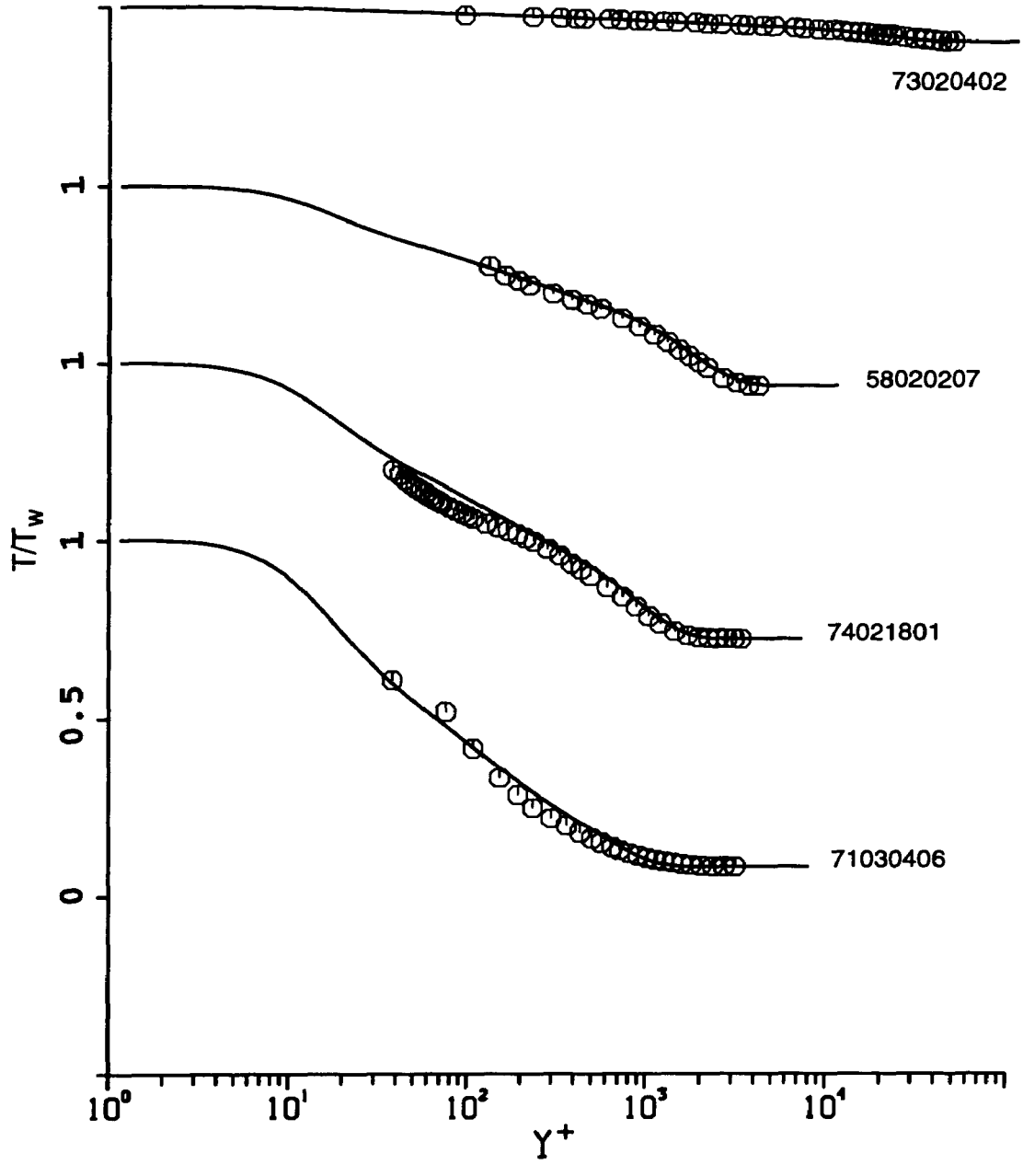

Figure 5.6b. Comparison of two-dimensional temperature data with the theoretical profile. Data from Fernholz and Finley, 1977 (5802-Stalmach; 7302-Winter and Gaude; 7402-Mabey et. al.; 7103-Fischer and Maddalon).

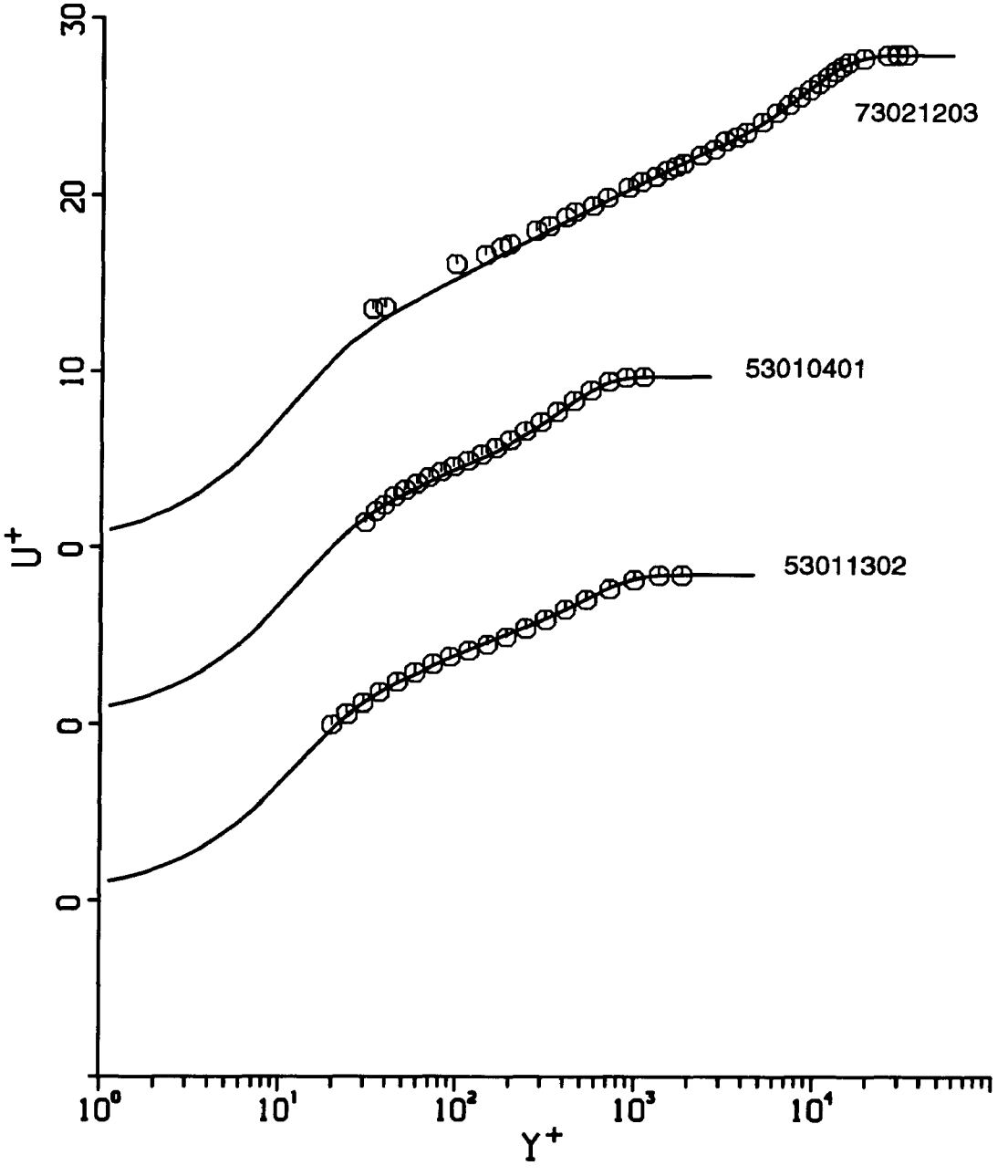

Figure 5.7a. Comparison of two-dimensional velocity data with the theoretical profile. Data from Fernholz and Finley, 1977 (5301-Coles; 7302-Winter and Gaude). Note the shifted origins.

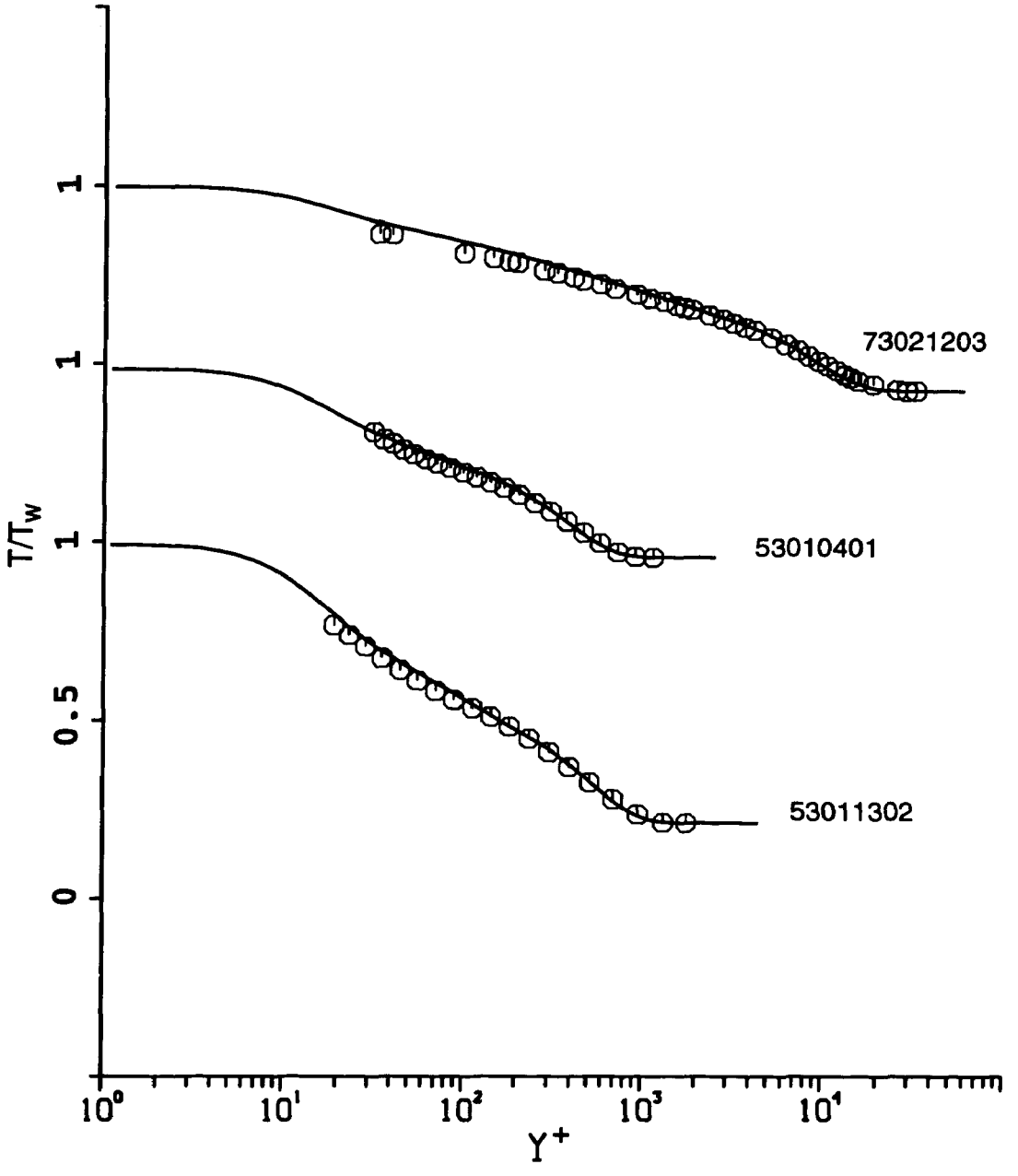

Figure 5.7b. Comparison of two-dimensional temperature data with the theoretical profile. Data from Fernholz and Finley, 1977(5301-Coles; 7302-Winter and Gaudel).

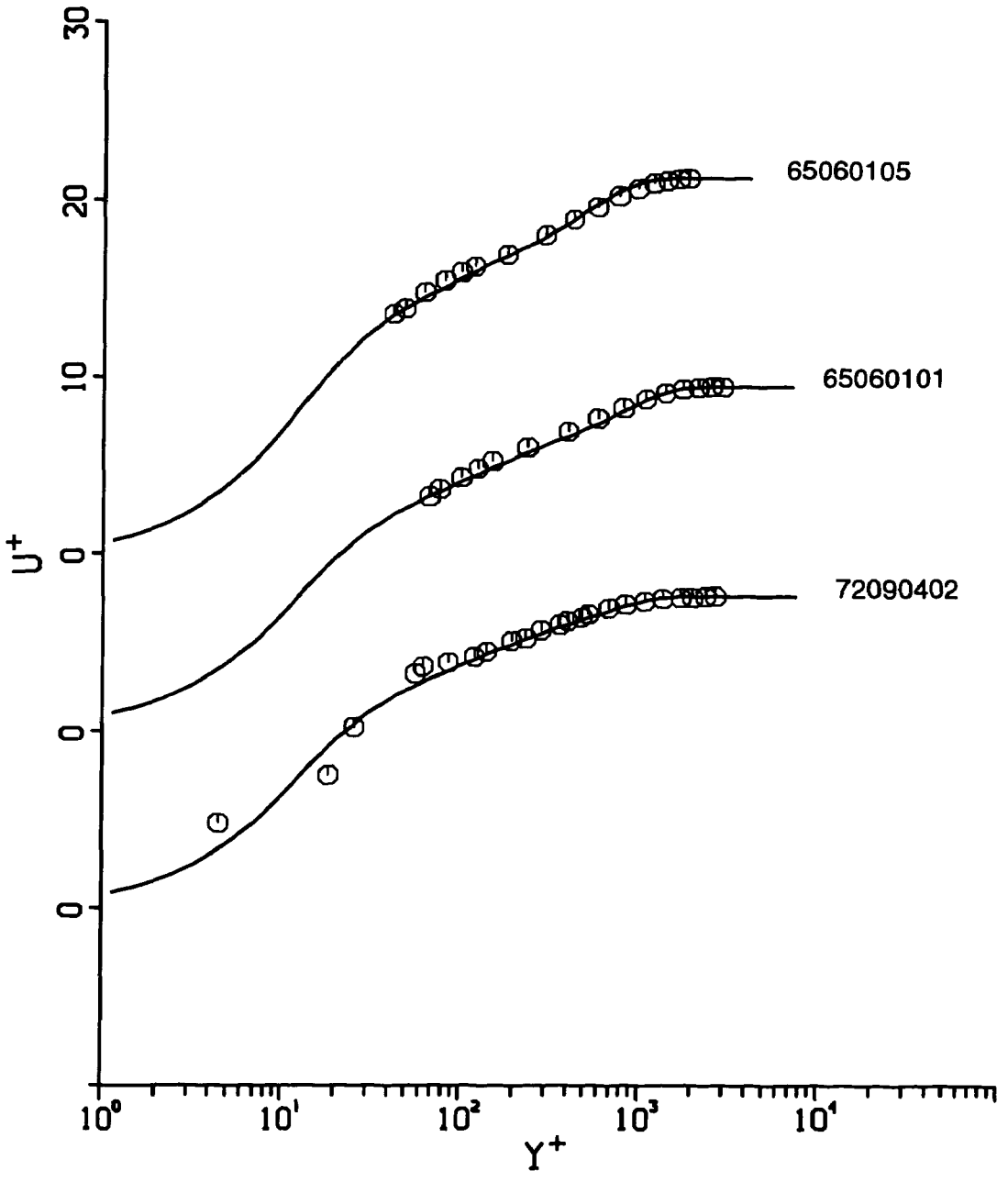

Figure 5.8a. Comparison of two-dimensional velocity data with the theoretical profile. Data from Fernholz and Finley, 1977 (6506-Young; 7209-Stone and Gary). Note the shifted origins.

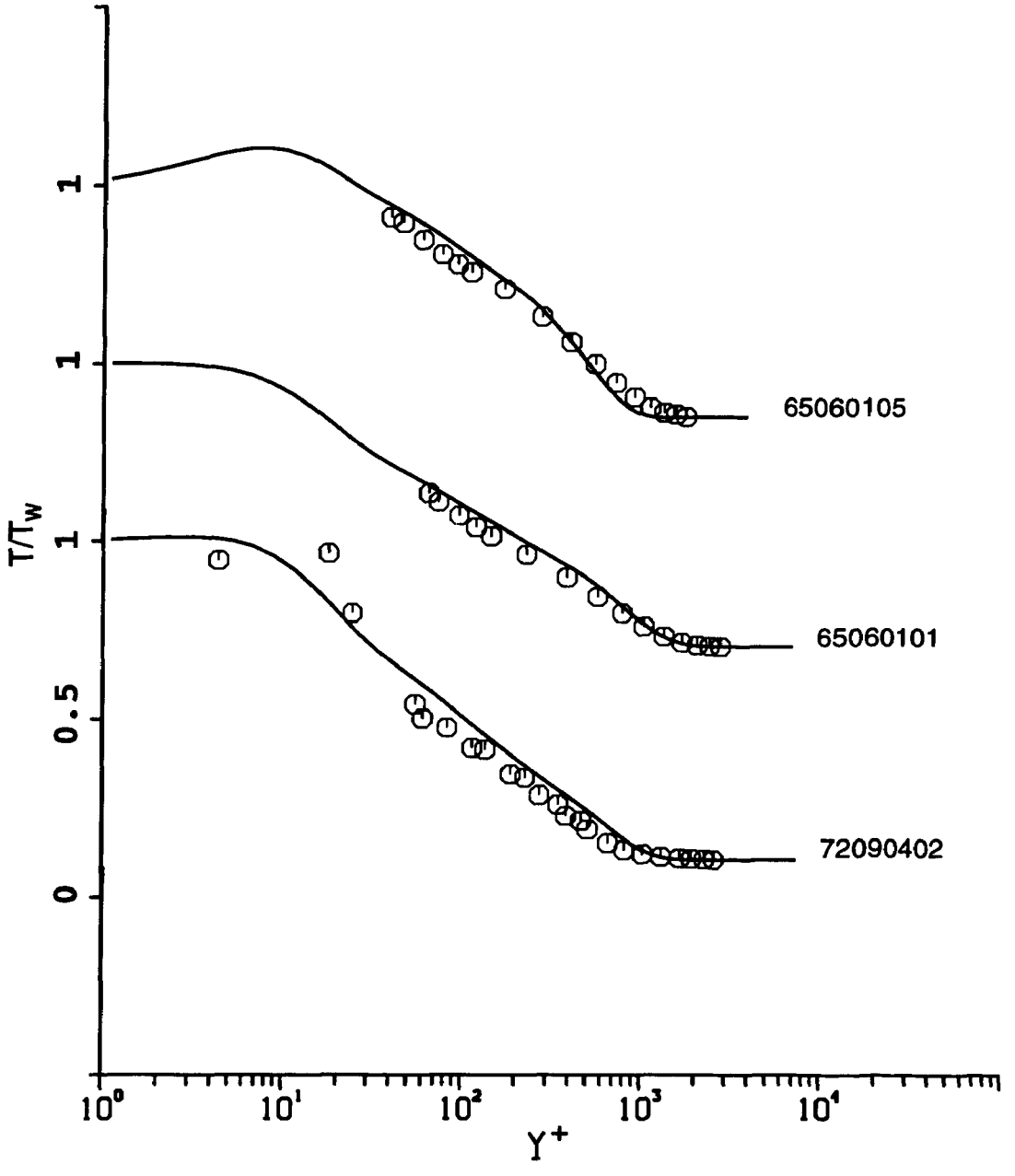

Figure 5.8b. Comparison of two-dimensional temperature data with the theoretical profile. Data from Fernholz and Finley, 1977 (6506-Young; 7209-Stone and Gary).

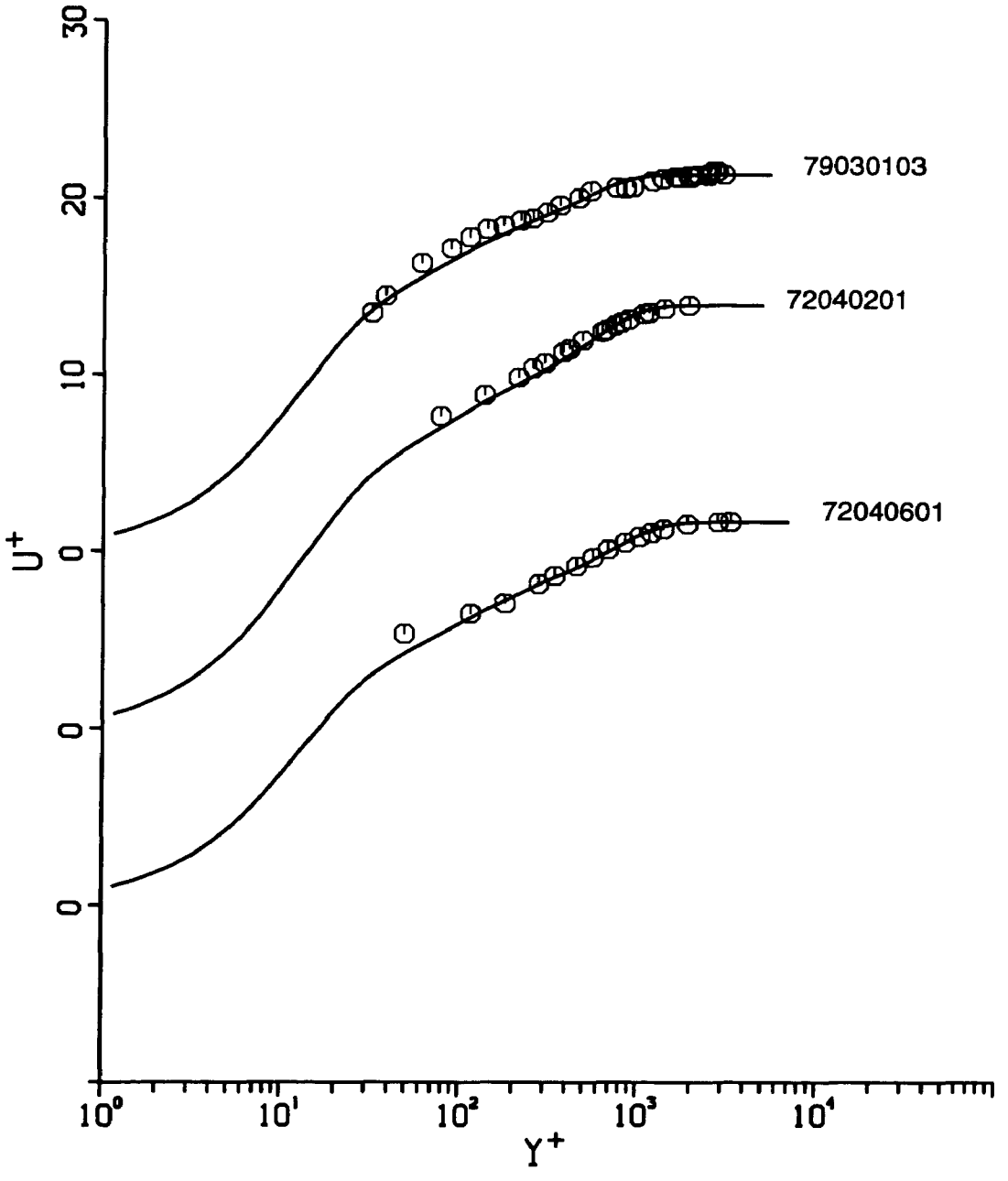

Figure 5.9a. Comparison of two-dimensional velocity data with the theoretical profile. Data from Fernholz and Finley, 1977 and 1981 (7204-Keener and Hopkins; 7903-Barlett et al.). Note the shifted origins.

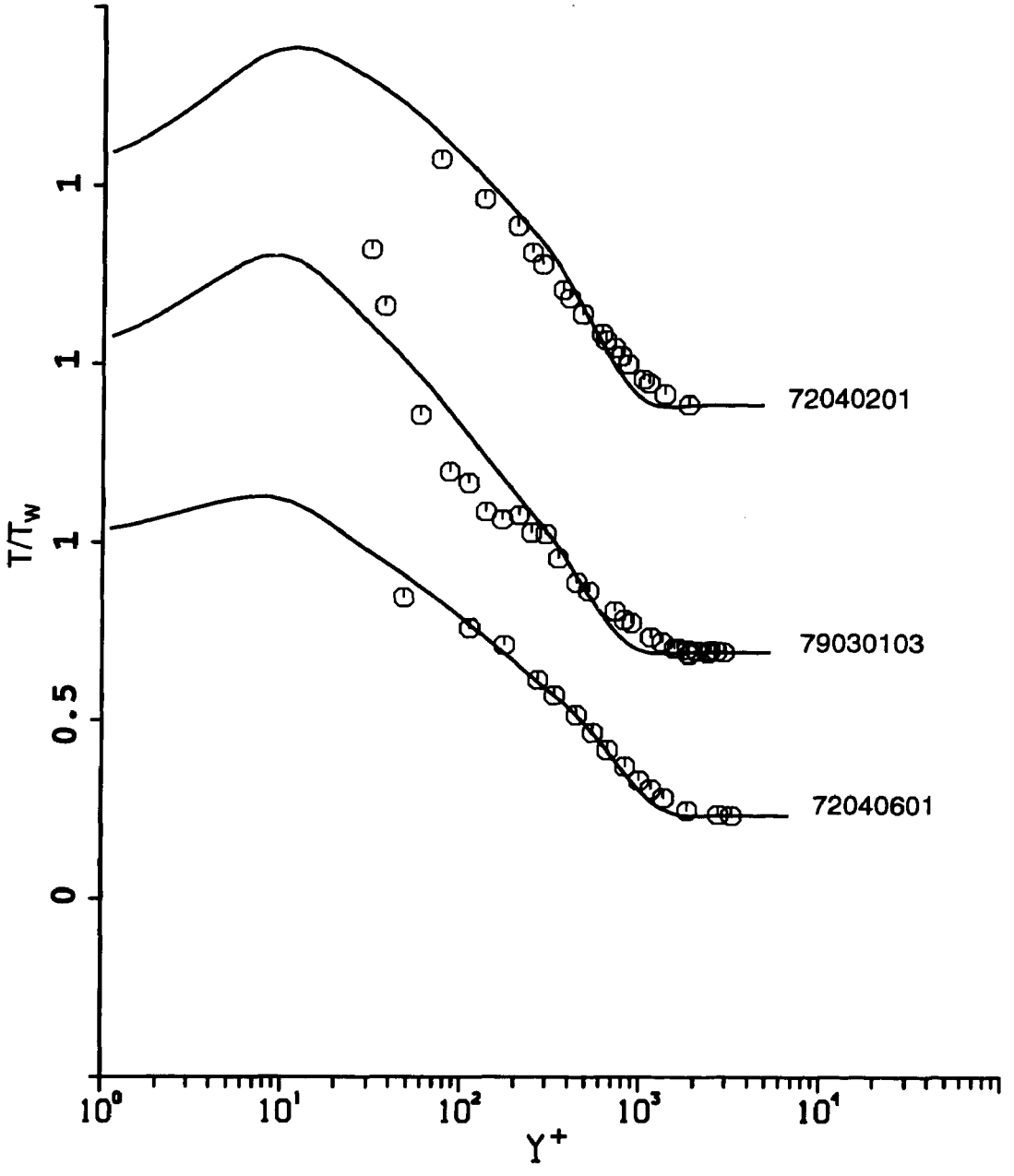

Figure 5.9b. Comparison of two-dimensional temperature data with the theoretical profile. Data from Fernholz and Finley, 1977 and 1981 (7204-Keener and Hopkins; 7903-Barlett et al.).

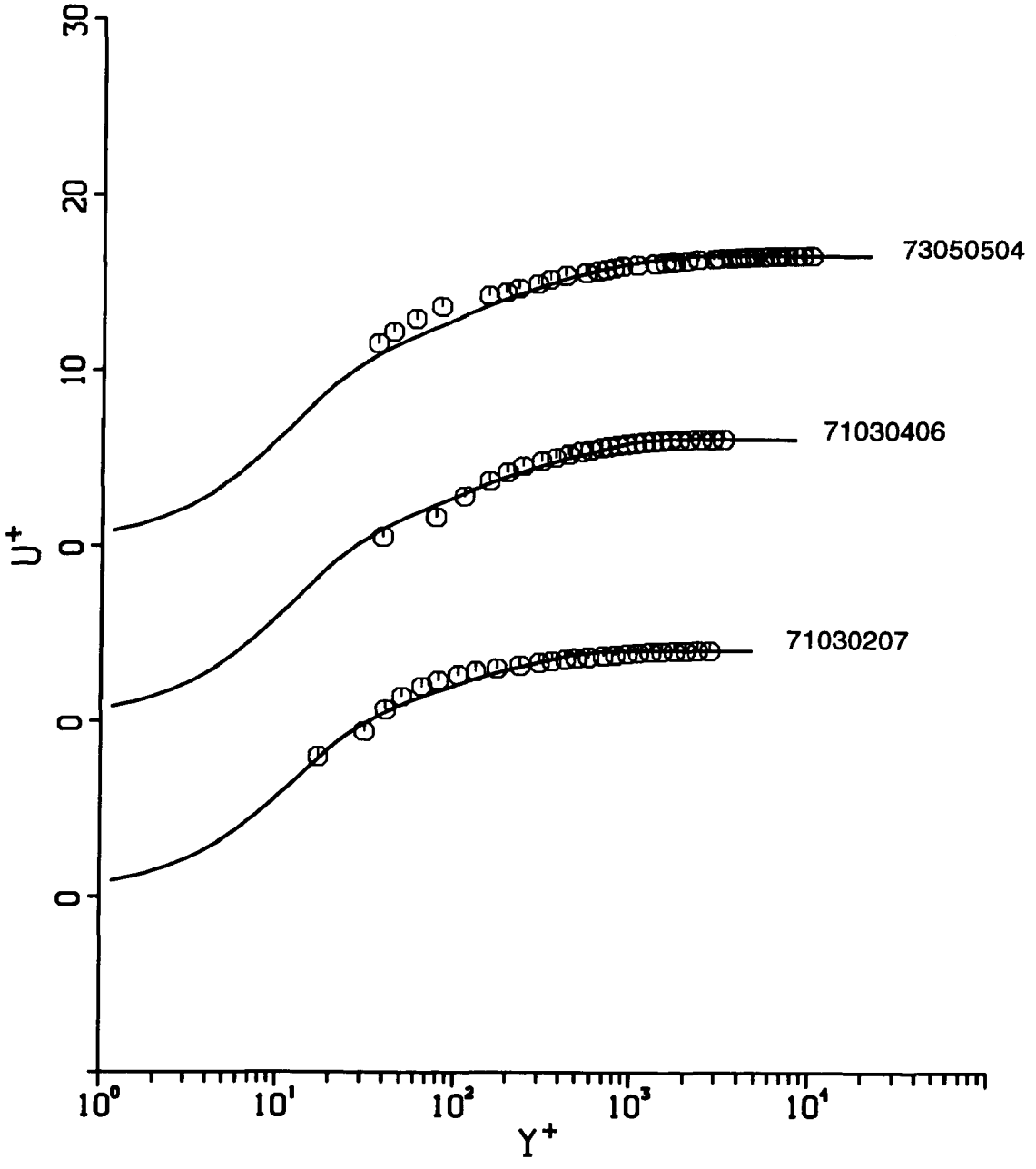

Figure 5.10a. Comparison of two-dimensional hypersonic velocity data with the theoretical profile. Data from Fernholz and Finley, 1977(7103-Fidcher and Maddalon; 7305-Watson et al.). Note the shifted origins.

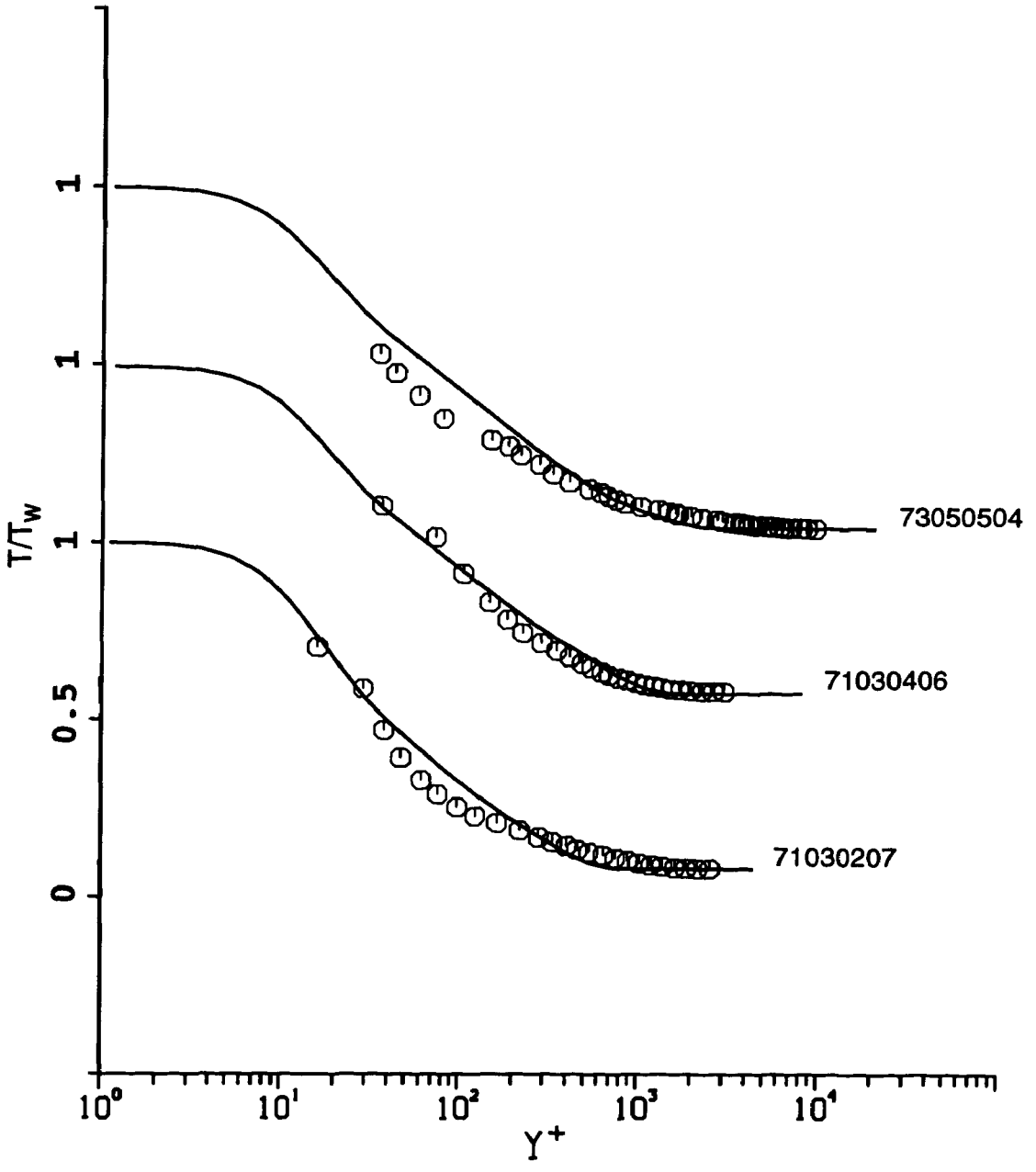

Figure 5.10b. Comparison of two-dimensional hypersonic temperature data with the theoretical profile. Data from Fernholz and Finley, 1977 (7103-Fidcher and Maddalon; 7305-Watson et al.).

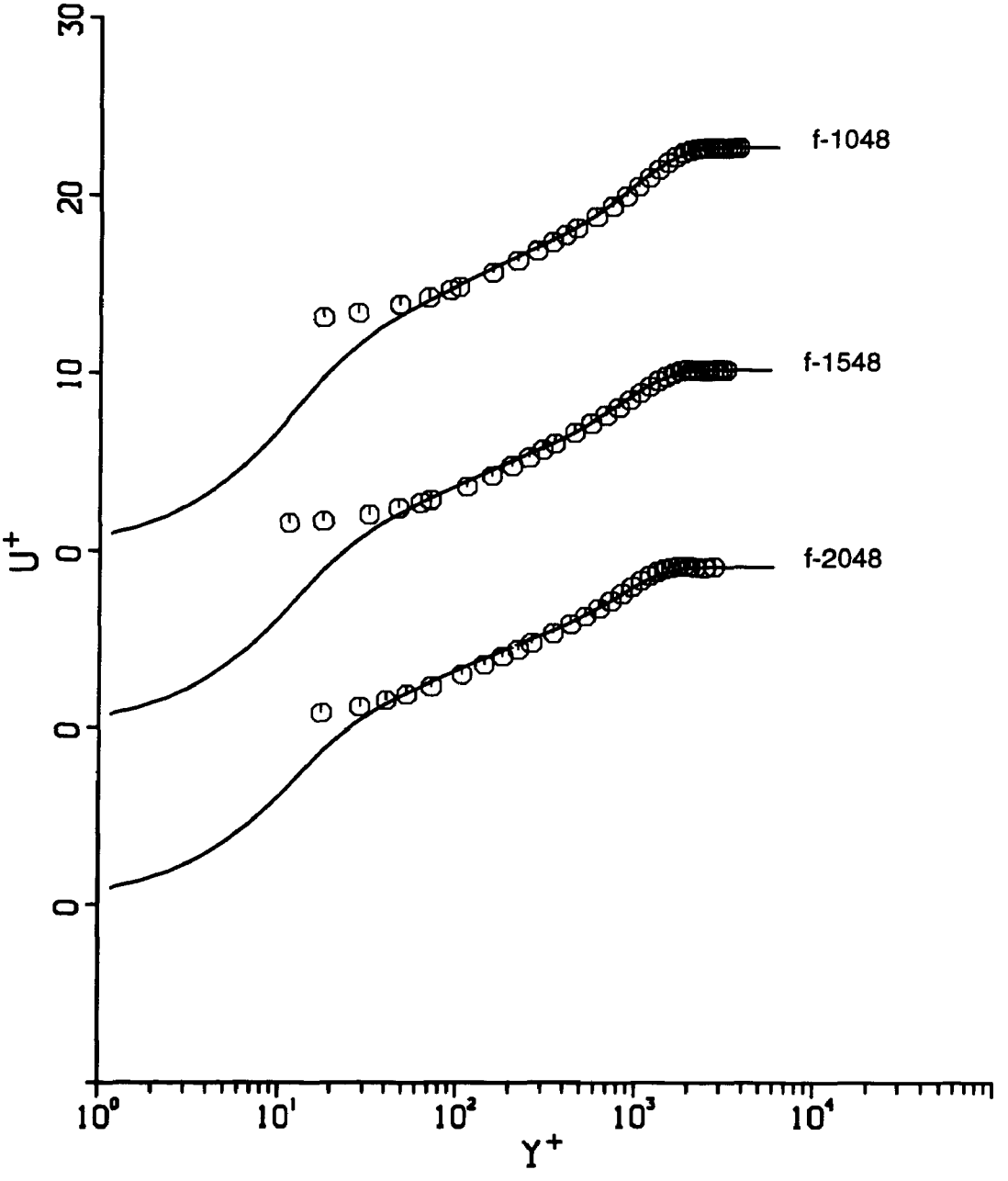

Figure 5.11a. Comparison of two-dimensional velocity data with the theoretical profile. Data from Carvin, 1988. Note the shifted origins.

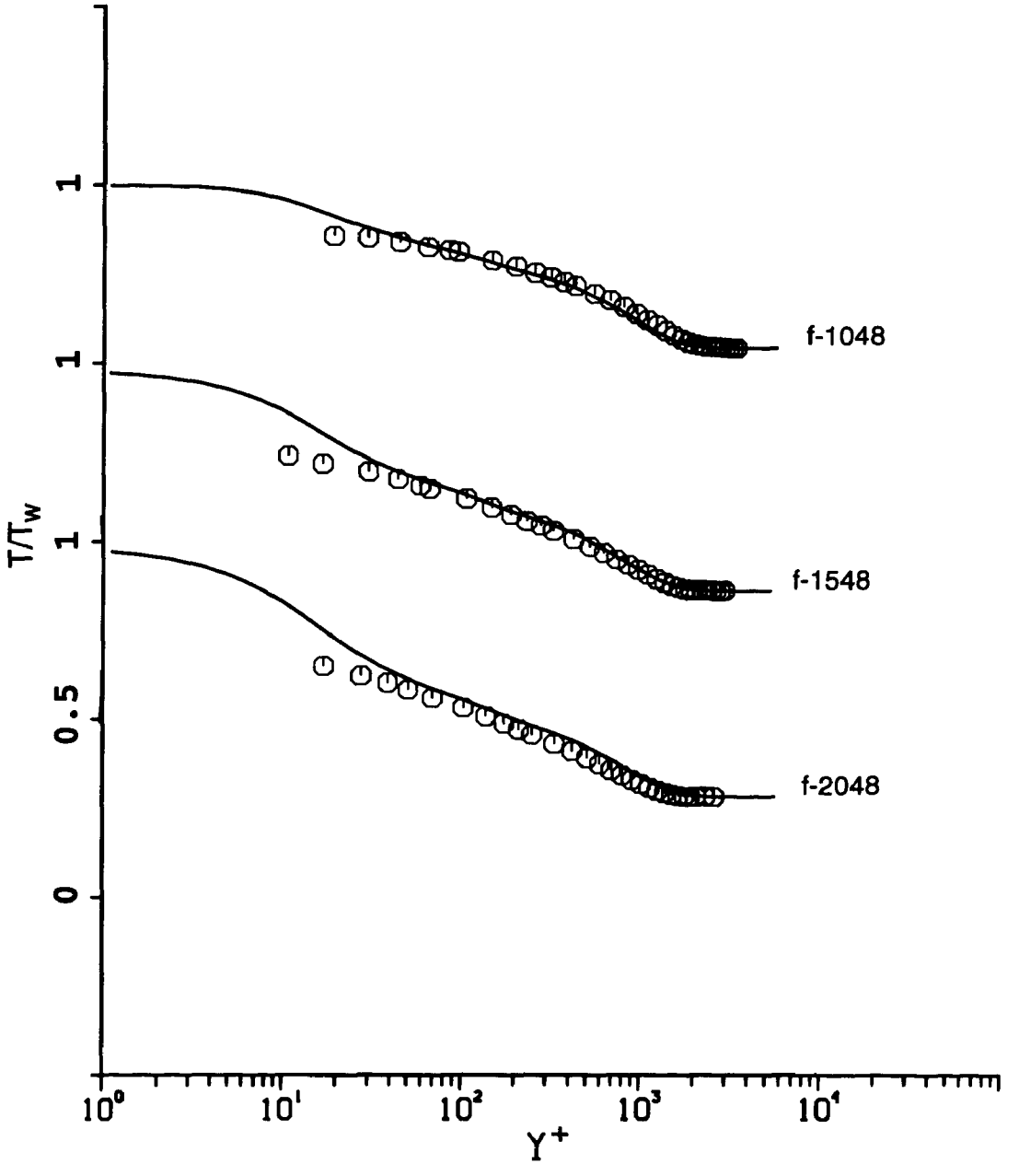

Figure 5.11b. Comparison of two-dimensional temperature data with the theoretical profile. Data from Carvin, 1988.

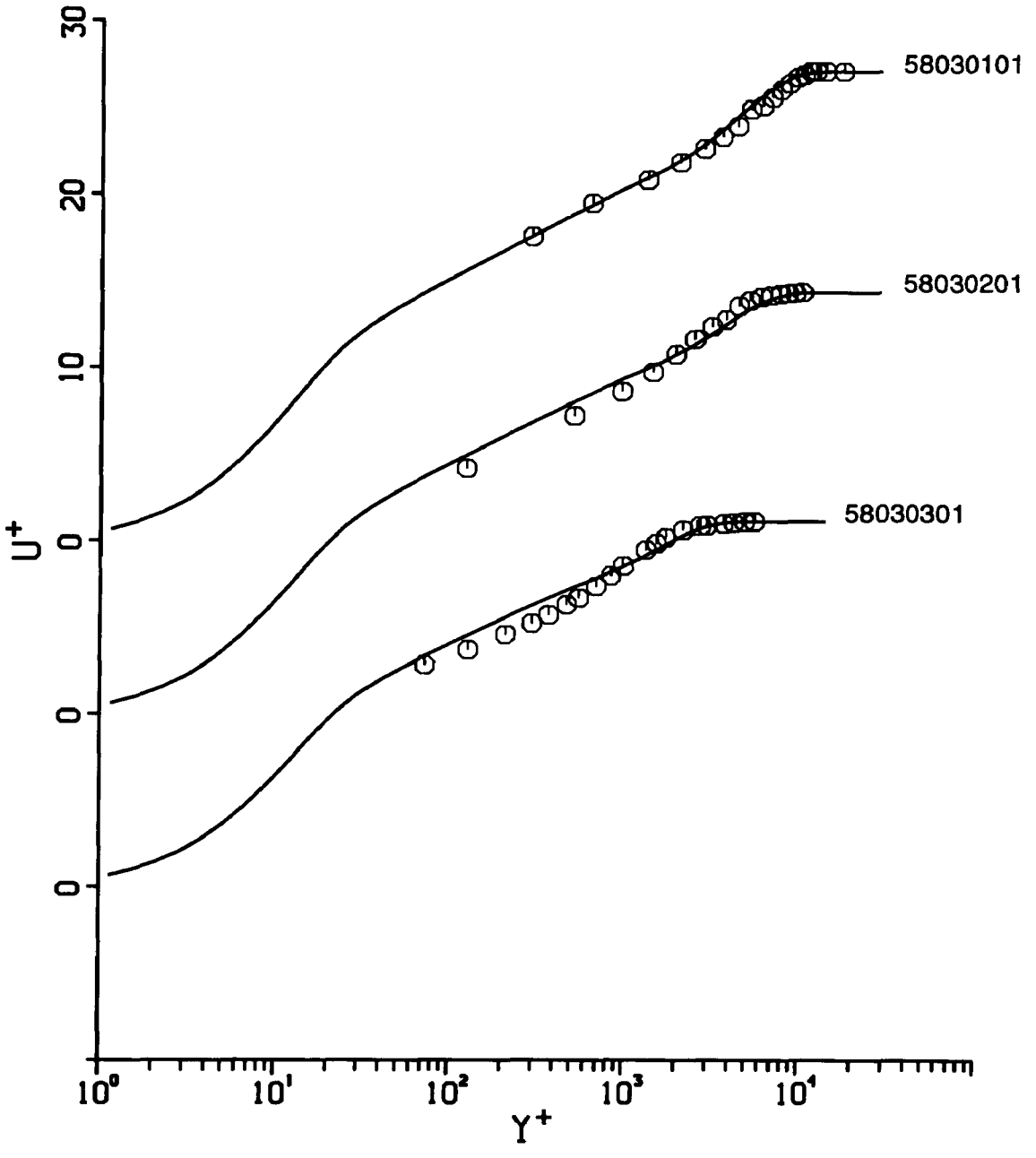

Figure 5.12a. Comparison of two-dimensional velocity data with the theoretical profile. Data from Fernholz and Finley, 1977 (5803-Kistler). Note the shifted origins.

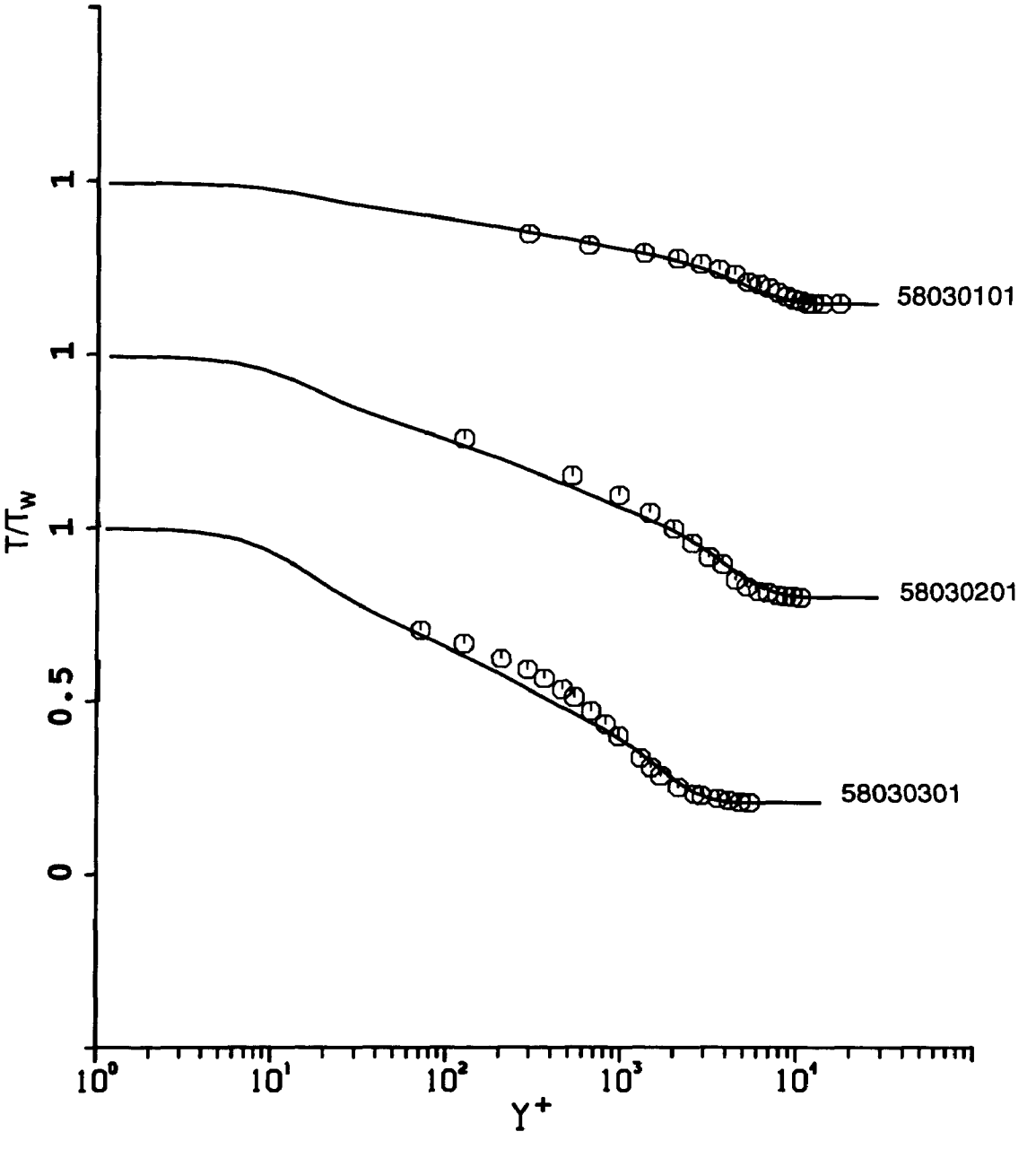

Figure 5.12b. Comparison of two-dimensional temperature data with the theoretical profile. Data from Fernholz and Finley, 1977 (5803-Kistler).

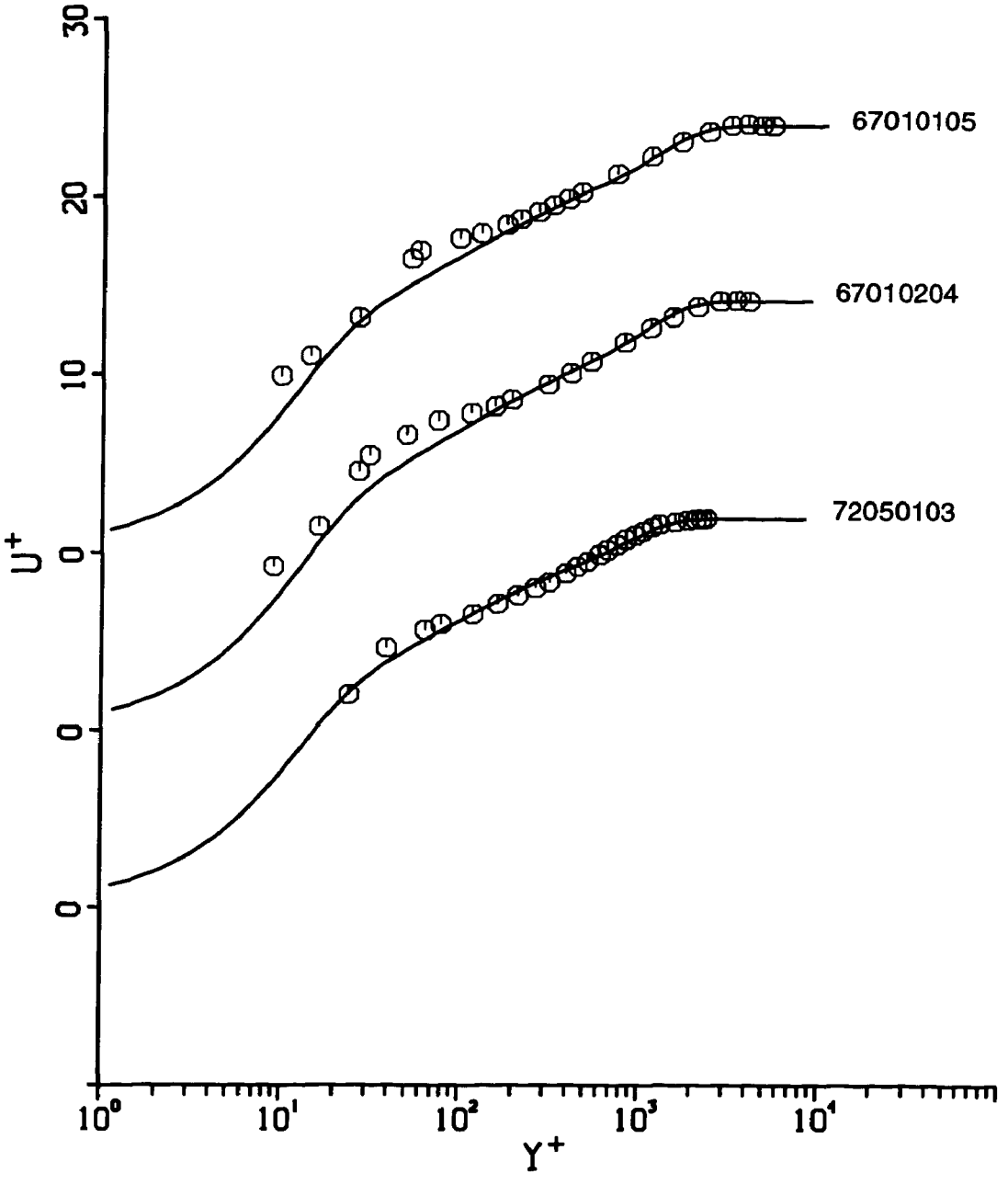

Figure 5.13a. Comparison of axi-symmetric velocity data with the theoretical profile. Data from Fernholz and Finley, 1977 (6701-Samuels et al.; 7205-Horstman and Owen). Note the shifted origins.

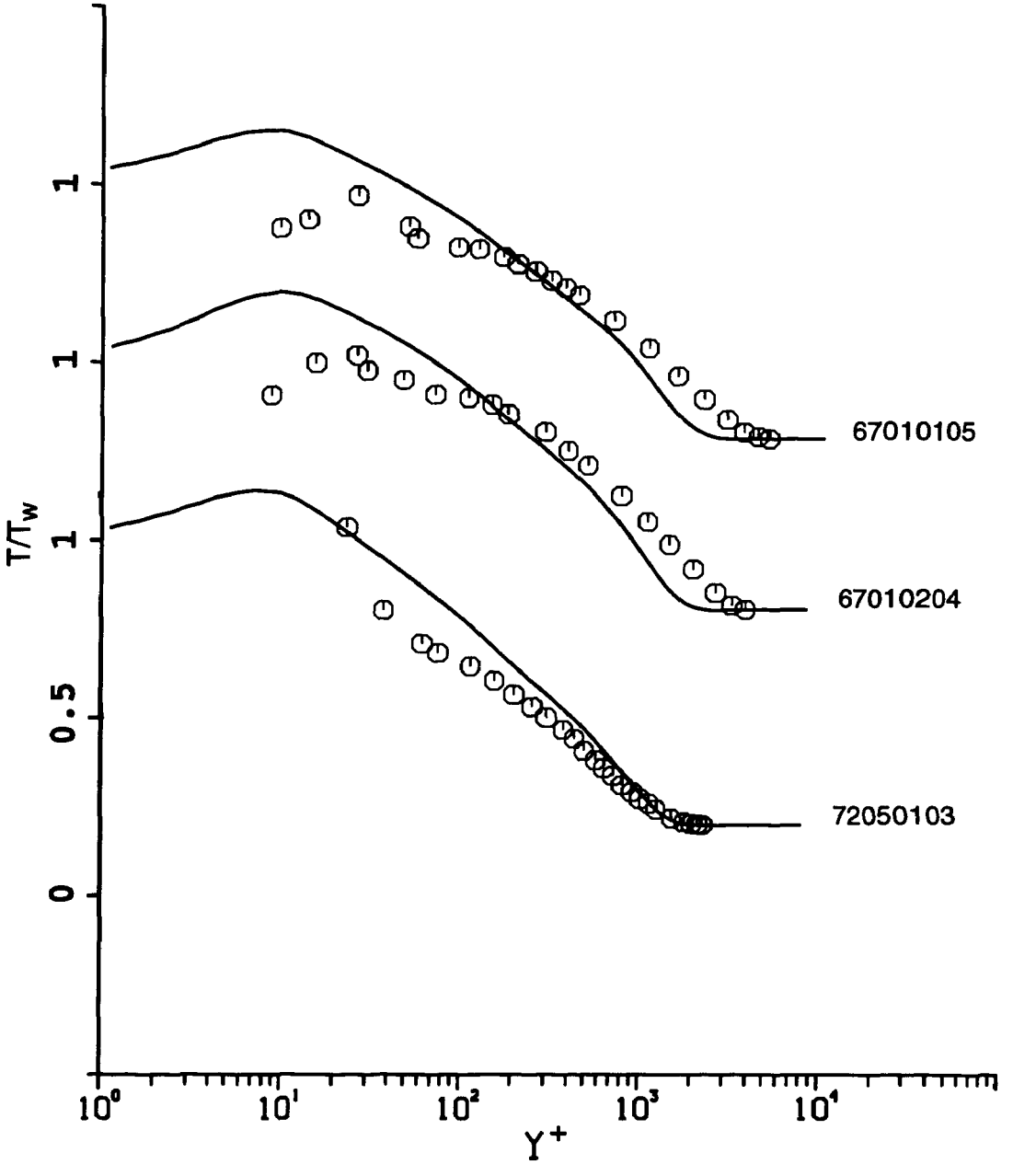

Figure 5.13b. Comparison of axi-symmetric temperature data with the theoretical profile. Data from Fernholz and Finley, 1977 (6701-Samuels et al.; 7205-Horstman and Owen).

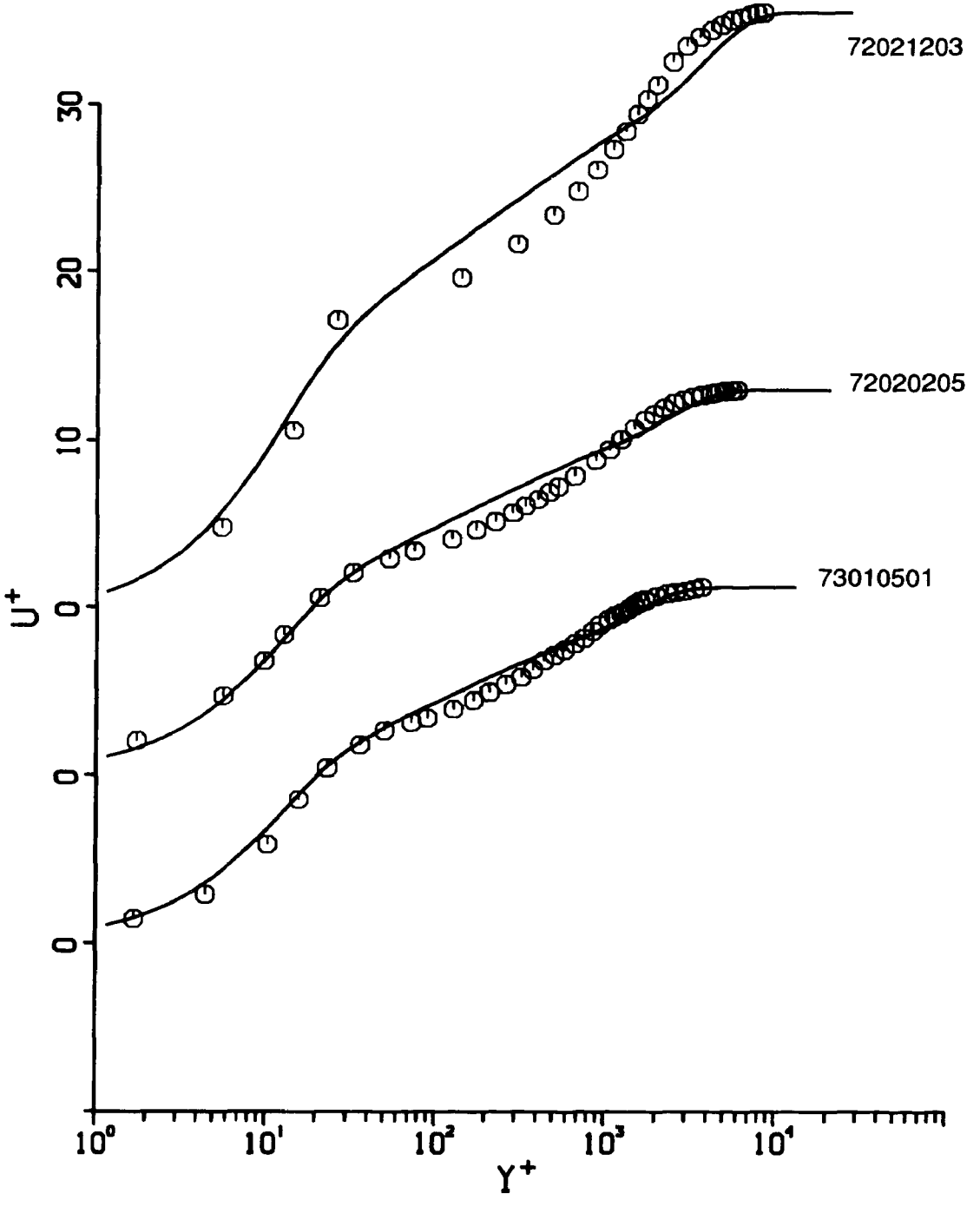

Figure 5.14a. Comparison of two-dimensional velocity data with the theoretical profile. Data from Fernholz and Finley, 1977 (7202-Voisinet and Lee; 7301-Gates). Flows are recovering from an upstream disturbance. Note the shifted origins.

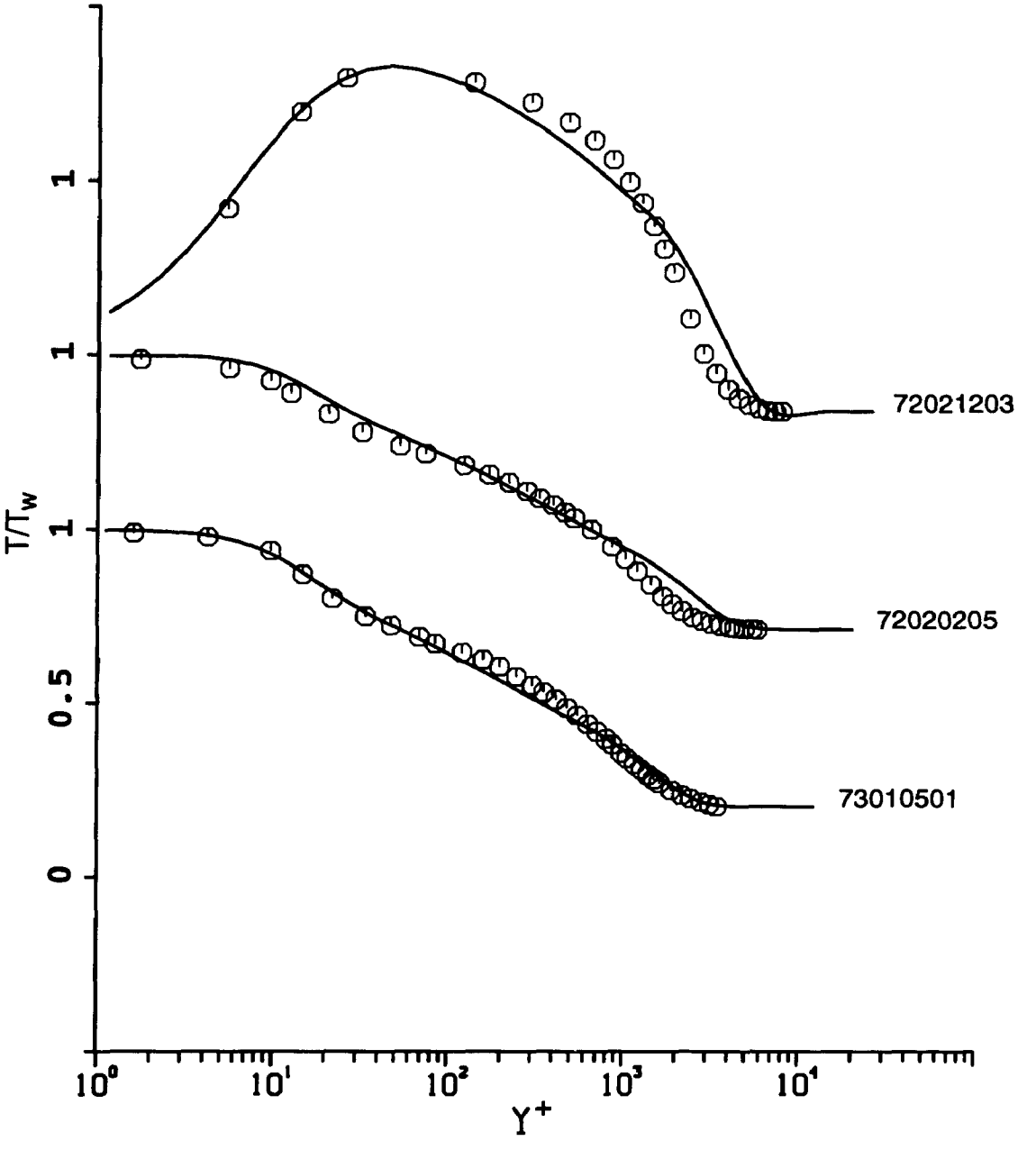

Figure 5.14b. Comparison of two-dimensional temperature data with the theoretical profile. Data from Fernholz and Finley, 1977 (7202-Voisinet and Lee; 7301-Gates). Flows are recovering from an upstream disturbance.

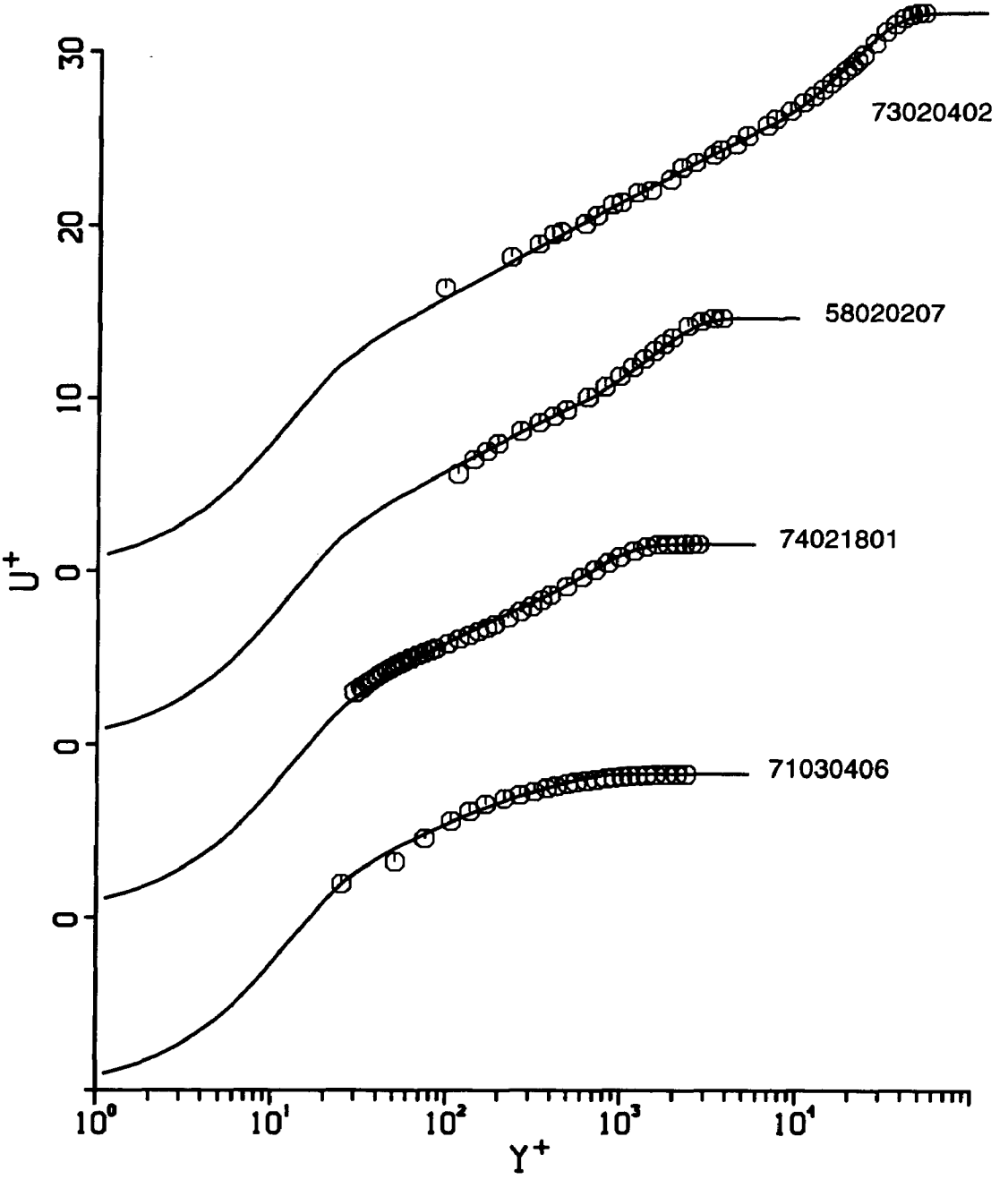

Figure 5.15a. Comparison of two-dimensional velocity data with the theoretical profile using the wall temperature as a reference condition. See Figure 5.6a for data identifications. Note the shifted origins.

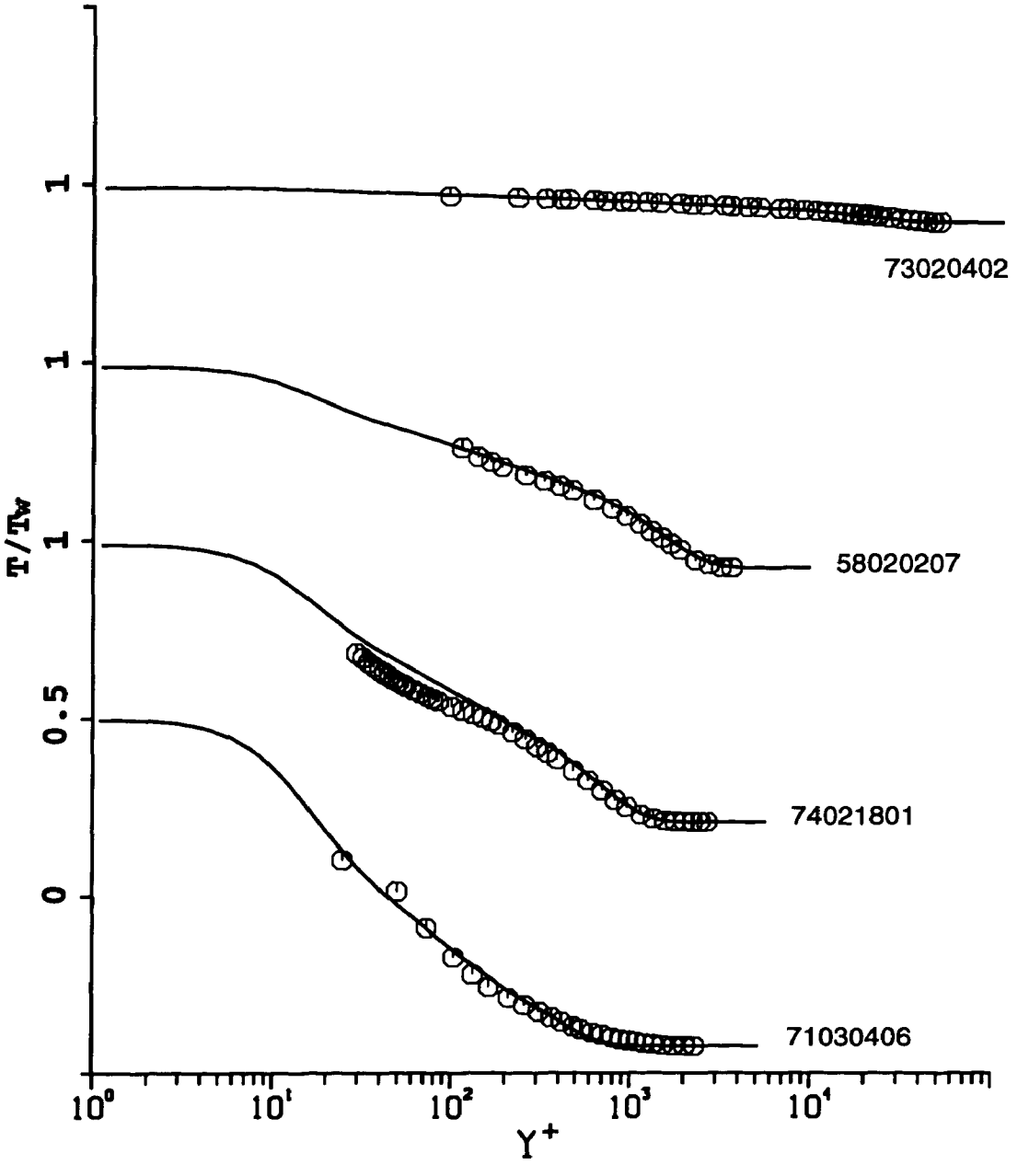

Figure 5.15b. Comparison of two-dimensional temperature data with the theoretical profile using the wall temperature as a reference condition. See Figure 5.6b for data identifications.

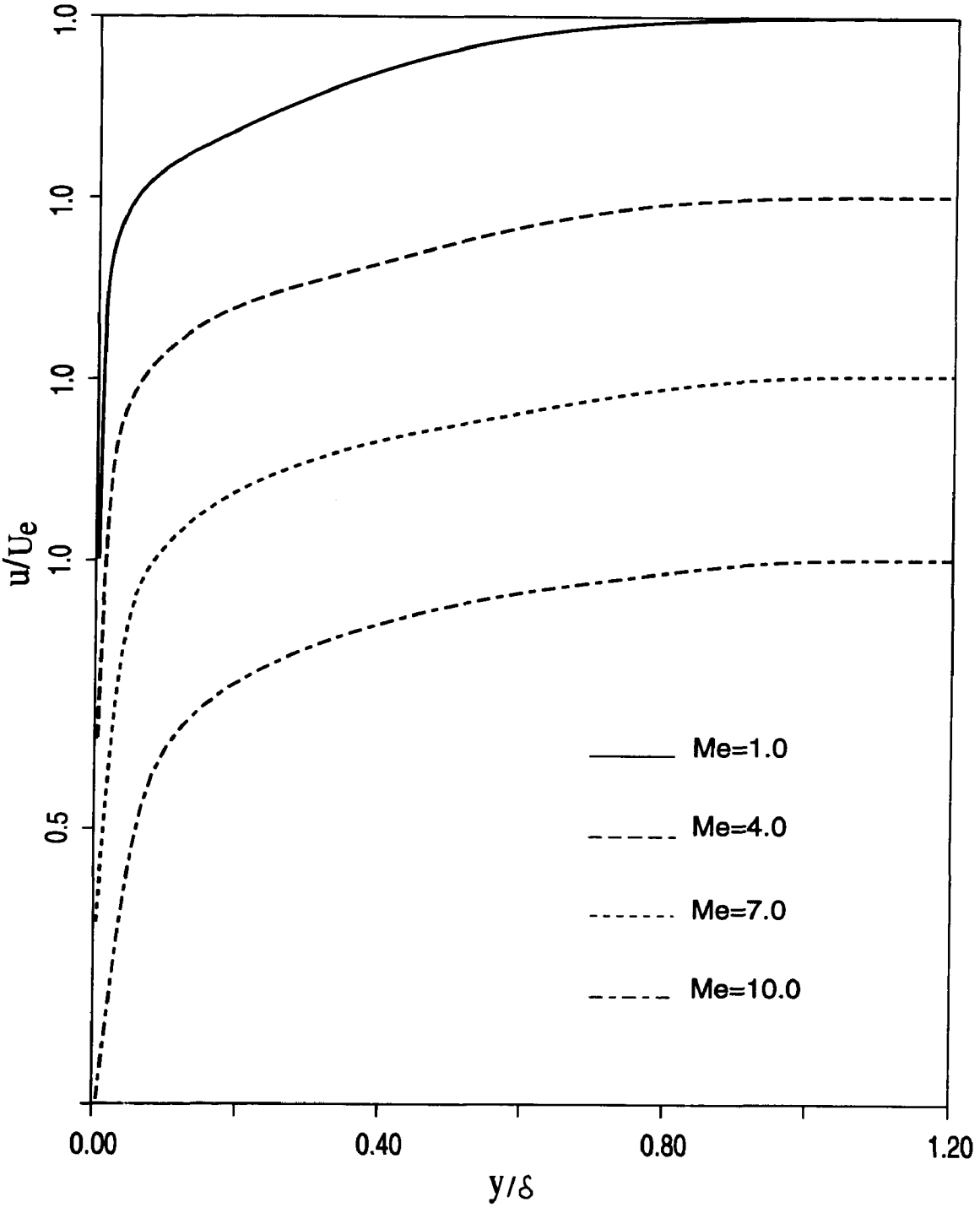

Figure 5.16. Variation of the velocity profile with Me for Re_{δ^*}=10,000.

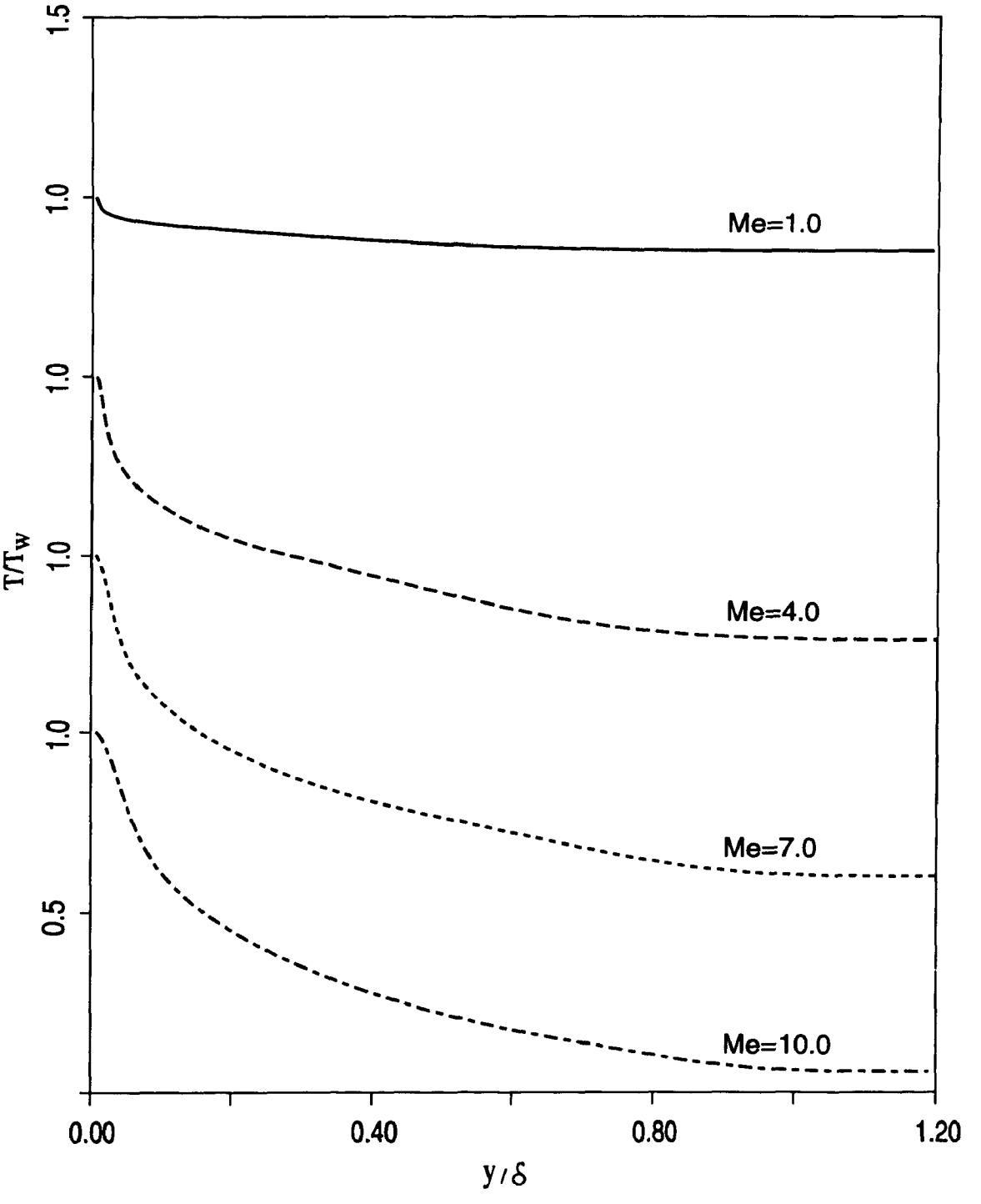

Figure 5.17. Variation of the temperature profile with Me for Re_{δ^*}=10,000.

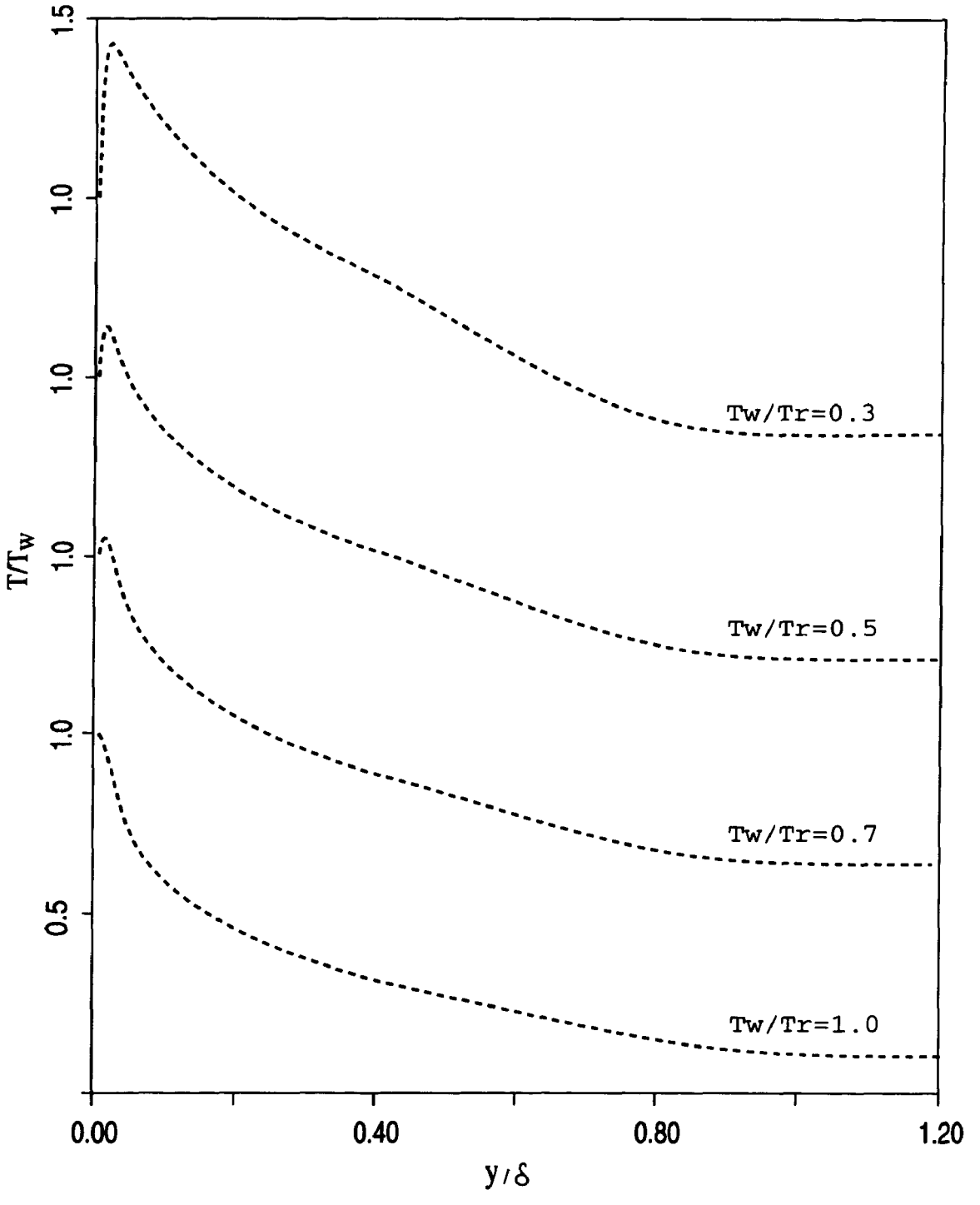

Figure 5.18. Variation of the temperature profile with the ratio of Tw/Tr for Re_{δ^*}=10,000 and Me=7.0.

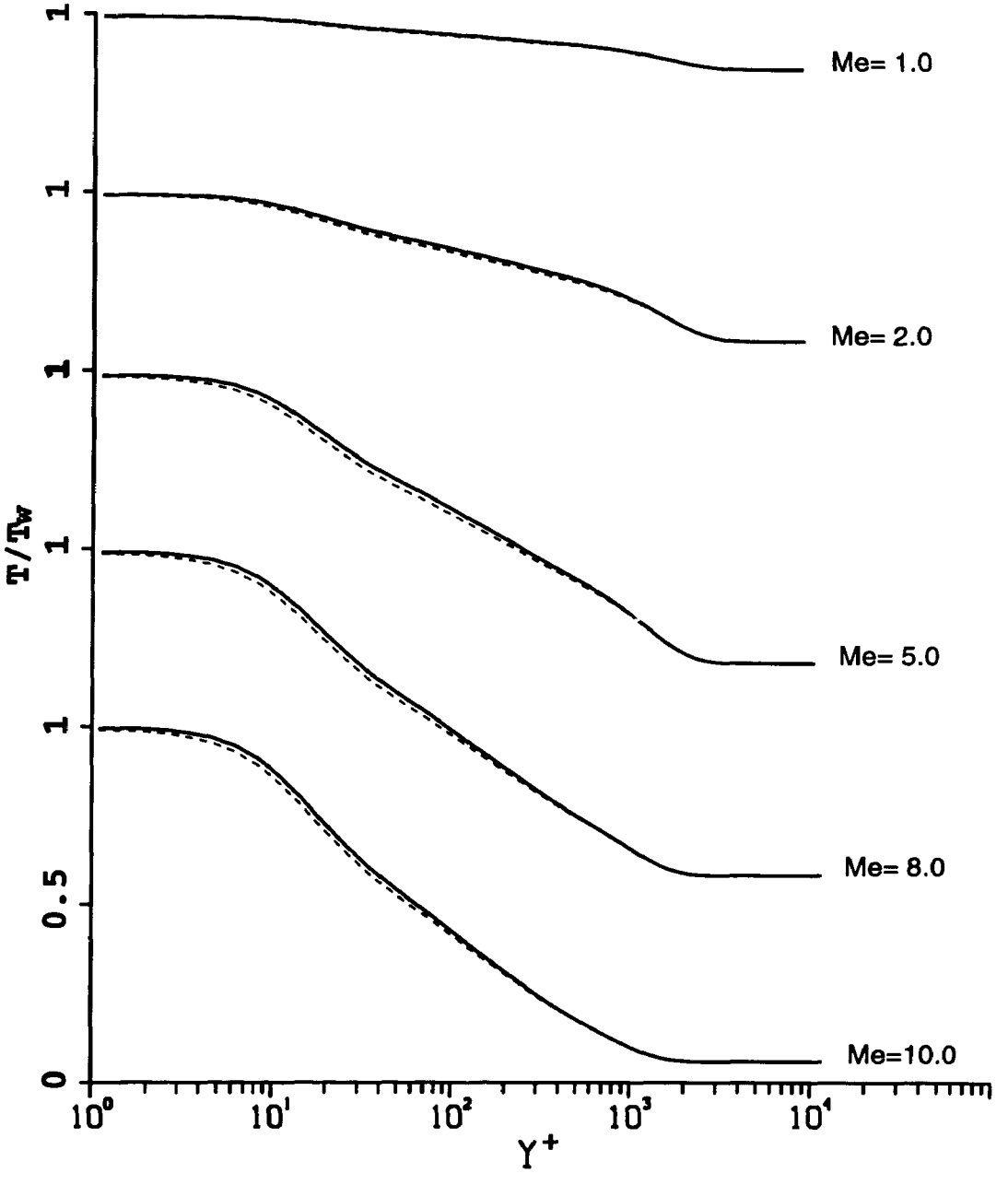

Figure 5.19a. Comparison of Crocco-Walz relationship (– – –) with the theoretical profile (———). Adiabatic flows with $Re_{\delta^*} = 10{,}000$. Note the staggered origins.

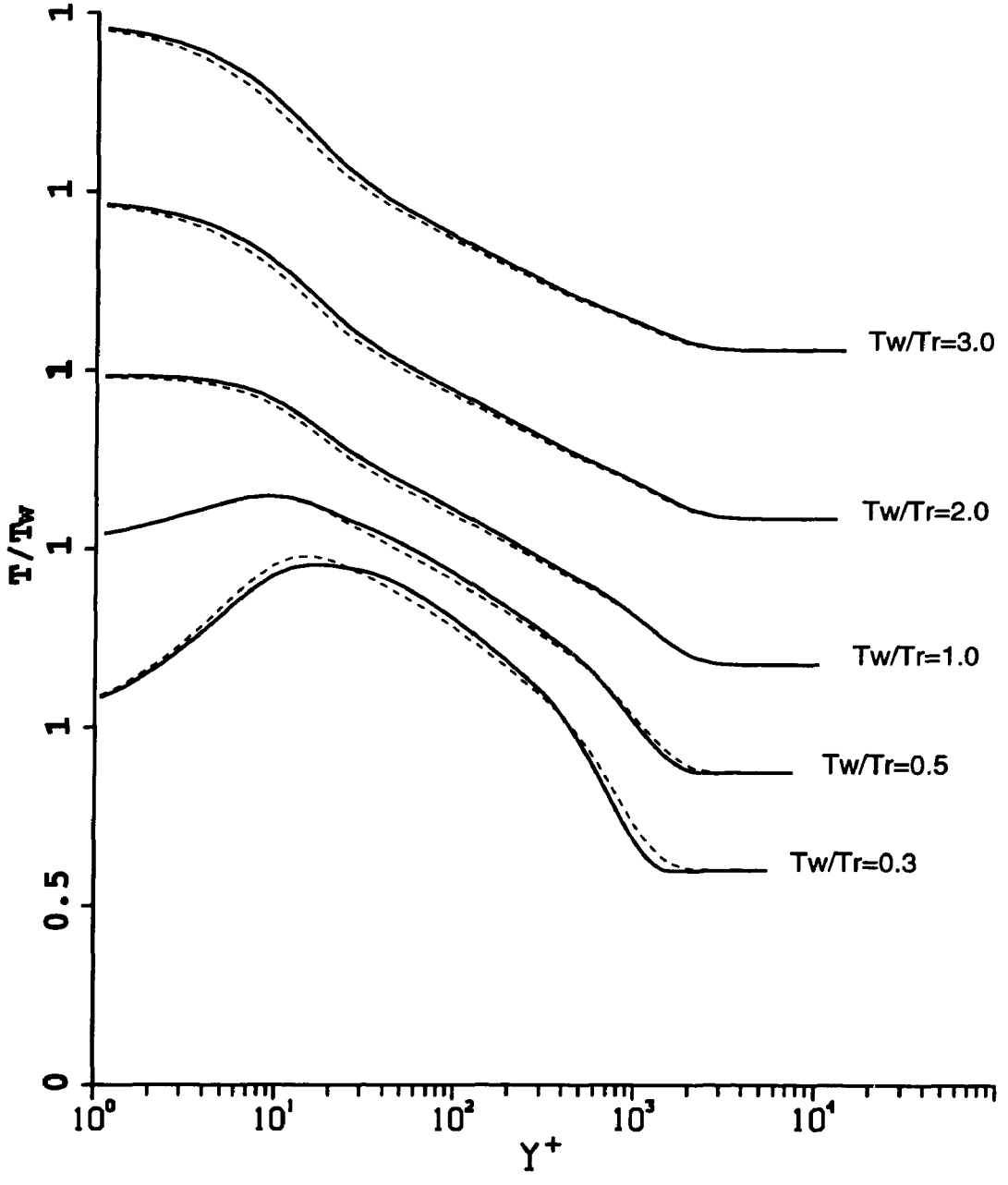

Figure 5.19b. Comparison of Crocco-Walz relationship (– – –·) with the theoretical profile (———). Me= 5.0, Re_{δ^*} = 10,000. Note the staggered origins.

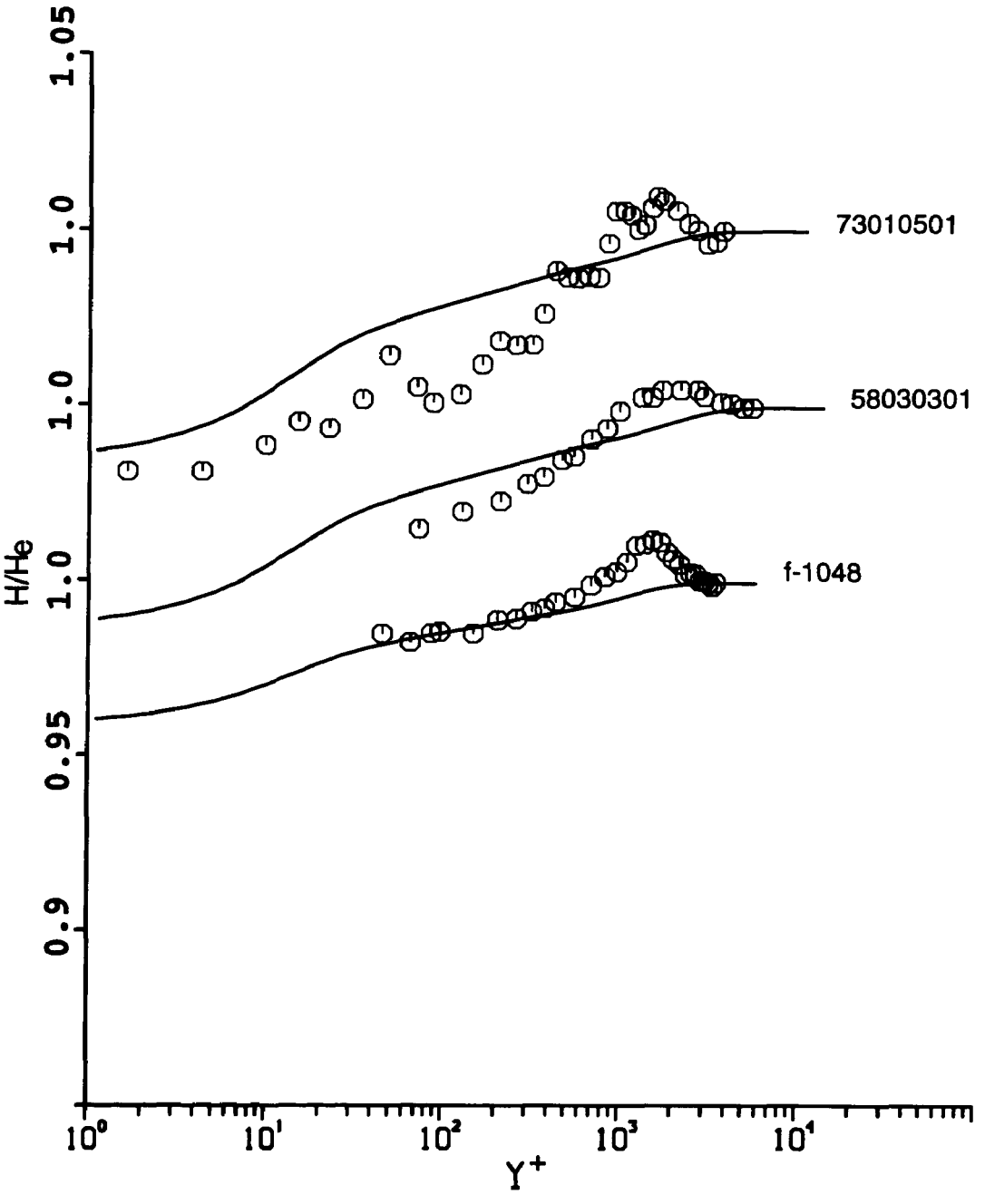

Figure 5.20. Comparison of total enthalpy data with the theoretical profile. Data from Fernholz and Finley, 1977 (5803-Kistler; 7301-Gates) and Carvin, 1988 (f-1048).

6. THE ADIABATIC WALL

6.1 Introduction

In this section, the effect of viscous dissipation on a high speed flow over an adiabatic surface will be addressed. Note that the total enthalpy equation contains a term associated with mean viscous dissipation which vanishes for a gas with Prandtl number unity; for convenience this term will be referred to throughout the study as being the "influence" or "effect" of viscous dissipation in the total enthalpy equation. It has been shown in §3 and §4 that in the limit of large Reynolds numbers and for mainstream Mach numbers O(1), the effects of mean viscous dissipation do not explicitly enter the leading-order equations if there is at least moderate heat transfer at the wall; this is consistent with the common view of the structure of the supersonic turbulent boundary layer. In general the dissipation term is believed to have only a limited effect on the mean temperature profile. Density and temperature changes reflect the combined effects of compressibility, viscous dissipation and/or heat transfer at the wall; the dissipation "effect" appears to be of little importance if only an expression for the mean temperature distribution is needed. This can be clearly seen by examining the data comparisons given in §5. However, the theory described in §5 cannot describe the total temperature overshoot near the boundary layer edge that is observed consistently in data; in this phenomenon, the total enthalpy increases monotonically from the near wall region and actually exceeds the mainstream value before decreasing toward the boundary-layer edge; this overshoot always occurs near the mainstream in the outer part of the boundary layer. The reason for the overshoot is not clear, but with increasing mainstream Mach number, viscous dissipation may become a

progressively important influence in the solution of the energy equation. In §4 it was shown that viscous dissipation first gives rise to a term in the expansion for total enthalpy in the wall layer as the quantity $D_{\tau o}$ becomes O(1) magnitude; this term eventually dominates in the wall-layer equation when heat transfer rate $q_w \to 0$. Only the limiting case of an insulated wall is considered in this section.

The leading order asymptotic analysis presented in §3 is valid when the effect of dissipation is negligible. When dissipation becomes significant, the asymptotic structure is expected to be modified. However, it is easily inferred that the expansions for the leading order momentum equation remains the same since the influence of dissipation only affects the velocity profile implicitly through density and temperature changes. The structure associated with the total-enthalpy equation evidently needs reconsideration. In order to concentrate solely on the influence of mean viscous dissipation for Prandtl numbers which are not equal to one, the case of supersonic flow with an adiabatic wall is considered exclusively here for large Reynolds numbers and mainstream Mach number O(1).

6.2 Asymptotic Structure

The basic equations governing the boundary layer flow were given in §3 and the energy equation is written again here, viz.

$$u\frac{\partial H}{\partial s} + \tilde{v}\frac{\partial H}{\partial Y} = \frac{1}{\bar{\rho}_o}\frac{\partial q}{\partial Y}\,, \tag{6.1}$$

where the total flux is defined as

$$q = \phi + \frac{\mu\rho}{\rho_o}\frac{1}{PrRe}\frac{\partial H}{\partial Y} + \frac{(\gamma-1)}{2}M_{ref}^2\frac{\partial}{\partial Y}\left[\left(1-\frac{1}{Pr}\right)\frac{\mu\rho}{\rho_o}\frac{1}{Re}\frac{\partial}{\partial Y}\left(u^2\right)\right]. \tag{6.2}$$

In this section the main interest is in the influence of viscous dissipation on the structure of the total enthalpy profile. The term associated with viscous dissipation is represented in the energy equation (6.1) by the second term on the right side of equation (6.2) for the flux q; this term is proportional to $u(\partial u/\partial n)$. To assess the behavior of this quantity, it is useful to examine a typical plot. First recall that in §5 a procedure was described for obtaining self-similar velocity profiles within a high-speed compressible boundary layer. A typical result for $U^+ = u/u_{\tau o}$ is shown in Figure (4.1) for an adiabatic flow at $M_e = 2.3$ (Carvin, 1988); it is evident that a close representation of measured velocity profile data has been obtained. On this same plot, $U^+(\partial U^+/\partial Y^+)$ is also shown; this quantity exhibits an absolute maximum deep within the wall layer (at $Y^+ \simeq 8$) and decreases rapidly toward zero near the outer edge of the wall layer. It is evident that the mean viscous dissipation is the largest in the wall layer and the influence of this quantity is expected to become progressively more important as M_e increases. Thus the wall layer is the starting point for the present analysis.

Now consider the energy equation (6.1) and introduce the inner normal variable Y^+ and velocity scaling. Again it follows that the convective terms are negligible to leading order and the energy equation reduces to

$$\frac{\partial q}{\partial Y^+} = 0\,. \tag{6.3}$$

This result also applies to flows with heat transfer but now $q_w = 0$, since the wall is

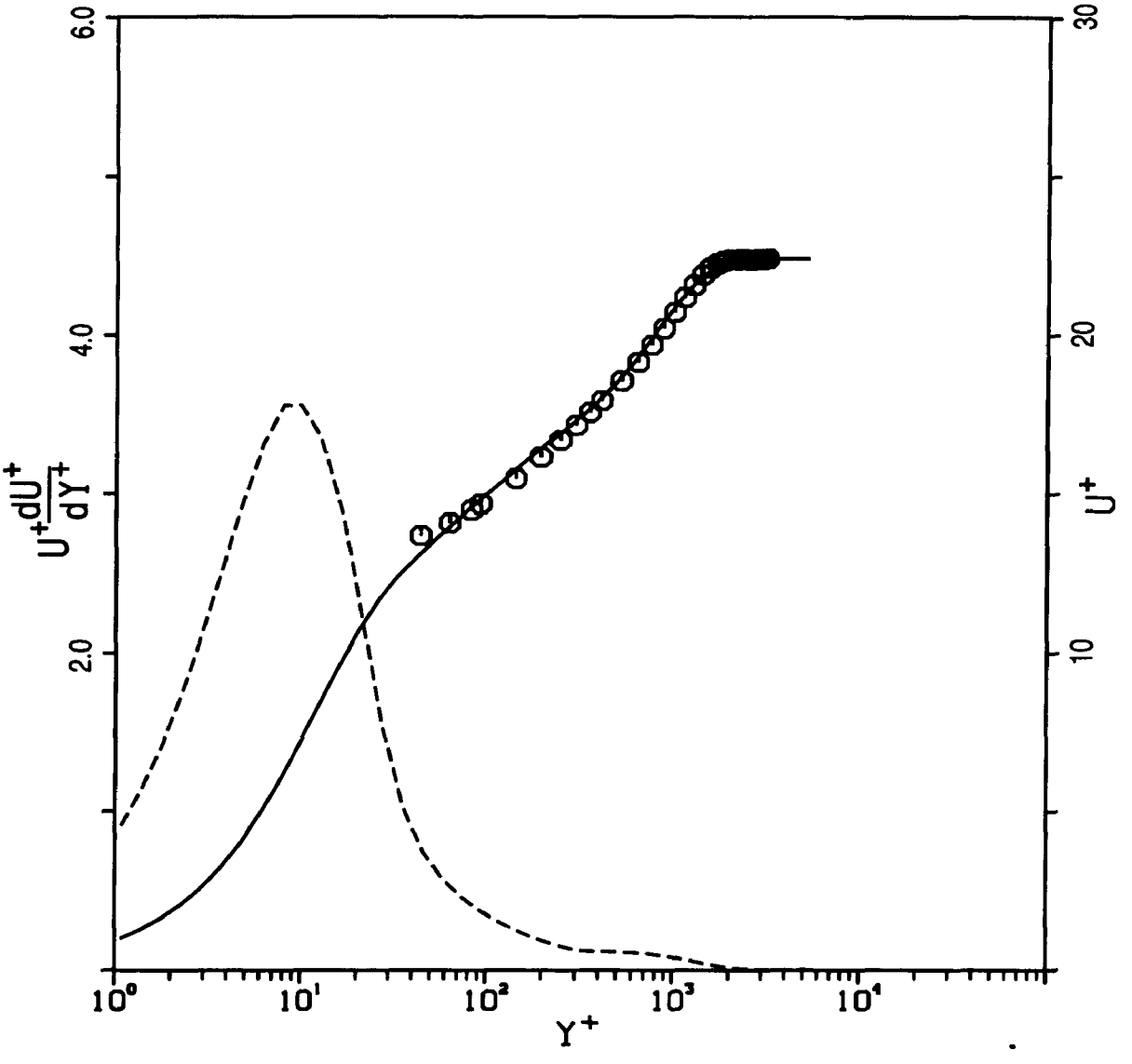

Figure 6.1. Typical velocity and mean dissipation distribution in a supersonic boundary layer; data is from Carvin, 1988, for adiabatic wall and with $M_e = 2.3$.

insulated and the integrated form of equation (6.3) is

$$\phi + \rho_o u_{\tau o} \left(\frac{\mu\rho}{\mu_w \rho_w}\right) \frac{1}{Pr} \frac{\partial H}{\partial Y^+}$$

$$+ \rho_o u_{\tau o}^3 \frac{(1-Pr)}{Pr} (\gamma - 1) M_{ref}^2 \left(\frac{\mu\rho}{\mu_w \rho_w}\right) \frac{\partial}{\partial Y^+} \left(\frac{u^2}{2}\right) = 0 \ . \tag{6.4}$$

Examination of equation (6.4) suggests that the wall-layer expansions should proceed as follows:

$$\phi = \alpha \rho_o u_{\tau o}^3 \frac{H_e}{U_e^2} \left(\frac{Pr-1}{Pr}\right) \phi_2(Y^+) + \cdots , \tag{6.5}$$

$$H = T_r + \alpha(1-Pr) H_e \left(\frac{u_{\tau o}}{U_e}\right)^2 \theta_2^+ (Y^+) + \cdots , \tag{6.6}$$

where T_r denotes a recovery temperature (or adiabatic wall temperature) defined as

$$T_r = T_e \left\{ 1 + \mathrm{r} \left(\frac{\gamma - 1}{2}\right) M_e^2 \right\} . \tag{6.7}$$

The form of the expansion (6.6) was also suggested by the unsteady wall-layer analysis for the limit $q_w \to 0$ (see §4.4). Substitution of equations (6.5) and (6.7) into equation (6.4) leads to

$$\phi_2 + \frac{\partial \theta_2^+}{\partial Y^+} = U^+ \frac{\partial U^+}{\partial Y^+} , \tag{6.8}$$

where the Chapman-Rubesin density-viscosity law has been used in obtaining equation (6.8). The right side of equation (6.8) should be regarded as a known function with asymptotic properties described in §3, which are

$$\frac{\partial U^+}{\partial Y^+} = 1, \quad U^+ = 0, \quad \text{at} \quad Y^+ = 0 \,, \tag{6.9}$$

and

$$U^+ \sim \tfrac{1}{\kappa} \log Y^+ + C_i \,, \quad \text{as} \quad Y^+ \to \infty \,. \tag{6.10}$$

In addition, at the wall

$$\phi_2 = \theta_2^+ = \frac{\partial \theta_2^+}{\partial Y^+} = 0 \quad \text{at} \quad Y^+ = 0 \,. \tag{6.11}$$

Note that both ϕ_2 and θ_2^+ are unknown, apart from conditions (6.11) and the fact that they satisfy equation (6.8). There is essentially no measured data for either the turbulence term or the total temperature near an adiabatic wall that can give guidance as to the general behavior of these functions in a supersonic boundary layer. Furthermore, since the gauge functions associated with these terms in equations (6.5) and (6.6) are relatively small, it is expected that experimental information concerning these quantities will not be forthcoming in the near future. In spite of these deficiencies, it is still possible to make progress in the determination of the asymptotic structure of the boundary layer. Integrating equation (6.8) from 0 to Y^+ results in

$$\theta_2^+ = \frac{1}{2}(U^+)^2 - \int_0^{Y^+} \phi_2 \, dY^+ \, . \tag{6.12}$$

The function ϕ_2 is associated with the turbulence and is unknown; however, it is assumed here that, at most,

$$\int_0^{Y^+} \phi_2 \, dY^+ \sim \frac{\Phi_2}{2}(\log Y^+)^2 + \Phi_1 \log Y^+ + \cdots \, , \tag{6.13}$$

as $Y^+ \to \infty$, where Φ_2, Φ_1, $\cdots$ are constants to be determined. Condition (6.13) implies that

$$\phi_2 \sim \Phi_2 \frac{\log Y^+}{Y^+} \quad \text{as} \quad Y^+ \to \infty \, . \tag{6.14}$$

Since it is anticipated that each term in equation (6.8) will approach zero as $Y^+ \to \infty$, equation (6.14) is equivalent to assuming that ϕ_2 does not decay slower than the right side of equation (6.8) as $Y^+ \to \infty$. It follows from equation (6.12) that

$$\theta_2^+ \sim \frac{1}{2}\left(\frac{1}{\kappa^2} - \Phi_2\right)(\log Y^+)^2 + \left(\frac{C_i}{\kappa} - \Phi_1\right)\log Y^+ \cdots \, , \tag{6.15}$$

as $Y^+ \to \infty$.

Now consider the outer layer where the velocity in the form of a defect law (cf. equation 3.110) is rewritten here according to

$$\frac{u}{U_e} = 1 + u_* \frac{\partial F_1}{\partial \eta} + \cdots \, . \tag{6.16}$$

The outer total-enthalpy expansion is also expected to be in defect form according to

$$I = \frac{H}{H_e} = 1 + u_* \Gamma_2 \Theta_2 + \cdots , \tag{6.17}$$

where Γ_2 is a gauge function to be determined. In the outer layer the deviations of the total enthalpy from its mainstream value are expected to be small and the form of equation (6.17) is assumed here subject to confirmation.

Substituting equation (6.17) into the energy equation gives,

$$\frac{\partial \Theta_2}{\partial s} - \frac{(\Delta_o r U_e)'}{(\Delta_o r U_e)} \eta \frac{\partial \Theta_2}{\partial \eta} = \frac{1}{\rho_o u_* \Delta_o U_e H_e \Gamma_2} \frac{\partial q}{\partial \eta} , \tag{6.18}$$

to leading order, where the prime denotes differentiation with respect to s and Δ_o is the outer length scale of the boundary layer and as discussed in §3 is $O(u_*)$. The boundary conditions associated with this equation are taken to have the form

$$\Theta_2 \sim \frac{1}{\kappa_a} \log\eta + B_o \quad \text{as} \quad \eta \to 0 , \tag{6.19}$$

and

$$\Theta_2 \to 0 \quad \text{as} \quad \eta \to \infty . \tag{6.20}$$

Here the quantity κ_a is the analogous quantity to the von Kármán constant but both κ_a and B_o are unknown at this stage. The asymptotic form (6.19) should be regarded as an assumption at this point, which is subject to confirmation and

which is motivated by the fact that a similar behavior is known to occur for H in flows with heat transfer at the wall; in addition, the logarithmic behavior is also suggested by the form of the inner expansion in equation (6.15).

Matching the wall-layer and outer-layer velocity profiles has been carried out in §3. Note that a relationship between inner variable Y^+ and outer variable η is obtained through the matching (see equation 3.116) according

$$\log Y^+ = \frac{\kappa}{u_*} + \log \eta + \kappa(C_o - C_i) \; . \tag{6.21}$$

Here to obtain a match of the total enthalpy expansions, relation (6.21) is substituted into the asymptotic form (6.15) and this yields

$$\theta_2^+ \sim \frac{1}{2u_*^2}\left(1 - \kappa^2\Phi_2\right) + \frac{1}{u_*}\left\{\left(\frac{1-\kappa^2\Phi_2}{\kappa}\right)\left[\log\eta + \kappa(C_o - C_i)\right] + C_i - \kappa\Phi_1\right\} + \cdots \tag{6.22}$$

to leading order. Using equations (6.6), (6.17) and (6.19), it may be confirmed that in order for the leading terms to match in the total enthalpy profile,

$$1 = I_r + \frac{\alpha}{2}\,(1 - Pr)\,(1 - \kappa^2\Phi_2) \; , \tag{6.23}$$

where $I_r = H_r/H_e = T_r/H_e$ is the ratio of total enthalpy at the wall to that in the mainstream for an adiabatic wall and α is given by equation (3.9). Similarly matching of the logarithmic terms in (6.17) and (6.22) yields an expression for the gauge function Γ_2 according to

$$\frac{\Gamma_2}{\kappa_a} = \frac{\alpha}{\kappa}\,(1 - Pr)\,(-\kappa^2\Phi_2)\ . \tag{6.24}$$

Using equation (6.22), it follows that

$$\frac{\Gamma_2}{\kappa_a} = \frac{2}{\kappa}\,(1 - I_r)\ . \tag{6.25}$$

The quantity κ_a is related to the slope of the total enthalpy profile in the overlap zone and is expected to be O(1); on the other hand, I_r is a function of M_e. It is convenient to select the gauge function Γ_2 in equation (6.17) from equation (6.25) according to

$$\Gamma_2 = 2(1 - I_r)\ . \tag{6.26}$$

It follows that

$$\kappa_a = \kappa\ , \tag{6.27}$$

and thus κ_a is equivalent to the von Kármán constant. It is noted that the quantity Φ_2, appearing in equation (6.22) and originally introduced in equation (6.13) in association with the assumed asymptotic behavior of the turbulence term, may be subsequently expressed in terms of the recovery factor; this will be considered in the next section.

Lastly it may be shown that an expression for the constant Φ_1 (c.f. equation (6.13)) may be obtained through matching of the terms $O(u_*)$; it can be shown that

$$\Phi_1 = \tfrac{1}{\kappa}\, C_i + \tfrac{1}{\kappa}\,(1-\kappa^2\Phi_2)\,(C_o - C_i - B_o)\ , \tag{6.28}$$

which in general defines Φ_1 as a function of s (streamwise distance along the surface). Note that for universal values of κ, C_i and Φ_2, $\Phi_1 = \Phi_1(s)$ since C_o and B_o are functions of s, in general, whose values depend on the specific outer-region turbulence model adopted in the momentum and energy equations, respectively.

At this point the outer-region total-enthalpy expansion may summarized as follows: the outer defect law takes the form

$$I = \frac{H}{H_e} = 1 + u_*\,[2(1-I_r)]\,\Theta_2 + \cdots\ , \tag{6.29}$$

with the limiting behavior of Θ_2 according to

$$\Theta_2 \sim \tfrac{1}{\kappa}\log\eta\ + B_o \quad \text{as} \quad \eta \to 0\ , \qquad \theta_2 \to 0 \quad \text{as} \quad \eta \to \infty. \tag{6.30}$$

Equation (6.29) implicitly contains a dependence on Mach number in I_r; as $M_e \to 0$, I_r approaches unity, and in this limit the total enthalpy is constant across the boundary layer. The hypersonic limit $M_e \to \infty$ will be considered subsequently, where it will be shown that I_r approaches a finite limit.

6.3 The Recovery Factor

It is known from the derivation of Crocco integral that if the molecular Prandtl number is unity and the turbulent transport terms $\rho\overline{u'v'}$ is exactly equal to $\rho\overline{v'H'}$, then the total enthalpy H must be constant across the boundary layer in an

adiabatic flow. However, the turbulence terms in the mainstream and energy equations are never identically equal, and in such cases and whenever Prandtl number is not unity, the total enthalpy is not constant. For most gases $Pr < 1$ and energy migrates from near the wall to regions near the edge of the boundary layer. In general it is observed that the wall temperature for adiabatic surfaces is greater than the mainstream static temperature but less than the mainstream total enthalpy. This experimental fact is characterized by the so-called recovery factor r defined by

$$\mathrm{r} = \frac{T_r - T_e}{(\gamma - 1)M_e^2/2}\,, \tag{6.31}$$

which in general lies between 0 and 1. From equation (6.31) it is easily shown that

$$I_r = \frac{H_r}{H_e} = 1 - \frac{\alpha}{2}\,(1 - \mathrm{r})\,, \tag{6.32}$$

where α is defined by equation (3.9). It is worthwhile to note that since $0 \leq \alpha < 2$ for $0 \leq M_e < \infty$, $I_r = 1$ when $M_e = 0$, and in the hypersonic limit $M_e \to \infty$, $I_r \to \mathrm{r}$.

Comparing equations (6.22) and (6.32), it follows that the recovery factor r is given in terms of the constant Φ_2 introduced in equation (6.13) by

$$\mathrm{r} = Pr + (1 - Pr)\kappa^2\Phi_2\,. \tag{6.33}$$

The recovery factor that is usually quoted for turbulent flow (see Cebeci and Smith, 1974) is $\mathrm{r} = Pr^{1/3}$; this value is a correlation of empirical data. It may be

noted that the functional dependence on Pr exhibited in equation (6.33) is different from the conventional relation; unfortunately, available experimental data for T_r is for gases having Prandtl numbers in the range 0.71 to 0.72, and this range is not sufficiently broad to discern a possible dependence on Pr in the data. If the conventional expression is equated to equation (6.33) for $Pr = 0.71$, a universal value of

$$\Phi_2 = 3.736 \tag{6.34}$$

is implied. In Figure (6.2), values of the recovery factor r computed from the compilation of data for adiabatic walls (Fernholz and Finley, 1977) and the recent experiments of Carvin (1988) are shown. For each point, r was calculated from the definition in equation (6.31) using the quoted experimental values of T_r, T_e and M_e. For the majority of the data $Pr = 0.71$ and the solid line denotes the standard value of the recovery factor of $(0.71)^{1/3}$ for which $\Phi_2 = 3.736$. A regression analysis was carried out for the points shown on Figure (6.2) and yielded the broken straight line having almost zero slope; this also tends to support the hypothesis of a constant value of Φ_2 given by equation (6.34), at least for an almost constant Pr. There is considerable scatter in the "data" shown on Figure (6.2) but to an extent this is to be expected because of the nature of the evaluation of r. Suppose for the sake of argument that $\bar{r} = (0.71)^{1/3}$ is the true value of r and that errors of ΔT_r and ΔT_e are present in the experimental data for T_r and T_e, respectively. Then it is easily shown from equation (6.31) that

$$r \simeq \bar{r} + \frac{T_r}{T_e}\left(\frac{\Delta T_r}{T_r} - \frac{\Delta T_e}{T_e}\right)\frac{2}{(\gamma-1)M_e^2} + \cdots . \tag{6.35}$$

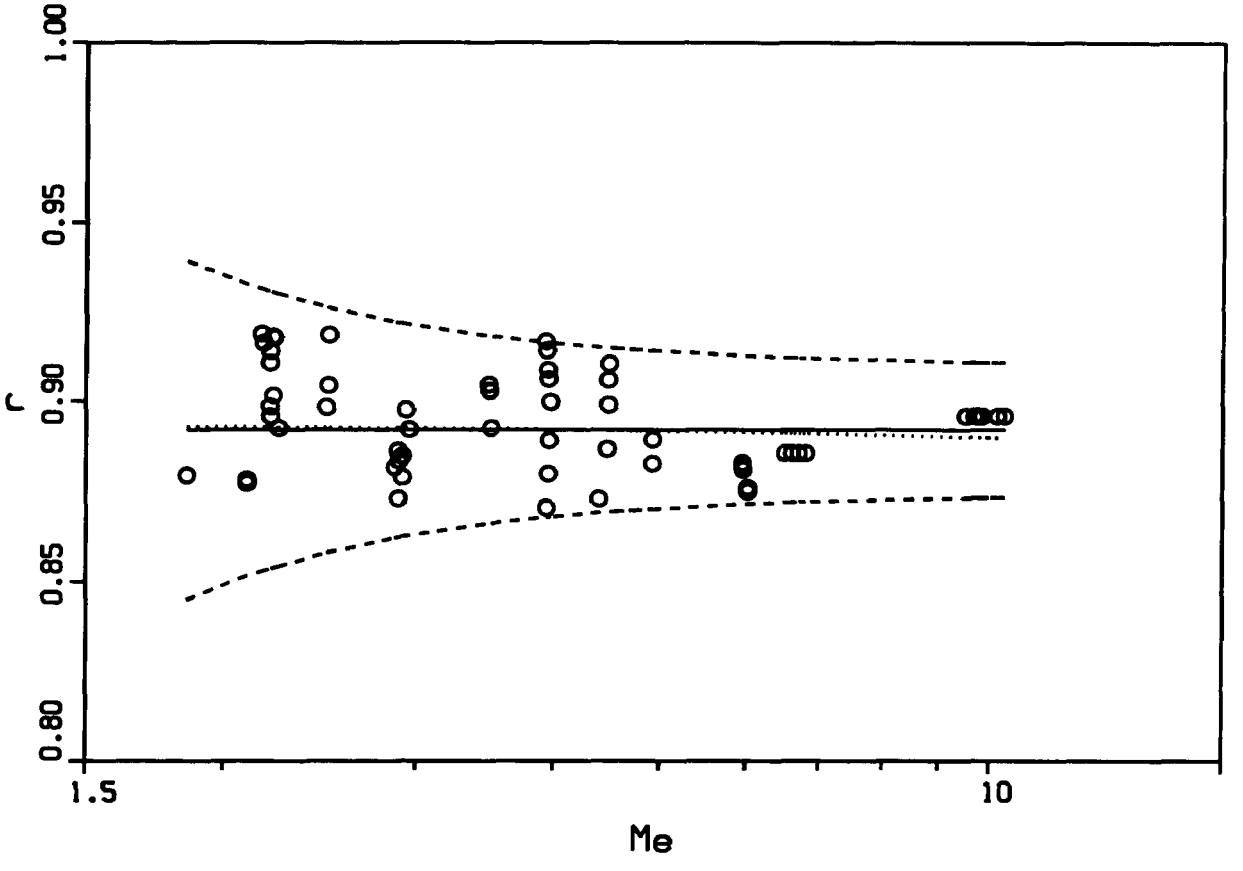

Figure 6.2. Experimental and theoretical values for recovery factor r : o evaluated from data; —— Φ_2=3.736; – – – maximum and minimum estimate for r for 1 percentage error in temperature data; ----- linear regression to data.

As an example, suppose that errors of 1% are present in the temperature data, then maximum and minimum values of r are given by

$$\mathrm{r} = \bar{\mathrm{r}} \pm \frac{0.04}{(\gamma-1)M_e^2}\frac{T_r}{T_e} \,. \tag{6.36}$$

These curves are shown in Figure (6.2) and are seen to bound most of the "data". For low values of M_e, there is considerable scatter in the data; in most of these experiments, there is uncertainty in the temperature data as well as whether or not the wall was truly adiabatic. Consequently, although Φ_2 could, in principal, be correlated as a function of M_e, neither the accuracy of presently available data or the trends in the data itself justifies such a correlation.

6.4 Turbulence Flux Modeling

In order to develop total-enthalpy profile for the outer region, it is now necessary to introduce specific turbulence models for q in the outer layer. In §5.2 it was argued that the Reynolds shear stress and flux can be modeled by Boussinesq's gradient-diffusion models having the form

$$\sigma = \rho\epsilon\,\frac{\partial u}{\partial n}\,, \qquad \phi = \rho\epsilon_H\,\frac{\partial H}{\partial n}\,, \tag{6.37}$$

where ϵ and ϵ_H are eddy viscosity and eddy conductivity, respectively. Here in this section, however, a rather unconventional model for turbulent flux term is proposed according to

$$\phi = \rho\epsilon_a \frac{\partial H}{\partial n} - \rho\epsilon \frac{2\mathrm{P}H_e(1-I_r)}{U_e^2} u\frac{\partial u}{\partial n}\,, \tag{6.38}$$

where ϵ_a denotes eddy-conductivity coefficient in an adiabatic flow. The form of equation (6.38) merits some discussion. Consider the energy equation (6.18) and using equations (6.19),it follows that for a self-similar flow ($\Theta_2 = \Theta_2(\eta)$)

$$\frac{\partial q}{\partial \eta} \sim -\frac{\rho_o u_* H_e \Gamma_2}{\kappa_a U_e} (\Delta_o U_e)' \quad \text{as} \quad \eta \to 0. \tag{6.39}$$

But for an adiabatic wall, $q_w = 0$ and since q is constant across the wall layer, it follows from equation (6.35) and (6.39) that

$$q \sim -\frac{2\rho_o u_* H_e (\Delta_o U_e)'}{\kappa U_e} (1-I_r)\,\eta \;\ldots \quad \text{as} \quad \eta \to 0. \tag{6.40}$$

Since $I_r < 1$ and $(\Delta_o U_e)' > 0$, it follows that q is negative for small η at the inner edge of the wall layer. Consequently, it is clear that if an attempt is made to model the turbulent heat flux in the outer layer, where from equation (6.2) $q \sim \phi$ to leading order, with an eddy conductivity formula such as the second of equations (6.37), then ϵ_H would have to be negative for small η and also quadratic in η. Formulae of this nature were not considered to be physically appealing, and although several were tried, it was not possible to find one which gave a satisfactory representation for H. For this reason the alternative given in equation (6.39) was considered. In fact there are two processes associated with dissipation of energy in the turbulent boundary layer, and these are associated with viscous dissipation and the production of turbulent kinetic energy, and in the outer layer it is the latter which dominates. Thus there is reason to believe that Reynolds stress

related work should be involved in the turbulence modeling as indicated in equation (6.37). Here ϕ is written in terms of an eddy conductivity plus an additional term representing turbulent dissipation, the form of which is suggested to some extent by equation (6.2). Here P is a constant whose value will be subsequently be defined. The form of the coefficient of the second term in equation (6.37) has been selected so that $\phi \to 0$ as $\eta \to 0$, as subsequently shown. It may be noted that the second term in equation (6.37) vanishes as $M_e \to 0$ and $I_r \to 1$. It is possible to model ϕ in other ways, but the relation (6.37) has proven to be effective in representing measured total temperature profiles for supersonic boundary layer layers with an adiabatic wall.

Consider first the formulation of eddy conductivity for small η. In terms of Howarth-Dorodnitsyn variable Y and then the scaled outer variable η

$$\phi = \frac{\rho^2}{\rho_o \Delta_o} \epsilon_a \frac{\partial H}{\partial \eta} - \frac{\rho^2}{\rho_o \Delta_o} \epsilon \frac{2\mathrm{P} H_e (1 - I_r)}{U_e^2} u \frac{\partial u}{\partial \eta} . \tag{6.39}$$

In the outer layer, u and H are both in the form of defect law and, according to equations (6.16) and (6.29), the defect functions are logarithmic for small η; also note from equation (5.111) that Reynolds stress $\sigma \sim \rho_o u_{\tau o}^2$ for small η. It follows that to leading order

$$\phi \sim \frac{\rho^2 \epsilon_a u_{\tau o} 2(H - H_r)}{\rho_o \Delta_o U_e \kappa \eta} - \frac{2\mathrm{P} H_e (1 - I_r)}{U_e} \rho_o u_{\tau o}^2 , \quad \text{as} \quad \eta \to 0 . \tag{6.40}$$

But from equations (6.5) and (6.14) it can be seen that the turbulence term $\phi \to 0$ as $Y^+ \to \infty$. It then follows that to provide a smooth transition between the inner

and outer layer, the eddy conductivity function must have the following form for small η

$$\epsilon_a \sim \frac{\rho_o^2}{\rho^2} u_{\tau o} \Delta_o(\mathrm{P}\kappa)\, \eta \ , \quad \text{as} \quad \eta \to 0 \ . \tag{6.41}$$

For large values of η, the form of eddy conductivity is taken to be same as ϵ_H, the eddy conductivity function used in §5, according to

$$\epsilon_a = \frac{\rho_o \rho_e}{\rho^2} \mathrm{K}_h U_e \delta^* \ . \tag{6.42}$$

It is worthwhile to note that in expression (5.14) for ϵ_H, the constant $\mathrm{K}_h = 0.0245$. This value of K_h was originally obtained from an extensive set of comparisons and synthesis of experimental data for static temperature in subsonic turbulent boundary layers (Weigand, 1978); it was utilized in the eddy-conductivity model for heat transfer problem in §5 and provided good agreement with supersonic data.

In the present case, the wall is adiabatic and some modification of the eddy-conductivity near the inner edge of the outer layer is necessary. However, the data base for supersonic boundary layers with adiabatic walls is not large, and in any case data near the wall is relatively scarce. Thus it is not possible to develop a model based purely on empiricism, and in order to make progress, it is necessary to postulate a functional form and investigate its performance. A convenient choice is to take

$$\epsilon_a(\eta) = \mathrm{P}\ \epsilon(\eta) \ , \tag{6.43}$$

where $\epsilon(\eta)$ is the eddy-viscosity function given by equation (5.26) and the constant P is now selected according to

$$\mathrm{P} = \mathrm{K}_h/\mathrm{K} = 1.4583 \; . \tag{6.44}$$

This choice is so that the eddy conductivity model has an outer form identical to the previous model for heat transfer, equation (5.27), in the outer portion of the boundary layer. Another motivation for selecting this model is that it proves possible to obtain exact analytical solutions for Θ_2 in the case of self-similar profiles which are described in the next section.

6.5 Self-Similar Profiles

In this subsection, a self-similar total-enthalpy profile is developed for adiabatic flows. This solution will subsequently used in the direct comparison with experimental data to validate the turbulence model adopted, as well as the general approach. Most of the measured total enthalpy data for adiabatic walls in supersonic boundary layer layers has been taken under constant pressure conditions, and here a solution of outer-region total enthalpy equation constant M_e is sought. The governing momentum equation for a constant Mach number is the same as that in §5.3, which is rewritten here, together with the energy equation (6.18)

$$\frac{\partial}{\partial \eta}\left\{\hat{\epsilon}\frac{\partial^2 F_1}{\partial \eta^2}\right\} + \mathrm{a}(s)\eta\,\frac{\partial^2 F_1}{\partial \eta^2} = \mathrm{c}(s)\,\frac{\partial^2 F_1}{\partial s \partial \eta}\;, \tag{6.45}$$

$$\frac{\partial}{\partial\eta}\left\{\mathrm{P}\hat{\epsilon}\frac{\partial\Theta_2}{\partial\eta}\right\}+\mathrm{a}(s)\eta\frac{\partial\Theta_2}{\partial\eta}=\mathrm{c}(s)\frac{\partial\Theta_2}{\partial s}+\frac{\partial}{\partial\eta}\left\{\hat{\epsilon}\frac{\partial^2 F_1}{\partial\eta^2}\right\}, \tag{6.46}$$

where the coefficients in these equations are given by equations (5.xx), (6.37), and (6.43), and the eddy-viscosity function for the modified Cebeci-Smith model is rewritten from §5 with

$$\hat{\epsilon}=\begin{cases}\mathrm{K}, & \eta>\eta_m\ ,\\ \kappa\eta/\eta_1, & \eta\le\eta_m\ ,\end{cases} \tag{6.47}$$

where

$$\eta_1(s)=\frac{\rho_e U_e\delta^*}{\rho_o\Delta_o u_{\tau o}}\ ,\qquad \eta_m=\frac{\mathrm{K}}{\kappa}\,\eta_1\ ,\qquad \mathrm{K}=0.0168\ . \tag{6.48}$$

Here η_m denotes the patch point between the two portions of the ramp function, The boundary conditions associated with these equations are

$$\frac{\partial F_1}{\partial\eta}\sim\tfrac{1}{\kappa}\log\eta+C_o\ \text{ as }\ \eta\to 0,\quad \Theta_2\sim\tfrac{1}{\kappa}\log\eta+B_o\ \text{ as }\ \eta\to 0 \tag{6.49}$$

and

$$\frac{\partial F_1}{\partial\eta}\ ,\quad \Theta_2\to 0\ ,\quad \text{as }\eta\to\infty\ . \tag{6.50}$$

For the self-similar solutions, a convenient choice for the outer length scale is the same as discussed in §5 and

$$\Delta_o=\frac{\rho_e U_e\delta^*}{\rho_o u_{\tau o}}\ , \tag{6.51}$$

where δ^* is the dimensionless "kinetic" displacement thickness defined by equation (5.8). This choice leads to a particularly simple formulation since $\hat{\epsilon}$ is then a function of η alone. Equations (6.45) and (6.46) reduce to

$$\frac{d}{d\eta}\left\{\hat{\epsilon}\frac{d^2F_1}{d\eta^2}\right\} + \mathrm{a}\,\eta\,\frac{d^2F_1}{d\eta^2} = 0\ , \tag{6.52}$$

$$\frac{d}{d\eta}\left\{\mathrm{P}\hat{\epsilon}\frac{d\Theta_2}{d\eta}\right\} + \mathrm{a}\,\eta\frac{d\Theta_2}{d\eta} = \frac{d}{d\eta}\left\{\hat{\epsilon}\frac{d^2F_1}{d\eta^2}\right\}\ , \tag{6.53}$$

respectively for the defect profile functions F_1 and Θ_2. Here a is the similarity constant and a method for determining a has previously been described in §5.5. Note that the difference between equations (6.53) and (5.43) is the non-zero right side in equation (6.53) which may be interpreted as the leading order contribution arising from turbulent dissipation. Integration of equation (6.53) across the boundary layer results in

$$\int_o^\infty \Theta_2(\eta)\ d\eta = 0\ , \tag{6.54}$$

from which it follows that Θ_2 must change sign in the outer region. The physical meaning of this result is evident. Since the flow is adiabatic, the total thermal energy in the boundary layer must remain constant. Thus, if one region of the flow has $H < H_e$, some other region must have $H > H_e$ and an overshoot must occur in total enthalpy.

The exact solution of equation (6.52) was given in §5.5. An exact solution of

the energy equation (6.53) may also be obtained. In the outer tier,

$$\Theta_2 = \frac{1}{(P-1)}\sqrt{\frac{\pi}{2aK}}\left\{\sqrt{P}\ e^{-aK/2\kappa^2 P}\ \mathrm{erfc}\left(\sqrt{\frac{a}{2KP}}\,\eta\right)\right.$$

$$\left. - P\ e^{-Ka/2\kappa^2}\mathrm{erfc}\left(\sqrt{\frac{a}{2K}}\,\eta\right)\right\}, \quad \eta > \eta_m \tag{6.55}$$

and in the inner tier

$$\Theta_2 = -\frac{1}{\kappa(P-1)}\left\{P\ E_1\left(\frac{a\eta}{\kappa}\right) - E_1\left(\frac{a\eta}{\kappa P}\right)\right\}$$

$$+ B_o - \frac{1}{\kappa}\left\{\gamma_o - \log\left(\frac{\kappa}{a}\right) + \frac{1}{P-1}\log P\right\}, \quad \eta \le \eta_m\,. \tag{6.56}$$

The outer-log-law constant for total enthalpy is given by

$$B_o = \frac{1}{\kappa}\left\{\gamma_o - \log\left(\frac{\kappa}{a}\right)\right\} + \frac{1}{\kappa(P-1)}\left\{P\ E_1\left(\frac{aK}{\kappa^2}\right) - E_1\left(\frac{aK}{\kappa^2 P}\right)\right.$$

$$\left. + \log P\right\} + \frac{1}{P-1}\sqrt{\frac{\pi}{2aK}}\left\{\sqrt{P}\ e^{-aK/2\kappa^2 P}\ \mathrm{erfc}\sqrt{\frac{aK}{2\kappa^2 P}}\right.$$

$$\left. - P e^{-aK/2\kappa^2}\ \mathrm{erfc}\sqrt{\frac{aK}{2\kappa^2}}\right\}. \tag{6.57}$$

In the above equations erfc and E_1 denote the complementary error function and exponential integral, respectively and $\gamma_o = 0.577215...$ is Euler's constant. The exact solutions (6.55) and (6.56) provide a convenient representation of the defect profiles for the simple eddy-conductivity function in equation (6.43). Together with the leading order defect-velocity profile (5.44), a complete set of outer-region solutions

has therefore been obtained. For the wall layer, an expansion for total enthalpy was given in equation (6.6), but the function θ_2^+ is unknown at this time except for conditions (6.11) and (6.15). A representative solution of θ_2^+ could be obtained in principle through unsteady wall-layer analysis as described in §4; however, the wall layer problem for θ_2^+ is significantly more difficult, and to leading order θ_2^+ is not needed. It may be noted from equation (6.6) that the second terms associated with θ_2^+ is small for $Y^+ = \mathrm{O}(1)$.

6.6 Comparison with Total Temperature Data

The solution described in (6.55) and (6.56) depends on the similarity constant a which must satisfy the condition (5.54). Assume that at a given streamwise location along an adiabatic surface, the following data are known for a specified gas: (a) the mainstream velocity U_e^*, temperature T_e^* and density ρ_e^*, and (b) the dimensional kinetic displacement thickness δ^{**}. The mainstream Mach number may now be determined by the relation

$$M_e^* = \frac{U_e^*}{\sqrt{\gamma R T_e^*}}\ , \tag{6.58}$$

and the wall temperature is then determined since $T_w^* = T_r^*$, where

$$T_r^* = T_e^* \left(1 + \mathrm{r}\,\frac{\gamma - 1}{2}\, M_e^{*2}\right). \tag{6.59}$$

The same iterative procedure as that in §5.5 may now be followed to determine a so that equation (6.54) is satisfied. The final solutions are then used to make direct

comparison with experimental profile data.

Comparisons for total enthalpy were carried out for several cases, and the results of six typical comparisons are shown in Figures 6.3 and 6.4 for the cases listed in Table 6.1. The majority of the data is taken from the compilation of data by Fernholz and Finley (1977) and again the same identification scheme is used; the exception is the recent data from Carvin (1988), f-1048. In many of the data sets compiled in Fernholz and Finley, the total temperature was often estimated by using some version of the Crocco integral from direct measurements of the velocity. However, there are some data sets in which the total temperature was actually measured, and only these were considered here. Unfortunately, this means that there is a relatively small data base suitable for direct comparisons.

Case No.	M_e	T_w/T_r	Re_{δ^*}	u_*	q_*
58030101	1.720	1.006	31521	0.0362	0.00
58030201	3.560	1.031	29121	0.0403	0.00
58030301	4.670	1.045	13621	0.0465	0.00
f-1048	2.160	1.012	6450.5	0.0439	0.00
73021203	2.80	1.00	66393	0.0360	0.00
73010501	4.742	1.0212	12352	0.0473	0.00

Table 6.1. Parameters associated with experimental data for an adiabatic wall and computed dimensionless friction velocity and heat flux.

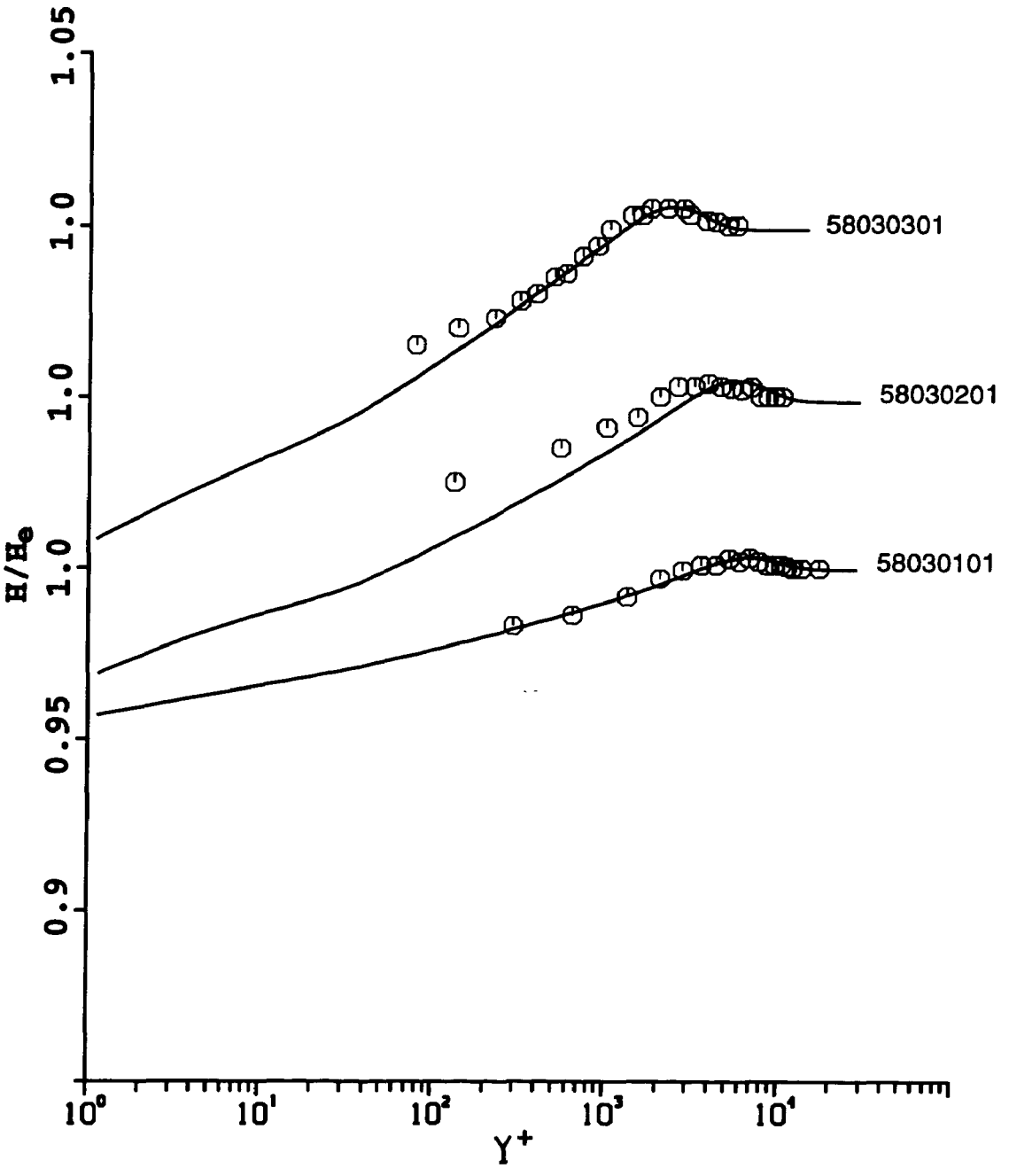

Figure 6.3. Comparison of total enthalpy data with the theoretical profile. Data from Fernholz and Finley, 1977 (5803-Kistler)

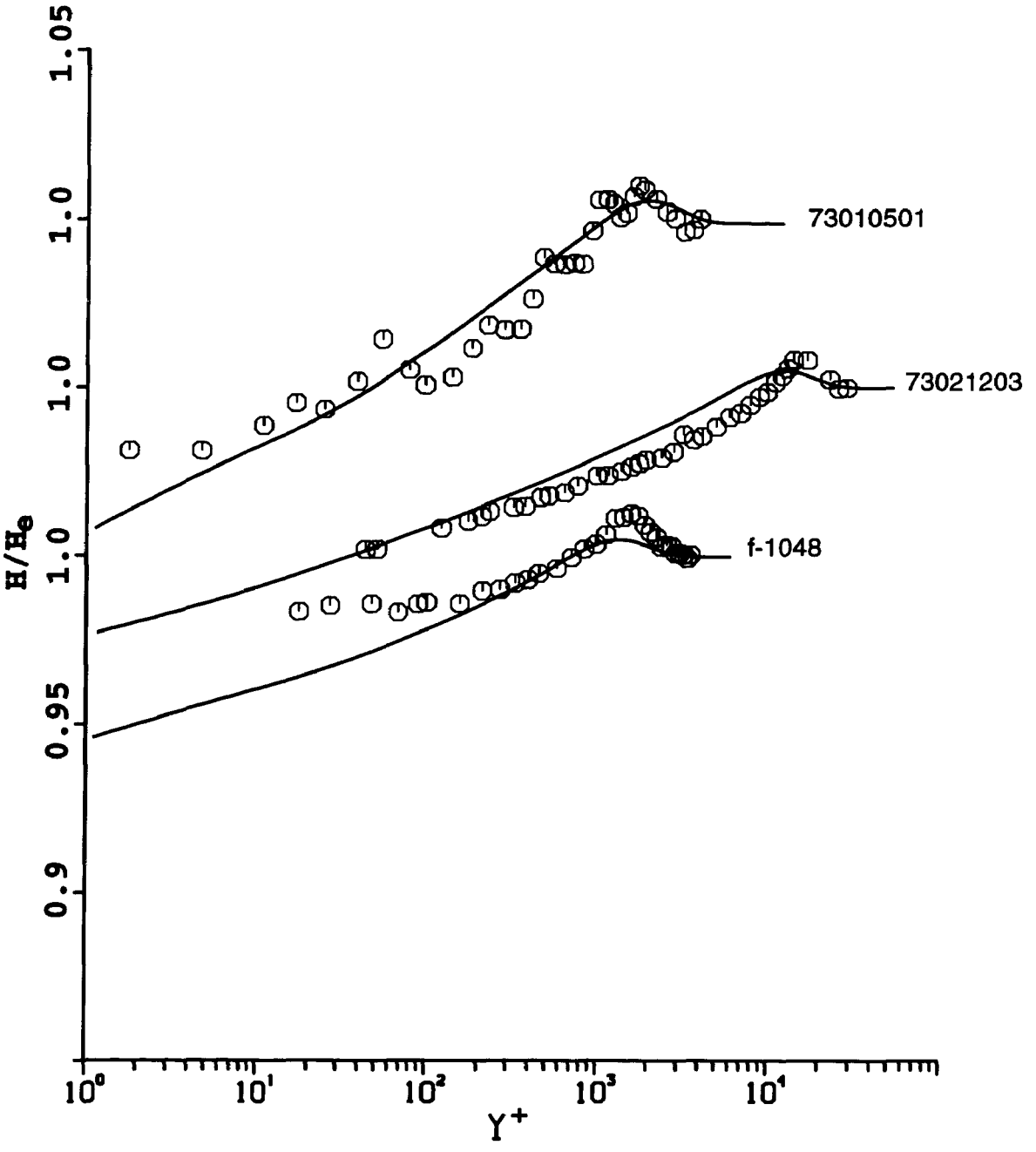

Figure 6.4. Comparison of total enthalpy data with the theoretical profile. Data from Fernholz and Finley, 1977 (7301-Gates; 7302-Winter and Gaudel), and Carvin, 1988.

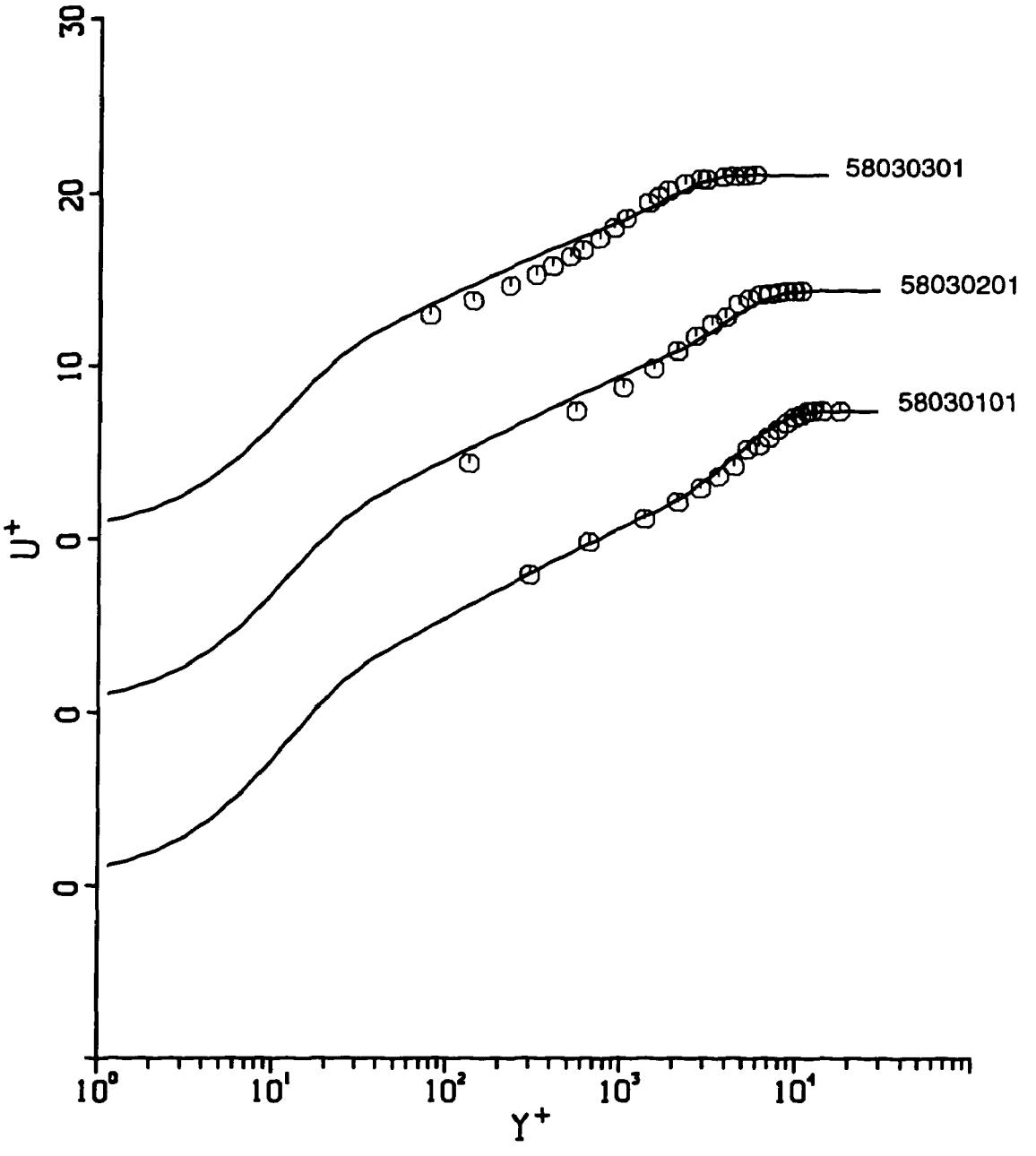

Figure 6.5. Comparison of velocity data with the theoretical profile. Data from Fernholz and Finley, 1977 (5803-Kistler).

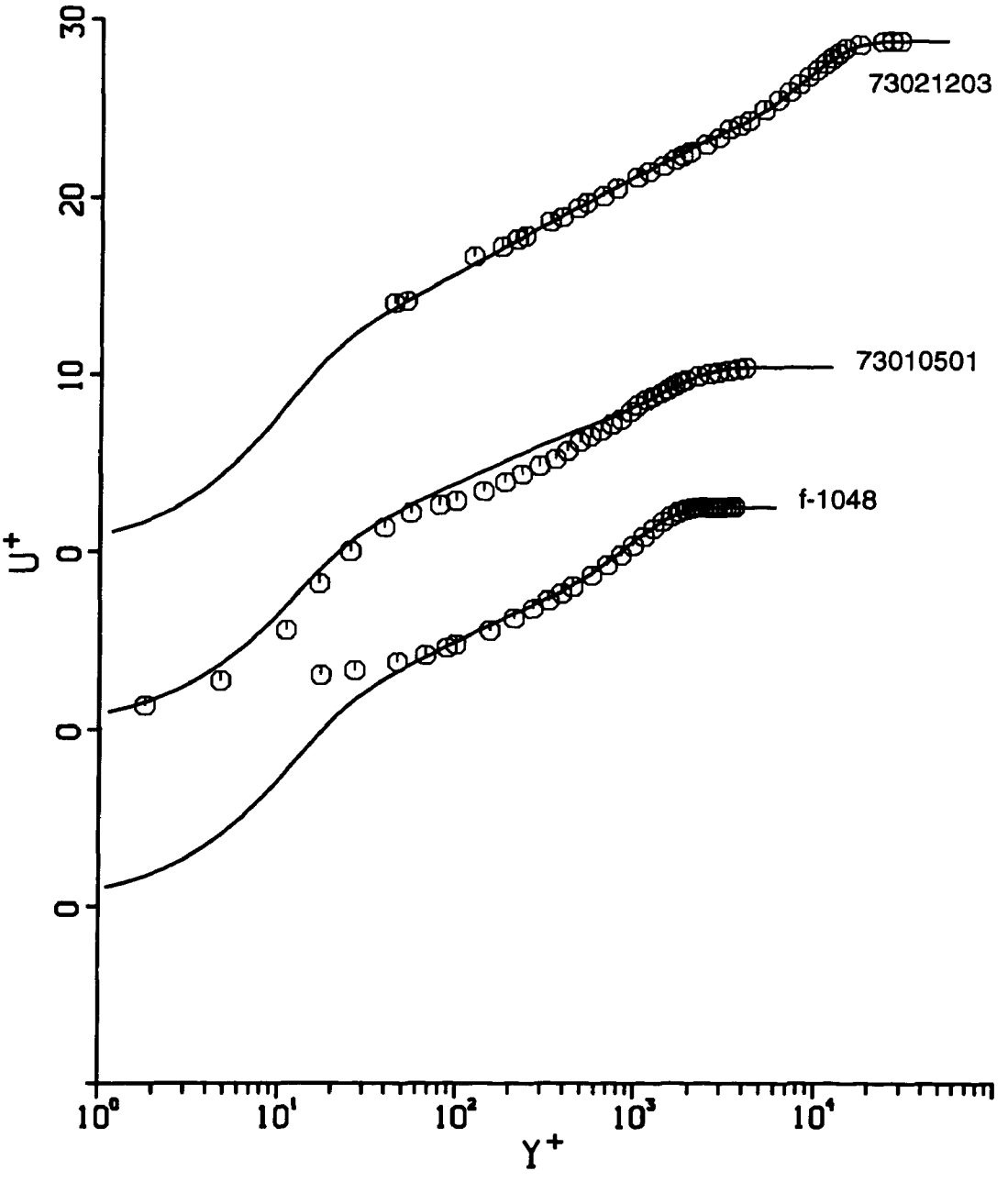

Figure 6.6. Comparison of velocity data with the theoretical profile. Data from Fernholz and Finley, 1977 (7301-Gates; 7302-Winter and Gaudel), and Carvin, 1988.

Again, profile distributions in a given experiment were selected closest to the end of the test section, since such profiles are expected to be closest to exhibiting self-similar behavior. Unfortunately, it is not possible to assess how close each situation is to equilibrium; in addition, it is also difficult to ascertain whether the wall is truly adiabatic in some of the experiments. Nevertheless, the results of the direct comparisons for total enthalpy are shown in Figures 6.3 and 6.4, the corresponding velocity results are in Figure 6.5 and 6.6; each data set is identified as listed in Table 6.1. It may be seen that the representation of the total enthalpy profiles are quite good over the entire range of Mach numbers listed in Table 6.1. The results for skin friction should be compared with those obtained using the theory in §5 and listed in Tables 5.8 and 5.11; note that the predicted values for u_* are very close. In addition the velocity profiles obtained using the present adiabatic wall theory are essentially identical to those shown in Figures 5.11 to 5.14. It is may be noted that the deviations of H from the mainstream value of H_e are not large and some scatter is evident in the data. Nevertheless, the present profiles correctly predict the shape of the distribution as well as the slope of the profile in the overlap zone. Note that the total enthalpy distribution reaches a maximum (above the mainstream value) within the boundary layer. For $Pr < 1$, $H_r < H_e$ and Θ_2 must be negative near the wall. In view of equation (6.54), Θ_2 must be positive further away from the surface and this behavior is reflected for all cases. Lastly, it should be emphasized that the theoretical profiles shown in Figures 6.3 and 6.4 are predicted results and that the comparisons have not been enhanced through adjustment of any model parameters. It should be noted that the total enthalpy overshoot from the value of H_e is relative small, therefore its influence on velocity profiles (Figures 5.5 and 5.6) is not noticeable comparing with the results obtained

in §5.

6.7 Summary

In this section, an algebraic turbulence model has been developed to represent the influence of viscous dissipation in supersonic turbulent boundary layers. The theory developed here is valid in the parameter range $(\gamma-1)M_e^2u_*^2 \leq O(1)$ but $(\gamma-1)M_e^2u_*^2 = o(1)$ in the limit $Re\rightarrow\infty$. The calculated total enthalpy profiles have been shown to agree well with measured experimental data. The variation of the self-similar profiles with Mach number is shown in Figures 6.7 and 6.8 for a fixed value of Re_{δ^*}; the trends shown here are similar for other values of Re_{δ^*}. Note overshoot that occurs in the total enthalpy profiles in the outer portion of the boundary layers; this overshoot appears to diminish at $M_e = 8$ but it should be noted that this hypersonic case is probably outside the range of validity of the present theory. It should be noted that the analysis described in this chapter is a limiting situation in supersonic boundary-layer flows, where the heat flux $q_w\rightarrow 0$. Another limiting case of $q_* = O(u_*)$ in which significant heat transfer occurs at the surface was discussed in §5. It may be noted that the results for velocity and static temperature obtained when the theory of chapter 5 is applied to nearly adiabatic wall cases are essentially the same as those obtained in the present chapter. The main difference is that the present theory is bale to capture the overshoot in total enthalpy for adiabatic walls whereas the theory in chapter 5 cannot.

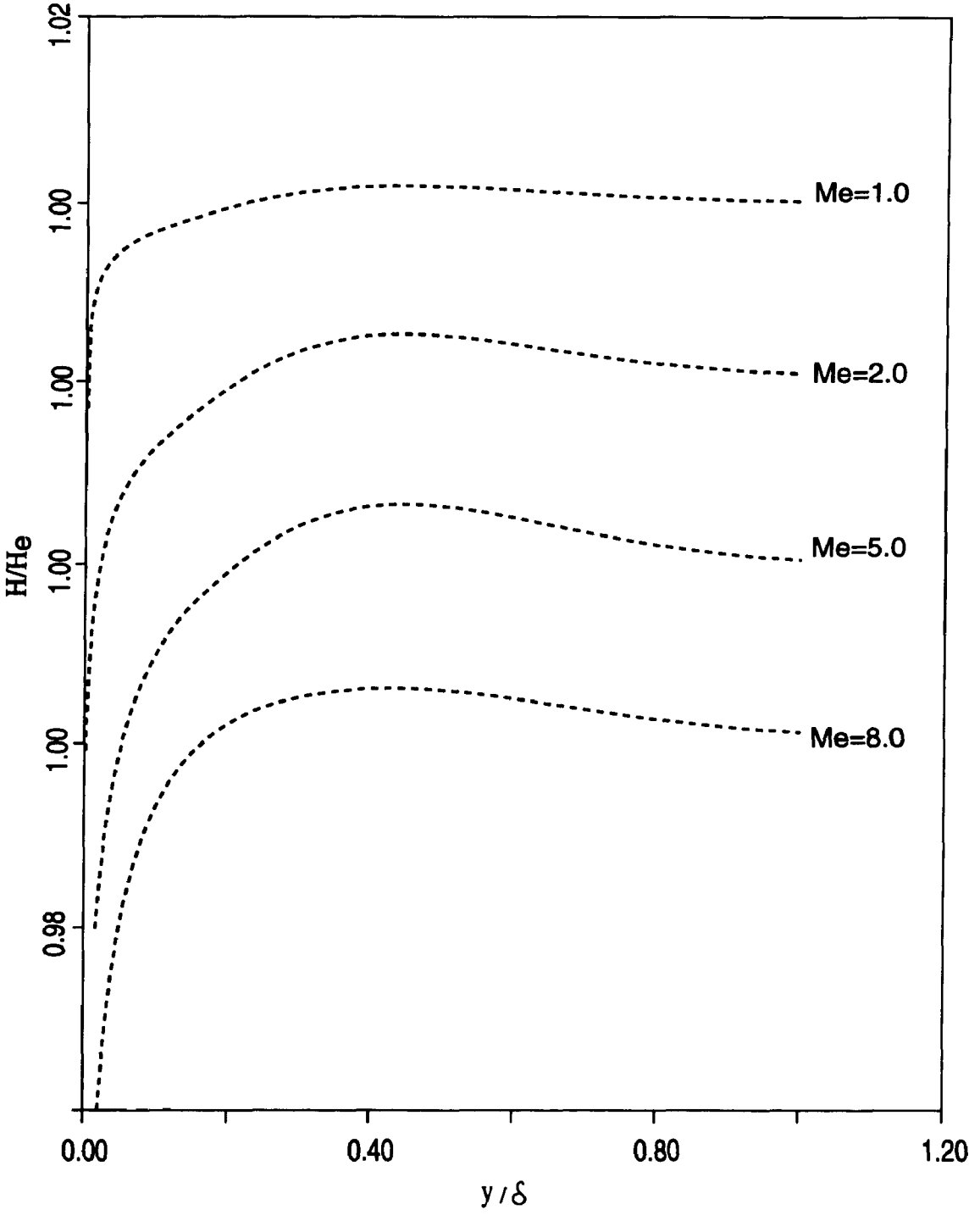

Figure 6.7. Variation of the total enthalpy profile with Me for Re_{δ^*}=10,000.

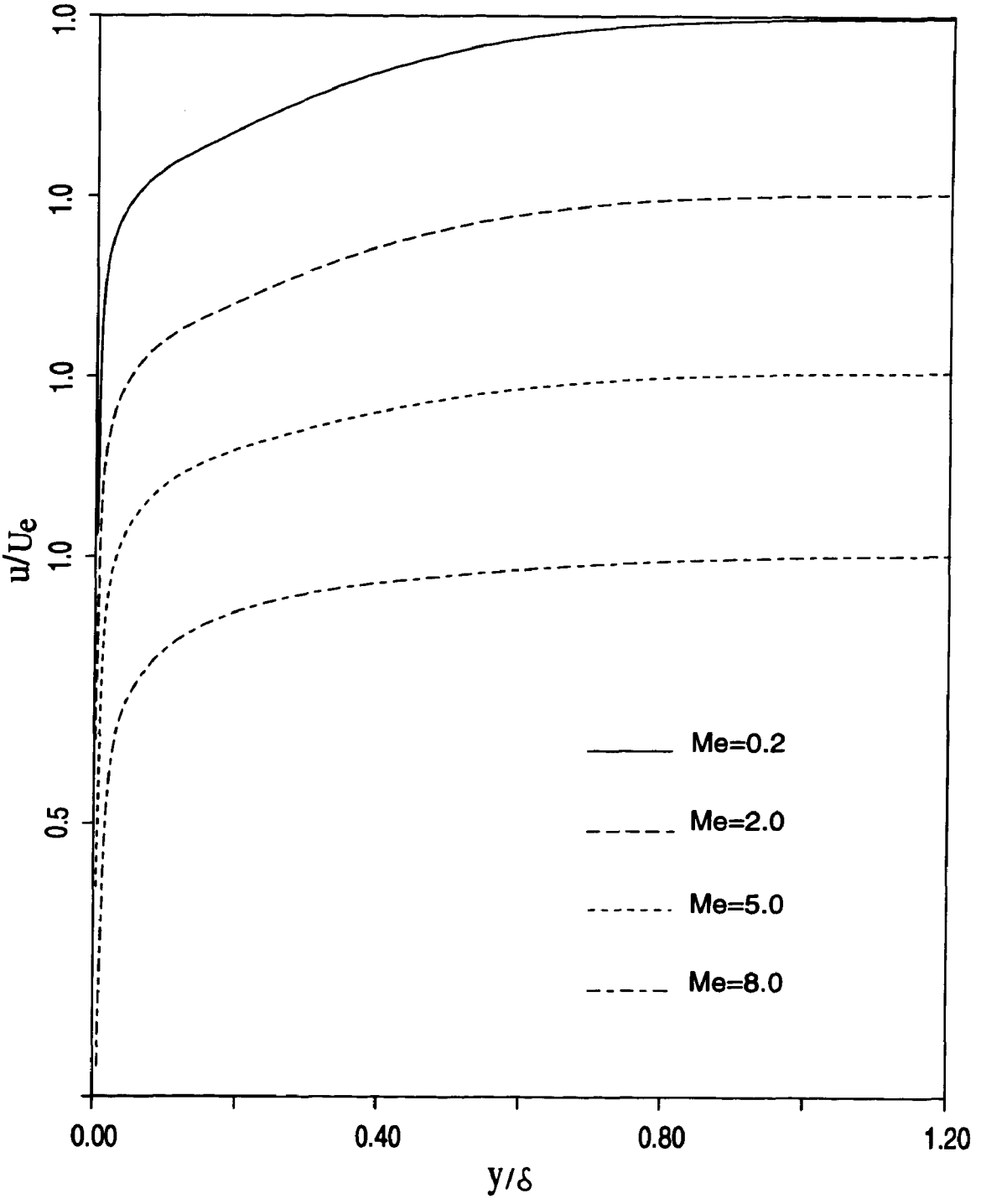

Figure 6.8. Variation of the velocity profile with Me for Re_{δ^*}=10,000.

7. Summary and Conclusions

The objectives of this study as outlined in §1.5 have been successfully met . The first objective was to determine the asymptotic time-mean structure of the compressible turbulent boundary layers for large Reynolds number and Mach number O(1). This was carried out in §3, with a detailed summary of the theoretical results given in §3.7. In summary the high-speed compressible boundary layer was to possess a self-consistent two layer structure. The important scaling parameter in the velocity problem was found to be $u_{\tau o} = \sqrt{\tau_w/\rho_o}$, where ρ_o denotes a reference density characteristic of the wall layer as a whole; in terms of the conventional friction velocity $u_{\tau o} = \sqrt{\rho_w/\rho_o} u_\tau$. For total enthalpy and important scaling parameter was determined to be $q_{\tau o} = q_w/\rho_o u_{\tau o}$ for flows with heat transfer; here q_w denotes a dimensionless heat flux at the wall. The case of the adiabatic wall was analyzed separately in chapter 6. The asymptotic analysis was carried out without recourse to a specific closure model, with a minimum of appeal to experiment. A major promise of this study is that the velocity and total enthalpy profiles are logarithmic in the Howarth-Dorodnitsyn variable within the overlap zone between the two regions of the boundary layer. Thus a new compressible law of the wall has been developed and confirmed through direct comparisons with data in §5.

In §4 a theory was presented for the mean flow in the wall layer which is based on the coherent structure of the near-wall turbulent flow. Through consideration of representative motions during a typical cycle in the wall layer, expressions for the mean profiles were produced via a time averaging over a cycle

and this process results analytic functions for velocity $U^+(Y^+)$, and total enthalpy function θ^+ across the entire wall layer.

In §5 self-similar profiles, which are uniformly valid across the outer layer, were developed by using simple eddy-viscosity and eddy-conductivity models for closure in the outer layer. The asymptotic results revealed a deficiency in the conventional form of outer-region algebraic models and a modification to account for density variations was proposed. In order to test the results of the asymptotic theory, as well as the new turbulence models, a limiting case was considered corresponding to constant pressure flows with heat transfer; in this situation, the governing equations in the outer region of the boundary layer reduce to ordinary differential equations, for which exact analytical solutions are found. Definitions of a reference density were proposed in §5 as either an average or a mean density for the inner layer. Data comparisons were carried out using the self-similar solutions to verify the selection of reference density ρ_o; it was found that the ρ_o evaluated as a mean average between $Y^+ = 0$ and $Y^+ = 60$ or a men value evaluated at $Y^+ = 23$ provided uniformly good results over the following range of Mach numbers and surface temperature: $M_e < 7$ and $0.3 \leq T_w/T_r \leq 1$ where T_w and T_r are the wall and recovery temperatures respectively. Direct comparisons with data show that the profiles give a good representation of measured mean velocity and temperature. It is worthwhile to note that closer correspondence with the data for a given profile can be achieved by adjusting the parameters in the turbulence models. However, the objective was to demonstrate that there is a degree of university over a range of Mach numbers using the present models, and so no attempt to "fit" the data was made; the profiles were produced solely from the known physical quantities at each

data station, and no adjustable parameters were used.

The limiting case of adiabatic flows in supersonic range with mainstream Mach number O(1) was discussed in §6. An algebraic model was developed to represent the influence of viscous dissipation in supersonic turbulent boundary layers. The theory developed here is valid in the parameter range $(\gamma-1)M_e^2 u_{\tau_o} = \mathrm{O}(1)$. The calculated profiles have been shown to agree well with measured experimental data for velocity and total enthalpy.

The work described in this thesis represents a first step toward extending the embedded-function methodology to the computation of turbulent supersonic flows. In addition, a set of models for boundary layers in a high-speed compressible flow has been developed. A further byproduct of the present study is a set of composite velocity and total enthalpy profiles which gives a good representation across the entire boundary layer. These profiles could be used to define an initial distribution of the flow quantities to initiate a Navier-Stokes solution in a more general flow environment, simply by estimating displacement thickness distributions along all walls.

The high speed compressible boundary-layer models developed in this study have been confirmed for zero pressure gradient flows. At present, it is not clear whether a self-similar structure can exist for flows with significant pressure gradients. The discussion of the conditions for self-similar in §5 concluded that the present theory does not describe self-similarity for flows with significant pressure gradient. However, a similarity profile may be possible with using alternate scalings. For this reason that future research might consider this situation.

The models in §5 and §6 covered the limiting cases of flow with significant

heat transfer and flow with an adiabatic wall respectively. Further study is needed to bridge the gap between these limiting situations for cases where both heat transfer transfer and the influence of viscous dissipation need to be considered simultaneously. Lastly the present theory become invalid for very high Mach numbers and it is of interest to develop the extension of the present theory to the hypersonic case.

REFERENCES

Baldwin, B. S. and Lomax, H. (1978), "Thin-layer approximation and algebraic model for turbulent separated flows", AIAA paper 78-257, January 1978.

Barwell, R. W. and Wahls, R. A. (1989), "A Skin Friction Law for Compressible Turbulent Boundary Layers", AIAA Paper 89-1864.

Boussinesq, J. (1877), "Theorie de l'écoulement tourbillant", Mem. Prés. Acad. Sci. XXIII, 46, Paris.

Bradshaw, P. (1977), "Compressible Turbulent Shear Layers", Annual Review of Fluid Mechaincs, Vol. 9, 1977, pp. 33-54.

Bushnell, D. M. and Morris, D. J. (1971), "Eddy Viscosity Distributions in a Mach 20 Turbulent Boundary Layer", AIAA Journal, Vol. 9, pp.764-766.

Carvin, C. (1988), "Etude Experimentale D'Une Couche Limite Turbulente Supersonique Fortement Chauffee", Ph.D. thesis, Universite' d'Aix Marseille.

Cebeci, T. and Smith, A. M. O. (1974), Analysis of Turbulent Boundary Layers, Academic Press, New York, 1974.

Clauser, F. H. (1954), "Turbulent boundary layers in adverse pressure gradients", Journal of Aeronautical Science, Vol. 21, pp. 91-108.

Clauser, F. H. (1956), "The Turbulent Boundary Layer", Adv. Appl. Mech. Vol. 1, pp. 1-51.

Coles, D. (1964), "The Turbulent Boundary Layer in a Compressible Fluid", The Physics of Fluids, Vol. 7, pp. 1403-1421.

Crawford, M. E. and Kays, W. M. (1980), Convective Heat and Mass Transfer, McGraw-Hill, New York.

Crocco, L. (1963), "Transformations of the Compressible Turbulent Boundary Layer with Heat Exchange", AIAA J. Vol. 1, pp. 2723-2731.

Degani, A. T., Walker, J. D. A., Ersoy, S. and Power, G. (1989), "On the Application of Algebraic Turbulence Models to High Mach Number Flows", AIAA Paper 89-1863.

van Driest, E. R. (1951), "Turbulent Boundary Layer in Compressible Fluids", J. Aero. Sci., Vol. 18, pp. 145-161.

van Driest, E. R. (1954), "The Laminar Boundary Layer with Variable Fluid Properties", Presented at the 1954 Meeting of the Heat Transfer and Fluid Mechanics Institute, Berkeley.

van Driest, E. R. (1956), "The Problem of Aerodynamic Heating", Aeronaut. Eng. Review, Vol. 15, pp. 26-41.

Economs, C. (1970), "A Transformation Theory for the Compressible Turbulent Boundary Layer with Mass Transfer", AIAA J., Vol. 8, pp. 758-764.

Fendell, F. E. (1972), "Singular Perturbation and Turbulent Shear Flow Near Walls", J. Astro. Sciences, Vol. 20, pp.129-165.

Fernholz, H. H. and Finley, P. J. (1977), "A Critical Compilation of Compressible Turbulent Boundary Layer Data", AGARD-AG-223.

Fernholz, H. H. and Finley, P. J. (1980), "A Critical Commentary on mean Flow Data for Two-dimensional Compressible Turbulent Boundary Layers", AGARD-AG-253.

Fernholz, H. H. and Finley, P. J. (1981), "A Further Compilation of Compressible Boundary Layer Data with a Survey of Turbulence Data", AGARD-AG-263.

He, J, Kazakia, J. Y. and Walker, J. D. A. (1990), "Embedded Function Methods for Supersonic Turbulent Boundary Layers", AIAA paper 90-0306.

Head, M. R. and Bandyopadhyay, P. (1981), "New Aspects of Turbulent Boundary-Layer Structure", Journal of Fluid Mechanics, Vol. 107, pp. 297-338.

Hopkins, E. J. and Inouye, M. (1971), "An Evaluation of Theories for Predicting Turbulent Skin Friction and Heat Transfer on Flat Plates at Supersonic and Hypersonic Mach Numbers", AIAA Journal, Vol.9, No. 6, pp. 993-1003

Howarth, L., "Concerning the Effect of Compressibility on Laminar Boundary Layers and Their Separation", Proceedings of the Royal Society of London, Ser. A, Vol. 194, 1948, pp. 16-42

Illingworth, C. R., "Steady Flow in the Laminar Boundary Layer of a Gas",Proceedings of the Royal Society of London, Ser. A, Vol. 199, 1949.

Johnson, J. A. and King, L. S. (1985), "A mathematically simple turbulence closure model for attached and separated turbulent boundary layers", AIAA Journal, Vol. 23, pp. 1684-1692.

Kistler, A. L. (1959), "Fluctuation Measurements in a Supersonic Turbulent Boundary Layer", The Physics of Fluids, Vol. 2, pp. 290-297.

Klebanoff, P. S. (1955),"Characteristics of Turbulence in a Boundary Layer with Zero Pressure Gradient", NACA TR 1247.

Kline, S. J., Reynolds, W. C., Schraub, F. A. and Runstadler, P. W. (1967), "The structure of turbulent boundary layers", Journal of Fluid Mechanics, Vol. 30, pp.741.

Laderman, A. J. and Demetriades, A. (1974), "Mean and Fluctuating Flow Measurements in the Hypersonic Boundary Layer Layer over a Cooled Wall", J. Fluid Mech., Vol. 63, pp. 121-144.

Laderman, A. J. and Demetriades, A. (1979), "Turbulent Shear Stresses in Compressible Boundary Layers", AIAA J., Vol. 17, pp. 736-744.

Lewis, J. E., Kubota, T. and Webb. W. H. (1970), "Transformation Theory for the Adiabatic Compressible Turbulent Boundary Layer with Pressure Gradient", AIAA J., Vol. 8, pp. 1644-1651.

Maise, G. and McDonald, H. (1968), "Mixing length and kinematic eddy viscosity in a compressible boundary layer", AIAA Journal, Vol. 6, pp. 73-80.

Mellor, G. L. (1972), "The Large Reynolds Number, Asymptotic Theory of Turbulent Boundary Layers", Int. J. Engrg. Sci. Vol. 10, pp. 851-873.

Morkovin, M. V. (1960), "The Structure of Supersonic Turbulent Boundary Layers", AGARD Wind Tunnel and Model Testing Panel.

Offen, G. R. and Kline, S. J. (1974), "Combined dye streak and hydrogen bubble visual observations of a turbulent boundary layer", Journal of Fluid Mechanics, Vol.62, pp. 223.

Prandtl, L. (1925), "Über die ausgebildete Turbulenz", ZAMM, 5, pp. 136-139

Preston, J. H. (1954), "The determination of turbulent skin friction by means of pitot tubes", Jl. R. Aeronautical Science, Vol. 58, pp. 109-121.

Robinson, S. K. (1985), "Instantaneous velocity profile measurements in a turbulent boundary layer", Chemical Engineering Communication, Vol 43, pp. 347.

Robinson, S. K. (1986), "Space-time correlation measurements in a compressible turbulent boundary layer", AIAA paper 86-1130.

Rotta, J. C. (1960), "Turbulent Boundary Layers with Heat Transfer in Compressible Flow", AGARD Report 281.

Smith, C. R. (1991), "On the Dynamics of Near-Wall Turbulence", Phil. Trans. R. Soc. London, A 336, pp.131-175

Spina E. F. and Smits, A. J. (1987), "Organized structures in a compressible, turbulent boundary layer", Journal of Fluid Mechanics, Vol. 182, pp. 85-109

Squire, H. B. (1951), "The Friction Temperature: A Useful Parameter in Heat-transfer Analysis", Proc. General Discus. Heat Transfer, Inst. Mech. Engrg. and ASME, pp. 185-186.

Stalmach, C. J. (1958), "Experimental investigation of the surface impact probe method of measuring local skin friction at supersonic speeds", CAT 5802.

Stewartson, K., "Correlated Incompressible and Compressible Boundary Layers", Proceedings of the Royal Society of London, Ser. 200, 1949, pp. 84-100.

Stewartson, K., The Theory of Laminar Boundary Layers in Compressible Fluids, Oxford University Press, 1964.

Talcott, N. A. and Kumar, A. (1985), "Two-Dimensional Viscous Simulation of Inlet/Diffuser Flows with Terminal Shocks", J. Propulsion, Vol. 1, pp. 103-108.

Townsend, A. A. (1956), The Structure of Turbulent Shear Flow, Cambridge University Press, Cambridge, Mass.

Townsend, A. A. (1960), "Equilibrium Layers and Wall Turbulence", J. Fluid Mech., Vol. 11, pp. 97-120.

Viegas, J. R., Rubesin, M. W. and Horstman, C. C. (1985), "On the Use of Wall Functions as Boundary Conditions for Two-Dimensional Separated Compressible Flows", AIAA Paper 85-0180.

Walker, J. D. A., Scharnhorst, R. K. and Weigand, G. G. (1986), "Wall layer models for the calculation of velocity and heat transfer in turbulent boundary layers", AIAA Paper 86-0213.

Walker, J. D. A., Werle, M. J. and Ece, M. C. (1987), "An embedded function approach for the calculation of turbulent flows near walls", UTRC 86-78, United

Technologies Research Center.
Walker, J. D. A., Abbott, D. E., Scharnhorst, R. K. (1989), "Wall Layer Model for the Velocity Profile in Turbulent Flows", AIAA Journal, Vol. 27, pp. 140-149.

Walker, J. D. A. 1990a "Wall Layer Eruptions in Turbulent Flows", Structure of Turbulence and Drag Reduction (A. Gyr, ed.), pp. 109-118.

Walker, J. D. A. 1990b "Models Based on Dynamical Features of the Wall Layer", Appl. Mech. Rev. 43, s232-s239.

Walz, A. (1959), "Compressible Turbulent Boundary Layers with Heat Transfer and Pressure Gradient in Flow Direction", J. Research Nat. Bureau of Standards, Vol. 63B, pp. 53-70.

Weigand, G. G., "Forced convection in a two-dimensional nominally steady turbulent boundary layer", Ph.D. thesis, Purdue University.

White, F. M. and Christoph, G. H. (1972), "Simple Theory for Two-Dimensional Compressible Turbulent Boundary layer", J. Basic Engrg. Vol. 94, pp. 636-642.

White, F. M. (1991), Viscous Fluid Flow, McGraw-Hill Book Company, New York.

Winter, K. G. (1977), "An Outline of the Techniques Available for the Measurement of Skin Friction in Turbulent Boundary Layers", Progr. Aerospace Sci., Vol. 18, pp. 1-57.

Yajnik, K. S. (1970), "Asymptotic Theory of Turbulent Shear Flows", J. Fluid Mech., Vol. 42, pp. 411-427.

Yuhas, L. J. and Walker, J. D. A. , "An optimization technique for the development of two-dimensional steady turbulent boundary layer models", AFOSR-TR-0417.

Appendix A

The Unsteady Wall Layer Model

In this appendix, the analytical embedded functions for the wall-layer profiles of mean velocity and total enthalpy are summarized (Walker et al., 1986, 1989). These mean profile functions are valid for the case of flow with heat transfer and are obtained by computing a time-average of the instantaneous velocity and total enthalpy over a typical interval between bursts in the wall layer. Both wall-layer profile models are of the form

$$U^+, \theta^+ = \left(1 + \frac{t_o^+}{T_B^+}\right)\left\{R(T_B^+, t_o^+)\, Q(\tilde{Y}^+) + Z(\tilde{Y}^+)\right\}$$

$$- \frac{t_o^+}{T_B^+}\left\{R(0,\, t_o^+)\, Q(\tilde{Y}_o^+) + Z(\tilde{Y}_o^+)\right\}. \qquad \text{(A.1)}$$

Here t_o^+ is a parameter (to be determined) and T_B^+ is the mean period between bursts in the wall layer having a typical value of $T_B^+ = 110.2$ (Walker et al., 1989). The functions in equation (A.1) are given by:

$$R(t,\, t_o^+) = C_i - \frac{1}{\kappa}\left(\frac{\gamma_o}{2} - \log 2\right) + \frac{1}{2\kappa}\log\left(t + t_o^+\right), \qquad \text{(A.2)}$$

$$Q(y) = \left(2y^2 + 1\right)\mathrm{erf}(y) + \frac{2}{\sqrt{\pi}}\, y\, \mathrm{e}^{-y^2}, \qquad \text{(A.3)}$$

$$Z(y) = \frac{4}{\kappa\sqrt{\pi}}\left\{(2y^2 + 1)\,\Xi(y) + y\,\Xi'(y) - \frac{\sqrt{\pi}}{8}\,(6y^2 + 1)\,\mathrm{erf}(y) - \frac{3}{4}\, y\, \mathrm{e}^{-y^2}\right\}. \qquad \text{(A.4)}$$

For the velocity profile U^+, C_i is the inner region log-law constant, κ is the von Kármán constant and γ_o is Euler's constant. For the total enthalpy profile θ^+, replace κ with κ_θ and C_i with B_i in equation (A.2). For the velocity profile U^+, the normal variables appearing in equation (A.1) are

$$\tilde{Y}^+ = \frac{Y^+}{2\sqrt{T_B^+ + t_o^+}}, \qquad \tilde{Y}_o^+ = \frac{Y^+}{2\sqrt{t_o^+}} \tag{A.5}$$

while for the total enthalpy profile θ^+, Y^+ is replaced with Y_θ^+ in equation (A.5) where $Y_\theta^+ = \sqrt{Pr}\, Y^+$. Finally, the function Ξ is defined by

$$\Xi(y) = \int_o^y \mathrm{e}^{-z^2} \int_o^z \mathrm{e}^{\xi^2} \int_o^\xi \mathrm{e}^{-x^2}\, d\xi dx dz\,. \tag{A.6}$$

A list of the properties of this function is given by Scharnhorst and Walker (1986) and, in particular, it may be shown that

$$\Xi(y) = \frac{\sqrt{\pi}}{4}\left(\log(y) + \frac{\gamma_o}{2} - \frac{1}{4y^2} + \cdots\right\}, \quad \text{as} \quad y \to \infty\,. \tag{A.7}$$

At the wall, the profile U^+ and θ^+ satisfy

$$U^+ = 0, \qquad \frac{\partial U^+}{\partial Y^+} = 1, \qquad \text{at} \quad Y^+ = 0\,, \tag{A.8}$$

$$\theta^+ = 0, \qquad \frac{\partial \theta^+}{\partial Y_\theta^+} = \sqrt{Pr}\,, \quad \text{at} \quad Y^+ = 0\,. \tag{A.9}$$

In addition, both profiles must satisfy the wall compatibility conditions which are

that second and third profile derivatives must vanish at $Y^+ = 0$; for the velocity profile U^+, these conditions require that (Walker et al. 1989)

$$\sqrt{T_B^+ + t_o^+}\left\{R(T_B^+, t_o^+) - \frac{1}{\kappa}\right\} - \sqrt{t_o^+}\left\{R(0, t_o^+) - \frac{1}{\kappa}\right\} = \frac{\sqrt{\pi}}{2} T_B^+, \tag{A.10}$$

$$\sqrt{T_B^+ + t_o^+}\ R(T_B^+, t_o^+) - \sqrt{t_o^+}\ R(0, t_o^+) = 0\ . \tag{A.11}$$

For the total enthalpy profile, κ_θ replaces κ in equations (A.10) and (A.11) and B_i replaces C_i in equation (A.2); in addition, the right side of equation (A.10) is multiplied by $\sqrt{Pr}$.

For the velocity profile U^+, it may be readily inferred that equation (A.1) contains the following parameters: (a) the von Karman constant κ, (b) the inner "log-law" constant C_i, (c) the burst period T_B^+ and (d) t_o^+. These parameters are not independent since equations (A.10) and (A.11) provide two interconnecting relations. For example, for the commonly used values of $\kappa = 0.41$ and $C_i = 5.0$, the solution of equations (A.10) and (A.11) gives

$$T_B^+ = 110.2, \quad t_o^+ = 0.00801 \tag{A.12}$$

and this value of T_B^+ compares favorably with experimental measurements of the period between bursts in the wall layer (Walker et al., 1989). Other values of κ and/or T_B^+ may be used to produce other values of C_i; in general T_B^+ is large with respect to t_o^+, and thus an expansion of equations (A.10) and (A.11) for small (t_o^+ / T_B^+) yields

$$C_i = \frac{1}{2}\sqrt{\pi T_B^+} + \frac{1}{\kappa}\left\{1 + \frac{\gamma_o}{2} - \frac{1}{2}\log\left(4T_B^+\right)\right\} = + \cdots , \tag{A.13}$$

to leading order. This relation gives C_i as an explicit function of κ and T_B^+; the estimate of C_i may be refined by iteratively solving equations (A.10) and (A.11) for given values of κ and T_B^+. For total enthalpy, a corresponding estimate of B_i is obtained by replacing κ by κ_θ and replacing T_B^+ by $T_B^+ Pr$ in the term on the right side of equation (A.10).

Appendix B

The Baldwin-Lomax Model

The turbulence closure model proposed by Baldwin and Lomax (1978), was partially patterned after that of Cebeci and Smith (1974). It is a simple eddy viscosity model which does not use the boundary-layer displacement thickness; this is advantageous in some situations, such as internal flows or near a backward-facing step, where it is difficult to identify a displacement thickness. In addition, the model is defined in terms of the vorticity which is invariant under coordinate transformations, and therefore, in principle, the model may be applied to three-dimensional configurations. Due to these advantages and an ease of implementation, the Baldwin-Lomax model has become a popular algebraic eddy viscosity model in computational aerodynamics and, therefore, was used in the present study. In this Appendix, a value for the model constant C_p appearing in equation (5.xx) is developed. Originally C_p was determined through numerical calculations to be approximately 1.6, in order that the Baldwin-Lomax model produces similar results to the Cebeci-Smith model at low Mach numbers and in incompressible flows. Here an exact value for C_p will be obtained according to the foregoing criterion.

According to §5, eddy viscosity ϵ in both the modified Cebeci-Smith and Baldwin-Lomax models may be written in the form

$$\epsilon = \frac{\rho_o \rho_e}{\rho^2} U_e \delta^* \hat{\epsilon}(\eta) \tag{B.1}$$

where

$$\hat{\epsilon} = \begin{cases} \mathrm{K}_\epsilon , & \eta > \eta_m \\ \kappa\eta/\eta_1 , & \eta \le \eta_m \end{cases} \tag{B.2}$$

and η_m and η_1 were given in equation (5.xx) by

$$\eta_1 = \frac{\rho_e U_e \delta^*}{\rho_o \Delta_o u_{\tau o}} , \qquad \eta_m = \frac{\mathrm{K}_\epsilon}{\kappa} \eta_1 . \tag{B.3}$$

The values of the parameter K_ϵ are given by

$$\mathrm{K}_\epsilon = \mathrm{K} , \tag{B.4}$$

for the Cebeci-Smith model and

$$\mathrm{K}_\epsilon = \mathrm{K} \left(\frac{C_p n_{max} \tilde{\mathrm{F}}_{max}}{U_e \delta^*} \right) , \tag{B.5}$$

for the Baldwin-Lomax model. In these formulae, K is a constant which normally has the value K=0.0168. For the Baldwin-Lomax model, n_{max} is the physical location where the function $\tilde{\mathrm{F}} = n \, | \partial u / \partial n |$ achieves a maximum and $\tilde{\mathrm{F}}_{max}$ is the corresponding value of $\tilde{\mathrm{F}}$; C_p is a constant which is to be adjusted so that the model produces the same results as the Cebeci-Smith model at low Mach numbers. Note that as $M_e \to 0$, equation (A.1) reduces to the incompressible form of either the Cebeci-Smith (1974) or Baldwin-Lomax (1978) model.

The differential equation for the velocity defect function $\partial F_1 / \partial \eta$ in the

limiting case of self-similar flow was given in equation (5.yy); in this equation the parameter a is a constant such that $a \to 1$ as $M_e \to 0$, and for self-similarity, the $\eta_1 = 1$ in equation (B.3). The solution for the defect function was given in equations (5.xx) and (5.yy).

Using this solution, it is possible to determine the constant C_p in the Baldwin-Lomax model. In the limit of $M_e \to 0$

$$\tilde{F} = n \frac{du}{dn} = \eta \frac{du}{d\eta} = u_{\tau o} \eta \frac{d^2 F_1}{d\eta^2} . \tag{B.6}$$

Upon differentiating equation (5.xx) and noting that $a = 1$ as $M_e \to 0$, it is easily shown that

$$\frac{C_p n_{max} \tilde{F}_{max}}{U_e \delta^*} = 1 , \tag{B.7}$$

or

$$C_p = \exp \left\{ \frac{1}{2} \left(1 + \frac{K}{\kappa^2} \right) \right\} . \tag{B.8}$$

Upon substituting $\kappa = 0.41$ and $K = 0.0168$ into equation (B.8), C_p can then be determined to be

$$C_p = 1.7332 \cdots \tag{B.9}$$

Direct comparisons of the two profiles show that the Baldwin-Lomax model having

the constant $C_p = 1.7332$ produces essentially the same results as the Cebeci-Smith model at low Mach numbers as well as in supersonic flows with M_e being O(1).

VITA

Mr. Jun He was born on August 25, 1956, in Beijing, China. He attended Beijing Yi-Wu-Jiu High School and graduated in January 1975. Mr. He attended Beijing Institute of Aeronautics and Astronautics and graduated with a BSME in January 1982. Upon graduation Mr. He was employed by Jet Propulsion Laboratory, Beijing Institute of Aeronautics and Astronautics and concurrent with this employment enrolled at the Institute and was awarded his MSME in June 1984. While at Beijing Institute of Aeronautics and Astronautics, Mr. He carried out research and development assignments working in the areas of turbomechinery, combustion engineering, and computational fluid dynamics. Mr. He enrolled at Lehigh University, Department of Mechanical Engineering and Mechanics in September 1988 to work toward the degree of Doctor of Philosophy.

In June 1984, Mr. He married Miss Beibin Li at Beijing, China. Their daughter, Meiheng He, was born at Beijing in July 1988.